UAV-ASSISTED WIRELESS COMMUNICATION SYSTEM FOR ON-DEMAND COVERAGE

A Thesis Submitted

in Partial Fulfilment of the Requirements

for the Degree of

DOCTOR OF PHILOSOPHY

by

Nishant Gupta

(2018EEZ0018)

DEPARTMENT OF ELECTRICAL ENGINEERING

INDIAN INSTITUTE OF TECHNOLOGY ROPAR

January, 2023

Nishant Gupta: *UAV-Assisted Wireless Communication System For On-Demand Coverage*

Dedicated to ***My Family***

and

My Teachers

Who are the inspiration and power behind the success of this work

Declaration of Originality

I hereby declare that the work which is being presented in the thesis entitled **UAV-ASSISTED WIRELESS COMMUNICATION FOR ON-DEMAND COVERAGE** has been solely authored by me. It presents the result of my own independent investigation/research conducted during the time period from January, 2019 to January, 2023 under the supervision of Dr. Satyam Agarwal, Assistant Professor, Department of Electrical Engineering, IIT Ropar. To the best of my knowledge, it is an original work, both in terms of research content and narrative, and has not been submitted or accepted elsewhere, in part or in full, for the award of any degree, diploma, fellowship, associateship, or similar title of any university or institution. Further, due credit has been attributed to the relevant state-of-the-art with appropriate citations and acknowledgments, in line with established ethical norms and practices. I also declare that any idea/data/fact/source stated in my thesis has not been fabricated/ falsified/ misrepresented. All the principles of academic honesty and integrity have been followed. I fully understand that if the thesis is found to be unoriginal, fabricated, or plagiarized, the Institute reserves the right to withdraw the thesis from its archive and revoke the associated Degree conferred. Additionally, the Institute also reserves the right to appraise all concerned sections of society of the matter for their information and necessary action (if any). If accepted, I hereby consent for my thesis to be available online in the Institute's Open Access repository, inter-library loan, and the title & abstract to be made available to outside organizations.

Signature 

Name: Nishant Gupta

Entry Number: 2018EEZ0018

Program: Ph.D.

Department: Electrical Engineering

Indian Institute of Technology Ropar

Rupnagar, Punjab 140001

Date: January 2023

Acknowledgement

First of all, I would like to thank my supervisor Dr. Satyam Agarwal for his guidance and encouragement which I received throughout my dissertation research journey. I am thankful to him for giving me the counsel and for painstakingly reading my reports. Without his invaluable advice and support it would not have been possible for me to complete this dissertation.

I take this opportunity to express my sincere thanks to Dr. Deepak Mishra for his valuable discussions and suggestions for improving my research work. I would like to thank Dr. Brijesh Kumbhani, Dr. Sam Darshi for their valuable feedback in improving my work.

I would like to thank all my fellow researchers of the Communication Group, who made this journey a memorable one. Further, I would like to extend them my best wishes for their future endeavors.

I express my heartfelt thanks to my parents who have been a constant source of inspiration to me all along and their encouraging words made this endeavor possible. Finally, I would like to thank my family, friends, and all others whose names are not mentioned here but have helped me to accomplish this work.

Certificate

This is to certify that the thesis entitled **UAV-Assisted Wireless Communication for On-Demand Coverage**, submitted by **Nishant Gupta (2018EEZ0018)** for the award of the degree of **Doctor of Philosophy** of Indian Institute of Technology Ropar, is a record of bonafide research work carried out under my guidance and supervision. To the best of my knowledge and belief, the work presented in this thesis is original and has not been submitted, either in part or full, for the award of any other degree, diploma, fellowship, associateship or similar title of any university or institution.

In my opinion, the thesis has reached the standard fulfilling the requirements of the regulations relating to the Degree.

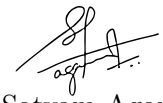

Dr. Satyam Agarwal
Assistant Professor
Department of Electrical Engineering
Indian Institute of Technology Ropar
Rupnagar, Punjab 140001
Date: January 2023

Lay Summary

This dissertation is inspired by the limited network coverage provided by the terrestrial base station, particularly in emergency and disaster-affected areas. In such cases, unmanned aerial vehicles (UAVs) can be programmed to act as aerial base stations (ABSs) to provide on-demand coverage to the users. In comparison to the terrestrial base stations, UAVs as ABSs can be deployed in a timely and energy-efficient manner. Thus, in this work, we consider UAVs that can be deployed as an ABS to enable communication service to ground users in a given area. However, there are multiple challenges that need to be addressed while deploying UAV as an ABS. Out of which, optimal deployment location of the UAV, the trajectory design of the UAV, and the limited battery available with the UAV are some of the challenges addressed in this dissertation.

In particular, we first identify the final location where the UAV can be deployed to provide maximum coverage to the ground users. Second, we design the path of the UAV to reach that location, given the limited battery of the UAV. Later, the UAV deployed at the final location will eventually run out of energy over time due to manoeuvring and hovering-related energy. Thus, to ensure that the UAV provides continuous coverage for longer durations, we show how the energy-depleted UAV can be replaced by another fully charged UAV. Furthermore, we also study the effect of communication channels on the UAV association probability, which refers to the probability by which the ground user is connected to a particular UAV.

Later, in this dissertation, we present the essential challenges that still need to be addressed in the context of using UAVs as ABSs in UAV-assisted communication networks.

Abstract

Unmanned aerial vehicles (UAVs) are thought to be the next-generation systems to enhance cellular coverage. The aerial nature of UAVs and their inherent characteristics, such as mobility, flexibility, and adaptive altitude, allow them to be deployed on an on-demand basis to assist the current cellular infrastructure by delivering additional coverage capabilities in either the hotspot or remote areas. Moreover, they can maintain line-of-sight (LoS) connection with the ground users leading to enhanced coverage and efficiency. Therefore, it is desirable to use the UAV as an aerial base station (ABS) to improve the wireless services and coverage in hotspot areas, such as football stadiums, fairs, public safety services (for example, firefighters and military operations), etc.

However, the use of UAVs as ABS requires some key design considerations, such as three-dimensional (3D) placement, communication-oriented trajectory design, energy efficiency, maximizing the performance metric, etc., to meet the application-specific requirements. Therefore, this dissertation intends to study a UAV-assisted communication system wherein a UAV is to be deployed in a timely and energy-efficient manner to provide optimum coverage to ground users.

In particular, we first study the optimal deployment location of the UAV to provide maximal performance to the ground users. After that, we obtain the UAV's path from the initial to the deployment location while meeting the UAV's energy and flight duration constraints. This scenario is very relevant to many practical applications where the deployment location is unknown and is based on ground users' location, such as providing high-speed connectivity to the first responders in emergencies, offloading traffic in a high-density area, such as football stadiums, or recovering the service in a disaster-affected areas.

We then study the velocity-acceleration and time profile to maximize the sum user throughput while considering the UAV kinematics (velocity and acceleration), mission completion time and UAV energy consumption as a function of velocity and acceleration as constraints. This is because the onboard energy available with the UAV, which is utilized in manoeuvring and hovering-related tasks, is determined by its flying velocity-acceleration profile and flight time.

Notably, in missions requiring long battery endurance, the battery limitation problem inhibits the UAV from delivering long-term service. As a result, to maintain coverage continuity, we propose a UAV replacement mechanism (a way to provide an uninterrupted long-term service). UAV replacement indicates that the existing serving UAV must be

replaced by another fully charged UAV when its available energy is exhausted. Finally, when multiple UAVs are deployed to provide service to multiple ground users spread over a given area, we study an association probability model based on a stochastic geometry framework for a UAV-assisted wireless communication network.

The above works/setups can be applied to many practical applications, such as establishing two-way communication between first responders and firefighters in areas with inadequate coverage or traffic offloading in a hotspot area, such as sports events.

Keywords: UAV-assisted wireless communication; on-demand coverage; UAV deployment and trajectory; UAV replacement; resource allocation; multi-UAV network; limited on-board energy;

List of Publications

Journal

- N. Gupta, S. Agarwal and D. Mishra, "Trajectory Design for Throughput Maximization in UAV-Assisted Communication System," in IEEE Trans. Green Commun. Netw., vol. 5, no. 3, pp. 1319-1332, Sept. 2021.
- N. Gupta, D. Mishra and S. Agarwal, "Energy-Aware Trajectory Design for Outage Minimization in UAV-Assisted Communication Systems," in IEEE Trans. Green Commun. Netw., vol. 6, no. 3, pp. 1751-1763, Sept. 2022.
- N. Gupta, S. Agarwal and D. Mishra, "Joint Trajectory and Velocity-Time Optimization for Throughput Maximization in Energy Constrained UAV," in IEEE Internet Things J., 2022, vol. 9, no. 23, pp. 24516-24528, Dec. 2022.
- N. Gupta, S. Agarwal, D. Mishra and B. Kumbhani, "Trajectory and Resource Allocation for UAV Replacement to Provide Uninterrupted Service," in IEEE Trans. Commun., 2022. (Under Review)

Conference Proceeding

- N. Gupta, D. Mishra and S. Agarwal, "3D-Trajectory Design for Outage Minimization in UAV-Assisted 5G Communication System," in Proc. IEEE 18^{th} Annual Consumer Commun. Netw. Conf. (CCNC), Las Vegas, USA, pp. 1-6, Jan. 2021.
- N. Gupta, S. Agarwal and D. Mishra, "UAV Deployment for Throughput Maximization in a UAV-Assisted Cellular Communications," in Proc. IEEE 32^{nd} Annual Int. Symp. Personal, Indoor Mobile Radio Commun. (PIMRC), Helsinki, Finland, pp. 1055-1060, Sep. 2021.
- N. Gupta, S. Agarwal and D. Mishra, "Multi-UAV Replacement and Trajectory Design for Coverage Continuity," in Proc. IEEE Int. Conf. Commun. (ICC), Seoul, South Korea, pp. 1-6, May 2022.
- N. Gupta, S. Agarwal and D. Mishra, "Impact of Fading on Association Probability in UAV-Enabled IoT Networks," in Proc. IEEE 95^{th} Veh. Technol. Conf. (VTC2022-Spring), Helsinki, Finland, pp. 1-5, June 2022.

Contents

Declaration iv

Acknowledgement v

Certificate vi

Lay Summary vii

Abstract viii

List of Publications x

1 Introduction 1

1.1 Background: UAV Meets Cellular Network 1

1.2 Opportunities and Challenges 3

1.3 Global Market of UAVs 5

1.4 UAV Rules, Regulations and Standards 6

1.5 Motivation 9

1.6 Objectives 10

1.7 Thesis Outline 12

2 System Model 15

2.1 UAV Trajectory Model 15

2.2 UAV Energy Consumption Model 17

2.2.1 Velocity Dependent Energy Model 18

2.2.2 Velocity-Acceleration Dependent Energy Model 19

2.3 A2G Channel Model 21

3 UAV Trajectory Design: Fixed Initial to Optimized Final Location 23

3.1 Introduction 23

3.1.1 State-of-the-Art 24

3.1.2 Contributions and Organization 26

3.2 System Model 27

3.2.1 Communication Setup 27

3.2.2 Performance Metric . . . 27
3.3 Problem Formulation . . . 28
3.4 Computation of Optimized Final Location . . . 29
3.4.1 Approximation and Concave Regions . . . 30
3.4.2 Solution using Alternating Optimization . . . 32
3.4.3 Convergence and Complexity . . . 32
3.5 UAV Trajectory Design towards Optimized Final Location . . . 33
3.5.1 Mathematical Analysis . . . 33
3.5.2 Algorithm Design . . . 35
3.5.3 Complexity Analysis . . . 38
3.6 Result and Discussions . . . 38
3.6.1 Optimal Location . . . 39
3.6.2 Trajectory Design Insights . . . 41
3.6.3 Performance Analysis of Proposed Scheme . . . 42
3.6.4 Performance Comparison with Benchmark Schemes . . . 43
3.7 Conclusion . . . 45

4 UAV Trajectory Design: Fixed Initial to Arbitrary Final Location 47
4.1 Introduction . . . 47
4.1.1 Related Works . . . 48
4.1.2 Contributions and Organization . . . 49
4.2 System Model . . . 51
4.2.1 Communication Setup . . . 51
4.2.2 Performance Metric . . . 51
4.3 Problem Formulation . . . 52
4.4 Vertex Approach: Proposed Solution I . . . 54
4.4.1 Vertex Computation . . . 54
4.4.2 UAV Trajectory without Energy and Velocity Constraint . . . 56
4.4.3 Proposed Vertex Approach . . . 57
4.4.4 Complexity Analysis . . . 60
4.5 Sequential Approach: Proposed Solution II . . . 61
4.5.1 Proposed Sequential Approach . . . 61
4.5.2 Complexity Analysis . . . 63
4.6 Simulation Results . . . 63
4.6.1 Trajectory Design Insights . . . 64

4.6.2 Performance Analysis of Proposed Scheme 66
4.6.3 Performance Comparison with Benchmark Schemes 68
4.7 Conclusion 69

5 UAV Kinematics Optimization **71**
5.1 Introduction 71
5.1.1 Related Work 71
5.1.2 Novelty, Motivation and Contribution 72
5.2 System Model 73
5.3 Problem Formulation 74
5.3.1 Sum Throughput Maximization 74
5.3.2 Energy Minimization 75
5.4 P1: Sum Throughput Maximization 75
5.4.1 Algorithmic Implementation of P1 75
5.4.2 Complexity and Convergence Analysis 77
5.5 P2: Energy Consumption Minimization 78
5.5.1 Algorithmic Implementation of P2 78
5.5.2 Complexity and Convergence Analysis 80
5.6 Results and Discussion 80
5.6.1 Sub-optimal Design Insights: Sum Throughput Maximization 81
5.6.2 Sub-optimal Design Insights: Energy Minimization 82
5.6.3 Performance Comparison 83
5.7 Conclusion 84

6 UAV Replacement for Coverage Continuity **85**
6.1 Introduction 85
6.1.1 Related Works 86
6.1.2 Contributions and Organization 88
6.2 System Model 89
6.2.1 Communication Model 89
6.2.2 Performance Metric 90
6.3 Problem Formulation 91
6.4 Proposed Methodology 92
6.4.1 Bandwidth Optimization 92
6.4.2 Trajectory Optimization 93

6.5 Overall Algorithm . . . 96
6.5.1 Trajectory Initialization Strategy . . . 97
6.5.2 Overall Algorithm . . . 97
6.5.3 Complexity and Convergence . . . 98
6.6 Results and Discussions . . . 99
6.6.1 Scenario 1: Single-user UAV Replacement Mechanism . . . 100
6.6.2 Scenario 2: Multi-user UAV Replacement Mechanism . . . 101
6.6.3 Scenario 3: Clustered-users UAV Replacement Mechanism . . . 105
6.7 Conclusion . . . 106

7 Impact of Fading on Association Probability 109
7.1 Introduction . . . 109
7.1.1 Motivation . . . 109
7.1.2 Related Works . . . 110
7.2 System Model . . . 111
7.2.1 Aerial Network Deployment . . . 111
7.2.2 A2G channel model . . . 111
7.3 Association Probability Analysis . . . 113
7.3.1 Key Statistical Results . . . 113
7.3.2 Exact Association Probability . . . 113
7.3.3 Special Case: Rayleigh Fading . . . 114
7.4 Approximate Association Probability . . . 115
7.4.1 Special Case: Low Altitude UAVs . . . 115
7.5 Result and Discussions . . . 116
7.5.1 Validation of Association Probability . . . 117
7.5.2 Performance Analysis . . . 117
7.5.3 Performance Comparison . . . 119
7.6 Conclusion . . . 120

8 Conclusion and Future Scope 123

A Appendix Title 125
A.1 Detailed Proofs of Chapter 3 . . . 125
A.1.1 Proof of Lemma 1: Individual Concave regions for step approximation 125
A.1.2 Proof of Lemma 2: Individual Concave regions for linear approximation . . . 126

A.2 Detailed Proofs of Chapter 4 128
A.2.1 Proof of Lemma 3: Pseudoconvexity of $e[n]$ with respect to $v[n]$ . . . 128
A.2.2 Proof of Lemma 4: Individual Pseudoconvexity of $\bar{P}_{out}$ in (x, y) for Fixed z and in z for fixed (x, y) 129
A.2.3 Proof of Lemma 5: Conditional Joint Convexity of $\bar{P}_{out}$ in x, y, and z131
A.3 Detailed Proofs of Chapter 6 132
A.3.1 Proof of Lemma 6 132
A.3.2 Proof of Lemma 7 133
A.3.3 Proof of Lemma 8 134
A.4 Detailed Proofs of Chapter 7 135
A.4.1 Proof of Lemma 9: Association probability of typical user with the LoS UAV 135
A.4.2 Proof of Lemma 10: Approximate association probability of typical user with LoS UAV 136

List of Figures

1.1 Summary of use-cases of UAVs in wireless communication. 7

1.2 UAV-assisted wireless communication system. 9

1.3 Thesis organization. 12

2.1 System model representing the coverage field having K ground users in a 2D plane along with UAV's initial and final locations. 16

2.2 Energy consumed with different accelerations for (a) level-straight flight, and (b) vertical flight of UAV. 20

3.1 Proposed scheme to obtain the optimal trajectory for problem (P3). 34

3.2 Validation of optimal location at (a) $y = y^*_{es}$, (b) $z = z^*_{es}$. 39

3.3 Variation of sum rate at optimal location with other schemes by varying number of users K. 40

3.4 Variation of sum rate at optimal location with other schemes by varying field radius r. 40

3.5 Insights on sub-optimal trajectories of UAV 41

3.6 Variation of average sum rate Q_{avg}, time slots attained by the UAV N^*, and β with maximum allowed time slots N_{av} for different values of on-board energy availability E_{max}. 42

3.7 Overall performance improvement in average sum rate over the inverted-L, straight flight trajectory and fly-hover scheme. 43

3.8 Variation in average sum rate with the change in the number of users, K, distributed in a field of radius $r = 500$ m. 44

3.9 Variation in the average sum rate with the change in velocity of UAV, V (m/s). 44

4.1 Motivation and brief description of proposed solutions. 54

4.2 *Vertex approach* to obtain the 3D UAV trajectory. 55

4.3 UAV 3D trajectory design under *sequential approach*. 61

4.4 Insights on sub-optimal trajectories of UAV. 64

4.5 Variation of (*a*) $x[n]^*$, (*b*) $y[n]^*$, (*c*) $z[n]^*$, and (*d*) $v[n]^*$ with number of time slots for different values of energy availability constraint, E_{max}. SA and VA are *sequential* and *vertex approach*, respectively. 64
4.6 Change in average outage probability with V_{max} for different flight time T. 66
4.7 Change in average outage probability with T for different maximum velocity V_{max}. 66
4.8 (*a*) v_{allow} of UAV due to energy constraint (4.4a) at different values of E_{max}. (*b*) Impact of E_{max} on average outage probability. 67
4.9 Comparison of proposed approaches with existing benchmark schemes. . . . 68

5.1 UAV dynamics with respect to sum rate maximization. 81
5.2 UAV dynamics with respect to energy minimization problem. 82
5.3 Performance of proposed scheme w.r.t. conventional schemes. 83

6.1 Model representing the UAV replacement framework. 89
6.2 Trajectory initialization based on straight-line path. 97
6.3 UAV trajectories for both UAV U_1 and UAV U_2 with $E_{left} = 5000$ J in (a) 3D-plane, and (b) XY-plane. 100
6.4 UAV trajectories for both UAV U_1 and UAV U_2 with $E_{left} = 2000$ J in (a) 3D-plane, and (b) XY-plane. 101
6.5 UAV trajectories for both UAV U_1 and UAV U_2 with $E_{left} = 5000$ J in (a) 3D-plane, and (b) XY-plane for Scenario 2. 102
6.6 UAV trajectories for both UAV U_1 and UAV U_2 with $E_{left} = 2000$ J in (a) 3D-plane, and (b) XY-plane for Scenario 2. 102
6.7 Optimal bandwidth allocated to (a) the user 1, and (b) user 2, when $E_{left} =$ 5000 J. 103
6.8 Optimal bandwidth allocated to (a) the user 1, and (b) user 2, when $E_{left} =$ 2000 J. 103
6.9 Comparison of proposed schemes with conventional schemes with different energy levels for Scenario 2. 104
6.10 UAV trajectories for both UAV U_1 and UAV U_2 with $E_{left} = 5000$ J in (a) 3D-plane, and (b) XY-plane for Scenario 3. 104
6.11 UAV trajectories for both UAV U_1 and UAV U_2 with $E_{left} = 2000$ J in (a) 3D-plane, and (b) XY-plane for Scenario 3. 105
6.12 Comparison of max-min throughput with different energy levels for a clustered-user UAV replacement scenario. 106
6.13 Comparison of achievable sum throughput of $K = 12$ users using different schemes for Scenario 3. 106

7.1 Validation of exact and closed-form expression with the simulation runs. . . 116
7.2 Impact of UAV's altitude on the LoS association probability for different environment scenarios. 117
7.3 Comparison of different fading scenario and validation of approximation LoS association probability. 117
7.4 Impact of UAV density, λ on the LoS association probability for (a) dense urban scenario, (b) sub-urban scenario. 118
7.5 Comparison of ergodic capacity of our proposed UAV scheme with the closest UAV scheme. 119
7.6 Comparison of LoS association probability of our proposed scheme with the closest UAV. 120

List of Tables

2.1 Energy consumption model parameters 18

4.1 Short summary of related works that considers energy constraint in their model. P.LoS is the probabilistic LoS channel model. 50

4.2 System Parameters Considered for Simulations 63

6.1 Key differences between the related existing literature with our work. PLoS here stands for probabilistic LoS channel. 87

Chapter 1

Introduction

1.1 Background: UAV Meets Cellular Network

In recent years, unmanned aerial vehicles (UAVs) have provided an effective solution to various kinds of applications, such as search and rescue, cargo delivery, military applications, commercial applications, telecommunications, precision agriculture, etc. [1], [2]. This is possible because of their inherent characteristics, such as controllable three-dimensional (3D) mobility, flexible deployment, and on-demand service. As a result, the global drone market is expected to reach US$58 billion by 2026, showing how fast the drone industry is evolving [3]. Furthermore, in the telecommunication industry, these appealing attributes have enabled them to provide communication-related service and assist the terrestrial wireless infrastructure [4].

Compared to the existing constrained terrestrial wireless infrastructure, UAVs are considered to be the next-generation systems to enhance cellular coverage. This is because, in special scenarios, such as search and rescue operations and on-demand emergency services, the deployment of an adequate ground infrastructure in a timely and economical manner is impractical due to high capital and operational costs, as well as substantial delay in deployment [5]. Thus, in many such scenarios, it is anticipated that the existing ground infrastructure might be insufficient to cater to the current needs.

The use of UAVs as network relays or aerial base stations (ABSs) can prove to be an effective solution due to their flexibility, on-demand coverage, and swift deployment. UAVs can maintain line-of-sight (LoS) communication links with the ground users/terminals and enhance the performance and coverage of the current cellular networks [6]. As a result, UAVs can be integrated with cellular networks by deploying them as an ABS or relays to support the terrestrial communication system [4]. These UAV functionalities have encouraged the governmental organizations and industry to develop policies for UAV operations.

Specifically, there are two typical use cases of UAVs in wireless communication: First,

the UAVs can be deployed on-demand as an ABS or relays to provide communication service in the desired areas. Second, UAVs as aerial user equipment's (UEs) to support the user applications, such as drone delivery and surveillance-related missions. This function of UAVs as UE's is referred to as cellular-connected UAVs.

From the above brief discussion, the two main roles or paradigms of UAVs when integrated into wireless communications systems are:

- Cellular-enabled UAV communication: In this paradigm, the UAVs operate as aerial users and have their own mission. Similar to ground users, aerial users are also served by ground base stations (BSs). Typical use cases of cellular-enabled UAV communication include cargo delivery, video surveillance, etc.

- UAV-assisted cellular communication: In this paradigm, UAVs operate as aerial platforms where the UAVs are either used as ABSs or relays to serve the ground users in cellular networks. Possible use case include traffic offloading in hotspot areas.

The UAVs integrated into wireless communication systems have numerous advantages. In particular, UAVs can offload traffic and can complement the existing BS. They can even provide coverage expansion in the areas where the BS deployment is difficult, such as in hard-to-reach rural areas. UAVs also offer several services to Internet of Things (IoT) applications [7]. IoT devices have low transmit power and cannot communicate over a long range. In such cases, UAVs can act as wireless relays to improve the coverage and connectivity of these IoT devices. UAVs also helps in surveillance, which is another key use case of IoT. Lastly, in regions (due to terrain constraints) where constructing a complete cellular setup is extremely expensive, UAVs become particularly useful as they eliminate the need for high-priced towers and infrastructure installations. The real-world projects that employ UAVs as ABS for wireless connectivity include Google's Loon project, where the UAVs were used to deliver airborne global Internet connectivity in developing countries [8]. Furthermore, Qualcomm and AT&T are also planning to deploy UAVs in the fifth-generation (5G) networks to enable wide-scale wireless communications. Likewise, Amazon Prime Air and Google's Project Wing programs are notable instances of cellular-connected UAV use cases.

Despite these promising advantages of UAVs, there are various challenges that must be resolved before using them for any given networking application. For example, performance characterization, optimal 3D deployment of UAVs, resource allocation, flight time minimization, energy-efficient communication, trajectory optimization, and network

planning are the primary design factors while employing UAVs as ABSs. Contrarily, the primary issues in the cellular-connected UAVs scenario include interference and handover management, low-latency communication, channel modeling, and localization. In this dissertation, we intend to study a UAV-assisted wireless communication system, where the UAV functions as an ABS to serve the ground users. Next, we present opportunities and challenges in a UAV-assisted communication system.

1.2 Opportunities and Challenges

In comparison to the ground BSs and fixed relays, UAVs as ABSs have the following new capabilities:

- Fast and flexible deployment: Traditional terrestrial infrastructures are often stationary; as a result, their design is limited to considering the long-term data traffic and distribution of the users in the given area. Whereas UAVs can be flexibly deployed as quasi-stationary ABSs to meet the real-time demand in a particular area and thus enhances the performance of the communication system. Notably, the fast, flexible and on-demand deployment of UAVs makes them a preferable alternative for providing ubiquitous cellular coverage in isolated, rural areas or hotspot events without the need to establish additional terrestrial infrastructure.

- Controllable 3D mobility: Besides serving as ABSs at specific locations, the controllable 3D mobility of UAVs allows them to function as mobile ABS capable of flying over the ground users in the serving area to provide more effective communication. Thus, in scenarios, such as user procession or first responders, the UAVs can track the mobility of the user and provide optimum coverage.

- LoS-dominant channel: Due to their controllable 3D mobility, the UAVs as an ABS has the capability to establish a LoS dominant channel by establishing LoS links with the ground users in rural or suburban environments. However, in urban environments, the UAV and ground user channel can be characterized via a probabilistic LoS channel wherein the LoS and non-LoS (NLoS) links have a certain occurrence probability.

As a result of the above capabilities, UAV-assisted wireless communication is anticipated to be a key technology for next-generation networks to meet the exponential growth in data traffic demands. Some common use cases are coverage expansion in isolated

areas without or with minimal terrestrial infrastructure; service recovery in emergency situations or disaster-affected areas; offload traffic from the ground BS in hotspot events; aerial relaying to connect far-flung ground users; and cost-effective and reliable data collection in machine-type communications, etc. [4].

However, the following design issues need to be addressed before realizing the enticing idea of UAVs as ABSs in wireless communication systems.

- 3D deployment for UAVs: Due to the additional degree of freedom (DoF) in the UAV's mobility and ability to adjust its altitude and horizontal location, the 3D deployment for UAVs as aerial platforms is more complicated than the traditional two-dimensional (2D) placement of terrestrial BS. Also, the deployment of UAVs as an aerial platform must ensure optimum coverage to all ground users.

- Communication-oriented trajectory design: The trajectory or the path traced by the UAVs must be planned to maximize the ground user's experience or the system's performance. For instance, a UAV can fly closer to a ground user and shorten the link distance with the ground users to achieve a high communication rate. This ensures an increase in capacity and a reduction in resources. Thus, the UAV trajectory must be designed while considering the limited resources available with the UAVs to further enhance the communication performance and for optimum utilization of communication resources.

- Energy-efficient communication: Besides the communication-related energy (energy consumed for signal processing and amplification), UAVs require additional energy to remain aloft in the air and move freely. This energy is referred to as propulsion energy consumption, which is typically far more substantial than the communication-related energy. For example, propulsion energy consumption is of the order of kilowatt versus watt in communication-related energy [9], [10]. The limited onboard energy available with the UAVs and the high propulsion energy consumption poses serious limitations when deployed to provide communication service in a specific area. Thus, energy-efficient design is essential to improve the long-term performance of UAVs in wireless communication.

To fully leverage the advantages of UAVs in wireless communication while also considering the above challenges, several research organizations, regulatory bodies, etc., are actively involved in conducting various trials and experiments. Therefore, we next

introduce the global market of UAVs, followed by the UAV rules, regulations, and standards for utilizing UAVs in enhancing wireless connectivity.

1.3 Global Market of UAVs

The rapid development of UAV technology in 5G has resulted in a myriad of wireless communication use cases. According to reports [11], 5G is expected to enable global economic outputs of 12.3 trillion and support the creation of 22 million jobs. The value chain is expected to generate a result of $3.5 trillion annually in 2035. Research is ongoing to harness the potential of UAVs to support the existing cellular systems [12].

Many research bodies are working towards this integration to target the applications of UAVs and terrestrial BSs. Two globally recognized telecommunication companies – Nokia and Qualcomm, begun a research project called the "5G!Drones" being funded by the European Union's Horizon 2020 Research and Innovation Programme, the biggest European Union research and innovation program to date with over 80 billion in funding [13]. Several research groups, such as Eurecom, Airbus, the University of Oulu, and many more, are also part of this project. The project is made up of a large consortium of businesses located throughout the European Union and Switzerland and is aimed at conducting trials of several UAV use cases and validating the attainment of 5G key performance indices (KPIs) for supporting such use cases [13]. As an outcome of their collaboration, several works, for example, [14], and [15], have been published identifying the optimal trajectories of UAVs.

Recently, Federal Government awarded $20 million across 19 5G projects that will trial 5G across the key sectors of the economy, including agriculture, construction, manufacturing, transport, and education and training. In particular, $1,496,627 in funding has been allocated to Rheinmetall Defence Australia Pty. Ltd. for 5G Remote Controlled Firefighting vehicle [16]. The purpose of this vehicle is to traverse extremely dangerous terrains to support rescue, path clearing, and firefighting missions.

Several communication societies are also targeting the UAV-cellular integration from various releases and standards. For example, the third-generation partnership project (3GPP) provides the recent definition of new UAV applications within Release 17 and a radio access network (RAN) work item for UAV support within Release 18.

1.4 UAV Rules, Regulations and Standards

As described in the previous subsection, the current market growth of UAVs has shifted the focus of researchers toward the development of communication technologies and protocols and the applications that support UAV operations. In addition, the industry has already begun to integrate UAVs into fourth-generation (4G) and 5G communication networks.

The standards organization for cellular networks, such as 3GPP, is actively participating in identifying the new wireless technologies and communication protocols for the usage of UAVs in wireless communication along with the current needs and requirements. The 3GPP has successfully completed the study that includes the support for UAVs as UEs in long-term evolution (LTE) in their Release 15 (Rel-15) Technical Report TR 36.777 in the year 2017. This study identifies the necessary enhancements that must be applied to LTE to maximize network efficiency when serving UAVs (as UEs). The important framework discussed regarding the UAV services is the development of a robust communications framework. This framework ensures authorization and maintains safety that incorporates the airspace regulation. These requirements were studied in Technical Specification TS 22.125 (in 2018) for providing UAV services.

In 2019, through TR 22.829, the 3GPP identified the required communications and networking performance enhancements as well as a number of UAV-enabled use cases and applications that will be supported by the 5G technology. In 2020, the 3GPP in the Rel-17 aimed to focus on the two major factors related to UAV communications: the processes for maintaining connectivity, identification, and tracking of UAVs, and the network infrastructure and application architecture to support UAV operations in TR 23.754, and TR 23.755, respectively. Currently, 3GPP is working on Rel-18, which is envisioned to enable the support of next-generation networks through 5G cellular systems. The growing interest in massive IoT and machine-type communication based services is the primary aim of studying UAV communication in 3GPP Rel 18.

Besides 3GPP, the Institute of Electrical and Electronics Engineers (IEEE) and the International Telecommunication Union (ITU) are also actively working in this domain of research. Different IEEE standards groups have developed standards for drone applications, traffic management for low-altitude UAVs, aerial communication, and networking standards [17]. In line with the 3GPP vision, the ITU develops a fully functional framework for UAVs that will act as UE's for IMT-2020 networks [18].

For effective communication with UAVs, the 3GPP has defined certain standards.

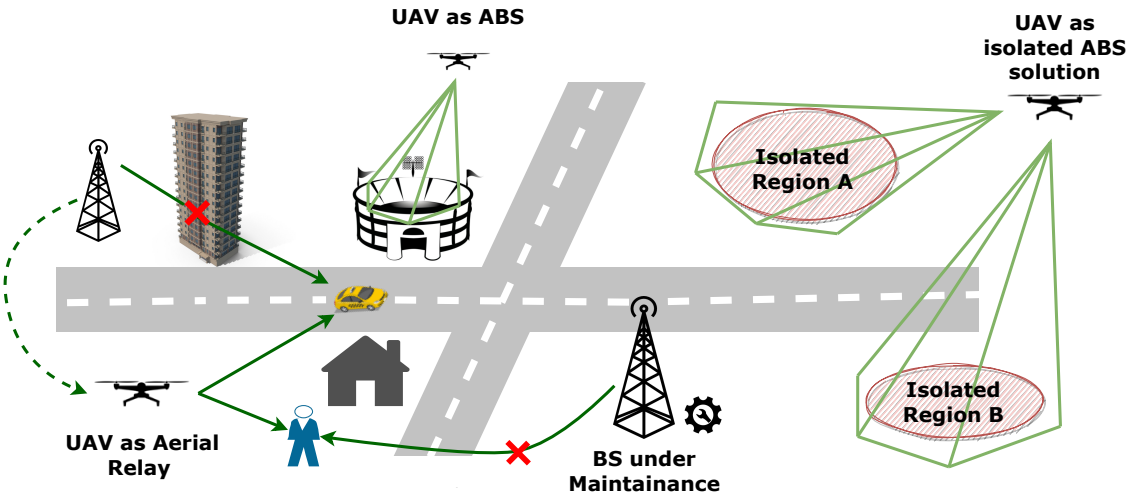

Figure 1.1: Summary of use-cases of UAVs in wireless communication.

First, the remote identification process, which requires the UAV nodes to register, authenticate and notify the network of their status regularly. The cellular network can then be used to enable services like control and communications. Second, for efficient management of airspace operations and to ensure safety, the UAV needs to provide regular updates of its presence to the airspace management system. This implies that in addition to the UAVs, the controller must also periodically validate their presence to the supporting network. This information is then transferred to UAV traffic management to ensure the safety of the aerial vehicles. The UAV traffic management supports remote identification of the aerial platforms, in-flight re-routing, strategic aerial de-confliction between coexisting missions, airspace authorization, and flight intent sharing with other authorizations [19].

Modern radios can be deployed on UAVs to provide high-quality data links for a variety of applications. This includes the UAV radio node to support terrestrial RANs, which can be used to extend the coverage or provide communication in isolated regions. As discussed in the previous subsections, it enables rapid deployment in emergency scenarios, such as supporting evacuation in disaster-affected areas or they can be used to provide on-demand communication at hotspot events. The summary of use cases of UAVs in wireless communication is illustrated in Figure 1.1.

However, as per the regulation protocol set by the 3GPP, before starting the predefined mission to provide wireless connectivity in the desired area, the UAV needs to be first authorized and then programmed only to perform a specific operation (with the defined regulations and objectives). After the authenticity, using spectral resources, the UAV can now be deployed at a particular location in a geographical area (specifying the no-fly zones) only for a provided mission time.

Since the UAVs are battery-operated, the overall flight time of the UAV is limited. Furthermore, there are other factors also, that reduce the operational time of UAVs, such as the size of the UAV, power rating of the onboard battery, size and weight of the payload, cargo, aerodynamics, and approved airspace laws that, in turn, enable the UAVs to take longer paths. As a result, the 3GPP systems are helping UAV nodes by allowing close monitoring and continuously reporting the power consumption status of the UAV, its location, trajectory, and environmental conditions. This constant monitoring and status reports of the UAV will help to maintain the appropriate quality-of-service (QoS) during its flight time and can easily manage UAV replacements when the power runs low on the UAV.

The research organizations and the industry are motivated to define the needs and requirements and standardize a set of services that can be offered to fully leverage the advantages of UAVs. Standardizing these services will enable service delivery and path planning by optimizing the operational parameters, and these services will assist in reduced in power consumption of UAV. To help standardize the services and requirements of UAV as an aerial node, significant R&D initiatives have been taken, and testbeds have been built to enhance UAV communications. These initiatives investigate the UAV performance requirements and protocol solutions to support a variety of real-life use cases. As a result, the experimental findings that are obtained in a regulated environment with real-time settings will speed up the process of UAV communication advancements. The several R&D initiatives are highlighted below.

Aerial Experimentation and Research Platform for Advanced Wireless (AERPAW): A large-scale testbed developed by the US in 2019 for the Advanced Wireless Research initiative. AERPAW enables the experimentation of systems of UAVs with advanced wireless technology. The aim of AERPAW is to support 5G and beyond 5G oriented research. Additionally, it also provides access to 5G networks that are suitable for commercial use and software radios that are deployed as payloads to enable UAV communications.

5G!Drones: An initiative taken by European Union in June 2019. Under 5G!Drones, several academic institutes, research centers, and network operators have come together to examine the use cases of UAVs over 5G networks. This project considers the following UAV use cases: UAV traffic management, public safety, and situational awareness. The goal of 5G!Drones is to evaluate the performance and capability of aerial nodes providing aerial services. They also provide feedback to aid performance improvement, requirements

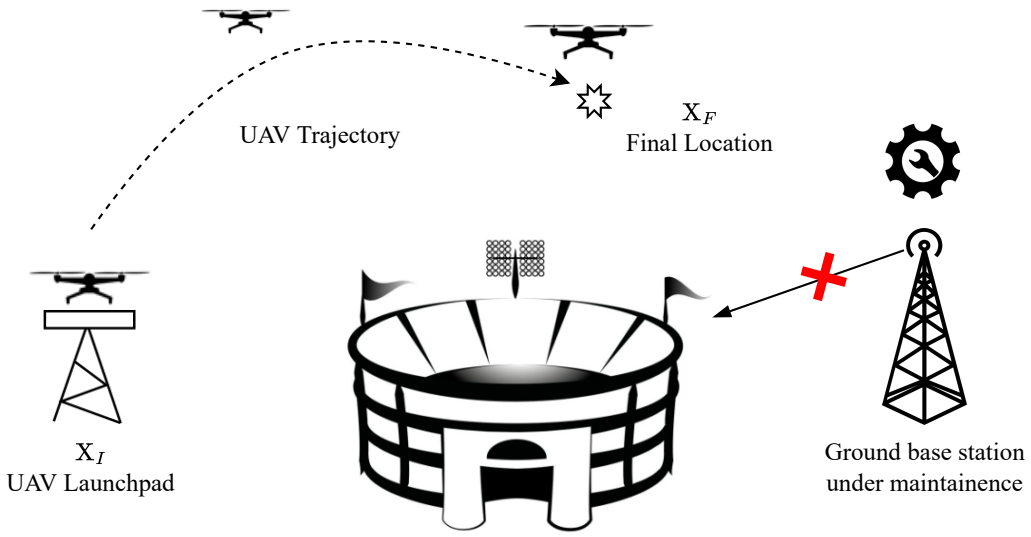

Figure 1.2: UAV-assisted wireless communication system.

and needs of a selected user case in 5G systems. 5G!Drones is part of the European Commission-funded 5G Public Private Partnership (5GPPP) projects.

5G-DIVE: The 5G-DIVE initiative was launched in October 2019 by a collaboration of vendors, service providers, network operators, small and medium-sized companies (SMEs), and academic and research centers from the European Union and Taiwan. The goal of 5G-Drive is to conduct real-world tests of several 5G technologies on the field to ensure that all the technical aspects are fulfilled before taking these technologies to the next level. The 5G-DIVE focuses on autonomous drone reconnaissance, which includes drone fleet navigation and cognitive image analysis. The European Union is funding 5G-DIVE under the H2020 Program.

1.5 Motivation

The use of UAVs as ABSs can prove to be an effective solution (as described in the previous sub-sections) to support the terrestrial communication systems [20]. Some common use cases include coverage expansion or offloading the traffic in a particular scenario, such as sports stadium, carnivals, and live concerts, where the present ground system is insufficient to provide adequate QoS, service restoration when the ground network infrastructure is interrupted, etc. [21]. Furthermore, in special scenarios, such as search and rescue operations, it is anticipated that the UAVs can be timely deployed to provide low-cost communication service in comparison to the existing ground infrastructure.

However, as specified in Section 1.4, there exist multiple challenges in deploying

the UAVs to enhance cellular coverage, such as optimal deployment in 3D space, communication-oriented trajectory design, and energy-efficient communication [22]. Furthermore, the limited onboard energy available with the UAV is a major concern due to which the operational time of the UAV is quite short.

In view of the above challenges, in this work, we introduce a framework to optimize the resources available with the UAV and the path of the UAV such that the communication performance is maximized. Specifically, as described in Figure 1.2, we consider the ground users to be present in the circular field. A UAV as an ABS is launched from the launchpad to provide communication in a given area while addressing the key challenges, such as 3D deployment, trajectory design of the UAV, resource allocation, and limited onboard energy of the UAV. This setup can be applied to many practical applications, such as establishing two-way communication between first responders and firefighters in an area with inadequate coverage or traffic offloading in a hotspot area, such as sports events.

1.6 Objectives

This dissertation intends to study a UAV-assisted communication system wherein a UAV is to be deployed in a timely and energy-efficient manner to provide optimum coverage to the ground users. The objectives formulated to study the communication system are as follows.

Objective 1: We consider a UAV-assisted communication scenario based on a user-centric approach wherein a UAV trajectory is optimized to provide maximum sum rate to the ground users while deploying the UAV at a suitably optimal location. This is because it is known that the maximal system performance is achieved when the final location is considered to be the optimal deployment location instead of considering the arbitrary final location [23]. So, the first step is to find the deployment location where the sum rate is maximum. After that, we obtain an optimal trajectory from the launchpad to the deployment location to maximize the average sum rate while meeting the energy and flight duration constraints of the UAV.

However, due to terrain limitations, legal restrictions, or some policies and regulations, the UAV might not be able to stay at the optimal location. In such cases, the final location can be a location other than the optimal location. Therefore, **Objective 2** considers the scenario where a UAV has to fly from the launchpad to an arbitrary final location in a stipulated time and with available onboard energy to provide coverage to a given set of users. Specifically, a trajectory optimization problem is formulated that optimizes the 3D

UAV trajectory while considering the velocity and total onboard energy availability as constraints.

The onboard energy available with the UAV is utilized in manoeuvring, which is determined by its flying velocity-acceleration profile and flight time [24]. In the prior objectives, we didn't consider the acceleration related energy consumption to handle the computational tractability of the problem. Thus, the communication system's design must consider energy consumption as a function of UAV velocity, acceleration, and time along with the other constraints. This is because the acceleration of the UAV also contributes to a significant energy consumption (as shown in Chapter 5). In this context, **Objective 3** studies the UAV kinematics optimization in an energy-aware UAV-assisted communication system, where we optimize the UAV velocity-acceleration and time profile in the presence of onboard energy, velocity, acceleration, and mission completion time constraints to maximize the performance of the UAV communication system, for a given trajectory of the UAV.

As the UAVs have limited onboard energy, its energy will become low after certain time. This is because manoeuvring and hovering consumes a significant amount of energy. Thus, to fully utilize the benefits of the UAV as an ABS, we need to find a way to provide an uninterrupted long-term service rather than short-term. Notably, in missions that require long battery endurance, we cannot solve the battery limitation problem by improving energy efficiency or energy management [25]. Thus, practical implementation of UAV applications requires UAV battery recharge or replacement. Therefore, the UAV must be grounded frequently at the charging station to replenish its battery. That is, if one UAV gets low on battery, another fully charged UAV can take its place to provide uninterrupted service to the ground users. As another UAV is launched for replacement, multiple key challenges like resource allocation and multi-UAV trajectory planning must be addressed by the communication system designer in the presence of UAV energy consumption constraints. Motivated by the UAV replacement scenario and its challenges, the **Objective 4** presents a novel framework for maintaining coverage continuity in a UAV-assisted wireless communication system by launching a fully charged UAV to replace the existing UAV, which is low on energy. This framework includes optimizing the 3D multi-UAV trajectory and bandwidth allocation to maximize the minimum achievable data rate by the ground users in the presence of onboard energy availability constraints.

Lastly, when multiple UAVs are deployed to provide communication to the ground users spread over a given area, a ground node is associated with the UAV that is closest.

Figure 1.3: Thesis organization.

However, in a UAV-assisted wireless communication, the UAV-user channel can be LoS or NLoS based on the channel conditions. In such a system, it may happen that a closer UAV may be in NLoS or may experience deep fade than a farther UAV with a LoS channel. Thus, instead of associating with the closest UAV, the ground user may want to associate with another UAV with a better channel for better communication. Therefore, **Objective 5** studies an association probability model based on stochastic geometry framework for UAV-assisted wireless communication where the UAV-user links are characterized by LoS or NLoS by taking fading into account. Since the channel between the UAV and the user is estimated through obtaining the instantaneous signal-to-noise ratio (SNR), which includes fading, it is necessary to study the impact of fading on the association probability.

1.7 Thesis Outline

The organization of this dissertation is as follows.

- **Chapter 2: System Model -** This chapter introduces a UAV trajectory model, velocity and acceleration-dependent energy consumption model, and air-to-ground (A2G) channel model. This chapter sets the stage for the rest of the chapters, where we utilize these models to build the communication setup and formulate the problem.

- **Chapter 3: UAV Trajectory Design: Launchpad to Optimal Deployment Location -** In this chapter, we address the problem of UAV deployment in 3D space to provide on-demand coverage to the users such that their sum rate is maximized. First, we find the optimal UAV location in 3D space where the sum rate is maximized for all ground users. Thereafter, an optimal trajectory is designed for the UAV to travel from the initial to the optimal location, such that the overall average sum rate during the flight is maximized while meeting the onboard energy availability and flight duration constraints.

- **Chapter 4: UAV Trajectory Design: Launchpad to Arbitrary Final Location -** In this chapter, an energy-aware trajectory optimization problem is formulated where the UAV is launched from the launchpad and moves to the arbitrary final location. In particular, we minimize the average outage probability of the system by optimizing the 3D trajectory of the UAV while considering the velocity and onboard energy as constraints.

- **Chapter 5: UAV Kinematics Optimization -** In this chapter, we provide a generalized framework for joint optimization of velocity and acceleration that can be applied to any existing UAV trajectory to maximize its performance. It optimizes the UAV velocity-acceleration profile in the presence of onboard energy, velocity, acceleration, and mission completion time constraints. This approach can be applied to both user-centric or UAV-centric applications and increases the UAV performance for the same trajectory by utilizing its energy optimally. In particular, we consider two problems, the sum throughput maximization, and energy consumption minimization.

- **Chapter 6: UAV Replacement for Coverage Continuity -** In this chapter, we present a novel framework for UAV replacement to maintain coverage continuity in a UAV-assisted wireless communication system when a serving UAV runs out of energy. Our objective during this replacement process is to maximize the minimum achievable throughput to the UAV-served ground users by jointly optimizing the 3D multi-UAV trajectory and resources allocated to the users from the individual UAVs.

- **Chapter 7: Impact of Fading on User Association Probability -** In this chapter, we consider a UAV-assisted wireless communication system where multiple UAVs are deployed to serve ground users. We model the A2G channel based on the instantaneous channel; we consider a generalized fading model, the

Nakagami-m model for the A2G link, to provide a more generic analysis. Through analytical insights, we obtain the exact and closed-form approximate expression of the association probability of the ground user with the UAV and infer the capacity enhancement obtained by considering fading compared to the average SNR scenario.

- **Chapter 8: Conclusion and Future Scope -** This chapter summarizes the key takeaways of each objective and highlights some possible future research direction in the UAV-assisted wireless communication system.

Chapter 2

System Model

In the previous chapter, we highlighted the requirements for a UAV-assisted communication system from the application's perspective and noted some key challenges that need to be addressed in this field. In this chapter, we describe the system model for the UAV-assisted communication system. In particular, we describe

- UAV trajectory model that presents the model involving the grounds users and UAV trajectory along with the mobility constraints
- Energy consumption model of a rotary-wing UAV
- A2G channel model

This sets the stage for rest of the chapters in this thesis, where we utilize these models to build the communication setup and formulate the problem.

2.1 UAV Trajectory Model

In this thesis, we consider a downlink communication setup as described in Figure 2.1, where a UAV serves K ground users, indexed by $\mathcal{K} \triangleq \{1, \cdots, K\}$, distributed randomly in a circular field of radius r. The users are static, and the location of the k^{th}-user is given by $(\mathbf{w}_k, 0)$, where $\mathbf{w}_k = [x_k, y_k] \in \mathbb{R}^{1\times 2}$, where $k \in \mathcal{N}$, and $\mathbb{R}$ denotes the set of real-valued numbers. For a mobile network with mobile ground users, we assume that the user location is known to the UAV but only at the beginning of every time slot. This can be achieved by employing tracking algorithms as presented in [26], and [27]. As the nodes are mobile, the future locations of the mobile users are difficult to be known at the current time instant. Hence, it is more challenging to achieve optimal performance metric for the communication system with mobile users. Future extensions include mobile node prediction in future times and UAV trajectory design for a mobile network.

We assume the UAV uses frequency division multiple access (FDMA) as the channel access technique to serve the ground users [28]. Under this FDMA scheme, we assume

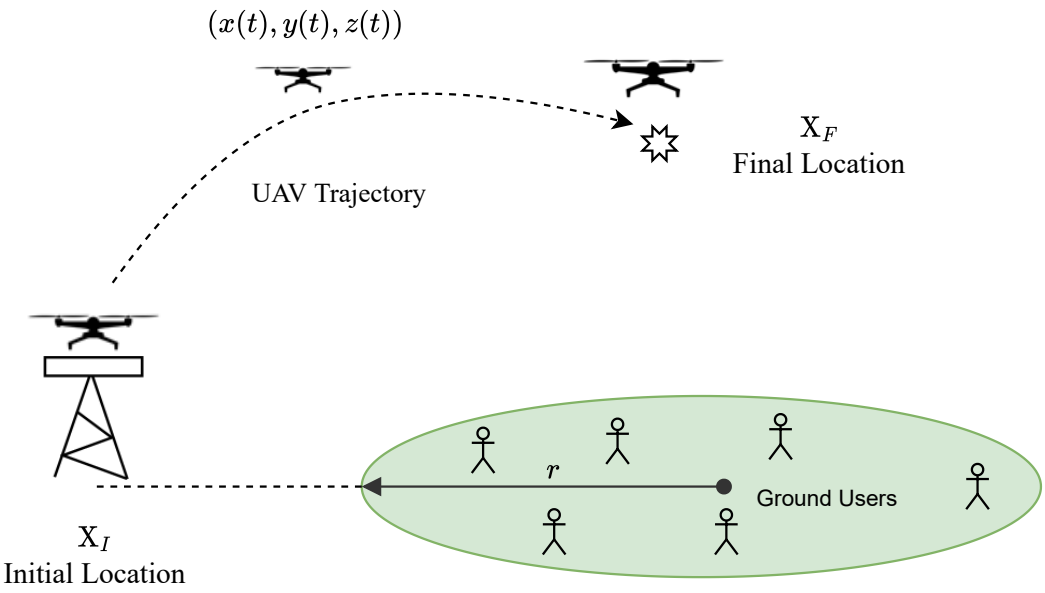

Figure 2.1: System model representing the coverage field having K ground users in a 2D plane along with UAV's initial and final locations.

that the UAV allocates equal channel bandwidth to each mobile ground user to maintain fairness and avoid interference. To serve the ground users, we deploy a single UAV, where the location of the UAV at time t is given as $(x(t), y(t), z(t))$. The UAV is launched from the initial location $\mathbf{X}_I$ with coordinates $(\mathrm{x}^{\mathrm{I}}, \mathrm{y}^{\mathrm{I}}, \mathrm{z}^{\mathrm{I}})$ and moves to the final location $\mathbf{X}_F$ with coordinates $(\mathrm{x}^{\mathrm{F}}, \mathrm{y}^{\mathrm{F}}, \mathrm{z}^{\mathrm{F}})$. Later, in this thesis, when we consider the multiple UAVs, we index the UAVs by $\mathcal{M} \triangleq \{1, \cdots, M\}$, and the location of the m^{th}-UAV is given by $(x_m(t), y_m(t), z_m(t))$. However, we include this notation after Chapter 6, from Chapter 2 to 5, we use $(x(t), y(t), z(t))$ as the UAV trajectory. Furthermore, we assume that the backhaul link provides sufficient capacity and does not pose any constraint on the UAV placement/trajectory design.

For ease of analysis, the total completion time available with the UAV to reach from the initial to the final location is divided into N slots, indexed by $\mathcal{N} = \{0, 1, \cdots, N\}$ and the n^{th}-slot is of duration $\tau[n]$, where $n \in \mathcal{N}$. The time slot duration is chosen such that the distance travelled by the UAV in a time slot is much smaller than the distance between the UAV and the ground users. Then, the UAV location in the n^{th}-time slot is expressed as $(x[n], y[n], z[n])$, where $n = 0$ implies the UAV is at the initial location and $n = N$ implies the UAV is at the final location. We assume that in the n^{th}-time slot, the UAV moves with a fixed acceleration $a[n]$ $(\mathrm{m/s^2})$ and the velocity achieved by the UAV at the end of the n^{th}-time slot is $v[n]$ (m/s). For all quantitative consideration, we consider the location of the UAV at the end of a given time slot to be the UAV location in that

time slot. Similarly, the UAV velocity at the end of the time slot is considered to be the velocity of the UAV in that slot for ease of analysis. This hold when $\tau[n]$ is sufficiently small.

Furthermore along with the UAV mobility model, to ensure a safe flight of the UAV, we also consider some practical mobility constraint which are described as follow. In a UAV-assisted communication system, to avoid obstacles/building, etc., we ensure that the UAV makes lateral movement only when its height is above a minimum threshold height H_{min} *i.e.,* the UAV only makes vertical movement when its height is below H_{min}. Apart from this due to the mechanical constraints, the UAV velocity and acceleration is restricted to a maximum velocity V_{max} and acceleration A_{max} obtainable by the UAV. Moreover, the total time of the UAV to transit from the initial to the final location is also restricted to T_{max}. We also consider that UAV has certain maximum onboard energy E_{max} which is required to remain aloft. Thus, we assume that UAV energy consumption must not exceeds the maximum available onboard energy E_{max}.

2.2 UAV Energy Consumption Model

From [24], we know that the UAV velocity, acceleration, and hence flight time are affected by the limited on-board energy. Thus, to analyze how energy consumption affects the trajectory, we consider the energy consumption model for a rotary-wing UAV. Rotary-wing UAV is considered in our work due to its better hovering features over fixed-wing UAVs [9]. Its energy consumption primarily comprises of propulsion energy consumption, which is required to support its movement and hovering related tasks. In general, UAV energy consumption consists of propulsion energy and communication-related energy. It has been shown in [10] that the communication energy that arises from the communication circuits, signal processing and signal radiation, etc., is far less than the propulsion energy. Therefore, in this work, we mainly focus on propulsion energy. As discussed in [29], the propulsion energy consumption comprises of two components: energy consumption during level-straight flight and energy consumption in vertical flight. Accordingly, the UAV velocity $v[n]$ in a time slot can be decomposed into two components, namely the horizontal and the vertical components denoted by $v^{xy}[n]$, and $v^{z}[n]$, respectively. Similarly, the UAV acceleration $a[n]$ in a time slot can be decomposed into horizontal and vertical components and is given as $a^{xy}[n]$, and $a^{z}[n]$, respectively. In the following subsections, we describe the two energy models, one is the velocity dependent energy consumption model and the other is the velocity-acceleration dependent energy consumption model. These models are

Table 2.1: Energy consumption model parameters

Parameter	Symbol
Profile drag coefficient	δ
Air density (kg/m^3)	ρ
Rotor solidity	ψ
Blade angular velocity (radians/second)	Ω
Rotor disc area (m^2)	A_{en}
Rotor radius (m)	R_{en}
UAV mass (kg)	M_{en}
Incremental correction factor to induced power	K_{en}
UAV weight (Newton)	W_{en}
Fuselage equivalent flat plate area (m^2)	S_{en}
Fuselage drag ratio	D_{en}
Mean rotor induced velocity in hovering	v_o

studied because in some cases, for the purpose of exposition and more tractable analysis, the UAV energy consumption caused by UAV acceleration/de-acceleration is ignored. This is reasonable for some scenarios, where the UAV's manoeuvring time is quite lesser than the UAV's operational time. Under such scenarios, we need to study the velocity dependent energy model. For the other case, we study the velocity-acceleration dependent energy consumption model.

2.2.1 Velocity Dependent Energy Model

In this subsection, we present the velocity-dependent energy consumption model for the rotary-wing model. The terminologies and notations that are used to present the energy model is shown in Table 2.1. By following the derivation from [9], the power required for hovering can be expressed as

$$P_h = \underbrace{\frac{\delta}{8}\rho\psi A_{en}\Omega^3 R_{en}^3}_{P_o} + \underbrace{(1+K_{en})\frac{W_{en}^{3/2}}{\sqrt{2\rho A_{en}}}}_{P_i}, \tag{2.1}$$

where P_o, and P_i are the constants whose values depend upon the value of parameters chosen. Then, the energy model of a rotary-wing UAV as a function of velocity is given as [30, Eq. 11]

$$\begin{aligned} e[n] =& P_o\tau[n]\left(1+\frac{3v^{xy}[n]^2}{\Omega^2 R_{en}^2}\right) + P_i\tau[n]\left(\sqrt{1+\frac{v^{xy}[n]^4}{4v_o^2}}-\frac{v^{xy}[n]^2}{2v_o^4}\right)^{\frac{1}{2}} \\ &+ \frac{1}{2}\tau[n]D_{en}\rho\psi A_{en}v^{xy}[n]^3 + W_{en}v^z[n], \end{aligned} \tag{2.2}$$

where $v^{xy}[n]$ and $v^{z}[n]$ represent the horizontal and vertical component of velocity, respectively, at the n^{th}-time slot, and physical meaning of other parameters are defined in Table 2.1. Then, the energy consumed by the UAV during its flight time is given by

$$e_{tot} = \sum_{n=1}^{N} e[n]. \tag{2.3}$$

2.2.2 Velocity-Acceleration Dependent Energy Model

From the UAV mechanics, we know that the UAVs generate forward thrust when the air is pushed in the direction opposite to flight. The forward thrust is proportional to the mass of the UAV multiplied by the rate of change in velocity (acceleration) of the UAV. To show that the acceleration plays a crucial role in the UAV trajectory design, we present the UAV energy consumption with the variation in acceleration in Figure 2.2. Figure 2.2(a) and Figure 2.2(b) shows the level-straight and vertical flight energy consumption, respectively. From Figure 2.2, it can be observed that as the acceleration increases, the energy consumption significantly increases for a fixed velocity. Therefore, we need to consider the acceleration of the UAV along with the UAV velocity to design a UAV trajectory. The relation between UAV velocity and acceleration is expressed as

$$v^{xy}[n] = \frac{2\|(x[n], y[n]) - (x[n-1], y[n-1])\|}{\tau[n]} - v^{xy}[n-1], \tag{2.4}$$

$$v^{z}[n] = \frac{2(z[n] - z[n-1])}{\tau[n]} - v^{z}[n-1], \tag{2.5}$$

$$a^{xy}[n] = \frac{v^{xy}[n] - v^{xy}[n-1]}{\tau[n]}, \tag{2.6}$$

$$a^{z}[n] = \frac{v^{z}[n] - v^{z}[n-1]}{\tau[n]}, \tag{2.7}$$

where (2.4)−(2.7) represent the kinematic equations to predict the unknown information about the UAV's motion. These equations represent the mathematical relationship between the UAV displacement in the n^{th}-time slot, UAV's velocities at the n^{th} and the $(n-1)^{th}$-time slot, and time duration of n^{th}-time slot for the horizontal and vertical components, respectively. Note that the overall velocity in a time slot is the resultant of the horizontal and vertical component *i.e,* $v[n] = \sqrt{(v^{xy}[n])^2 + (v^{z}[n])^2}$, and similarly, $a[n] = \sqrt{(a^{xy}[n])^2 + (a^{z}[n])^2}$.

Among all the analytical formulations of the propulsion energy consumption models for a rotary-wing UAVs present in the literature [9, 29, 31], we have utilized the most realistic

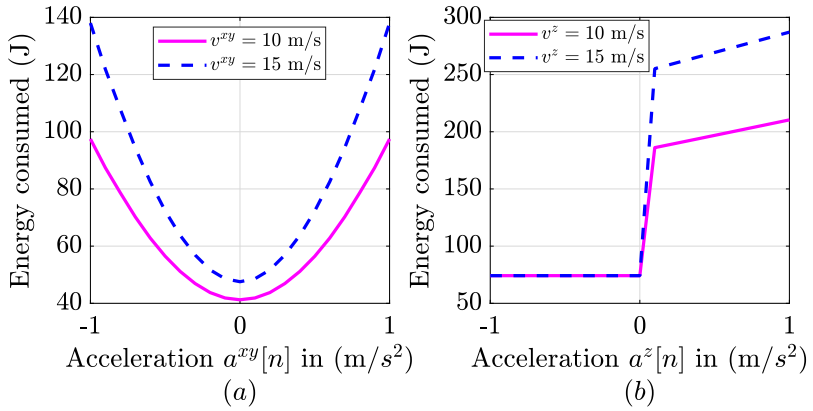

Figure 2.2: Energy consumed with different accelerations for (a) level-straight flight, and (b) vertical flight of UAV.

$$e^{xy}[n] = \tau[n]\Big(P_0(1 + C_1(v^{xy}[n])^2) + P_1\sqrt{1 + (C_2(v^{xy}[n])^2 + C_3 a^{xy}[n]v^{xy}[n])^2)} \cdot\sqrt{\sqrt{1 + (C_2(v^{xy}[n])^2 + C_3 a^{xy}[n]v^{xy}[n])^2 + C_4^2(v^{xy}[n])^4} - C_4(v^{xy}[n])^2} + C_5(v^{xy}[n])^3\Big) \tag{2.8}$$

$$e^{z}[n] = \tau[n]\left(P_2 + \frac{W_{en}v^z[n] + M_{en}a^z[n]v^z[n]}{2} + \frac{W_{en} + M_{en}a^z[n]}{2} \times \sqrt{(v^z[n])^2 + \frac{2(W_{en} + M_{en}a^z[n])}{\rho A_{en}}}\right) \tag{2.9}$$

model that takes into account the UAV velocity, acceleration/deacceleration, and time duration as presented in [29]. Then, as defined in [29], the propulsion energy consumption of a rotary-wing UAV under individual horizontal and vertical components for the n^{th}-time slot is given by $e^{xy}[n]$ in (2.8), and $e^{z}[n]$ in (2.9), respectively. Here, P_o and P_i are the constants as defined in the (2.1). P_2, C_1, C_2, C_3, C_4, and C_5 are the constants whose values depend upon the mechanical parameters of the UAV and is given as

$$P_2 = P_o + K_{en}\frac{W_{en}^{3/2}}{\sqrt{2\rho A_{en}}}, C_1 = \frac{3}{\Omega^2 R_{en}^2}, C_2 = \frac{\rho S_{en}}{2W_{en}}, C_3 = \frac{M_{en}}{W_{en}}, C_4 = \frac{\rho A_{en}}{W_{en}}, C_5 = \frac{1}{2}D_{en}\rho\psi A_{en},$$

where the physical meaning of the parameters are defined in Table 2.1. Then, the total energy consumed by the UAV during its flight time is given by

$$e_{tot} = \sum_{n=1}^{N} e^{xy}[n] + \sum_{n=1}^{N} e^{z}[n]. \tag{2.10}$$

Next, we present the channel model for the A2G communication.

2.3 A2G Channel Model

Although UAVs has the ability to adjust altitude to maintain a LoS communication link, in some instances, the A2G link is more prone to blockage due to the presence of obstacles and buildings, such as in the urban environment. Therefore, it is necessary to consider the channel model, including the LoS and NLoS links. This work considers a realistic probabilistic LoS channel model wherein the LoS and NLoS links have a certain occurrence probability [23]. Then, the path loss for LoS and NLoS links are expressed as

$$L_k[n] = \begin{cases} d_0 d_k[n]^{-\bar{\alpha}}, \text{ for LoS link, and} \\ \kappa d_0 d_k[n]^{-\bar{\alpha}}, \text{ for NLoS link,} \end{cases} \tag{2.11}$$

where d_0 represents the path loss at a reference distance of 1 meter (m), $\bar{\alpha}$ represents the path loss exponent, and $\kappa < 1$ accounts for additional attenuation factor due to NLoS component and $d_k[n]$ represents the distance between the k^{th}-user and the UAV, given by $d_k[n] = \sqrt{(x[n]-x_k)^2 + (y[n]-y_k)^2 + z[n]^2}$. The probability that the k^{th}-user is in LoS with the UAV at time slot n is represented as a logistic function of elevation angle [32] and is given by

$$P_k^L[n] = \frac{1}{(1 + C\exp(-D[\phi_k[n] - C]))}, \tag{2.12}$$

where C and D are parameters depending on environment, such as rural, sub-urban and urban. $\phi_k[n]$ (in degrees) is the elevation angle of UAV from the k^{th}-user at time slot n given as $\phi_k[n] = \frac{180}{\pi}\sin^{-1}\left(\frac{z[n]}{d_k[n]}\right)$.

The average path loss $h_k[n]$ between the UAV and the k^{th}-user at time slot n is expressed as

$$\begin{aligned} h_k[n] &= P_k^L[n] d_0 d_k[n]^{-\bar{\alpha}} + (1 - P_k^L[n])\kappa d_0 d_k[n]^{-\bar{\alpha}} \\ &= d_0 \frac{(1-\kappa)P_k^L[n] + \kappa}{((x[n]-x_k)^2 + (y[n]-y_k)^2 + z[n]^2)^{\alpha}}, \end{aligned} \tag{2.13}$$

where $\alpha = \frac{\bar{\alpha}}{2}$.

The above pathloss $h_k[n]$ is considered in the subsequent chapters to derive the performance metric, such as outage probability and throughput.

Chapter 3

UAV Trajectory Design: Fixed Initial to Optimized Final Location

3.1 Introduction

Deploying a UAV as an ABS is a promising technology that enables service connectivity in areas where the terrestrial BS is insufficient to provide service to ground users or is under maintenance. For example, in remote areas, crowded areas, and areas affected by disasters or emergencies. In such scenarios, we need to compute the optimal deployment location of the UAV in 3D space where high-quality service to the ground user is ensured. Thereafter, we need to design the path of the UAV to reach the optimal deployment location. Thus, in this chapter, we address the problem of UAV deployment and trajectory design in 3D space to provide on-demand coverage to ground users such that their sum rate is maximized.

We first find the optimal UAV location in 3D space where the sum rate is maximized for all ground users. Thereafter an optimal trajectory is designed for the UAV to travel from the initial to the optimal location, such that the overall average sum rate during the flight is maximized while meeting the onboard energy availability and flight duration constraints. The problem formulated is non-convex. To obtain the optimal location, we approximate the rate expression to obtain the concave regions and apply alternating optimization. An iterative scheme is proposed to obtain the optimal UAV trajectory, which computes the optimal location in each time slot sequentially, followed by a greedy approach to reach the final location. Simulation results provide useful insights into the optimal location and the UAV trajectory problem and show on an average 16.5% improvement over the benchmark schemes.

This scenario is very relevant to many practical applications where the deployment location is unknown and is based on ground users' location, such as providing high-speed connectivity to the first responders in emergencies, offloading traffic in a high-density area, such as football stadiums, or recovering the service in a disaster-affected areas.

3.1.1 State-of-the-Art

Performance enhancement in the UAV-assisted communication system has been an active area of research in recent years. We broadly classify the state-of-the-art into two objectives: UAV deployment and UAV trajectory design for performance enhancement.

UAV deployment

From the UAV deployment perspective, researchers have focused on finding the optimal UAV placement, where the UAVs act as an aerial quasi-static BS to support ground users in a given area [33, 34, 32, 35, 36]. Thus, the altitude and horizontal locations of the UAV are optimized either independently or jointly based on different QoS requirements of the users. In particular, [32] optimized the UAV altitude to provide maximum coverage to the ground users. In contrast, the UAV horizontal location was optimized in [35] by fixing the UAV altitude to minimize the number of UAVs required to provide coverage in a given area. In 3D space, the problem of a drone-enabled small cell placement optimization was explored in [36] to maximize the number of users to be served. Similarly, in [37], and [38], a drone placement for maximizing the number of users served was considered in the presence of minimum rate requirement for each user.

Some works [39, 40, 41] focused on UAV deployment with an objective to maximize throughput. The authors in [39] maximized the communication rate by optimizing the UAV's flying altitude and antenna beamwidth. In [40], the authors maximized the achievable sum rate in the presence of a constant-modulus constraint for the beamforming vector in millimeter-wave communications. However, in their work, the authors fixed the altitude of the UAV. The multi-UAV deployment problem was investigated in [41] by maximizing the minimum rate for all ground users while assuming the channel to be dominated by LoS links.

UAV Trajectory Design

Some researchers have focused on UAV trajectory design for maximizing the throughput of the system under different scenarios. The authors in [42] maximized the minimum throughput over the ground users by optimizing the UAV trajectory over a finite time horizon. However, in their model, they assumed that the UAV flew only at a fixed altitude. In [43], the authors maximized the throughput of a UAV relay system by optimizing the UAV trajectory and transmit power considering the mobility constraints. The throughput was also maximized for UAV-enabled multi-user downlink communication

in [44]. The authors in [45] maximized the total system capacity by jointly optimizing the UAV trajectory, user scheduling, and transmission power. They assumed the LoS dominant scenario where a full-duplex UAV-BS was employed to serve the targeted small cell users from a fixed altitude. In [46], the sum rate was maximized by optimizing the UAV trajectory at the edge of multiple cells. Moreover, the authors in [47] optimized the 3D UAV trajectory to minimize the average outage probability over all users by considering the probabilistic LoS channel model.

In the above works [42, 43, 44, 45, 46, 48], the energy consumption in UAV was not considered. The significance of UAV on-board energy was first emphasized in [20]. Because of the limited availability of on-board energy, it must be used as efficiently as possible. To establish a relationship between the propulsion energy and the UAV flight status, the authors in [10] first proposed a mathematical propulsion energy model for a fixed-wing UAV. Subsequently, a propulsion model for a rotary-wing UAV was proposed in [9]. For both the UAVs, it was shown that the UAV propulsion energy consumption is a function of velocity as well as the acceleration of the UAV. The authors in [10] studied energy-efficient communication and optimized the UAV trajectory. In addition, they assumed that the UAV flew at a fixed altitude and considered a simple path loss channel model. Transmit power, user scheduling, UAV trajectory, and bandwidth allocation were jointly optimized in [49] to maximize the energy efficiency while satisfying the user quality-of-experience requirements. Similarly, [50], and [30] jointly optimized the resource allocation and UAV trajectory to maximize energy efficiency, where the former considered the UAV to fly in a circular path while the latter considered the fuel-powered UAV.

In practice, the UAV-assisted communication system is constrained by not only the on-board energy but also via the mission completion time [22]. Towards this end, the authors in [51], presented energy versus flight duration tradeoff for meeting a required minimum rate. They optimized the UAV trajectory by considering the free-space path loss model. On the other hand, the authors in [52] considered the energy budget constraints of the UAV and rate constraint for each device to minimize the mission completion time via optimizing the UAV 2D trajectory and transmit power. Moreover, [53], and [54] considered the propulsion energy consumption of a fixed-wing UAV as a constraint to optimize the UAV trajectory when flying at a fixed altitude while considering the LoS channel for UAV-user link. In particular, [53], and [54] formulated a max-min average sum rate problem and maximized the achievable sum rate of the ground user, respectively. Additionally, rotary-wing UAV has been considered in [55] to maximize the number of

users served.

Similarly, in [10], [9] and [56], energy efficiency was maximized while including a rate constraint to the optimization problem. The authors in [57] considered the energy efficiency and throughput jointly while designing the UAV trajectory over a finite flight time. However, they assumed the UAV to be flying at a fixed altitude.

3.1.2 Contributions and Organization

Towards this direction, our current work bridges the gap in the existing literature by finding first, an optimal deployment location for UAV in 3D space where the sum rate over all ground users is maximized while considering a realistic UAV-user channel model. Thereafter, we obtain an optimal 3D UAV trajectory from the initial to the final location in a time bounded fashion while ensuring on-board energy availability to maximize the sum rate of the users. The current work considers a practical communication setup, where the channel is modelled having LoS and NLoS components [23]. To the author's knowledge, there is no work reported on enhancing the sum rate of the system by optimizing the UAV trajectory in the presence of on-board energy and flight duration constraints. Our current setup can also be applied to UAV-assisted mm-wave communication systems, first responders, hotspot areas, etc.

The key contributions of this chapter are as follows:

- Firstly, we formulate a 3D deployment problem that computes the optimal location for UAV deployment in 3D space by maximizing the sum rate over all users. Secondly, we formulate a trajectory optimization problem that finds an optimal UAV path from the initial to the final location by maximizing the sum rate averaged over time in the presence of on-board energy and flight duration constraints.

- The 3D deployment problem is non-convex and NP-hard. Thus, a closed-form approximation of rate expression is provided, and conditional concavity is explored to obtain the optimal location for the 3D deployment problem.

- An efficient algorithm is proposed to obtain the sub-optimal solution for the trajectory optimization problem. The sub-optimal solution is obtained sequentially by searching for the optimal location in each time slot using the steepest ascent method.

- Finally, numerical results provide useful insights into the optimal deployment location and the UAV trajectory. Firstly, the effectiveness of the proposed approach

to obtain the optimal location is shown. Secondly, the performance of the sub-optimal trajectory is explored. Our proposed scheme provides on an average 16.5% improvement over the benchmark schemes.

The remaining part of this chapter is organized as follows. System model and problem definition are described in Section 3.2 and 3.3, respectively. Sections 3.4 and 3.5 present the methodology adopted to solve the UAV location and trajectory problem, respectively. Numerical results are provided in Section 3.6. The chapter is concluded in Section 3.7.

3.2 System Model

3.2.1 Communication Setup

As shown in Figure 2.1 in Chapter 2, a downlink communication setup is considered, where the UAV serves the K ground users. To serve the users, we deploy a single UAV that starts from a pre-defined initial location $\mathbf{X}_I$ $(\mathrm{x^I}, \mathrm{y^I}, \mathrm{z^I})$ and moves to an optimal final location. The final location is the location of the UAV in 3D space where the sum rate over all ground users is maximum. In this chapter, we assume that the UAV flies with a fixed velocity V m/s. The time dependent distance between the UAV and the k^{th}-user at the n^{th}-time slot is given by $d_k[n] = \sqrt{(x[n]-x_k)^2 + (y[n]-y_k)^2 + z[n]^2}$.

3.2.2 Performance Metric

We consider a probabilistic LoS channel model, whose average path loss $h_k[n]$ expression is given in Chapter 2, equation 2.13. Let P_{tr} denote the UAV transmit power. The achievable rate in bits/second (bps) between the UAV and the k^{th}-user is given by [9, Eq. 10],

$$R_k[n] = \frac{B}{K}\log_2\left(1 + \frac{P_{tr}h_k[n]}{\sigma^2}\right), \tag{3.1}$$

where B denotes the total channel bandwidth available to the UAV, and σ^2 is the channel noise power at the receiver. Substituting (2.13) in (3.1), we get

$$R_k[n] = \frac{B}{K}\log_2\left(1 + \frac{\tilde{\gamma}_o \widehat{P}_k^L[n]}{((x[n]-x_k)^2 + (y[n]-y_k)^2 + z[n]^2)^{\alpha}}\right), \tag{3.2}$$

where $\tilde{\gamma}_o \triangleq P_{tr}d_0/\sigma^2$, $\widehat{P}_k^L[n] = (1-\kappa)P_k^L[n] + \kappa$ and $\alpha \triangleq \bar{\alpha}/2$.

3.3 Problem Formulation

Our objective in this chapter is to provide on-demand coverage to the ground users by optimizing the UAV trajectory and deploying it at an optimal location in 3D space. To begin with, we decouple our objective into two problems:

Problem 1: Given a circular field with K users, what is the optimal location in 3D space where the UAV should be deployed to maximize the sum rate capacity?

Problem 2: Given the UAV initial and final locations, what should be the UAV trajectory to maximize the sum rate averaged over time in the presence of on-board energy and flight duration constraints?

We begin by defining *Problem 1* and *Problem 2* mathematically. For *Problem 1*, we formulate a sum rate maximization problem to obtain the optimal location as

$$\text{(P1)}: \quad \max_{\{x,y,z\}} \quad Q \triangleq \sum_{k=1}^{K} R_k$$

$$\text{subject to (s.t.)}: \; -r \leq x, y \leq r, \tag{3.3a}$$

$$H_{min} \leq z \leq H_{max}, \tag{3.3b}$$

where H_{min} is the minimum height required by the UAV to avoid ground obstacles and make horizontal movements, and H_{max} is the maximum height achievable by the UAV. Note that we omit [n] in calculation of R_k in (3.2). Since all the users are present in the circular field of radius r centered at the origin, then it can be easily interpreted that the optimal values of x and y will also lie in the circular field. Therefore, we restrict the search space of x and y to the radius of circular field *i.e.,* $-r \leq x, y \leq r$.

We treat the optimal location $\mathcal{X}^* = (x^*, y^*, z^*)$ obtained from (P1) to be the final location where the UAV will be deployed to provide service to the users. Thus, in *Problem 2*, we obtain an optimal UAV trajectory in flying from the initial location $(\mathrm{x^I}, \mathrm{y^I}, \mathrm{z^I})$ to the final location $\mathcal{X}^*$ in the presence of energy and flight durations constraints. *Problem 2* is formulated as follows

$$\text{(P2)}: \quad \max_{\substack{N,\{x[n],y[n],z[n]\} \\ \forall\, n\in\{1,\cdots,N\}}} \quad \frac{1}{N}\sum_{n=1}^{N}\sum_{k=1}^{K} R_k[n]$$

$$\text{s.t. } (C1) : (x[N], y[N], z[N]) = (x^*, y^*, z^*), \tag{3.4a}$$

$$(C2) : z[n] \geq H_{min}, \forall n \in \{1, \cdots, N-1\}, \tag{3.4b}$$

$$(C3) : \|(x[n], y[n], z[n]) - (x[n-1], y[n-1], z[n-1])\| = \tau V, \forall n \in \{1, \cdots, N-1\}, \tag{3.4c}$$

$$(C4) : \|(x^*, y^*, z^*) - (x[N-1], y[N-1], z[N-1])\| \leq \tau V, \tag{3.4d}$$

$$(C5) : N \leq \min\left\{\frac{E_{max}}{\mathcal{E}}, N_{av}\right\}, \tag{3.4e}$$

where $R_k[n]$ is defined in (3.2). Constraint (3.4a) represents the final location constraint, (3.4b) represents the minimum altitude required by the UAV to avoid obstacles. Constraint (3.4c) represents the distance travelled by the UAV in a particular time slot, where for $n = 1$, $(x[0], y[0], z[0]) = (\mathrm{x^I}, \mathrm{y^I}, \mathrm{z^I})$. Similarly, (3.4d) represents the distance travelled in the final time slot. N_{av} in (3.4e) represents the maximum number of time slots a UAV can take to reach the final location. E_{max} represents the total on-board energy available with the UAV. Since the energy consumed by the UAV $\mathcal{E}$ is fixed due to fixed UAV velocity, the ratio $E_{max}/\mathcal{E}$ gives the number of time slots the UAV can fly before exhausting its on-board energy E_{max}. Thus, according to the constraint (3.4e), the UAV can at most consume the time slots out of N_{av} or $E_{max}/\mathcal{E}$, whichever is minimum. To ensure that the UAV reaches the final location without exhausting its resources, velocity V should be greater than the minimum velocity required by the UAV to reach the final location via straight-line path *i.e.,* $V \geq \frac{\|(x^*,y^*,z^*)-(\mathrm{x^I},\mathrm{y^I},\mathrm{z^I})\|}{\min\left(\frac{E_{max}}{\mathcal{E}},N_{av}\right)}$. Both problems (P1) and (P2) are non-convex due to the presence of non-concave objective function. Therefore, for *Problem 1*, we find the optimal location in 3D space by using alternating maximization that uses a combination of golden section search (GSS) and linear search as discussed in Section 3.4. For *Problem 2*, we propose an iterative scheme that successively searches for optimal location in each time slot, as discussed in Section 3.5.

3.4 Computation of Optimized Final Location

In this section, we obtain the solution to the problem (P1). R_k defined in (3.2) is a function of not only the distance between the UAV and the k^{th}-user but also $\widehat{P}_k^L[n]$, which makes R_k difficult to handle. R_k defined in (3.2) is a non-concave function, hence it is difficult to obtain the optimal solution of (P1). Exhaustive search (ES) can be used to obtain the

global solution, albeit with high computational complexity.

From the problem (P1), we analyzed that for specific ranges of x, y, and z, the function is concave if the variable $(x, y, \text{or}\, z)$ is taken individually. Note that it remains non-concave if the variables are considered jointly. Thus to have a faster solution, we exploit this unique feature of the objective function in the next sub-section to find the concave regions. We break the domain of the function under individual variable (x, y, or z) into two parts, concave and non-concave. In the concave region, we can apply faster search algorithms like GSS [58], whereas in the non-concave region, we can use linear search to find the maxima in the specified interval.

GSS is an effective search technique to find the maxima in a specified interval, where the function is concave (or unimodal). It operates by successively narrowing the search range of maxima over the specified interval. In particular, in each iteration, it reduces the search region by a fraction of 0.618 (golden ratio) than the previous iteration. On the other hand, linear search sequentially obtains the value of the objective function at each point spaced ϵ-apart and computes the maxima. Thereafter we use an alternating maximization to solve (P1) where the objective function over individual variable is maximized using GSS in the concave region and linear search in the non-concave region.

In general, it is difficult to evaluate the closed-form expression for the region where the sum rate $Q \triangleq \sum_{k=1}^{K} R_k$ is concave. Thus, to get analytical insights on the concavity, we approximate the sigmoidal function in $\widehat{P}_k^L[n]$ described in (2.12) and (2.13) to obtain a closed-form approximation for the concave region in Q. Thereafter, for maximization over the concave domain in a single variable, GSS is used, which reduces the computations significantly.

3.4.1 Approximation and Concave Regions

We provide an approximation to the sigmoidal function defined in the expression of R_k. We propose two approximations to R_k, namely step and linear approximation as discussed below.

Step Approximation

For higher values of D, *i.e.,* $D \gg 1$ and sufficient UAV height in (2.12), $P_k^L[n]$ tends to one *i.e.,* $P_k^L[n] \approx 1, \forall k \in \mathcal{K}$. The approximate R_k is given as

$$\widetilde{R}_k^S = \frac{B}{K} \log_2 \left(1 + \frac{\tilde{\gamma}_o}{((x - x_k)^2 + (y - y_k)^2 + z^2)^{\alpha}} \right). \tag{3.5}$$

$\widetilde{R}_k^S$ defined above is still a non-concave function of x, y, and z. However, we can obtain the domain over which the function is concave in x, y, and z individually. Next, we present a lemma to find the region of concavity.

Lemma 1. *The region over which* $\widetilde{Q}^S \triangleq \sum_{k=1}^{K} \widetilde{R}_k^S$ *is individually concave in* x*,* y*, and* z *is given by* $\mathcal{R}_x^S = \bigcap_{k=1}^{K} \mathcal{R}_{xs}^k, \mathcal{R}_y^S = \bigcap_{k=1}^{K} \mathcal{R}_{ys}^k$*, and* $\mathcal{R}_z^S = \bigcap_{k=1}^{K} \mathcal{R}_{zs}^k$ *as defined in* (A.1.7)*, where* $\widetilde{R}_k^S$ *is defined in* (3.5)*.*

Proof. See Appendix A.1.1. □

Linear Approximation

If the value of D is small, *i.e.,* $D \ll 1$ in (2.12), then the sigmoidal function in (2.12) can be approximated as $\frac{z}{\sqrt{(x-x_k)^2+(y-y_k)^2+z^2}}$. Then, R_k defined in (3.2) is approximated as

$$\widetilde{R}_k^L = \frac{B}{K} \log_2 \left(1 + \tilde{\gamma}_o \frac{\frac{(1-\kappa)z}{\sqrt{(x-x_k)^2+(y-y_k)^2+z^2}} + \kappa}{((x-x_k)^2 + (y-y_k)^2 + z^2)^{\alpha}} \right). \tag{3.6}$$

Again, $\widetilde{R}_k^L$ in (3.6) is non-concave with respect to x, y, and z. Next, we present a lemma to find the region of individual concavity of $\widetilde{Q}^L \triangleq \sum_{k=1}^{K} \widetilde{R}_k^L$ in x, y, and z.

Lemma 2. $\widetilde{Q}^L \triangleq \sum_{k=1}^{K} \widetilde{R}_k^L$ *defined above is individually concave with respect to* x*,* y*, and* z *in the region defined by* $\mathcal{R}_x^L = \bigcap_{k=1}^{K} \mathcal{R}_{xl}^k, \mathcal{R}_y^L = \bigcap_{k=1}^{K} \mathcal{R}_{yl}^k$*, and* $\mathcal{R}_z^L = \bigcap_{k=1}^{K} \mathcal{R}_{zl}^k$ *as defined in* (A.1.14)*, respectively.*

Proof. See Appendix A.1.2. □

From Lemmas 1 and 2, we obtained the regions where $\widetilde{Q}$ is concave in x, y, and z, individually, using step or linear approximations, respectively. Note that $\widetilde{Q} = \widetilde{Q}^S$ if $D \gg 1$ and $\widetilde{Q} = \widetilde{Q}^L$ if $D \ll 1$.

The advantage of using the step and linear approximation is used to get the analytical insights on R_k. It reduces the computational complexity to obtain maxima by finding the concave regions. It is observed that, for $D \gg 1$ in (2), the $P_k^L[n] \approx 1, \forall k \in \mathcal{K}$. This implies for environments like rural areas or when the UAV is present at high altitude such that there always exists a LoS link between the UAV and the users, the R_k can be approximated using step function to R_k^S. Linear approximation, on the other hand, is ideal for dense environments or low-altitude UAVs since $P_k^L[n]$ becomes a linear function of the elevation angle $\phi_k[n]$. Hence, the use of approximation depends upon the type of environment and the ability to maintain LoS links with the UAV.

3.4.2 Solution using Alternating Optimization

Alternating optimization is employed to obtain a sub-optimal solution of (P1). In alternating optimization, the function is maximized over a single variable successively, and the algorithm iterates to obtain a sub-optimal solution. While optimizing the function over a single variable x, y or z, the domain of the function is divided into two parts: concave and non-concave. Over the concave region, GSS is used, while in the non-concave region, linear search is employed. The individually concave regions are defined as $\mathcal{R}_\psi$, $\psi \in \{x, y, z\}$ that are obtained either using the step or linear approximation. Let $\mathcal{B}_x$, $\mathcal{B}_y$, and $\mathcal{B}_z$ be the region spanned by $-r \leq x \leq r$, $-r \leq y \leq r$, and $H_{min} \leq z \leq H_{max}$ for x, y, and z, respectively. Then, the non-concave regions are given by $\mathcal{B}_\psi \backslash \mathcal{R}_\psi$.

The algorithm repetitively gives the alternating individual optimization sequence of x^*, y^* and z^* at the l^{th} iteration. Q_k is the sum rate at the l^{th}-iteration. The algorithm iterates until $Q_l - Q_{l-1} \geq \epsilon$, where ϵ is the acceptable tolerance threshold. In each alternating maximization subproblem, we obtain two solutions, one corresponding to the GSS applied over the concave region and the second corresponding to the linear search over the non-concave region. The best among the two is chosen as the solution to the alternating optimization subproblem. The steps to obtain the sub-optimal solution of (P1) are presented in Algorithm 1. Later, in the numerical section, it is observed that the sub-optimal solution obtained by using this low complexity algorithm is very close to the globally optimal solution obtained using ES. The solution obtained for (P1) is named as $\mathcal{X}^* = (x^*, y^*, z^*)$.

3.4.3 Convergence and Complexity

Since (P1) is a non-convex problem, we used alternating optimization to obtain the deployment location of UAV by applying GSS in the concave region and linear search in the non-concave region. The number of iterations involved in the convergence of alternating optimization is as follows. In each iteration for concave region, the search space $\Delta x = (x^{ub} - x^{lb})$, $\Delta y = (y^{ub} - y^{lb})$, and $\Delta z = (z^{ub} - z^{lb})$ reduces by a factor of 0.618 [58]. ψ^{ub} and ψ^{lb} denote the upper and lower bound of the concave region in the search space, respectively, that are computed either by using (A.1.7) or (A.1.14), where $\psi \in \{x, y, z\}$. Let $L_\psi = \frac{\psi^{ub} - \psi^{lb}}{\epsilon}$, $\psi \in \{x, y, z\}$, denote the number of computations required to find the maximum sum rate in ψ in the non-concave region. Then, the average iterations are given by $L_{itr} = 2L_p \left(\ln\left(\frac{\Delta x}{\epsilon}\right) + \ln\left(\frac{\Delta y}{\epsilon}\right) + \ln\left(\frac{\Delta z}{\epsilon}\right) + L_x + L_y + L_z \right)$, where L_p denotes the number of executions of the main loop in Algorithm 1. The term in

Algorithm 1 Alternating optimization to obtain sub-optimal solution of (P1)

Input: r, H_{min}, H_{max}, $\mathcal{B}_x$, $\mathcal{B}_y$, $\mathcal{B}_z$, N, $(x_k, y_k), \forall k \in \mathcal{K}$ and ϵ.
Output: Q^* along with $\mathcal{X}^* = (x^*, y^*, z^*)$.
1: Initialize $k = 1$, $y = -r$, $z = H_{min}$, $Q_0 = 0$, and $Q_1 = 0.1$.
2: Calculate $\mathcal{R}_x$, $\mathcal{R}_y$, and $\mathcal{R}_z$, obtained either by step or linear approximation using (A.1.7) or (A.1.14), respectively.
3: **while** $Q_l - Q_{l-1} \geq \epsilon$ **do**
4: $l = l + 1$.
5: **for** $\psi \in \{x, y, z\}$ **do**
6: For $\mathcal{R}_\psi$, compute $\psi_1^* = arg \max_{\psi} Q \triangleq \sum_{k=1}^{K} R_k$, using GSS within acceptable tolerance ϵ.
7: Evaluate $\psi_2^* = arg \max_{\psi} Q$, through linear search with step size ϵ by varying ψ over the region $\mathcal{B}_\psi \backslash \mathcal{R}_\psi$.
8: Find $\psi^* = arg \max_{\{\psi_j^*\}} Q$ for $j \in \{1, 2\}$.
9: Substitute $\psi = \psi^*$ in Q.
10: Set $Q_l = Q$.
11: Set $Q^* = Q_l$.

parenthesis are the number of iterations involved to obtain the optimal value for each variable in concave and non-concave region. The worst-case number of iterations of (P1) in alternating optimization when no concave regions are found is $L_{itr} = L_p(L_x + L_y + L_z)$.

Whereas using ES, the total number of computations taken to find the optimal location with maximum sum rate is $L_x L_y L_z$.

3.5 UAV Trajectory Design towards Optimized Final Location

3.5.1 Mathematical Analysis

In this section, we find the optimal trajectory of the UAV in travelling from initial to final location by solving (P2), where final location corresponds to $\mathcal{X}^*$ obtained by solving (P1) in the previous section. In problem (P2), constraint (3.4b) states that the UAV height is always above the minimum height H_{min} to avoid obstacles, *i.e.,* $z[n] \geq H_{min}$, $\forall n \in \{1, \cdots, N-1\}$. If the UAV initial height $\mathrm{z^I}$ is less than $(H_{min} - \tau V)$, then the UAV cannot attain a minimum height H_{min} in a time slot. In such a case, we assume that the UAV only makes vertical movement in z-direction until it attains a height $\bar{z}_\mathrm{I} \geq H_{min} - \tau V$. The number of time slots required to reach the location $(\mathrm{x^I}, \mathrm{y^I}, \bar{z}_\mathrm{I})$ that satisfies $\bar{z}_\mathrm{I} \geq H_{min} - \tau V$ is given by $S_h = \left\lfloor \frac{H_{min} - \mathrm{z^I}}{\tau V} \right\rfloor$ and $\bar{z}_\mathrm{I}$ is given as $\bar{z}_\mathrm{I} = \mathrm{z^I} + \tau S_h V$. Energy consumed in travelling from $(\mathrm{x^I}, \mathrm{y^I}, \mathrm{z^I})$ to $(\mathrm{x^I}, \mathrm{y^I}, \bar{z}_\mathrm{I})$ is given by $\mathcal{E}_I = S_h \mathcal{E}$. Therefore, when the UAV height is less than H_{min}, the UAV is constrained to move vertically in

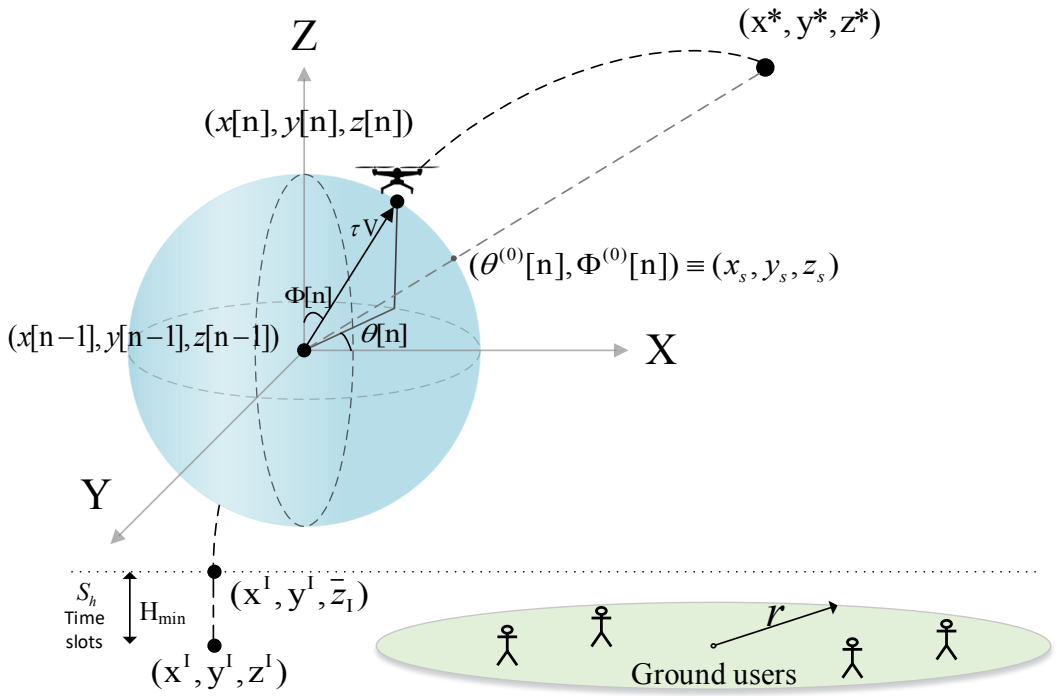

Figure 3.1: Proposed scheme to obtain the optimal trajectory for problem (P3).

z-direction to reach $(\mathrm{x}^{\mathrm{I}}, \mathrm{y}^{\mathrm{I}}, \bar{z}_{\mathrm{I}})$. Thereafter, we re-frame the problem (P2) to optimize the UAV trajectory in travelling from $(\mathrm{x}^{\mathrm{I}}, \mathrm{y}^{\mathrm{I}}, \bar{z}_{\mathrm{I}})$ to the deployment location by adjusting the energy availability and time elapsed in going from the initial to $(\mathrm{x}^{\mathrm{I}}, \mathrm{y}^{\mathrm{I}}, \bar{z}_{\mathrm{I}})$ as follows

$$(\mathrm{P3}): \max_{\substack{N,\{x[n],y[n],z[n]\} \\ \forall\, n\in\{S_h+1,\cdots,N\}}} \quad Q_{avg} \triangleq \frac{1}{N}\sum_{n=S_h+1}^{N}\sum_{k=1}^{K} R_k[n] \tag{3.7a}$$

$$\text{s.t. (3.4a), (3.4d),} \tag{3.7b}$$

$$z[n] \geq H_{min}, \forall n \in \{S_h+1, \cdots, N-1\}, \tag{3.7c}$$

$$\|(x[n], y[n], z[n]) - (x[n-1], y[n-1], z[n-1])\| = \tau V, \forall n \in \{S_h+1, \cdots, N-1\}, \tag{3.7d}$$

$$N - S_h \leq \min\left\{\frac{E_{max} - \mathcal{E}_I}{\mathcal{E}}, N_{av} - S_h\right\}. \tag{3.7e}$$

Constraint (3.7e) represents the total time slots available with the UAV (*i.e.,* N time slots) in travelling from the initial to the final location while accounting for the initial S_h time slots utilized in vertical take-off. $\frac{E_{max}-\mathcal{E}_I}{\mathcal{E}}$ denotes the available time slots as per the on-board energy availability after reaching $(\mathrm{x}^{\mathrm{I}}, \mathrm{y}^{\mathrm{I}}, \bar{z}_{\mathrm{I}})$. $N_{av} - S_h$ denotes the remaining time slots to reach the final location. Then, according to (3.7e), the UAV can at most consume the time slots out of $\frac{E_{max}-\mathcal{E}_I}{\mathcal{E}}$ or $N_{av} - S_h$, whichever is minimum.

3.5.2 Algorithm Design

Problem (P3) is still a non-convex problem due to the presence of non-concave function $R_k[n]$. Therefore, to solve (P3), we propose an iterative scheme that searches for the best location in each time slot sequentially to reach the final location. A UAV flying with velocity V can reach a distance of τV in a time slot. Therefore, the search space for a new location in time slot n is a sphere of radius τV, centered at the previous time slot location, *i.e.,* $(n-1)^{th}$-time slot location $(x[n-1], y[n-1], z[n-1])$. This procedure is repeated for every time slot until the final location is reached. Figure 3.1 presents the proposed scheme to solve (P3).

For ease of analysis, we switch to spherical coordinate system. A point in spherical coordinate system is defined by the azimuth Φ and polar angle θ from the origin. Thus, instead of directly computing the UAV location for the n^{th}-time slot, we find the value of $\Phi[n]$ and $\theta[n]$ from the $(n-1)^{th}$ location. Origin in our case is considered to be the $(n-1)^{th}$-time slot location *i.e.,* $(x[n-1], y[n-1], z[n-1])$. Thereafter, we convert the spherical coordinates to Cartesian coordinates to obtain the UAV location using

$$\begin{aligned} x[n] &= x[n-1] + \tau V \sin\Phi[n]\cos\theta[n], \\ y[n] &= y[n-1] + \tau V \sin\Phi[n]\sin\theta[n], \quad \text{and} \\ z[n] &= z[n-1] + \tau V \cos\Phi[n]. \end{aligned} \tag{3.8}$$

Substituting (3.8) in (3.2), $R_k[n]$ in terms of $\theta[n]$ and $\Phi[n]$ is expressed as

$$R_k[n] = \frac{B}{K}\log_2\left(1 + \tilde{\gamma}_o \frac{\frac{1-\kappa}{1+Ce^{-D\left(\frac{180}{\pi}\sin^{-1}\left[\frac{\tau V\cos\Phi[n]}{\sqrt{l_k[n]}}\right]-C\right)}} + \kappa}{(l_k[n])^{\alpha}}\right), \tag{3.9}$$

where $l_k[n] = (x[n-1]+\tau V\sin\Phi[n]\cos\theta[n]-x_k)^2 + (y[n-1]+\tau V\sin\Phi[n]\sin\theta[n]-y_k)^2 + (z[n-1]+\tau V\cos\Phi[n])^2$.

In each time slot, the UAV moves to the best location where the sum rate $\widehat{R}_G(\theta[n], \Phi[n])$ is maximum. Sum rate in time slot n is defined as

$$\widehat{R}_G(\theta[n], \Phi[n]) \triangleq \sum_{k=1}^{K} R_k[n], \tag{3.10}$$

where $R_k[n]$ is defined in (3.9). Since (3.10) is non-concave, obtaining a trajectory when travelling towards the optimal location in each time slot sequentially does not ensure

Algorithm 2 Steepest ascent algorithm to compute the trajectory

Input: S_h, β, $(x_k, y_k)\ \forall k \in \mathcal{K}$, τ, V, ϵ, $(\mathrm{x^I}, \mathrm{y^I}, \bar{z}_\mathrm{I})$ and $\mathcal{X}^*$.
Output: $x^*[n]$, $y^*[n]$, $z^*[n]$, $\forall n \in \{S_h + 1, \cdots, N_{av}\}$ and $N^* = N_{av}$.

for $n = S_h + 1$ to β **do**
  Make a sphere of radius τV from $(x[n-1], y[n-1], z[n-1])$, and a line segment joining the $(x[n-1], y[n-1], z[n-1])$ and $\mathcal{X}^*$. Denote the intersection point between $(x[n-1], y[n-1], z[n-1])$ and $\mathcal{X}^*$ as (x_s, y_s, z_s).
  Evaluate $\theta^{(0)}[n] = \tan^{-1}\left(\frac{y_s - y[n-1]}{x_s - x[n-1]}\right)$ and $\Phi^{(0)}[n] = \tan^{-1}\left(\frac{\sqrt{(x_s - x[n-1])^2 + (y_s - y[n-1])^2}}{z_s - z[n-1]}\right)$. Set the initial guesses as $\theta^{(0)}[n]$ and $\Phi^{(0)}[n]$.
  Compute $\nabla \widehat{R}_G(\theta[n], \Phi[n])$ evaluated at $\theta^{(0)}[n]$ and $\Phi^{(0)}[n]$, where $\widehat{R}_G(\theta[n], \Phi[n])$ is defined in (3.10).
  Set $k = 1$.
  while $-\nabla \widehat{R}_G(\theta[n], \Phi[n]) \geq \epsilon$ **do**
    Find the search direction $\left[\theta_s^{(k)}, \Phi_s^{(k)}\right] = \nabla \widehat{R}_G(\theta^{(k)}[n], \Phi^{(k)}[n])$.
    Calculate step size $\widetilde{\alpha}^{(k)} = \arg\ \max_{\widetilde{\alpha}}\ \widehat{R}_G(\theta^{(k)}[n] + \widetilde{\alpha}^{(k)}\theta_s^{(k)}, \Phi^{(k)}[n] + \widetilde{\alpha}^{(k)}\Phi_s^{(k)})$.
    Update the result $\theta^{(k+1)}[n] = \theta^{(k)}[n] + \widetilde{\alpha}^{(k)}\theta_s^{(k)}$ and $\Phi^{(k+1)}[n] = \Phi^{(k)}[n] + \widetilde{\alpha}^{(k)}\Phi_s^{(k)}$.
    $k = k + 1$.
  Set $\theta^*[n] = \theta^{(k)}[n]$ and $\Phi^*[n] = \Phi^{(k)}[n]$.
  Find $x^*[n], y^*[n]$, and $z^*[n]$ using (3.8).
  Make a straight line path from $\mathcal{X}_0$ to $\mathcal{X}^*$ with velocity V. Set $N^* = (\beta - 1) + \left\lceil \frac{\|\mathcal{X}_0 - \mathcal{X}^*\|}{\tau V} \right\rceil$. Save the solution as $(x^*[n], y^*[n], z^*[n])_{m=\beta}^{N^*}$.

that the UAV will reach the final location in the specified time frame (N_{av}) or meet the on-board energy constraints. Therefore, we split our proposed scheme into two parts: 1.) UAV searches for the optimal location in each time slot and reaches that location. 2.) UAV takes a greedy approach to reach the final location *i.e,* it takes a straight-line path to reach the destination. This implies, in the earlier time slots, we maximize (3.10) to obtain the optimal location. Then, after certain time slots (say $\beta \in \{S_h + 1, \cdots, N\}$), we take a straight-line path from the previous time slot to the final location. β depends upon the number of available time slots such that the UAV reaches the final location within the specified time slots *i.e.,* $N^* = \min\left\{\frac{E_{max} - \mathcal{E}_I}{\mathcal{E}}, N_{av} - S_h\right\} + S_h$.

The optimal location with a maximum sum rate in each time slot is computed using the steepest ascent method described in Algorithm 2. In time slot n, we start the steepest ascent method by taking the initial starting point as $\theta^{(0)}[n]$ and $\Phi^{(0)}[n]$, corresponding to (x_s, y_s, z_s). This starting point is obtained by drawing a line segment between the UAV location at $(n-1)^{th}$-time slot and the final location $\mathcal{X}^*$. The point obtained by the intersection of the sphere of radius τV and line segment between the $(n-1)^{th}$-time slot and $\mathcal{X}^*$ is taken as the initial starting point for the steepest ascent algorithm.

After computing the initial starting point, at the l^{th}- iteration the algorithm computes the positive gradient $v_s^{(l)}$, $v \in \{\theta, \Phi\}$, of the function at the current point. The steps 6-10 of Algorithm 2 generates the next iteration point $v^{(l+1)}[n]$, $v \in \{\theta, \Phi\}$, which takes a step size $\tilde{\alpha}^{(l)}$ in the direction $v_s^{(l)}$, $v \in \{\theta, \Phi\}$, starting from the previous point $v^{(l)}[n]$. The direction $v_s^{(l)}$ decides which direction to search next, and the step size $\tilde{\alpha}^{(l)}$ determines how far we must go in that particular direction to obtain the maximum sum rate. This $\tilde{\alpha}^{(l)}$ is chosen such that $\widehat{R}_G(v^{(l)}[n] + \widetilde{\alpha}\, v_s^{(l)})$ is maximized. Thus,

$$\widetilde{\alpha}^{(l)} = \arg \max_{\widetilde{\alpha}} \widehat{R}_G(v^{(l)}[n] + \widetilde{\alpha}\, v_s^{(l)}), \tag{3.11}$$

where $\widehat{R}_G(.)$ is defined in (3.10) and is solved using GSS. This algorithm continues its search in the direction which will maximize the function value, given the current point. The steepest ascent iterates until $-\nabla \widehat{R}_G(\theta[n], \Phi[n]) \geq \epsilon$, and later converges to the local solution $\theta^*[n]$ and $\Phi^*[n]$, where ϵ is the acceptable tolerance threshold. Then, using (3.8), we change the coordinate system from spherical to Cartesian to compute $(x^*[n], y^*[n], z^*[n])$.

Thus, for $n < \beta$, a similar approach is followed in each time slot to obtain the optimal location of UAV for that time slot. In other words, Algorithm 2 describes the steps involved to obtain the trajectory using steepest ascent for $n = \{S_h + 1, \cdots, \beta\}$. Next, we discuss how to obtain optimal β.

The appropriate choice of β depends upon the constraint (3.7e). Algorithm 3 is used to compute β and its corresponding sub-optimal trajectory. The procedure followed in Algorithm 3 is as follows. It first initializes the value of β to N_{av}. Thereafter, it calls Algorithm 2 to obtain the UAV trajectory for given $\beta = N_{av}$ using the steepest ascent algorithm. If constraints (3.4a) and (3.7e) are satisfied, then the obtained trajectory is the sub-optimal final solution, and the algorithm terminates. Otherwise, it decrements the value of β by 1 *i.e.,* $\beta = \beta - 1$. Now, to obtain the trajectory corresponding to this new β, for $n = \{S_h + 1, \cdots, \beta - 1\}$, it uses the same locations as obtained from Algorithm 2 in the previous case (with $\beta = N_{av}$). For $n \geq \beta$, it follows straight-line trajectory to reach the final location. After computing the trajectory for this new β, it outputs the total number of time slots (N^*) required to reach the final location. This implies that (3.4a) is satisfied. However, constraint (3.7e) needs to be checked. If (3.7e) is satisfied, then the obtained solution is the sub-optimal trajectory for the given problem. Otherwise, we decrement the value of β by 1 and follow similar steps to compute the sub-optimal trajectory.

The main benefit of this proposed scheme is that we do not have to compute the

Algorithm 3 Proposed scheme to obtain solution of (P3)

Input: $(\mathrm{x^I}, \mathrm{y^I}, \bar{z}_\mathrm{I})$, $\mathcal{X}^*$, S_h, $\mathcal{E}_I$, $\mathcal{E}$, N_{av}, $(x_k, y_k)\ \forall k \in \mathcal{K}$, V, ϵ, E_{max}.
Output: Q^*_{avg} along with optimal N^* and $(x^*[n], y^*[n], z^*[n])$, $\forall n \in \{S_h+1, \cdots, N^*\}$.

1: Call Algorithm 2 with V and $\beta = N_{av}$ to obtain $\{x^*[n], y^*[n], z^*[n]\}_{m=S_h+1}^{N_{av}}$ and N^*.
2: **if** $N^* < \min\left\{\frac{E_{max}-\mathcal{E}_I}{\mathcal{E}}, N_{av}-S_h\right\} + S_h$ and $(x^*[N_{av}], y^*[N_{av}], z^*[N_{av}]) = \mathcal{X}^*$ **then**
3: The obtained trajectory $\{x^*[n], y^*[n], z^*[n]\}_{n=S_h+1}^{N^*}$ is the sub-optimal final trajectory.
4: **else**
5: **while** $N^* > \min\left\{\frac{E_{max}-\mathcal{E}_I}{\mathcal{E}}, N_{av}-S_h\right\} + S_h$ **do**
6: Set $\beta = \beta - 1$.
7: Make a straight-line path from $\mathcal{X}_0 = (x^*[\beta-1], y^*[\beta-1], z^*[\beta-1])$ to $\mathcal{X}^*$ with velocity V. Set $N^* = (\beta-1) + \left\lceil \frac{\|\mathcal{X}_0 - \mathcal{X}^*\|}{\tau V} \right\rceil$. Save the solution as $(x^*[n], y^*[n], z^*[n])_{n=\beta}^{N^*}$.
8: Calculate $R_k[n]$ defined in (3.2), $\forall n \in \{S_h+1, \cdots, N^*\}$ and then evaluate $Q^*_{avg} = \frac{1}{N^*}\sum_{n=S_h+1}^{N^*}\sum_{k=1}^{K} R_k[n]$.

trajectory using the steepest ascent method for every β. Instead, it stores the locations of the UAV obtained by using the steepest ascent method for $\beta = N_{av}$ and uses these stored locations when $\beta < N_{av}$. For $n \geq \beta$, a greedy approach is followed in each iteration to computes the sub-optimal trajectory. In this way, Algorithm 3 computes β, and N^* and average sum rate Q_{avg} corresponding to β.

3.5.3 Complexity Analysis

The computation cost of Algorithm 3 depends primarily on the complexity of steepest ascent. The worst-case complexity of steepest ascent at which the norm of objective function's gradient is less than ϵ is $\mathcal{O}\left(1/\epsilon^2\right)$ [59]. Since the steepest ascent algorithm is called for N_{av} time slots, the complexity of trajectory using steepest ascent is $\mathcal{O}\left(\frac{N_{av}}{\epsilon^2}\right)$. $\mathcal{O}\left(N_{av}\right)$ is the computations to compute the appropriate value of β. The total complexity to compute the sub-optimal solution is $\mathcal{O}\left(\frac{N_{av}}{\epsilon^2}\right)$.

3.6 Result and Discussions

In this section, numerical results are provided to validate the proposed UAV trajectory model. We consider a system with 10 users [60] that are distributed randomly in a circular field of radius 150 m, centered at origin. The total communication bandwidth B is set to 1 MHz. The reference SNR at distance $d_0 = 1$ m is taken as $\tilde{\gamma}_o = 80$ dB. The modelling parameters are set as $C = 10$, $D = 0.6$, $\kappa = 0.2$, and $\bar{\alpha} = 2.3$ [9]. The minimum height H_{min} to be attained by the UAV as described in (3.7c) is 15 m. The fixed time slot

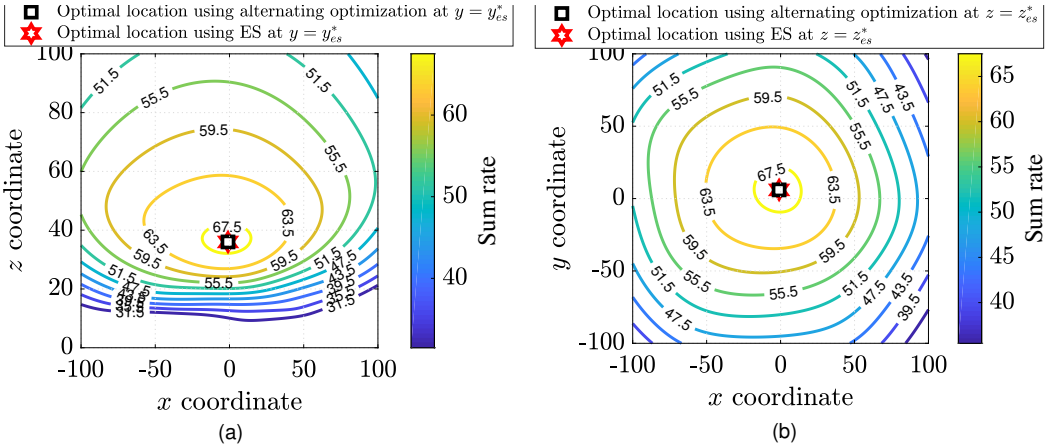

Figure 3.2: Validation of optimal location at (a) $y = y^*_{es}$, (b) $z = z^*_{es}$.

duration τ is set to 0.2 s. The UAV's initial location is set to $(\mathrm{x^I}, \mathrm{y^I}, \mathrm{z^I})$ = (-200,0,0) m. The acceptable tolerance is taken as $\epsilon = 1 \times 10^{-6}$. The simulation values taken for energy consumption model are as follows: $P_o = 79.86$W, $P_i = 88.63$W, $U_{tip} = 120$, $v_o = 4.03$ m/s, $d_f = 0.6$, $\rho = 1.225$, $s = 0.05$, and $A_r = 0.503$ [9].

3.6.1 Optimal Location

To validate the optimal location for UAV deployment, we plot Figure 3.2. The solution using ES is $(x^*_{es}, y^*_{es}, z^*_{es})$. In Figures 3.2(a) and (b), contour lines for sum rate is plotted against x and z for a given $y = y^*_{es}$, and x and y for a given $z = z^*_{es}$, respectively. The figure also shows that the low-complexity solution obtained using alternating optimization for the problem (P1) converges to the solution obtained by using ES. On performing simulations on Intel Core $i7$ processor with 3.20 GHz CPU clock, the time taken to obtain the optimal location using ES is approximately 180 minutes, whereas it took approximately 15 minutes to solve the problem using alternating optimization. Thus, we infer that the proposed alternating optimization scheme provides a better complexity compared to ES. To validate the proposed optimal deployment location, we compare it with the other schemes as follows:

- Optimized altitude [39]: Here, the UAV altitude is optimized to obtain a maximum sum rate of the system while fixing the horizontal coordinates to the center of the field.

- QoS-aware UAV placement [38]: This scheme finds the 3D placement of UAV by considering the different QoS requirements of the ground users to maximize the achievable sum rate.

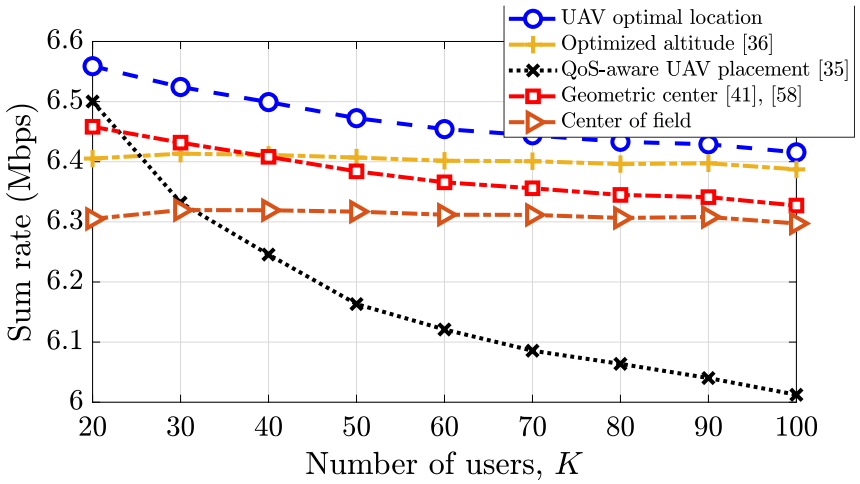

Figure 3.3: Variation of sum rate at optimal location with other schemes by varying number of users K.

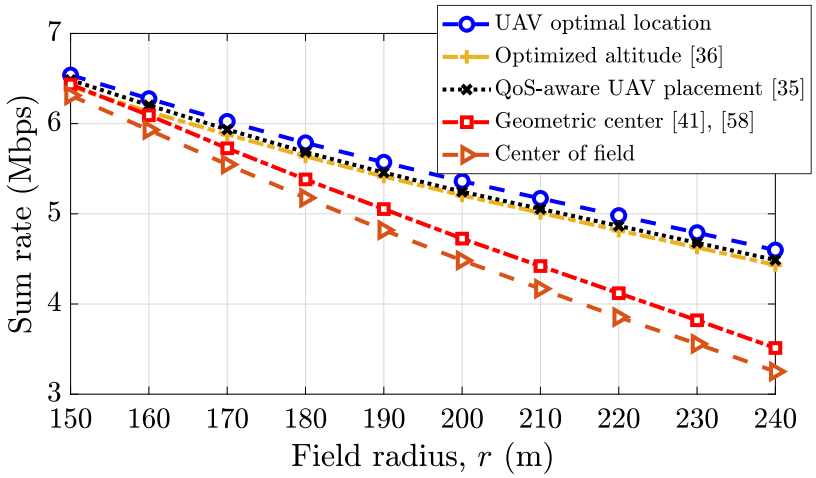

Figure 3.4: Variation of sum rate at optimal location with other schemes by varying field radius r.

- Geometric center [44], [61]: In this scheme, the horizontal location of the UAV is set to the geometric center of all users while the UAV altitude is fixed to 25 m.
- Center of the field: In this scheme, the horizontal location is set to the center of the field while the UAV altitude is set to 25 m.

Figure 3.3 shows the sum rate comparison of the proposed scheme with different schemes as addressed above and is plotted by varying the number of users in a circular field of radius $r = 150$ m. It is observed that the sum rate of the optimal location is higher than the other schemes. It is because the proposed scheme jointly optimizes the horizontal and vertical coordinates of the UAV. In contrast, the other schemes either optimize the UAV altitude or consider the fixed UAV altitude. Also, a sharp decrease in the QoS-aware UAV placement scheme is observed because the QoS-based scheme focuses on rate fairness

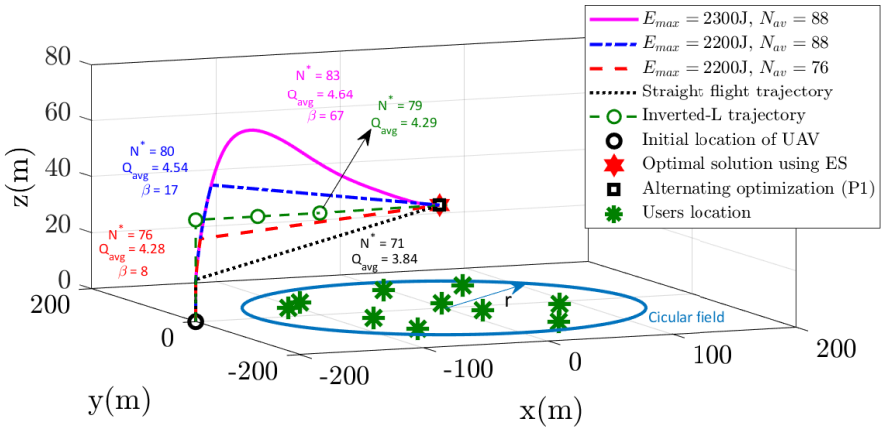

Figure 3.5: Insights on sub-optimal trajectories of UAV

rather than maximizing the sum rate.

Figure 3.4 is plotted for $K = 20$ users by varying the radius of the circular field. As the field radius r increases, the path loss increases. Thus, the sum rate decreases with an increase in the field radius. Here the performance of QoS-aware UAV placement is better than other schemes due to the fixed number of users in a field. Intuitively, the optimal UAV height should increase with an increase in the field radius. Due to fixed UAV height in the geometric center and the center of the field cases, the sum rate worsens with an increase in the field radius. As a result, it gives lower sum rate in comparison to other schemes.

3.6.2 Trajectory Design Insights

Through Figure 3.5, we give insights on the UAV trajectory for the proposed scheme when velocity V is set to 15 m/s. The figure is plotted for different values of total on-board energy availability E_{max} and the maximum allowed time slots N_{av} in (3.7e). Figure 3.5 also presents the benchmark schemes *i.e.,* straight flight, and inverted-L. In a straight flight trajectory, UAV follows the straight-line path from the initial location to the destination. In the inverted-L trajectory, the UAV first moves vertically until the optimal height z^* is reached. Then, it makes a horizontal movement in a straight-line path to reach the final location. Along with the UAV trajectories, the figure also shows the globally optimal final location obtained using ES and low-complexity sub-optimal solution obtained by using alternating optimization for the problem (P1).

In our proposed scheme, the UAV first moves up to the region where the sum rate is high and, after that, moves to the optimal location. Unlike the other benchmark schemes, because our UAV quickly reaches the high sum rate region, (though it is not the maximum

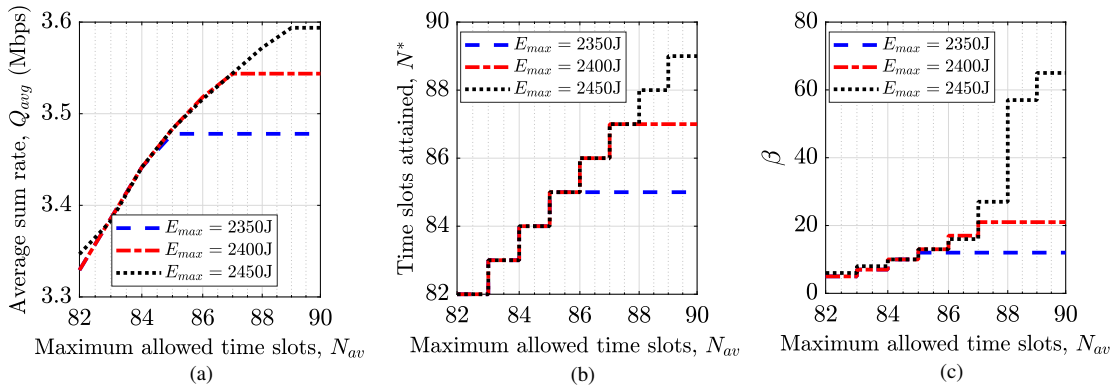

Figure 3.6: Variation of average sum rate Q_{avg}, time slots attained by the UAV N^*, and β with maximum allowed time slots N_{av} for different values of on-board energy availability E_{max}.

sum rate but close to the maximum) our trajectory provides better performance than the benchmark schemes. As stated in Section 3.5, the UAV first travels by calculating the optimal location for each time slot as long as n is less than β, and afterwards, it travels in a straight-line to reach the final location. The same can also be observed from Figure 3.5. Also, the value of β decreases with a decrease in either E_{max} or N_{av}. This occurs in order to meet the constraint (3.7e).

Note that to make a fair comparison between the proposed and the benchmark schemes, we utilize the concept of time normalization. Under the time normalization framework, the total time span considered for each of the schemes is the maximum time required by our proposed scheme to reach the optimal location. Thus, while the UAV in a straight flight trajectory reaches the destination early, it stays there until the UAV in our proposed path reaches the destination to compute the average sum rate.

3.6.3 Performance Analysis of Proposed Scheme

To study the variation in average sum rate Q_{avg}, time slots required by the UAV to reach the destination N^*, and β with the change in maximum allowed time slots N_{av}, we plot Figure 3.6(a)-(c). The figures are plotted for different values of $E_{max} = \{2350, 2400, 2450\}$ J. As we know, in early stage, the UAV travels by computing optimal location in each time slot and later takes a straight-line trajectory to reach the final location. Thus, as N_{av} increases, β also increases. This implies that the UAV now follows the optimal path (obtained using steepest ascent method) for more number of time slots. As a result, N^* and Q_{avg} also increases.

E_{max} also plays an important role in $N^* = \left\{\frac{E_{max}-\mathcal{E}_I}{\mathcal{E}}, N_{av} - S_h\right\} + S_h$. As we decrease E_{max}, β also decreases, and for lower values of E_{max}, the UAV takes a straight-line

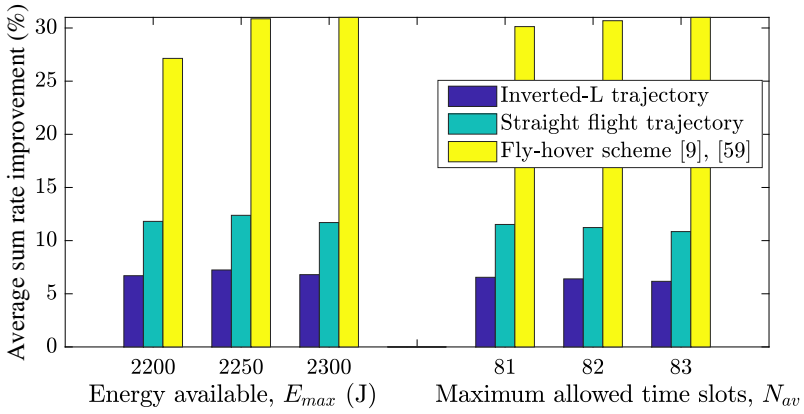

Figure 3.7: Overall performance improvement in average sum rate over the inverted-L, straight flight trajectory and fly-hover scheme.

trajectory to reach the final location. Hence, more the on-board energy available, the better is the average sum rate Q_{avg}. Similarly, less restriction in energy will increase β, as a result, the number of time slots N^* consumed to reach the final location will also increase. When the energy constraint is met with equality, there is no change in Q_{avg}, β, and N^* as seen in Figure 3.6(a)-(c).

3.6.4 Performance Comparison with Benchmark Schemes

In this sub-section, we compare the proposed scheme's performance with the benchmark schemes *i.e.,* straight flight, inverted-L, and fly-hover scheme [9], [62]. In the fly-hover scheme, the UAV first visits the hovering locations (*i.e.,* user's location with a fixed altitude H_{F-H}) before reaching the destination. This scheme first computes the visiting sequence of the hovering locations to maximize the average sum rate. Thereafter, it obtains the UAV trajectory with the given velocity while keeping in view the energy consumption and flight duration constraints. Next, we first present the overall percentage improvement in the average sum rate of our proposed scheme. Secondly, we provide the performance comparison in a high-scale environment *i.e.,* with a large number of users in a larger area with high UAV velocity.

To present the overall percentage improvement in the average sum rate of our proposed UAV flight trajectory as compared to the benchmark schemes, we plot Figure 3.7. These benchmark schemes are compared by varying the total energy available E_{max} and the time slots available N_{av} for the UAV to reach the final location. It is observed that the proposed scheme always outperforms the benchmark schemes. This is because, in our proposed scheme, the UAV takes a path wherein it quickly reaches a region where a high sum rate can be achieved by first travelling in the vertical direction to attain height and

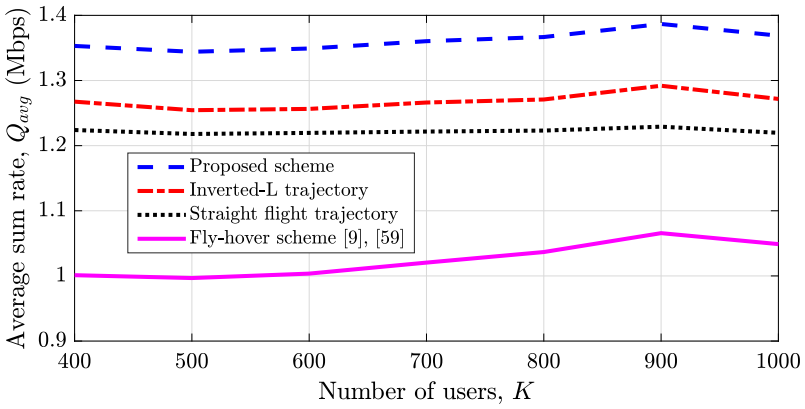

Figure 3.8: Variation in average sum rate with the change in the number of users, K, distributed in a field of radius $r = 500$ m.

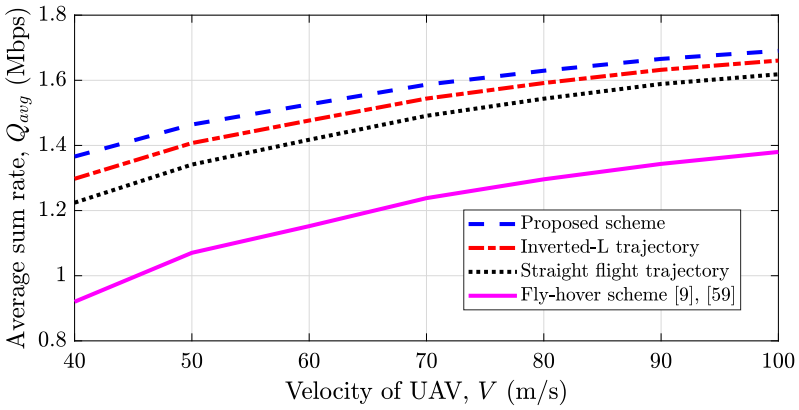

Figure 3.9: Variation in the average sum rate with the change in velocity of UAV, V (m/s).

then travelling towards the final location. On an average, our proposed scheme provides 13%, 7%, and 30% improvement over the straight flight, inverted-L, and fly-hover scheme, respectively.

Figure 3.8 is plotted by varying the number of users in a circular field of radius $r = 500$ m, at the flying velocity $V = 50$ m/s. We assume that the UAV starts its journey from the initial location at $(-550, 0, 0)$ m and flies towards the final location. The UAV's on-board energy and available time slots are set to $E_{max} = 20$ kJ and $N_{av} = 80$, respectively. As the number of users and their locations vary, the proposed scheme first computes the optimal location to compute the UAV trajectory. It can be observed that the proposed scheme outperforms the other benchmark schemes, and our proposed algorithm can be applied to a scenario with a large number of users.

Figure 3.9 is plotted by varying the UAV's velocity to serve $K = 800$ ground users randomly distributed in a circular field of radius $r = 500$ m. At low velocity, the UAV will take more time to reach the final location. On the other hand, at high velocity, the UAV

reaches the final location quickly, and the rest of the time slots are utilized for hovering at the optimal location. Thus, as the UAV's velocity increases, the average sum rate also increases. Also, the proposed scheme performs relatively better in comparison to the other schemes and can be applied to a scenario with a large number of users and high velocity.

3.7 Conclusion

This chapter optimizes the 3D UAV trajectory to maximize the average sum rate over all users. It is achieved by first computing the optimal deployment location. The optimal deployment location is computed by obtaining the concave regions and then applying alternating optimization. The 3D UAV trajectory is optimized to reach the deployment location using an iterative scheme wherein the UAV travels by searching the optimal location in each time slot using the steepest ascent method. Results show that the deployment location obtained using alternating maximization yielded a low complexity solution while providing a solution close to the globally optimal solution. The UAV trajectory obtained using our proposed scheme outperformed the benchmark schemes, with a performance improvement of around 16.5%, on an average. Note that our work is equally applicable to mobile users, provided that the users' location is known to the UAV in each time slot. Our proposed scheme can assist the UAV deployment in on-demand high-traffic applications where quick network deployment is required, such as first-responders in emergencies, service recovery in disasters, etc.

This chapter assumes the UAV to be deployed at an optimal deployment location. However, in real-world scenarios, there may be some terrain constraints or legal restrictions; as a result, we cannot deploy the UAV at an optimal location for a long time duration. In that case, we need to deploy the UAV to the pre-defined fixed final location as specified by the regulatory authorities. Therefore, it is necessary to analyze the system when the final location is different from the optimal deployment location.

Thus, in the next chapter, we proposed a framework where we optimize the trajectory of the UAV from the initial location to the pre-defined final location in a stipulated time in the presence of onboard energy constraints.

Chapter 4

UAV Trajectory Design: Fixed Initial to Arbitrary Final Location

4.1 Introduction

This chapter studies the flight trajectory of UAV to provide 5G cellular service in a given area. We consider a single UAV launched from the pre-defined initial to a pre-defined final location in a stipulated time, during which it serves the ground users that are distributed in a circular field. UAV's limited on-board energy has been a major concern affecting the system's performance. Therefore, in this work, we minimize the average outage probability of the system by optimizing the 3D trajectory of the UAV while considering the velocity and on-board energy as constraints. To solve this problem, we propose two approaches: the low-complexity vertex and the high-performance sequential approach. The vertex approach involves two steps. Firstly, it obtains the optimal solution while relaxing the velocity and on-board energy constraints. Secondly, a greedy solution is proposed for the original problem. The sequential approach finds the optimal location in each time slot sequentially. Simulation results compare the two approaches and show that our proposed strategies provide on an average 41% improvement in average outage probability over the benchmark schemes. Additionally, we show that the sequential approach is better than the vertex approach, though at the cost of high computational complexity.

Our present work is motivated by practical scenarios, such as providing coverage to first responders or providing connectivity in a crowded region, wherein a UAV is to be deployed in a timely and energy-efficient manner. This setup can be applied to many practical applications, such as establishing two-way communication between first responders, and fire-fighters in an area with inadequate coverage or traffic offloading in a hotspot area, such as sports events, etc.

4.1.1 Related Works

A trajectory design for the UAV-assisted communication system needs to address two main concerns, namely, communication-related performance and energy consumption in UAV manoeuvring. Over the last few years, a substantial number of studies have been carried out in the above areas, for which we provide a survey on the relevant prior work.

In communication-oriented trajectory design, UAV as an amplify-and-forward relay was considered in [63] to optimize the trajectory and transmit power of the UAV by minimizing the outage probability of the relay system. In [45], UAV 2D trajectory was optimized for full-duplex UAV aided small cell wireless systems to maximize the total system capacity. The authors in [64] jointly optimized buoy sensors communication scheduling, UAV trajectory, and system power to minimize the maximum average outage probability among all buoy sensors. In [47], the UAV trajectory was optimized by minimizing the average outage probability over all users considering a probabilistic LoS channel model. Due to the limited resources available with the UAVs, user scheduling and UAV trajectory were jointly optimized in [65] and [44] to maximize the minimum data collection rate in UAV-enabled wireless sensor networks.

As there is limited on-board energy available with the UAVs, their energy must be utilized effectively to increase the system's performance. The above works on communication-oriented trajectory design do not consider the energy availability at the UAV. The energy consumed by the UAV was first emphasized in [10] for a fixed-wing UAV and in [9] for a rotary-wing UAV. In both works, the authors maximized energy efficiency while achieving the user's minimum rate requirement. Similarly, [66] considered coverage as a constraint to optimize the trajectory and minimize the energy consumption. The 3D trajectory of a UAV relay was designed in [30] to maximize the system energy efficiency while meeting the constraints on UAV trajectory, data rate requirement, and communication and mechanical energy consumption. The authors in [49] focussed on jointly optimizing the user scheduling, power, and bandwidth allocation along with the trajectory to maximize the UAV energy efficiency in the presence of quality-of-experience (QoE) requirements of the users. On the same note, the aim in [50] was to serve the edge users and assist in traffic offloading while the UAV flew in a circular path. Similarly, the works [67], and [68] also considered the energy efficiency to design the 2D trajectory of the UAV.

The works presented so far have focused on UAV trajectory design based on energy efficiency and outage minimization, individually. In all of the above-highlighted

works, energy efficiency was considered as an objective function for obtaining an optimal UAV trajectory. However, from the perspective of communication systems, communication-related performance metrics, such as outage, throughput, etc., should be regarded as objective functions, while energy consumption can be included in the constraints. This UAV energy consumption as a constraint ensures that the UAV completes its mission without completely exhausting the available on-board energy. Towards this end, the authors in [69] and [53] considered the energy consumption constraint to optimize the UAV flight trajectory when flying at a fixed altitude while considering the LoS UAV-user channel model. In particular, [69] considered UAV flying energy consumption to be independent of velocity while [53] considered the energy consumption model for a fixed-wing UAV. Moreover, in [70], the authors considered LoS channel model with an objective to maximize coverage to a number of ground users to design the 2D trajectory of the UAV in the presence of energy constraints. Whereas, the authors in [71] considered the 2D trajectory under a probabilistic LoS channel model but assumed the UAV to move with a fixed velocity. Also, the work in [72] took the energy constraint and minimized total outage duration in a LoS channel.

The above works [69]-[72] considered the energy constraint to design the 2D trajectory of the UAV. However, for a rotary-wing UAV, there are very few works for 3D trajectory design in a probabilistic LoS channel model. Some of the works are as follows. The authors in [73] studied the 3D trajectory design by considering the energy consumption as a constraint to maximize the overall throughput of the system but considered the UAV to move with the fixed maximum velocity. This is not applicable to scenarios when UAV have a less limited energy, where the decrease in UAV velocity saves certain amount of energy. To this extent, the authors in [74], considered the variable speed to design UAV trajectory for the same scenario. However, they designed the UAV trajectory while considering the analysis only under the LoS condition and not considering the NLoS condition which is oversimplified. Table 4.1 describes the short summary of related work with key differences that considers the energy constraint.

4.1.2 Contributions and Organization

We consider the scenario where a UAV has to fly from a pre-defined initial to a pre-defined final location in a stipulated time and energy availability to provide coverage to a given set of users. Compared to the prior works [73] and [74], our present work considers a 1) realistic trajectory design (with varying altitude). 2) Practical UAV-user channel model

Table 4.1: Short summary of related works that considers energy constraint in their model. P.LoS is the probabilistic LoS channel model.

Ref.	Objective	Channel/Traj.	Key differences
[69]	Maximize the system's throughput to optimize the UAV trajectory	LoS / 2D	Considered 2D trajectory and LoS dominant links
[53]	Minimum average rate maximization and energy efficiency	LoS / 2D	Considered the analysis with fixed-wing UAV
[70]	Maximize coverage to a number of ground users	LoS / 2D	Coverage as a performance metric
[71]	Maximize the throughput of the network during the flight time	P.LoS / 2D	Considered the UAV to move with fixed velocity
[72]	Minimization of total outage duration	LoS / 2D	LoS dominant links and the UAV with fixed height
[73]	Overall throughput maximization	P.LoS / 3D	UAV moves with fixed maximum velocity
[74]	Maximize the minimum throughput	P.LoS / 3D	Analysis only under the LoS conditions

i.e., Probabilistic LoS channel model [23] considering probabilities of both the LoS and NLoS links, as opposed to [74] which only examines LoS links for analysis. 3) Velocity dependent energy consumption model for a rotary-wing UAV such as drones [9] in the presence of mobility constraints, which [73] assumed the UAV to fly with a fixed velocity. Based on the above differences, this work considers the UAV deployment from a practical standpoint which cannot be derived from the prior works in the literature due to their unrealistic assumptions, such as fixed UAV velocity or LoS channel model.

The key contributions of this work are listed below:

- An optimization problem is framed to minimize the average outage probability over all ground users by optimizing the 3D UAV trajectory, while considering the velocity and total on-board energy constraints under probabilistic LoS channel model that incorporates the probabilities of LoS link and NLoS link separately.

- Noting the non-convexity of the problem, we present the low-complexity *vertex approach* in Section 4.4, where the 3D location with minimum outage probability is computed followed by greedy approach to obtain a UAV trajectory. To obtain 3D location, the optimal location problem is framed and the globally optimal solution within acceptable tolerance is obtained.

- To improve upon the *vertex* solution, we present a high-performance *sequential approach* discussed in Section 4.5. It starts from the initial location and searches for the optimal UAV location in each time slot sequentially.

- Numerical results provide useful insights on the UAV trajectory obtained from both the approaches and compares them with the benchmark schemes. For both the approaches, the impact of velocity on the average outage probability is shown, and

a trade-off between UAV velocity and energy availability is studied.

- In particular, our proposed *vertex* and *sequential* approaches show on an average 31% and 52% improvement over the benchmark schemes, respectively.

Rest of the chapter is organized as follows. Section 4.2 provides the overview of the communication system model. Section 4.3 presents the problem formulation. Section, 4.4 and 4.5 describe the methodologies proposed followed by their computational complexities. Numerical results are provided in Section 4.6, followed by conclusion in Section 4.7.

4.2 System Model

4.2.1 Communication Setup

For a given downlink communication model and UAV trajectory model as described in Chapter 2 and also shown in Figure 2.1, the UAV has to complete its mission (going from the initial location $\mathbf{X}_I$ to the final location $\mathbf{X}_F$ to serve the K ground users in N time slots while assuming the time slot duration to be fixed for each time slot, i.e., $\tau[n] = \tau$, $\forall n$. Given the ground users and the UAV location at the n^{th}-time slot, the distance between the UAV and the k^{th}-user at any time slot n is given by $d_k[n] = \sqrt{(x[n] - x_k)^2 + (y[n] - y_k)^2 + z[n]^2}$. Velocity of the UAV within each time slot is given by

$$v[n] \triangleq \frac{1}{\tau}\big((x[n] - x[n-1])^2 + (y[n] - y[n-1])^2 + (z[n] - z[n-1])^2\big)^{\frac{1}{2}}. \tag{4.1}$$

4.2.2 Performance Metric

In this work, we assume that alongside Probabilistic LoS channel model, the channel between the UAV and the user also undergoes the small-scale fading due to rich scattering. Thus, the channel between the UAV and the k^{th}-user at the n^{th}-time slot is modelled as $g_k[n] = \sqrt{h_k[n]}\tilde{h}_k[n]$, where $\tilde{h}_k[n]$ accounts for small-scale fading while $h_k[n]$ accounts for large-scale attenuation which includes path loss as described in (2.13).

Then, the received SNR, denoted by $\gamma_k[n]$, between the k^{th}-user and the UAV at time slot n is given as $\gamma_k[n] = \frac{P_{tr}|g_k[n]|^2}{\sigma_n^2}$, where P_{tr} represent the transmit power of the UAV, and σ_n^2 is the noise power. Furthermore, for simplicity and without loss of generality, we assume Rayleigh fading channel so that the probability density function of SNR $\gamma_k[n]$ follows exponential distribution $f_{\gamma_k[n]}(\gamma_k[n]) = \frac{1}{\bar{\gamma}_k[n]} e^{\frac{\gamma_k[n]}{\bar{\gamma}_k[n]}}$, where $\bar{\gamma}_k[n]$ is the average SNR

given by $\bar{\gamma}_k[n] = \frac{P_{tr}\mathbb{E}[h_k[n]]}{\sigma_n^2}$. This is in line with [75] and is obtained when $\mathbb{E}[|\tilde{h}_k[n]|^2] = 1$, and $\mathbb{E}[h_k[n]]$ as defined in (2.13). Substituting $\mathbb{E}[h_k[n]]$ in $\bar{\gamma}_k[n]$, we get

$$\bar{\gamma}_k[n] = \frac{\tilde{\gamma}_o((1-\kappa)P_k^L[n] + \kappa)}{((x[n]-x_k)^2 + (y[n]-y_k)^2 + z[n]^2)^{\alpha}}, \tag{4.2}$$

where $\tilde{\gamma}_o \triangleq P_{tr}d_0/\sigma_n^2$ and $\alpha \triangleq \bar{\alpha}/2$.

Outage probability of the k^{th}-user, defined as the probability that the received SNR falls below the threshold γ_{th} [76]. Here, for a Rayleigh fading channel, the outage probability $P_{out}^k[n]$ of k^{th}-user follows $P_{out}^k[n] = 1 - e^{-\frac{\gamma_{th}}{\bar{\gamma}_k[n]}}$. Using (4.2), the outage probability of k^{th}-user is given as

$$P_{out}^k[n] = 1 - e^{\left(-\frac{\gamma_{th}}{\tilde{\gamma}_o}\frac{((x[n]-x_k)^2+(y[n]-y_k)^2+z[n]^2)^{\alpha}}{(1-\kappa)P_k^L[n]+\kappa}\right)}. \tag{4.3}$$

In this work, we minimize the outage probability (4.3) averaged over all users and time to obtain the optimal trajectory.

Lemma 3. *The energy consumed by the UAV defined in* (2.2) *is a pseudoconvex function with respect to* $v^{xy}[n]$.

Proof. See Appendix A.2.1. □

4.3 Problem Formulation

We intent to minimize the outage probability averaged over time and users by optimizing UAV trajectory ($x[n]$,$y[n]$,$z[n]$), while meeting the constraints on trajectory and energy consumption model. Our optimal designs are aimed at serving applications with a UAV communication system-centric goal, rather than individual user-level, where the best-effort delivery is desired to minimize the aggregate outage probability. Then, the optimization problem is formulated as

$$\begin{aligned}
(\text{P1}): \quad & \min_{\substack{\{x[n],y[n],z[n]\} \\ \forall n \in \mathcal{N}}} \frac{1}{NK}\sum_{n=1}^{N}\sum_{k=1}^{K} P_{out}^k[n] \\
& \text{subject to (s.t.)} : \sum_{n=1}^{N} e[n] \leq E_{max}, && \text{(4.4a)} \\
& (x[N], y[N], z[N]) = (\mathrm{x^F}, \mathrm{y^F}, \mathrm{z^F}), && \text{(4.4b)} \\
& z[n] \geq H_{min}, \forall n \in \mathcal{N}, && \text{(4.4c)} \\
& v[n] \leq V_{max}, \forall n \in \mathcal{N}, && \text{(4.4d)}
\end{aligned}$$

where (4.4a) is the energy consumption constraint with $e[n]$ defined in (2.2) and $v[n]$ is defined in (4.1). E_{max} in (4.4a) represents the on-board energy available with UAV for completing the mission. Constraint (4.4b) ensures that the UAV reaches the final location within N slots, and (4.4c) represents the minimum height H_{min} required by UAV to avoid collisions. We assume $\mathrm{z^F} \geq H_{min}$. If $\mathrm{z^I} < H_{min}$, we constrained the UAV to move vertically in z-direction until minimum height H_{min} is achieved. Constraint (4.4d) represents the maximum velocity constraint of the UAV. To obtain the solution to the above problem, we first present the following proposition.

Proposition 1. *Using* $\widehat{P}^k_{out}[n]$ *defined below in* (4.5) *instead of* $P^k_{out}[n]$ *defined in* (4.3) *in problem (P1) is equivalent.*

$$\widehat{P}^k_{out}[n] \triangleq \frac{\frac{\gamma_{th}}{\bar{\gamma}_o}((x[n]-x_k)^2+(y[n]-y_k)^2+z[n]^2)^{\alpha}}{(1-\kappa)\,P^L_k[n]+\kappa}. \tag{4.5}$$

Proof. Using $e^{-a} \approx 1-a$, $\forall a \ll 1$, in (4.3), since the P^k_{out} is a strictly increasing function of $\widehat{P}^k_{out}$, the two optimization problems with objective functions $\widehat{P}^k_{out}$ and P^i_{out} are equivalent and share the same set of optimal points $(x^*[n], y^*[n], z^*[n])$ [77]. The optimal values are related as $P^{k*}_{out} = 1 - e^{-\widehat{P}^{k*}_{out}}$. □

Accounting the above proposition, we modify (P1) by substituting $\widehat{P}^k_{out}[n]$ instead of $P^k_{out}[n]$ as follows

$$\text{(P2)}: \min_{\substack{\{x[n],y[n],z[n]\}\\ \forall\, n\in\mathcal{N}}} \widehat{P}_{avg} \triangleq \frac{1}{NK}\sum_{n=1}^{N}\sum_{k=1}^{K}\widehat{P}^k_{out}[n],$$

$$\text{s.t.}: \text{(4.4a)} - \text{(4.4d)}.$$

The objective function in (P2) is non-convex with respect to $x[n]$, $y[n]$ and $z[n]$, $\forall n \in \mathcal{N}$. We propose two solutions based on computational complexity, namely, a low-complexity *vertex approach* with moderate performance and a high performance *sequential approach* with higher complexity. However, the high computational complexity of *sequential approach* limits its practical usage when deploying the UAV in a realistic scenario for faster deployment. Thus, to mitigate this issue, we need to have a faster solution. Therefore, we introduce the *vertex approach*. The *vertex approach* is practically a very fast algorithm than the *sequential* one, but we have to sacrifice a bit on the performance to adopt this algorithm. Thus, there exists a trade-off between the performance and the complexity.

Moreover, the *vertex approach* is a greedy scheme that computes the optimal location of the UAV in 3D space, where the average outage probability is minimum, and builds a trajectory by using this optimal location (as discussed in Section 4.4). On the other

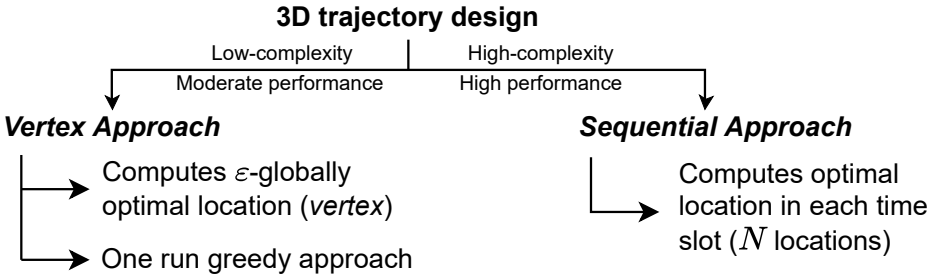

Figure 4.1: Motivation and brief description of proposed solutions.

hand, the *sequential approach* is a sub-optimal scheme that forms the trajectory while computing the optimal location at every time slot (shown in Figure 4.3, Section 4.5). The higher complexity of the *sequential approach* than that of the *vertex approach* is discussed in Section 4.6.1. The brief description on the two approaches is shown in Figure 4.1.

In this section, we propose a low-complexity greedy solution. The key idea is to first relax the on-board energy and velocity constraints i.e., (4.4a) and (4.4d), respectively, in (P2), then obtain the optimal trajectory that comprises of the initial location, the optimal location (we call it *vertex*), and the final location. Note that the UAV will not directly go to the final location as the outage at the final location may not be minimum. Thus, the UAV will stay at the *vertex* till $n < N$. Accordingly, we relax (4.4a) and (4.4d), and introduce a new problem to obtain the best location in 3D space (*vertex*) where the average outage probability is minimum. Then, we utilize this *vertex* to obtain a greedy solution to (P2) while accounting for velocity and on-board energy constraints. This approach is named as *vertex approach* because it constructs the UAV trajectory by following the *vertex* as shown in Figure 4.2.

4.4 Vertex Approach: Proposed Solution I

4.4.1 Vertex Computation

In this sub-section, our objective is to compute the *vertex* by relaxing (4.4a) and (4.4d) in (P2). As the outage probability $\widehat{P}_{out}^{k}[n]$ defined in (4.5) is a function of the location of fixed ground users $(x_k, y_k), \forall k \in \mathcal{K}$ and UAV, we will get a single location in 3D space where the average outage probability is minimum. Next, we define a new optimization problem (P3) to compute the *vertex* while omitting [n] as follows

$$\begin{aligned} (\text{P3}): \quad & \min_{\{x,y,z\}} \quad \bar{P}_{out}, \\ & \text{s.t.} \quad |x|, |y| \leq r; H_{min} \leq z \leq H_{max}, \end{aligned}$$

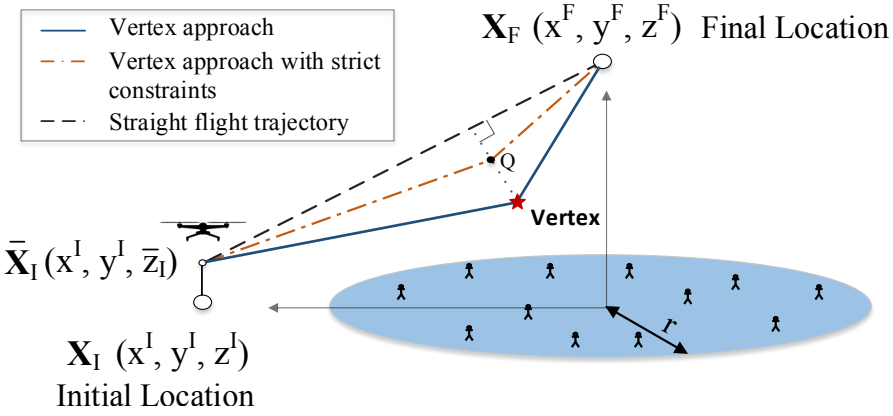

Figure 4.2: *Vertex approach* to obtain the 3D UAV trajectory.

Algorithm 4 Solution of (P3) using alternating optimization

Input: $-r \leq x \leq r$, $-r \leq y \leq r$, $H_{min} \leq z \leq H_{max}$, K, $(x_k, y_k), \forall k \in \mathcal{K}$, and ϵ.
Output: $\bar{P}^*_{out}$ along with $\mathcal{X}^* = (x^*, y^*, z^*)$.
1: Initialize $l = 1$, $\bar{P}^0_{out} = 1$, $\bar{P}^1_{out} = 0.99$, $x^1 = y^1 = -r$, and $z^1 = H_{min}$.
2: **while** $\bar{P}^{l-1}_{out} - \bar{P}^l_{out} \leq \epsilon$ **do**
3: Apply 2D GSS on $\bar{P}_{out}$ to obtain x^{l+1} and y^{l+1} for fixed z^l.
4: Apply 1D GSS on $\bar{P}_{out}$ to obtain z^{l+1} for fixed x^{l+1} and y^{l+1}.
5: Compute $\bar{P}^{l+1}_{out}$ for $(x^{l+1}, y^{l+1}, z^{l+1})$.
6: Set $l = l + 1$.
7: Set $(x^*, y^*, z^*) = (x^l, y^l, z^l)$ and $\bar{P}^*_{out} = \bar{P}^l_{out}$.

where $\bar{P}_{out} \triangleq \frac{1}{K}\sum_{i=1}^{K} \widehat{P}^k_{out}$ with $\widehat{P}^k_{out}$ defined as in (4.5). As users are present in the coverage field of radius r centered at origin, it is convenient to assume that the optimal points x^* and y^* will lie within the coverage field. Thus, $-r \leq x \leq r$, $-r \leq y \leq r$, and z is constraint by H_{max}. H_{max} is maximum flying height of the UAV. Since $\bar{P}_{out}$ is non-convex in x, y, and z, it is difficult to obtain the globally optimal solution.

We apply alternating optimization to obtain the solution to (P3). In alternating optimization [78], we iteratively optimize the objective function with respect to the horizontal (x, y) and vertical (z) coordinates by applying the GSS [79] to compute the minimum in each dimension *i.e.,* horizontal (x, y) and vertical (z) coordinates. To show that the GSS converges to the optimal solution in each iteration, we present a proof for pseudoconvexity of $\bar{P}_{out}$ in the horizontal (x, y) and vertical (z) coordinates as follows

Lemma 4. *$\bar{P}_{out}$ is a jointly pseudoconvex function of x and y for any given value of z, and $\bar{P}_{out}$ is a pseudoconvex function of z for any given value of x and y.*

Proof. See Appendix A.2.2. □

Lemma 2 ensures that the GSS converges to the optimal location in each iteration.

Algorithm 5 ϵ-globally optimal solution

Input: $-r \leq x \leq r$, $-r \leq y \leq r$, $H_{min} \leq z \leq H_{max}$, N, $(x_k, y_k), \forall k \in \mathcal{K}$, and ϵ.
Output: $\bar{P}^*_{out}$ with $\mathcal{X}^* = (x^*, y^*, z^*)$.

1: Compute $\mathcal{R}_C$ using (A.2.13), as defined in Appendix A.2.3.
2: Let $\mathcal{X} = (x, y, z)$. For $\mathcal{R}_C$, compute $\mathcal{X}_1^* = arg \min_{\mathcal{X}} \bar{P}_{out}$ using steepest descent with ϵ.
3: Evaluate $\mathcal{X}_2^* = arg \min_{\mathcal{X}} \bar{P}_{out}$ using linear search over the region $\mathcal{R}_{NC} = \mathcal{R}/\mathcal{R}_C$ by keeping step size ϵ.
4: Obtain $\mathcal{X}^* = arg \min_{\{\mathcal{X}_j^*\}} \bar{P}_{out}$ for $j \in \{1, 2\}$.
5: Set $\bar{P}^*_{out}$ to $\bar{P}_{out}$ corresponding to $\mathcal{X}^*$.

Algorithm 4 describes the steps involved in the alternating optimization. In each iteration l, we optimize (x, y) fixing the z obtained in the last iteration, and then obtain optimal z by fixing (x, y). The algorithm converges when $\bar{P}^{l-1}_{out} - \bar{P}^{l}_{out} \leq \epsilon$, where $\bar{P}^{l-1}_{out}$ and $\bar{P}^{l}_{out}$ are the outage probability obtained at $(l-1)^{th}$ and l^{th} iterations, respectively, and ϵ is the pre-defined tolerance threshold.

Next, we propose a ϵ-globally optimal solution where the obtained solution lies in the ϵ-neighbourhood of the globally optimal solution. In this, we first obtain the conditional convexity of $\bar{P}_{out}$. Thereafter, we apply steepest descent in the convex region and linear search in the non-convex region to obtain a low-complexity solution. In the following, we provide the region over which the function is convex.

Lemma 5. *The region over which $\bar{P}_{out}$ is jointly convex in x, y, and z is given by $\mathcal{R}_C$, where $\mathcal{R}_C$ is defined in* (A.2.13).

Proof. See Appendix A.2.3. □

Thus, the problem (P3) is convex in region $\mathcal{R}_C$ and non-convex in region $\mathcal{R}_{NC} = \mathcal{R}/\mathcal{R}_C$, where $\mathcal{R}$ is the region defined by $-r \leq x \leq r$, $-r \leq y \leq r$, and $H_{min} \leq z \leq H_{max}$. Then first, by applying steepest descent in $\mathcal{R}_C$ with acceptable tolerance ϵ and later using linear search in $\mathcal{R}_{NC}$ by taking step size ϵ, we can obtain two optimal solutions within an acceptable tolerance ϵ. Best among the two solutions is termed as ϵ-globally optimal solution for which $\bar{P}_{out}$ is minimum. Algorithm 5 describes the steps to obtain the ϵ-globally optimal solution $\mathcal{X}^*$ for (P3).

4.4.2 UAV Trajectory without Energy and Velocity Constraint

The solution to (P3) is called the *vertex* ($\mathcal{X}^*$) represents the solution obtained by using Algorithm 4 or Algorithm 5. Then, the path traced by the UAV in travelling from the

initial ($\mathbf{X}_I$) to $\mathcal{X}^*$ and then to the final location ($\mathbf{X}_F$) while hovering at $\mathcal{X}^*$ for all $n \in \mathcal{N}\backslash\{N\}$ is defined as the optimal path of (P2) when (4.4a) and (4.4d) are relaxed.

The UAV velocity V_{opt} is obtained for the slot over which the distance travelled by UAV is maximum which is given by

$$V_{opt} = \max\left\{\frac{\|(\mathrm{x^F}, \mathrm{y^F}, \mathrm{z^F}) - \mathcal{X}^*\|}{\tau}, \frac{\|(\mathrm{x^I}, \mathrm{y^I}, \mathrm{z^I}) - \mathcal{X}^*\|}{\tau}\right\}. \tag{4.6}$$

4.4.3 Proposed Vertex Approach

As seen earlier, the optimal trajectory when the energy and velocity constraints are relaxed consists of only three distinct locations - the initial, the *vertex*, and the final locations, where for all $m \in \mathcal{N}\backslash\{N\}$ slots, the UAV hovers at the *vertex*. The presence of on-board energy (4.4a) and velocity (4.4d) constraints will restrict the UAV to reach the *vertex* $\mathcal{X}^*$ in a single time slot.

At the *vertex* $\mathcal{X}^*$, the average outage probability is minimum. Our objective is to reach this *vertex* as quickly as possible and stay there for longer time periods to minimize the average outage. In case, due to insufficient on-board energy or low velocity, if the UAV cannot reach the *vertex*, then it should at least approach the *vertex* while transiting towards the final location. This implies that the UAV will move with velocity V_{max} in this approach.

Assuming that the sufficient energy is available with the UAV, whenever $V_{max} \geq V_{opt}$ in (4.4d), with V_{opt} defined in (4.6), the velocity constraint will not affect the trajectory. This is because the UAV can still reach the *vertex* $\mathcal{X}^*$ in a single time slot. Then, V_{opt} can be treated as upper bound on the velocity. However, if $V_{max} < V_{opt}$, the UAV will first move in the direction of $\mathcal{X}^*$ and then towards the final location. This implies the UAV now takes multiple time slots to reach $\mathcal{X}^*$. As a result, the UAV path consists of many locations while travelling towards $\mathcal{X}^*$ and then towards the final location. Here, the outage at all other locations will be higher than $\mathcal{X}^*$. Therefore, $\widehat{P}_{avg}$ in this case will always be higher than that obtained when energy and velocity constraints are relaxed. Therefore, the $\widehat{P}_{avg}$ obtained in (P2) while relaxing (4.4a) and (4.4d) is defined as the asymptotic outage of $\widehat{P}_{avg}$.

To obtain the solution of (P2) *i.e.,* while considering the on-board energy consumption, we present Algorithm 6. The steps involved in Algorithm 6 are as follows

Algorithm 6 *Vertex approach* to obtain solution of (P2)

Input: $(\mathrm{x^I}, \mathrm{y^I}, \mathrm{z^I})$, $(\mathrm{x^F}, \mathrm{y^F}, \mathrm{z^F})$, K, N, V_{max}, $(x_k, y_k), \forall k \in \mathcal{K}$, E_{max}, τ, and ϵ.
Output: $\widehat{P}^*_{avg}$ with optimal $x^*[n]$, $y^*[n]$, and $z^*[n], \forall n \in \mathcal{N}$.

1: Find the *vertex* $\mathcal{X}^*$ using Algorithm 4 or 5.
2: **if** $\mathrm{z^I} < H_{min}$ **then**
3: UAV flies vertically up with V_{max} for $N_I = \left\lceil \frac{H_{min} - \mathrm{z^I}}{\tau V_{max}} \right\rceil$ time slots. Set $\bar{z}_I \triangleq z[N_I] = \mathrm{z^I} + N_I \tau V_{max}$ and $\mathcal{E}_I \triangleq N_I \mathcal{E}(V_{max})$ be the energy to reach $\bar{z}_I$. Calculate $\widehat{P}^k_{out}[n]$ using (4.5), $\forall n \in \{1, \cdots, N_I\}$.
4: **else**
5: Set $\bar{z}_I = \mathrm{z^I}$ and $N_I = \mathcal{E}_I = 0$.
6: Initially, set $v_{allow} = V_{max}$ and assuming there is sufficient energy available.
7: Calculate $N_1 = \left\lceil \frac{\|(\mathrm{x^I}, \mathrm{y^I}, \bar{z}_I) - \mathcal{X}^*\|}{\tau V_{allow}} \right\rceil$ and $N_2 = \left\lceil \frac{\|\mathcal{X}^* - (\mathrm{x^F}, \mathrm{y^F}, \mathrm{z^F})\|}{\tau V_{allow}} \right\rceil$. Set $N_v = N_1 + N_2$.
8: **if** $N_v \leq N - N_I$ **then**
9: Make a straight line from $(\mathrm{x^I}, \mathrm{y^I}, \bar{z}_I)$ to $\mathcal{X}^*$ and from $\mathcal{X}^*$ to $(\mathrm{x^F}, \mathrm{y^F}, \mathrm{z^F})$ each containing N_1 and N_2 locations, respectively. For $N - N_I - N_v$ time slots, the UAV will stay at $\mathcal{X}^*$.
10: Set the obtained locations as solution *i.e.,* $(x^*[n], y^*[n], z^*[n])$, $\forall n \in \{N_I + 1, \cdots, N\}$, and obtain $\widehat{P}^*_{avg} \triangleq \frac{1}{NK} \sum_{n=1}^{N} \sum_{k=1}^{K} \widehat{P}^k_{out}[n]$ by calculating $\widehat{P}^k_{out}[n]$ using (4.5).
11: **else**
12: Solve optimization problem (4.7), where Q passes through a location in a line segment drawn perpendicular to the straight flight trajectory from the $\mathcal{X}^*$.
13: Repeat step 7 and step 9 with Q instead of $\mathcal{X}^*$ to obtain trajectory and calculate $\widehat{P}^*_{avg}$ using step 10.
14: Calculate $v[n]$ and then $e[n], \forall n \in \{N_I + 1, \cdots, N\}$, using (4.1) and (2.2), respectively. Then, calculate $\mathcal{E}_h = \sum_{n=N_I+1}^{N} e[n]$.
15: **if** $\mathcal{E}_h + \mathcal{E}_I \leq E_{max}$ **then**
16: The obtained is feasible and is the proposed *vertex* solution.
17: **else**
18: Find percentage energy decrease: $\mathcal{E}_R = \left(\frac{\mathcal{E}_h + \mathcal{E}_I - E_{max}}{\mathcal{E}_h + \mathcal{E}_I} \right) \times 100$.
19: Find $\mathcal{E}(v_{allow})$ by substituting $v[n] = v_{allow}$ into (2.2).
20: Obtain new energy per slot: $\mathcal{E}_N = \mathcal{E}(v_{allow}) - [(\mathcal{E}_R/100) \times \mathcal{E}(v_{allow})]$.
21: Solve equation (2.2) *i.e.,* $\mathcal{E}(v[n]) = \mathcal{E}_N$ for $v[n]$. Denote the roots as: $\mathcal{V}_1$ and $\mathcal{V}_2$. Set $v_{allow} = \max\{\mathcal{V}_1, \mathcal{V}_2\}$.
22: **while** $\mathcal{E}_R > 0$ **do**
23: Repeat steps 7 to 22 with v_{allow} and set the solution.

Initial Check on $\mathrm{z^I}$

Whenever $\mathrm{z}_0 < H_{min}$, we constrained the UAV to move vertically in z-direction until minimum height H_{min} is achieved. Thus, if $\mathrm{z^I} < H_{min}$, the UAV will take $N_I = \left\lceil \frac{H_{min} - \mathrm{z^I}}{\tau V_{max}} \right\rceil$ slots to reach a $z[N_I] = \mathrm{z^I} + \tau N_I V_{max}$. Beyond this, the UAV can make horizontal movement. Let $\bar{z}_I \triangleq z[N_I] = \mathrm{z^I} + N_I \tau V_{max}$, and $\mathcal{E}_I \triangleq N_I \mathcal{E}(V_{max})$ be the energy required to reach $\bar{z}_I$, where $\mathcal{E}(V_{max})$ is calculated using (2.2) with $v[n] = V_{max}$.

Time Constrained Trajectory

While we relax the energy constraint, the UAV moves with velocity V_{max} first to reach the *vertex* and then to the final location. The minimum time taken to reach the final location is $N_v = \left\lceil \frac{\|(\mathrm{x^I},\mathrm{y^I},\bar{z}_I)-\mathcal{X}^*\|}{\tau V_{max}} \right\rceil + \left\lceil \frac{\|\mathcal{X}^*-(\mathrm{x^F},\mathrm{y^F},\mathrm{z^F})\|}{\tau V_{max}} \right\rceil$. If the UAV cannot reach the final location in the stipulated time, then to reduce its flight time, the UAV takes a shorter path closer to the straight-line path as shown in Figure 4.2. We draw a perpendicular from the *vertex* to the shortest path. The UAV passes through one of the locations through this perpendicular such that it passes through a point close to the *vertex* and the time taken by the UAV is equal to N. This point Q as shown in Figure 4.2 can be obtained by solving the following optimization problem

$$\begin{aligned} &\min_{Q} \quad \|Q-\mathcal{X}^*\| \\ &s.t. \left\lceil \frac{\|Q-\bar{\mathbf{X}}_I\|}{\tau V_{max}} \right\rceil + \left\lceil \frac{\|Q-\mathbf{X}_F\|}{\tau V_{max}} \right\rceil + \left\lceil \frac{\|\bar{\mathbf{X}}_I-\mathbf{X}_I\|}{\tau V_{max}} \right\rceil \leq N, \end{aligned} \tag{4.7}$$

where $\bar{\mathbf{X}}_I = (\mathrm{x^I}, \mathrm{y^I}, \bar{z}_I)$. This part is described in Step 6-13 of Algorithm 6.

Time and Energy Constrained Trajectory

After obtaining the UAV trajectory with given velocity, we compute the total energy consumed by the UAV in travelling from the initial $\bar{\mathbf{X}}_I \triangleq (\mathrm{x^I}, \mathrm{y^I}, \bar{z}_I)$ to the final location using $\mathcal{E}_h \triangleq \sum_{n=N_I+1}^{N} e[n]$, with $e[n]$ defined in (2.2). If the energy consumed by the UAV is lesser than the total on-board energy available *i.e.,* $\mathcal{E}_h + \mathcal{E}_I \leq E_{max}$, then the obtained solution is feasible and this is our final *vertex* solution. However, if $\mathcal{E}_h + \mathcal{E}_I > E_{max}$, we compute a new velocity, to meet the energy consumption constraint. This is done by calculating the percentage energy to be decreased from each slot to get the new energy requirement as described in Step 18 *i.e.,* $\mathcal{E}_R = \left(\frac{\mathcal{E}_h+\mathcal{E}_I-E_{max}}{\mathcal{E}_h+\mathcal{E}_I}\right) \times 100$. This new energy requirement will result in the new maximum allowed UAV velocity denoted by v_{allow}, which is obtained by solving (2.2) for $v[n]$. After computing v_{allow}, the UAV now travels with v_{allow} instead of V_{max}. With this new v_{allow}, we again compute trajectory using Step 7-13 of Algorithm 6. Then with this new trajectory and velocity, we compute the energy consumed and iterate to meet the energy as well as time requirements. Therefore, v_{allow} is a result of the trade-off between constraints (4.4a) and (4.4d). Finally, the algorithm returns the greedy solution of (P2).

Remark 1. *The implementation of the Algorithm 6 is based on the fact that the users' location is known to the UAV. However, when the users location/mobility is unknown,*

various estimation methodologies must be used to aware the UAV with the locations of the ground users.

4.4.4 Complexity Analysis

In this sub-section, we discuss the computational complexity of the *vertex approach*. First, we obtain the computations in obtaining the *vertex* location using Algorithm 4 and 5. Thereafter, we state the complexity of the proposed *vertex approach*.

Alternating Optimization: Algorithm 4 presents the solution to problem (P3) using alternating optimization. The algorithm gives the alternating optimization sequence until $(\bar{P}_{out}^{l-1} - \bar{P}_{out}^{l}) \leq \epsilon$. It works iteratively by applying 2D GSS followed by 1D GSS in every iteration. In GSS, the search spaces $\Delta x = (x^{ub} - x^{lb})$, $\Delta y = (y^{ub} - y^{lb})$, and $\Delta z = (z^{ub} - z^{lb})$ reduces by a factor of 0.618 in each iteration. $\mathcal{X}^{lb}$ and $\mathcal{X}^{ub}$ denote the lower and upper bounds on variable $\mathcal{X} \in \{x, y, z\}$, respectively. Values of the bounds are set as $x^{lb} = y^{lb} = -r, z^{lb} = H_{min}$, and $x^{ub} = y^{ub} = r$, $z^{ub} = H_{max}$. Let L_l represents the average number of executions, then the number of iterations are given as $L_{itr} = 2L_l \left(\ln \left(\frac{\max\{\Delta x, \Delta y\}}{\epsilon} \right) + \ln \left(\frac{\Delta z}{\epsilon} \right) \right)$, where the first and the second term are the iterations involved in step 3 and step 5 of Algorithm 4, respectively.

ϵ-globally optimal solution: Algorithm 5 presents the solution to problem (P3). The algorithm first computes the convex region using (A.2.13) and then apply steepest descent in the convex region and linear search in the non-convex region. The steepest descent can take $\mathcal{O}\left(\epsilon^{-2}\right)$ iterations to find an iterate where the Euclidean norm of the gradient is lesser than a pre-defined tolerance [80]. The worst-case complexity of Algorithm 5 when no convex regions are found is given by $\mathcal{O}(L^3)$, where L represents the set of x, y, and z. Then the number of iterations are given as $L_{itr} = \mathcal{O}\left(\epsilon^{-2}\right)\mathcal{O}(L^3)$.

Proposed vertex approach: Algorithm 6 finds the solution to (P2) using the greedy algorithm. The number of iterations involved in Algorithm 6 while ignoring Step 1 depends upon obtaining the velocity v_{allow} that satisfies the energy constraint. Let L_e denote the iteration count. Then, the overall iterations involved in the *vertex approach* is given by $L_{itr} + L_e$, where L_{itr} is for ϵ-globally optimal solution or alternating optimization.

The numerical value obtained for L_e is described in Section 4.6.1. The term low-complexity used for the *vertex approach* will be verified when we discuss the average number of iterations involved in proposed approaches in Section 4.6.1.

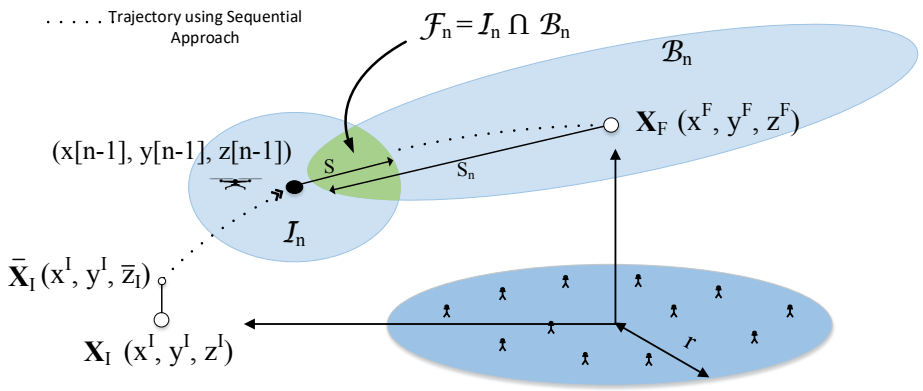

Figure 4.3: UAV 3D trajectory design under *sequential approach*.

4.5 Sequential Approach: Proposed Solution II

4.5.1 Proposed Sequential Approach

Intuitively, whenever the UAV is away from the coverage field, to achieve low outage or better LoS link, the UAV has to make large upward movement. In the *vertex approach*, the greedy solution to (P2) does not guarantee an optimal trajectory. Thus, to obtain a better trajectory, in this section, we propose a *sequential approach*. Unlike *vertex approach* that travels in a single direction towards the *vertex*, the *sequential approach* searches for an optimal location in each slot sequentially to reach the final location by keeping in view the velocity constraint. Thereafter, the energy constraint is met in the same way as in *vertex approach*. Note that, as seen in *vertex approach*, if $z^I < H_{min}$, then UAV will make vertical movement to $\bar{z}_I$ as shown in Section 4.4.3.

The reach of the UAV in each slot depends upon its location in the previous slot, since it is constrained by velocity. We adopt a heuristic approach where the UAV starts with the initial location and moves to an optimal new location in the next slot. Similarly, the UAV moves in further slots until the $(N-1)^{th}$-time slot. In this way, we sequentially obtain the optimal points in each slot to determine the UAV trajectory.

To find the optimal location in the n^{th}-time slot, we first determine the region where the UAV should move to. To determine this, we first define the reachable region of the UAV within a slot from the $(n-1)^{th}$-time slot as $\mathcal{I}_n$. Here $\mathcal{I}_n$ is a sphere of radius $S = \tau V_{max}$. Similarly, $\mathcal{B}_n$ defines the region from which the final location is reachable in $(N-n)$ time slots. So, $\mathcal{B}_n$ is a sphere of radius $S_n = \tau(N-n)V_{max}$, centered at the final location. The regions $\mathcal{I}_n$ and $\mathcal{B}_n$ are shown in Figure 4.3. Then, the feasible region for

Algorithm 7 *Sequential approach* to obtain solution of (P2)

Input: $(\mathrm{x^I}, \mathrm{y^I}, \mathrm{z^I})$, $(\mathrm{x^F}, \mathrm{y^F}, \mathrm{z^F})$, K, N, V_{max}, $(x_k, y_k), \forall k \in \mathcal{K}$, E_{max}, τ, $\mathcal{R}_C$ and ϵ.
Output: $\widehat{P}^*_{avg}$ with optimal $x^*[n]$, $y^*[n]$, and $z^*[n], \forall n \in \mathcal{N}$.

1: Repeat steps 2 to 5 of Algorithm 6 to find $\bar{z}_I$, N_I, and $\mathcal{E}_I$ and calculate $\bar{P}_{out}[n] \triangleq \frac{1}{K}\sum_{k=1}^{K} \widehat{P}^k_{out}[n]$, $\forall n \in \{1, \cdots, N_I\}$, with $\widehat{P}^k_{out}[n]$ defined in (4.5).
2: Let $\mathcal{X}_0 = (\mathrm{x^I}, \mathrm{y^I}, \bar{z}_I)$, $\mathcal{X}_F = (\mathrm{x^F}, \mathrm{y^F}, \mathrm{z^F})$, and set $v_{allow} = V_{max}$.
3: **for** $n = N_I + 1 : N - 1$ **do**
4: Set $S = v_{allow}\tau$ and make a sphere of radius S centered at $\mathcal{X}_0$ and denote the region as $\mathcal{I}_n$.
5: Set $S_n = v_{allow}(N-n)\tau$ and make a sphere of radius S_n centered at $\mathcal{X}_F$ and denote it by $\mathcal{B}_n$.
6: Find $\mathcal{F}_n = \mathcal{I}_n \bigcap \mathcal{B}_n$.
7: Calculate $\mathcal{R}_1 = \mathcal{F}_n \bigcap \mathcal{R}_C$ and $\mathcal{R}_2 = \mathcal{F}_n / \mathcal{R}_1$.
8: Let $\mathcal{X}[n] = (x[n], y[n], z[n])$. For $\mathcal{R}_1$, compute $\mathcal{X}^*_1[n] = arg \min_{\mathcal{X}[n]} \bar{P}_{out}[n] \triangleq \frac{1}{K}\sum_{k=1}^{K} \widehat{P}^k_{out}[n]$, using GSS with ϵ.
9: Evaluate $\mathcal{X}^*_2[n] = arg \min_{\mathcal{X}[n]} \bar{P}_{out}[n]$ using linear search over the region $\mathcal{R}_2$ by keeping step size ϵ.
10: Obtain $\mathcal{X}^*[n] = arg \min_{\mathcal{X}^*_j[n]} \bar{P}_{out}[n]$ for $j \in \{1, 2\}$.
11: Update $\mathcal{X}_0 = \mathcal{X}^*[n]$ and set $\bar{P}^*_{out}[n] = \bar{P}_{out}[n]$.
12: Calculate $\widehat{P}^*_{avg} = \frac{1}{N}\sum_{n=1}^{N} \bar{P}^*_{out}[n]$.
13: Repeat steps 14-21 of Algorithm 6 to update v_{allow} and find $\mathcal{E}_R$.
14: **while** $\mathcal{E}_R > 0$ **do**
15: Repeat steps 3 to 13 with v_{allow} and find the solution.

the UAV to move to in the n^{th}-time slot is given by $\mathcal{F}_n = \mathcal{I}_n \bigcap \mathcal{B}_n$. Therefore, instead of the entire region $\mathcal{I}_n$, the optimal location in each time slot is searched in region $\mathcal{F}_n$. To obtain the optimal location in $\mathcal{F}_n$, we identify the regions in $\mathcal{F}_n$, where the function is convex/non-convex and then use the search methods to obtain the next slot location to move to. The region over which the function is convex can be computed using (A.2.13) as described in Lemma 5.

Therefore, in $\mathcal{F}_n$, the convex region is given by $\mathcal{R}_C \bigcap \mathcal{F}_n$ ($\mathcal{R}_C$ is defined in (A.2.13)), while the non-convex region is given by $\mathcal{F}_n / (\mathcal{R}_C \bigcap \mathcal{F}_n)$. In the convex region, we use faster search technique like GSS [58] while in the non-convex region, we obtain the optimal point using linear search with ϵ-tolerance to find the minima in the specified interval. In each iteration, two solutions are obtained, one corresponding to the GSS applied over convex region and other corresponding to the linear search over non-convex region. The minimum among the two is chosen as the solution for the n^{th}-time slot.

The steps describing the *sequential approach* are defined in Algorithm 7. On-board energy (4.4a) and velocity (4.4d) constraints in (P2) are satisfied using the same concept as discussed in Section 4.4.3. Flight duration constraint is automatically met as the search area is restricted to $\mathcal{F}_n = \mathcal{I}_n \bigcap \mathcal{B}_n$.

Table 4.2: System Parameters Considered for Simulations

Parameter	Symbol	Value
Reference, threshold SNR	$\tilde{\gamma}_o$, γ_{th}	52.5 dB, −3.01 dB
Environment parameters	C, D	10, 0.6
Additional attenuation factor	κ	0.2
Pathloss exponent	$\bar{\alpha}$	2.3
Blade profile, induced power	P_o, P_i	79.86 W, 88.63 W
Tip of rotor blade	$U_{tip} = \Omega R_{en}$	120
Fuselag drag ratio	D_{en}	0.6
Fuselag equipment plate area	S_{en}	0.0151 m^2
Mean rotor induced velocity	v_o	4.01 m/s
Air density	ρ	1.225 kg/m^3
Rotor disc area	A_{en}	0.503 m^2
Aircraft's weight	W_{en}	20 N

Remark 2. *In contrast to the vertex approach, where the UAV follows a single direction to reach the vertex location, the sequential approach follows a more accurate path that leads the UAV into a region with low outage in minimum possible time. This happens because the increase in the computation of UAV locations in the sequential approach will enable it to find the optimal location in every slot while reaching the vertex location. However, in the sequential approach, if we constrain the UAV to move in one particular direction, the obtained location will overlap with the vertex location in the vertex approach. Thus, the vertex approach can be viewed as a subset of the sequential approach.*

4.5.2 Complexity Analysis

In the *sequential approach*, the sub-optimal solution is achieved sequentially by obtaining the optimal location in each time slot. As discussed in Algorithm 7, in each iteration to obtain the optimal location, the 3D GSS is applied on convex region and linear search on the non-convex region for $N-1$ time slots. In 3D GSS, the search spaces $\Delta x = (x^{ub} - x^{lb})$, $\Delta y = (y^{ub} - y^{lb})$, and $\Delta z = (z^{ub} - z^{lb})$ reduces by a factor of 0.618 in each iteration [81]. $\mathcal{X}^{lb}$ and $\mathcal{X}^{ub}$ denote the lower and upper bounds on variable $\mathcal{X} \in \{x, y, z\}$, respectively. Let L_{fe} denote the number of iterations to compute v_{allow}. Then, the overall number of iterations involved in Algorithm 7 is given by $2L_f L_{fe}\left(\ln\left(\frac{\max\{\Delta x, \Delta y, \Delta z\}}{\epsilon}\right)\right)$, where $L_f = N - 1$. In Section 4.6, we provide the numerical values of L_{fe}.

4.6 Simulation Results

In this section, we present the 3D UAV trajectory and its performance for the proposed strategies and compare it with the benchmark schemes. We consider a setup with 10

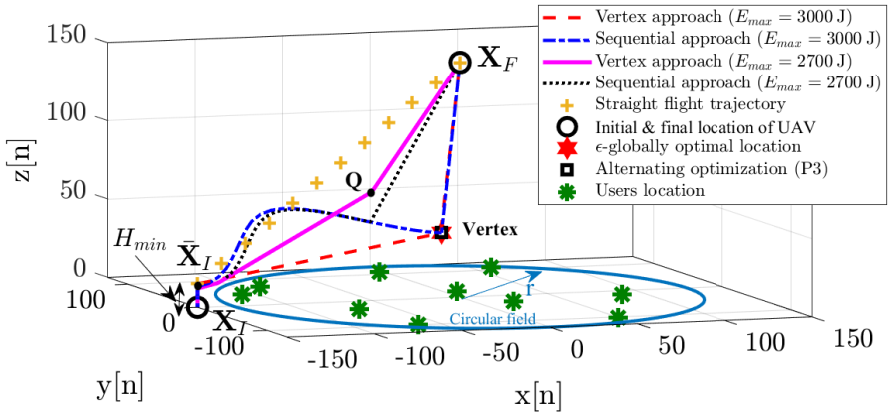

Figure 4.4: Insights on sub-optimal trajectories of UAV.

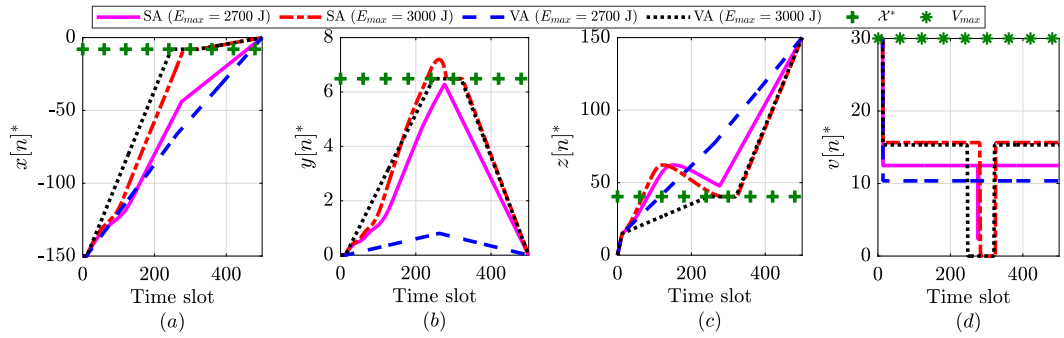

Figure 4.5: Variation of (a) $x[n]^*$, (b) $y[n]^*$, (c) $z[n]^*$, and (d) $v[n]^*$ with number of time slots for different values of energy availability constraint, E_{max}. SA and VA are *sequential* and *vertex approach*, respectively.

ground users [73], randomly distributed in a circle of radius 120 m, centered at origin. The UAV is assumed to fly from the initial location $(-150, 0, 0)$ m to the final location $(0, 0, 150)$ m. The system parameters taken for simulations are listed in Table 4.2.

4.6.1 Trajectory Design Insights

Through Figure 4.4, we provide insights into the 3D UAV trajectory. It is plotted for both *vertex* and *sequential approaches* with $V_{max} = 30$ m/s, $T = 20$ s, $N = 500$, and $H_{min} = 15$ m for different values of $E_{max} = \{3000, 2700\}$ J. Along with the proposed trajectories from *vertex* and *sequential approaches*, the *vertex* point obtained using ϵ-globally optimal algorithm and alternating optimization approach. It can be observed that the solution obtained from alternating optimization almost converges to the ϵ-globally optimal solution, thus it can be inferred that the low-complexity alternating optimization approach can be applied to obtain a *vertex* point. As shown in the Figure 4.4, for *vertex approach* with $E_{max} = 3000$ J, the UAV first travels towards the *vertex* and then travels to the final location in a straight line with velocity V_{max} while hovering at the *vertex*. For the

sequential approach, it first attains some height and then reaches the location with the minimum average outage probability. This is because it does not follow *vertex* location but instead searches the best location with minimum average outage probability in each time slot sequentially. On the other hand, when $E_{max} = 2700$ J, for *vertex approach*, due to less energy available, UAV cannot reach the *vertex*. Thus, it tries to approach the *vertex* by passing through point Q depending upon the energy available. Also, it can be seen that UAV initially moves vertically to point $\bar{\mathbf{X}}_I$ to attain a minimum height H_{min} as defined in Section 4.4.3.

In the *vertex approach*, to obtain v_{allow}, the average number of iteration L_e counts to 12. On the other hand, in the *sequential approach*, the average number of iterations counted for L_{fe} and L_f is 9 and 49, respectively. Further, to analyze the complexity of both approaches, we use Matlab on an Intel Core $i7$ processor with a 3.20 GHz CPU clock to perform simulations. We consider the UAV maximum velocity as $V_{max} = 30$ m/s, total flight time as $T = 20$ s which is discretized in $N = 50$ time slots and total on-bard energy availability as $E_{max} = 4000$ J. The total execution time to obtain the UAV trajectory using the *vertex approach* is approximately 12.4 s, whereas, the *sequential approach* took around 45.6 s to optimize the trajectory. This difference increases further when the number of time slots N increases. Hence, we conclude that the *vertex approach* gives a low-complexity solution compared to the *sequential approach*. The performance comparison of both approaches will be studied in the next sub-section.

To gain further insights into the UAV trajectory obtained using the proposed approaches, we plot Figure 4.5 to show how the optimal $x[n]^*$, $y[n]^*$, $z[n]^*$, and $v[n]^*$ of UAV is changing with time. Figure 4.5(a)-(d) is plotted with respect to $E_{max} = \{2700, 3000\}$ J in (4.4a) when V_{max}, T, H_{min}, and N are set to 30 m/s, 20 s, 15 m, and 500, respectively. The presence of energy constraint restricts the UAV to fly with V_{max} and finds the new maximum allowed velocity v_{allow} at which the UAV should fly. Increasing E_{max} in constraint (4.4a), will increase v_{allow}. As a result, for both approaches, the UAV can reach the *vertex* and stay there for longer periods of time. For example, in Figure 4.5(a)-(c), when $E_{max} = 2700$ J, the UAV does not arrive at the optimal location; instead, it flies to the final location from a certain midway point near the *vertex* point. However, for $E_{max} = 3000$ J, it reaches the optimal location and stays there for some time. From Figure 4.5(d), it is observed that the UAV first travels with V_{max} in the z-direction without changing the (x, y) coordinates to satisfy (4.4c) as discussed in Section 4.4.3 and then travels with v_{allow}. Also, zero UAV velocity in Figure 4.5(d) corresponds to hovering

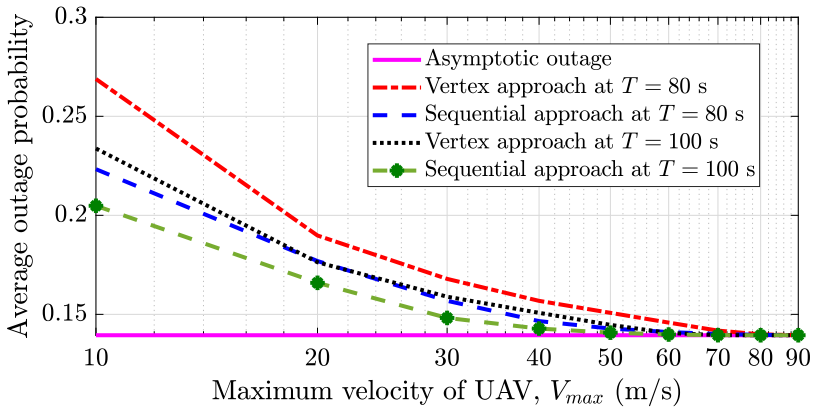

Figure 4.6: Change in average outage probability with V_{max} for different flight time T.

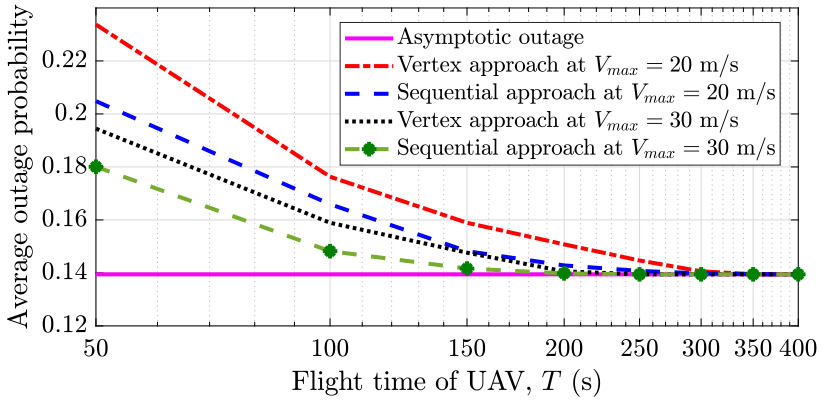

Figure 4.7: Change in average outage probability with T for different maximum velocity V_{max}.

at the *vertex* point.

4.6.2 Performance Analysis of Proposed Scheme

To understand the impact on $\widehat{P}_{avg}$ for different V_{max} and flight time T, while assuming sufficient on-board energy availability at the UAV, we plot Figure 4.6, and Figure 4.7. In Figure 4.6, $\widehat{P}_{avg}$ is plotted against V_{max} for $T = \{80, 100\}$ s. In Figure 4.7, $\widehat{P}_{avg}$ is plotted against T for $V_{max} = \{20, 30\}$ m/s. From Figure 4.5(d), we observe that the UAV flies with velocity v_{allow} in both the approaches if the on-board energy is limited. However, if sufficient on-board energy is available, the UAV flies with V_{max}. At higher velocity, UAV reaches the optimal location quickly and therefore, the outage probability is minimized. The same is applicable to flight time.

Therefore, for both higher velocity and flight time, the UAV will spend more time at the *vertex*. Since the *vertex* corresponds to the location of minimum outage probability, spending more time at *vertex* will decrease the outage probability, and it will finally

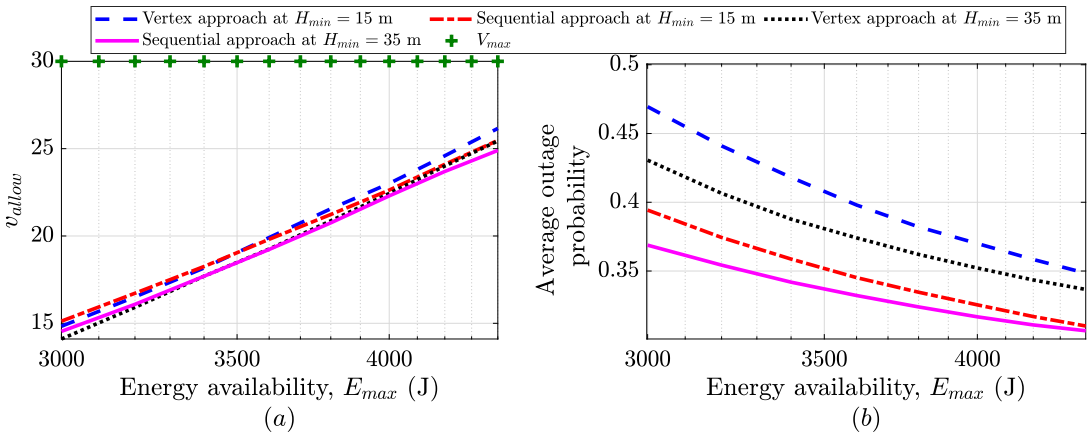

Figure 4.8: (*a*) v_{allow} of UAV due to energy constraint (4.4a) at different values of E_{max}. (*b*) Impact of E_{max} on average outage probability.

converge to the asymptotic outage of $\widehat{P}_{avg}$ in (P2). It can be observed that the *sequential approach* performs better than the *vertex approach* for any fixed value of V_{max} and T because the *sequential approach* searches the best location in every time slot instead of following the *vertex*.

From Lemma 3, we have seen that the energy consumption is a pseudoconvex function of the UAV velocity. Therefore, it will have an impact on the velocity by which the UAV should fly. Figure 4.8(a) shows how the total energy available, E_{max}, affects the UAV velocity, with $V_{max} = 30$ m/s and $T = 20$ s. We consider the case when the energy consumed by the UAV when flying at V_{max} always exceeds the energy threshold E_{max} *i.e.,* step 15 of Algorithm 6 is not satisfied for both the approaches. From Figure 4.6, we observed that more the V_{max}, lower is $\widehat{P}_{avg}$. However, increasing $V_{max} > V_0$ results in higher energy consumption, where V_0 is the velocity at which the energy consumption is minimal as obtained in (A.2.3). Hence, to obtain the minimum $\widehat{P}_{avg}$, the constraint in (4.4a) should be satisfied with equality. Because of this, there exists a trade-off in the velocity by which the UAV moves, denoted by v_{allow}. It is observed that increasing the value of E_{max} will increase v_{allow}. As we increase H_{min} for fixed E_{max}, more number of time slots are consumed to reach the minimum height H_{min}, therefore, $\mathcal{E}_I$ will increase. Certainly, the energy left for the rest of the time will decrease. As a result, to compensate the energy left for the $n \in \{N_I, \cdots, N\}$ time slots, v_{allow} will further reduce. Therefore, v_{allow} decreases as H_{min} increases.

Similarly, in Figure 4.8(b), we study the impact of E_{max} on average outage probability using the same values of V_{max} and T. The monotonic decreasing nature of $\widehat{P}_{avg}$ is desired because v_{allow} increases with an increase in E_{max} as observed from Figure 4.8(a). Thus, the UAV reaches the *vertex* quickly and spends longer time at that location, decreasing

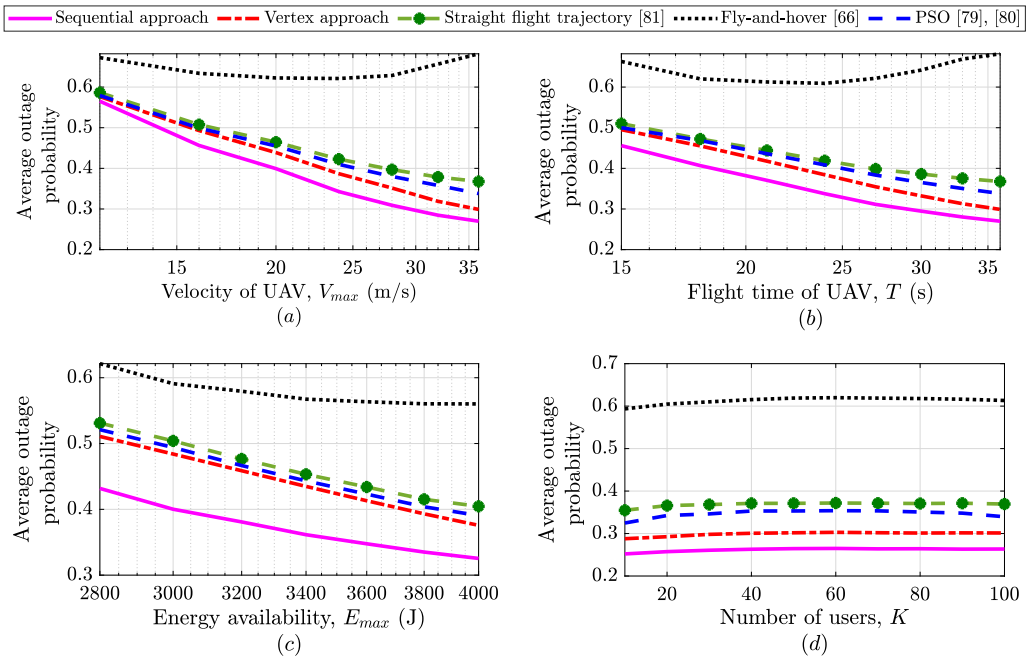

Figure 4.9: Comparison of proposed approaches with existing benchmark schemes.

$\widehat{P}_{avg}$.

4.6.3 Performance Comparison with Benchmark Schemes

To show the effectiveness of the proposed approach, in Figure 4.9(a)-(d), we compare the proposed approaches with the benchmark schemes. The approaches are compared by varying the maximum velocity V_{max}, the flight time T of the UAV, on-board energy availability E_{max}, and number of users N. Figure 4.9(a) is plotted with $T = 20$ s, $K = 10$, and $E_{max} = 6000$ J. Figure 4.9(b) is plotted with $V_{max} = 20$ m/s, $K = 10$, and $E_{max} = 6000$ J. Figure 4.9(c) is plotted with $V_{max} = 30$ s, $T = 20$ s, and $K = 10$. Figure 4.9(d) is plotted with $V_{max} = 20$ s, $T = 20$ s, and $E_{max} = 4000$ J. Minimum height H_{min} and time slots N are set to 15 m and 50, respectively, for all the sub-figures. The benchmark schemes considered for comparison are the fly-and-hover scheme [69], particle swarm optimization (PSO) [82]-[83], and straight flight trajectory [84]. In the fly-and-hover scheme, the UAV flies sequentially over the users before reaching the destination. It first computes the sequence of users to be visited to minimize the average outage probability. Following that, it obtains the UAV trajectory while keeping in view the energy consumption constraint. Thus, the horizontal coordinate (x, y) will change according to the user's location, whereas the vertical coordinate (z) of the UAV is set to the z-coordinate of the *vertex* till the UAV covers all the users. In PSO, each particle refers to a randomly initialized possible solution. The velocity and position of each particle are then updated in each iteration based on

information about the particle's prior velocity, the particle personal best, and the best position ever occupied by any particle in the swarm. On the other hand, the straight flight trajectory, as shown in Figure 4.4 is the straight-line path between the initial and final locations.

Flying over users reduces the outage probability of that particular user but does not ensure a decrease in the average outage probability for all users. Whereas in PSO, the non-convexity of the objective function obstructs the UAV to reach the *vertex* but instead travels through a high outage locations. The *vertex approach* computes the optimal location where the average outage probability over all users is minimum rather than focussing on the single user. On the other hand, *sequential approach*, computes that location in every time slot. Therefore, the two proposed trajectory designs, namely the *vertex* and *sequential approach* outperform the other schemes and achieves a minimum average outage probability. Furthermore, the trajectory obtained by the *sequential approach* achieves better performance than the *vertex approach*. On an average our proposed *vertex* and *sequential approach* provide on an average 31% and 52% improvement over the benchmark schemes, respectively.

4.7 Conclusion

In this chapter, a framework to optimize the UAV trajectory has been presented with an objective to minimize the average outage probability in a UAV-assisted 5G communication system. The UAV is constrained with both the maximum velocity and on-board energy availability. To solve this problem, we propose two trajectory optimization approaches: the *vertex* and the *sequential approach*. The *vertex approach* is based on finding an optimal location with minimum average outage probability and constructing the trajectory based on that location. On the other hand, the *sequential approach* adopts a heuristic method to obtain the trajectory by searching the best location sequentially in each time slot. This approach provides better performance at the cost of complexity when compared to the *vertex approach*. Extensive simulations show that both approaches achieve better average outage probability compared to the benchmark schemes. Besides, the optimal location obtained in the *vertex approach* could be used as a referential baseline to obtain the asymptotic outage of average outage probability while assuming the sufficient on-board energy is available with the UAV.

However, in this chapter, we consider the velocity-dependent energy consumption model of the rotary-wing UAV. In general, the energy consumed by the UAV in

manoeuvring-related tasks is determined by both the UAV's velocity and acceleration. Moreover, in cases where the UAV manoeuvring time is much larger than the UAV hovering time, the UAV accelerated related energy cannot be ignored. Therefore, for a more accurate and realistic analysis, we study the UAV's velocity, acceleration, and time profile in the next chapter while considering a more realistic energy consumption model of a rotary-wing UAV.

Chapter 5

UAV Kinematics Optimization

5.1 Introduction

For the purpose of exposition and more tractable analysis, in the previous chapters, we have ignored the acceleration/de-acceleration related UAV energy consumption. Since the UAV consumes a significant amount of energy while accelerating (as shown in Figure 2.2 of Section 2.2.2), we need to consider the velocity and acceleration related energy for more accurate analysis when designing the UAV trajectory in the presence of onboard energy constraint.

Therefore, in this chapter, we consider a scenario where the path which the UAV would take is predefined. It could be an optimized path based on maximizing some performance metric, or it could be based on certain regulatory or environmental constraints such as buildings, trees, etc., or it could be the pre-specified path through which the UAV has to move, such as air corridors. In such a case, for a given trajectory, we show how much impact the velocity-acceleration profile has on the UAV energy consumption and subsequently on network performance, and service delivery. The performance metric could be anything, depending on the scenario. Particularly, in this chapter, we consider two performance measures (1) user-centric (sum throughput) and (2) UAV-centric (energy consumption). A generalized optimization framework is presented in this chapter to account for UAV velocity and acceleration dependent energy consumption and a velocity-acceleration profile of the UAV for its optimal operation. The proposed problem is challenging since it includes multiple non-convex functions; approximations are proposed to efficiently solve this non-convex optimization problem.

5.1.1 Related Work

The related work of the UAV-enabled communication system is divided into two parts; the energy efficiency and the user throughput. To keep the literature short, we have considered only those works that takes the onboard energy as constraints.

Several techniques have been developed in the literature to improve the energy efficiency of the UAV-assisted communication system. From the rotary-wing UAV perspective, the propulsion energy model was developed in [9], and [29], where the authors minimized the energy consumption to optimize the trajectory and scheduling subject to the throughput requirement of the ground nodes. In addition, the authors in [49], and [30] considered the resource allocation apart from the UAV trajectory to maximize the energy efficiency.

The authors in [85] considered the onboard energy as a constraint to maximize the minimum throughput while optimizing the UAV trajectory, user scheduling and bandwidth allocation. However, the energy consumption model chosen was for fixed-wing UAV. Similar to [85], the authors in [86] maximized the data collection rate but considered the UAV to hover at a fixed height. Moreover, in [52], the authors minimized the completion time via optimizing the UAV trajectory, and transmit power subject to onboard energy constraints. The recent works, [73], and [74] considered the throughput as an objective to optimize the 3D UAV trajectory while considering the onboard energy constraint for a rotary-wing UAV. However, [73] assumed the UAV to fly with a fixed maximum speed, as a result, the energy consumed in a particular slot remains fixed. On the other hand, [74] considered the maximum velocity constraint but ignored the acceleration of the UAV.

5.1.2 Novelty, Motivation and Contribution

In general, the propulsion energy consumption model of a rotary-wing UAV depends upon its mobility, which is determined by the UAV's velocity-acceleration profile in horizontal and vertical directions, and the flight duration [29]. Many prior works have considered either fixed velocity of the UAV throughout its flight trajectory or they do not consider acceleration dependent energy consumption or UAV mobility constraints such as velocity and acceleration. UAV acceleration results in significant amount of energy consumption and plays a critical role in designing the trajectory of the UAV. To the best of author's knowledge, the aforementioned velocity-acceleration dependent energy model has not been considered in the prior works. Therefore, in this chapter, we consider velocity and acceleration dependent energy consumption model of a UAV and optimize the UAV velocity, and acceleration to maximize the system performance metrics. We consider two performance metrics 1) user-centered (sum throughput) and UAV-centered (energy consumption).

This work can be applied to any given UAV trajectory irrespective of the objective

chosen and the channel between the UAV and the user. From the results, we observe that when a UAV keeps the same trajectory, this approach provides significant improvement in terms of lesser energy consumption.

5.2 System Model

Based on the UAV trajectory presented in the previous works, we assume here the trajectory of a UAV going from its initial to the final location is pre-specified. This scenario can be applied in Urban Air Mobility, where the UAV moving in air corridors [87] have pre-specified waypoints through which it has to pass and move in a pre-specified air corridor. The transition of a UAV from the initial to the final location is subjected to some practical constraints, such as velocity, acceleration, onboard energy availability, etc.

As specified before, the UAV takes a predefined trajectory. The different waypoints the UAV passes through during its flight is known. As the time slot duration is variable which will be optimized later, we consider these waypoints correspond to the UAV location at different time slots. These waypoints can be at varying distances from each other. Thus, the UAV is aware of its location at each time slot denoted by $(x[n], y[n], z[n]), \forall n$.

There could be various performance metric that could be optimized for the UAV to optimally adjust its velocity-acceleration profile. For example, in a UAV-centered setting, the UAV may want to minimize its energy consumption in going from the initial to the final location. Another example could be a user-centric case, wherein, the UAV moves in such a way so that the sum-rate to all users is maximized. There could be other performance measures as well. However, in this chapter, we focus on two objectives namely, energy minimization and throughput maximization. For any other performance measures, similar technique as discussed in this work can be used.

Since the trajectory is known, sum user throughput at each UAV location (waypoint) is known. This sum user throughput at the n^{th}-time slot is obtained by using $R[n] = \sum_{k=1}^{K} \frac{B}{K} \log_2(1+\text{SNR}_k)$, where K is the total number of users, B is the available bandwidth in Hertz (Hz), and SNR is the signal-to-noise ratio. SNR_k of k^{th}-user is calculated by assuming the probabilistic LoS channel between the UAV and user. Then, overall sum throughput $\mathcal{R}$ averaged over time is given by

$$\mathcal{R} = \frac{\sum_{n=1}^{N} \tau[n] R[n]}{\sum_{n=1}^{N} \tau[n]}. \tag{5.1}$$

5.3 Problem Formulation

Our objective in this work is to minimize the UAV's total energy consumption and to maximize the overall sum throughput $\mathcal{R}$ of the system by obtaining an velocity-time profile of the UAV in going from the initial to the final location in the presence of velocity, acceleration, energy and time constraints. UAV follows a predefined trajectory wherein UAV position at different times is given as $\mathcal{X}[n] \triangleq (x[n], y[n], z[n])$. At each times, sum rate to the users is also known which is dependent on UAV locations at time slot n and is denoted by $R[n]$. From the given trajectory, the distance travelled by the UAV in the n^{th}-time slot is also known which is denoted by $d^s[n] \triangleq \|(x[n], y[n], z[n]) - (x[n-1], y[n-1], z[n-1])\|, \forall n$, where $\mathcal{X}[n]$ and $\mathcal{X}[n-1]$ represent the UAV locations. The two optimization problems formulated are given as follows.

5.3.1 Sum Throughput Maximization

In a user-centric approach, the UAV moves while providing communication service to the ground users. Here our goal is to maximize the sum user throughput by suitably adjusting the UAV velocity and acceleration. Based on UAV kinematics relations in a slot, *i.e.,* distance, velocity, acceleration and time are interlinked. Therefore, optimizing one adjusts the other. So, out of these distances in known as the waypoints or UAV location at each time slot is fixed. In this work, we attempt to optimize the velocity and time slot duration. It results in suitable change in acceleration which can be obtained from (2.6) and (2.7). The optimization problem can be formulated as (P1).

$$
\begin{aligned}
(\text{P1}): \quad & \max_{v[n],\tau[n],\forall n} \quad \frac{1}{T_{max}} \sum_{n=1}^{N} \tau[n] R[n] \\
\text{s.t.} \quad & v[n] - v[n-1] - A_{max}\tau[n] \leq 0, \forall n, && \text{(5.2a)} \\
& v[n] + v[n-1] - \frac{2d^s[n]}{\tau[n]} = 0, \forall n, && \text{(5.2b)} \\
& v[0] = 0, v[N] = 0, && \text{(5.2c)} \\
& |a[n]| \leq A_{max}, \forall n, && \text{(5.2d)} \\
& v[n] \leq V_{max}, \forall n, && \text{(5.2e)} \\
& \sum_{n=1}^{N} \tau[n] = T_{max}, && \text{(5.2f)} \\
& e_{tot} \triangleq \sum_{n=1}^{N} e_{xy}[n] + \sum_{n=1}^{N} e_z[n] \leq E_{max}. && \text{(5.2g)}
\end{aligned}
$$

(5.2a) and (5.2b) represents the constraints on the dynamics and kinematics of UAV, where $d^s[n] \triangleq \|(x[n], y[n], z[n]) - (x[n-1], y[n-1], z[n-1])\|, \forall n$, denotes the distance travelled by the UAV in the n^{th}-time slot. (5.2c) state that the initial and the final velocity of the UAV is zero. (5.2d), and (5.2e) denote the maximum acceleration and velocity constraint, respectively, where A_{max} and V_{max} represent the maximal acceleration and velocity, respectively, that a UAV can attain. T_{max} in (5.2f) denotes the total flight time of the UAV. Due to the stringent energy storage of the UAV, we have added an onboard energy constraint in (5.2g) such that the UAV reaches the final location before exhausting its given energy E_{max}.

5.3.2 Energy Minimization

Energy minimization problem is more suitable for a UAV-centric approach wherein the UAV minimizes its energy consumption in reaching to the destination while at the same time provide a minimum sum rate to all users. The energy minimization problem is formulated as

$$\begin{aligned} (\text{P2}): \quad & \min_{v[n],\tau[n],\forall n} \quad e_{tot} = \sum_{n=1}^{N} e_{xy}[n] + \sum_{n=1}^{N} e_z[n] \\ \text{s.t.} \quad & (5.2a) - (5.2f), \\ & \sum_{n=1}^{N} \tau[n] R[n] \geq R_{th}, \end{aligned} \tag{5.3a}$$

(5.3a) represents the achievable sum rate of the UAV path should be greater than the threshold rate. Here $R[n]$ is the sum throughput over all users at the n^{th}-time slot and R_{th} is the minimum rate required during its transition from the initial to the final location.

5.4 P1: Sum Throughput Maximization

5.4.1 Algorithmic Implementation of P1

Problem (P1) is difficult to solve directly due to the non-linear constraint (5.2a), non-affine constraint (5.2b) and non-convex constraint (5.2g). To tackle this issue, we first relax the energy constraint (5.2g) and solve (P1). We name this modified problem as (P1a). To solve problem (P1a), a two-stage alternating optimization is proposed. In the first stage, the time slot duration $\tau[n]$ is optimized by fixing $v[n]$. Then, in the second stage, $v[n]$ is optimized for the obtained $\tau[n]$. The two stages are solved alternatively until convergence.

Algorithm 8 Proposed approach for solving (P1)

Input: $R[n]$ (sum user throughput at each waypoint).
Output: $\tau[n]^*$ (optimized $\tau[n]$), $v[n]^*$ (optimized $v[n]$), $\forall n \in \{1, \cdots, N\}$.
1: Set $l = 0$.
2: Set $r = 0$, and initialize $v[n]^r$.
3: **repeat**
4: With given $v[n]^r$ solve (P1a) to obtain $\tau[n]^{r+1}$ by using (5.4) instead of (5.2b).
5: With given $\tau[n]^{r+1}$ solve (P1a) to obtain $v[n]^{r+1}$.
6: Set $r = r + 1$.
7: **Until** The objective function converges.
8: Calculate $v^{xy}[n]$ and $v^z[n]$, and $a^{xy}[n]$ and $a^z[n]$ using (2.4)-(2.7), respectively. Then, calculate $e^{xy}[n]$ and $e^z[n]$ defined in (2.8), and (2.9), respectively, to calculate e^l_{tot}.
9: **repeat**
10: $l = l + 1$.
11: Update constraint (5.2e) using (5.5).
12: Repeat Steps 2-13.
13: **Until** $e^l_{tot} < E_{max}$

The solution to (P1a) is checked against energy consumption constraint. If the constraint is satisfied, the solution obtained is a final solution. Otherwise, (P1a) is again executed with a modified V_{max} constraint as defined later in this section.

In the first stage, for a given $v[n]$, (5.2b) is a non-affine constraint in $\tau[n]$. To tackle this non-affine constraint, we use first-order Taylor expansion at a point $\tau_r[n]$ to make (5.2b) linear, where $\tau_r[n]$ denotes the value of $\tau[n]$ in the r^{th}-iteration. Accounting this, (5.2b) can be rewritten as

$$v[n] + v[m-1] - 2d^s[n]\left(\frac{1}{\tau_r[n]} + \frac{\tau[n] - \tau_r[n]}{\tau_r[n]^2}\right) = 0. \tag{5.4}$$

Using (5.4) in place of (5.2b) makes the problem (P1a) a linear programming problem in $\tau[n]$ for a given $v[n]$.

In the second stage, for a given $\tau[n]$ it can be observed that the problem (P1a) is a linear programming problem in $v[n]$ since constraints (5.2a) and (5.2b) are both linear in $v[n]$. Thus, to optimize $v[n]$ and $\tau[n]$ alternatively, interior point method can be used to solve (P1a). To get an initial $v[n]$ and $\tau[n]$, we assume the UAV takes maximum acceleration in the starting to reach the peak velocity V_{max} and then continue its flight.

The solution of (P1a) is checked against energy consumption constraint (5.2g). Energy consumption is computed using equations (2.8), (2.9), and using e_{tot}. If the energy consumption constraint is met, this is the final solution. Otherwise V_{max} is adjusted to reduce the overall energy consumption of the UAV. From (2.8) and (2.9), we understand that the UAV energy consumption is directly proportional to velocity and acceleration

i.e., higher the velocity/acceleration, higher the energy consumption. Therefore, we adjust V_{max} to reduce energy consumption of the UAV. The new V_{max}^{l} is defined as

$$V_{max}^{l} = \frac{E_{max}}{e_{tot}^{l-1}} \times V_{max}^{l-1}, \tag{5.5}$$

where V_{max}^{l} is the updated velocity in the l^{th}-iteration, V_{max}^{l-1} is the velocity in the previous iteration $(l-1)$, and e_{tot}^{l-1} is the energy consumption in the $(k-1)^{th}$-iteration. Algorithm 8 presents the solution to (P1).

5.4.2 Complexity and Convergence Analysis

The complexity of (P1) lies in solving (P1a) using alternating optimization and the number of iterations needed to satisfy the energy constraint in (5.2g). In alternating optimization, the time slot duration and velocity are optimized sequentially using the interior point method. Then, the complexity to optimize each variable optimally is given as $\mathcal{O}(N^{3.5}\log(1/\epsilon))$, with a given solution accuracy ϵ [88]. Accounting the alternating optimization iterations with $\log(1/\epsilon)$ of complexity, the total computational complexity of a two-stage alternating optimization is given by $\mathcal{O}(N^{3.5}\log^2(1/\epsilon))$. Let l_{max} denote the number of iterations utilized to satisfy the energy constraint. Then, the overall computations required to solve (P1) is given by $\mathcal{O}\left(l^{\max}N^{3.5}\log^2(1/\epsilon)\right)$.

Define $\mathcal{R}_{\text{P1a}}(\tau[n], v[n])$ and $\mathcal{R}^{\dagger}_{\text{P1a}}(\tau[n], v[n])$ as the value of objective function to the original problem (P1) and approximation of (P1a), respectively. Then at r^{th}-iteration, we have

$$\begin{aligned}\mathcal{R}_{\text{P1a}}(\tau[n]^r, v[n]^r) &\overset{(a)}{=} \mathcal{R}^{\dagger}_{\text{P1a}}(\tau[n]^r, v[n]^r)\\ &\overset{(b)}{\leq} \mathcal{R}^{\dagger}_{\text{P1a}}(\tau[n]^{r+1}, v[n]^r)\\ &\overset{(c)}{\leq} \mathcal{R}_{\text{P1a}}(\tau[n]^{r+1}, v[n]^r),\end{aligned} \tag{5.6}$$

where (a) holds because the first-order Taylor expansion defined in (5.4) is tight at a local point, (b) holds since the problem is solved optimally, and (c) holds since the objective function of the approximate problem is the lower bound of the original problem where we optimize $\tau[n]$ by fixing $v[n]$. Thus, (5.6) implies that even though we have considered the approximate problem to obtain the solution, the objective function defined in (P1a) is still non-decreasing after each iteration. Since the problem to optimize $v[n]$ is convex,

then accordingly we have

$$\mathcal{R}_{\text{P1a}}(\tau[n]^{r+1}, v[n]^{r}) \leq \mathcal{R}_{\text{P1a}}(\tau[n]^{r+1}, v[n]^{r+1}). \tag{5.7}$$

Based on (5.6) and (5.7), we observe that the objective value is non-decreasing after every iteration. Thus, (P1a) is guaranteed to converge. Furthermore, only convex optimization problems are solved in each iteration. Thus, it can be effectively implemented with a faster convergence.

5.5 P2: Energy Consumption Minimization

5.5.1 Algorithmic Implementation of P2

Problem (P2) is non-convex due to the non-convex objective function in $v_{xy}[n]$ and $v_z[n]$. To solve this problem, we approximate the non-convex objective function into convex and obtain an approximate solution. This is done by substituting $a_i[n] = (v_i[n] - v_i[n-1])/\tau[n], \forall i \in \{xy, z\}$ in (P2) and introducing slack variables defined as follows.

$$\mathcal{X}_1[n] \geq C_2 v_{xy}[n]^2 + C_3 \mathcal{X}_5[n], \forall n, \tag{5.8}$$

$$\mathcal{X}_2[n] \geq 0, \tag{5.9}$$

$$\mathcal{X}_2[n]^2 \leq \sqrt{1 + \mathcal{X}_1[n]^2 + C_4^2 v_{xy}[n]^4} + C_4 v_{xy}[n]^2, \forall n, \tag{5.10}$$

$$\mathcal{X}_3[n]^2 \geq v_z[n]^2 + \frac{2W_{en}}{\rho A_{en}} + \frac{2M_{en}}{\rho A_{en}} \mathcal{X}_4[n], \forall n, \tag{5.11}$$

$$\mathcal{X}_4[n] \geq \frac{v_z[n] - v_z[n-1]}{\tau[n]}, \forall n, \tag{5.12}$$

$$\mathcal{X}_5[n] \geq \frac{v_i[n]^2}{\tau[n]} - \frac{v_i[n] v_i[n-1]}{\tau[n]}, \forall i \in \{xy, z\}, \forall n. \tag{5.13}$$

The above slack variables transforms $e_{xy}[n]$ defined in (2.8) into

$$\tilde{e}_{xy}[n] = P_o(1 + C_1 v_{xy}[n]^2) + P_i \frac{1 + \mathcal{X}_1^2[n]}{\mathcal{X}_2[n]} + C_5 v_{xy}[n]^3, \tag{5.14}$$

and $e_z[n]$ defined in (2.9) into

$$\tilde{e}_z[n] = P_2 + \frac{W_{en} v_z[n]}{2} + M_{en} \mathcal{X}_5 + \frac{W_{en} \mathcal{X}_3}{2} + \frac{M_{en} \mathcal{X}_4}{2}. \tag{5.15}$$

As a result, the horizontal and vertical component of velocity-acceleration energy model as described in (2.8) and (2.9) can be equivalently represented by (5.14), (5.15) and the

variables $\mathcal{X}_j[n], \forall j \in \{1, \cdots, 5\}$ defined in (5.8)-(5.13).

Then, problem (P2) is reformulated as

$$\text{(P2e)}: \min_{\substack{v[n],\tau[n],\forall n \\ \mathcal{X}_j[n],\forall n \forall j \in \{1,2,3,4,5\}}} e_{tot} = \sum_{n=1}^{N} \tilde{e}_{xy}[n] + \sum_{n=1}^{N} \tilde{e}_z[n]$$

$$\text{s.t.} \quad (5.2\text{a}) - (5.3\text{a}), (5.8) - (5.13).$$

From (P2e), it can be observed that the objective is convex, while the constraints (5.10), (5.12), (5.13) are non-convex. To tackle these constraints, we utilize first-order Taylor expansion. Define $v_{xy,l}[n]$, $v_{z,l}[n]$, $\tau_l[n]$ to be the values of $v_{xy}[n]$, $v_z[n]$, $\tau[n]$ at the l^{th}-iteration, respectively.

To deal with constraint (5.13), on the right hand side $\frac{v_i[n]^2}{\tau[n]}$ is convex. However, $\frac{v_i[n]v_i[n-1]}{\tau[n]}$ is not concave. Then, using Taylor expansion at a point $v_{i,l}[n]$, $v_{i,l}[n-1]$, and $\tau_l[n]$, we get

$$\frac{v_i[n]v_i[m-1]}{\tau[n]} = f\left(\frac{v_{i,l}[n]v_{i,l}[m-1]}{\tau_l[n]}\right) + \begin{bmatrix} \frac{v_{i,l}[n-1]}{\tau_l[n]} \\ \frac{v_{i,l}[n]}{\tau_l[n]} \\ \frac{-v_{i,l}[n]v_{i,l}[m-1]}{\tau_l[n]^2} \end{bmatrix} \cdot \begin{bmatrix} v_i[n] - v_{i,l}[n] & v_i[m-1] - v_{i,l}[m-1] & \tau[n] - \tau_l[n] \end{bmatrix}. \tag{5.16}$$

Similarly, following the same steps, constraint (5.12) can be converted into the convex constraint.

For constraint (5.10), it can be observed that the right hand side is a convex function in $\mathcal{X}_1[n]$ and $v_{xy}[n]$. Therefore to make (5.10) a convex constraint, we use

$$\begin{aligned} &\sqrt{1 + \mathcal{X}_1[n]^2 + C_4^2 v_{xy}[n]^4} + C_4 v_{xy}[n]^2 \geq (1 + \mathcal{X}_1[n]^2 + C_4^2 v_l^{xy}[n]^4)^{-\frac{1}{2}} \\ &\times \left[\mathcal{X}_{1,l}[n](\mathcal{X}_1[n] - \mathcal{X}_{1,l}[n]) + 2C_4^2 v_{xy,l}[n]^3 (v_{xy}[n] - v_{xy,l}[n])\right] \\ &+ \sqrt{1 + \mathcal{X}_{1,l}[n]^2 + C_4^2 v_{xy,l}[n]^4} + C_4 v_{xy,l}[n]^2 + 2C_4(v_{xy}[n] - v_{xy,l}[n]) \triangleq b_{xy}^l. \end{aligned} \tag{5.17}$$

Using the transformation defined for (5.13), (5.12), (5.10), problem (P1e) can be approximated to form a convex optimization problem wherein interior point method is used to get the solution to (P2e).

Problem (P2e) can be solved iteratively using the interior point method to get the optimal solution of (P2). Algorithm 9 shows the steps to obtain the solution of problem (P2e). The initial point is obtained again by considering that the UAV takes maximum

Algorithm 9 Proposed approach to obtain solution of (P2e)

Input: $R[n]$, acceptable tolerance ϵ.
Output: $\tau[n]^*$, $v[n]^*$, $\forall n \in \{1, \cdots, N\}$.
1: Set $l = 0$, and initialize $\mathbf{X}^0$ and objective e_{tot}^0, where $\mathbf{X} = \{v[n], \tau[n], \mathcal{X}_j[n], \forall j\}$.
2: **repeat**
3: Substitute $\mathbf{X}^0$ to problem (P2e) and solve convex problem (P2e).
4: Obtain the solution $\mathbf{X}^*$ and objective e_{tot}^*.
5: Set $l = l + 1$, $\mathbf{X}^l = \mathbf{X}^*$, and $e_{tot}^l = e_{tot}^*$.
6: **Until** $|e_{tot}^l - e_{tot}^{l-1}| \leq \epsilon$.

acceleration in the starting to reach the peak velocity and then it continues its flight with V_{max}.

5.5.2 Complexity and Convergence Analysis

The computational complexity of (P2e) is determined by finding the number of iterations and the computational complexity for solving the convex optimization problem in each iteration. In each iteration, $7N$ variables are solved. Therefore, the overall complexity of (P1e) is $\mathcal{O}(r_{max}(7N)^{3.5}\log(1/\epsilon))$, where r_{max} is the number of iterations required until the solution converges. The proposed solution for solving (P2e) is guaranteed to converge. This convergence can be again proved using similar steps (ref. eq. (5.6)) as presented for earlier case.

5.6 Results and Discussion

In this section, we provide the numerical results to validate the proposed solution. From the system perspective, the initial and final location of the UAV is set to $(-150, 0, 0)$ m and $(-1, 0, 36)$ m, respectively. We consider 10 ground users distributed in a circular field of radius 120 m. The sum user rate $R[n]$ at each time slot is calculated using the probabilistic LoS channel model [9] and finally the rate is calculated using (5.1). The total flight of the UAV is taken to be $T_{max} = 15$ s, which is discretized in $N = 80$ slots. The maximum velocity and acceleration is set to $V_{max} = 20$ m/s and $A_{max} = 5$ m/s^2, respectively [89]. The total bandwidth B available for communication is set to 20 MHz. The simulation values taken for the energy model are as shown in Table 2.1, Section 2.2 [29].

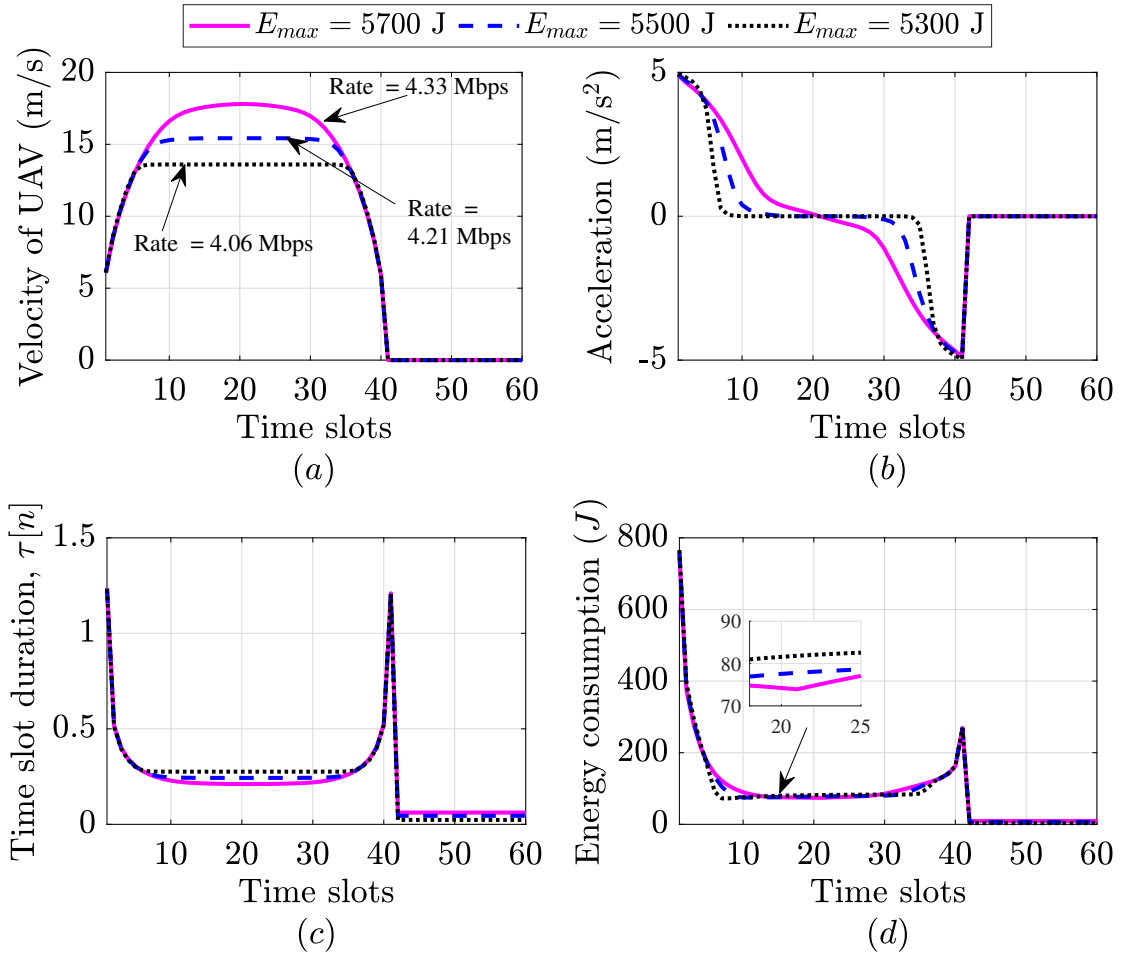

Figure 5.1: UAV dynamics with respect to sum rate maximization.

5.6.1 Sub-optimal Design Insights: Sum Throughput Maximization

For problem (P1), Fig. 5.1 provides insights on how the velocity, acceleration, and time profile varies with the change in the onboard energy availability E_{max} when a simple conventional straight flight trajectory is considered wherein UAV moves in straight line path from initial to the final location. The velocity profile shows that to maximize the system's performance, in the given trajectory, the UAV always moves with maximum velocity. This is because the final location is the optimal deployment location where the sum throughput over all ground users is maximum. In such a case, high throughput is ensured when the UAV spends more time at the locations where the sum throughput is high. Also, it can be observed that for all energy levels, the UAV first increases its velocity, accounting the acceleration constraint and later de-accelerates to reach the final location. Zero velocity indicates the UAV is hovering at the final location.

Similarly, the acceleration plot in Fig. 5.1(b) shows the acceleration profile of the UAV. It can be seen that the accelerating or de-accelerating peaks are obtained when the UAV

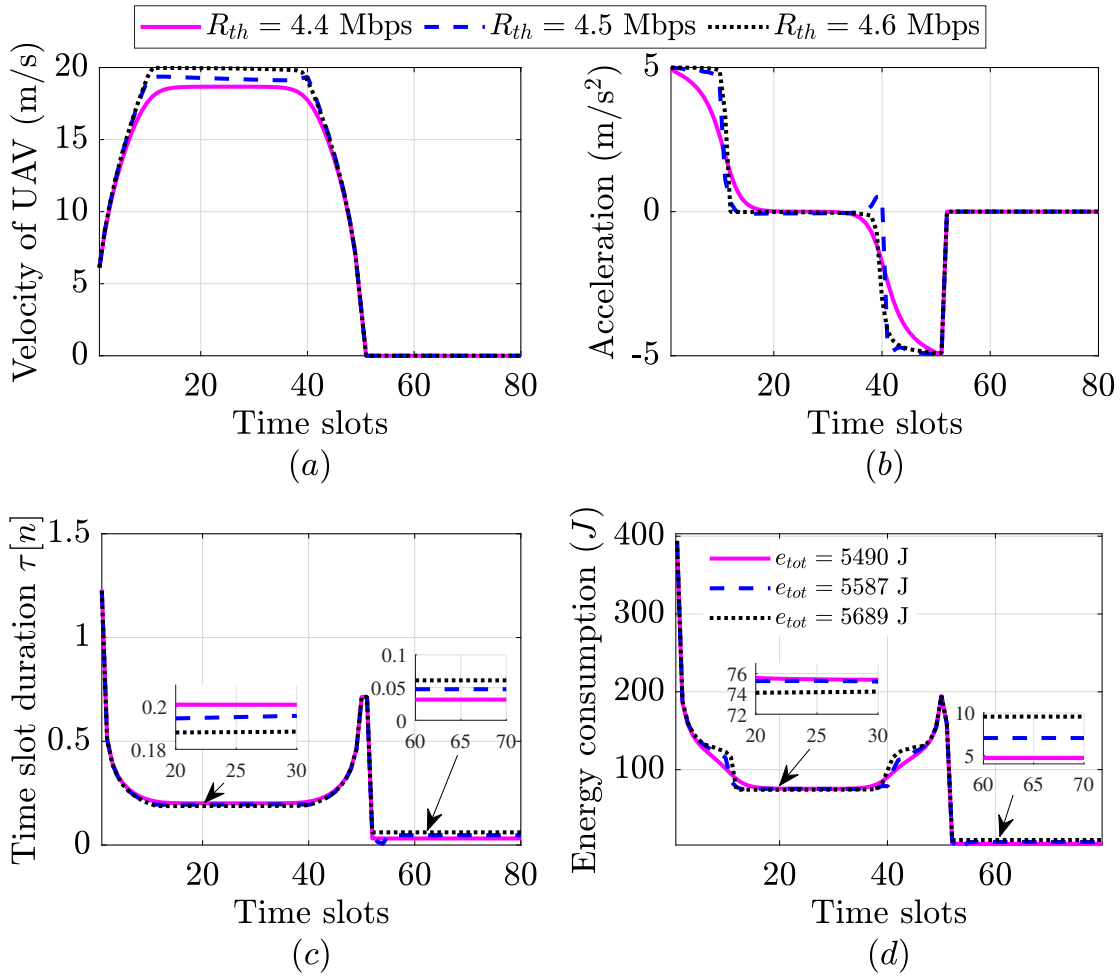

Figure 5.2: UAV dynamics with respect to energy minimization problem.

attains maximum velocity from zero velocity or decreases from maximum velocity to zero velocity at the final location. A similar explanation can also be applied to the time slot duration $\tau[n]$ plot shown in Fig. 5.1(c). The duration of time slot $\tau[n]$ depends strictly upon the total time available with the UAV *i.e.,* T_{max}. Since energy consumed in a time slot is a function of time slot duration and velocity-acceleration profile in that slot, when a peak occurs in Figs. 5.1(b)-(c), the UAV also consumes high energy.

5.6.2 Sub-optimal Design Insights: Energy Minimization

Fig. 5.2, shows the variation in UAV velocity, acceleration, time and energy consumption for different value of minimum rate threshold R_{th} defined in (5.1). Here an inverted-L shaped trajectory is considered [73] wherein the UAV first attains the height equal to z^F (z-coordinate of the final location) and then travels horizontally to reach the final location. It can be observed that as the rate requirement increases, the UAV consumes more energy in travelling from the initial to the final location. This is because the UAV

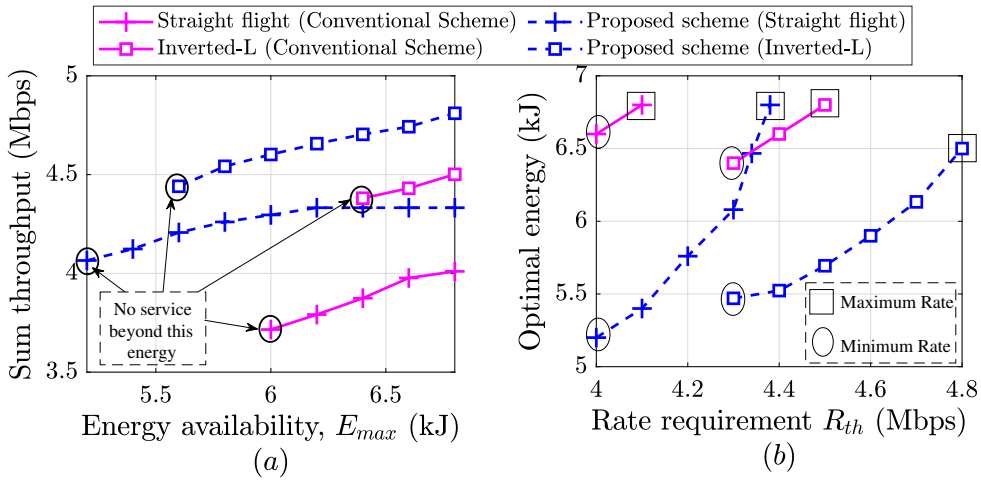

Figure 5.3: Performance of proposed scheme w.r.t. conventional schemes.

attains maximum velocity to reach the final location (as it is the optimal location to provide maximum throughput) and thus consumes more energy. However, at the optimal energy, the UAV achieves a lower data rate, which is desired as both are complementary to each other. Thus, to appropriately design the communication system there needs a trade-off between the sum throughput and the energy consumption.

5.6.3 Performance Comparison

To show the effectiveness of our proposed scheme, we compare its performance with the *simple* conventional schemes, namely, straight flight and inverted-L shaped trajectory [73]. In both the schemes, the UAV accelerates with A_{max} to reach V_{max}, and thereafter moves with constant velocity V_{max}. Finally it de-accelerates to reach the final location with $v[n] = 0$. To the best of author's knowledge, none of the prior works in literature have optimized the velocity, acceleration, and time profile. Therefore, we have considered this simple conventional scheme for comparison.

Fig. 3(a) shows the improvement in sum throughput with the variation in E_{max}, and Fig. 3(b) shows the optimal energy consumption with different minimum rate requirement R_{th}. It is observed that the proposed velocity-acceleration optimization applied over the given trajectories performs better than the conventional approach due to its ability to optimize velocity, acceleration and time in every time slot. Compared to the conventional schemes, optimizing the velocity, acceleration, and time using our proposed approach provides additional flexibility by consuming lesser energy in the pre-specified path. From Fig. 3(b), it is observed that as R_{th} increases, the UAV consumes higher energy. This is because the UAV travels with a higher velocity to provide a higher sum rate. From

results, for a user-centric applications, our proposed scheme provides 9% improvement in sum rate when UAV consumes same energy in both the proposed and conventional schemes. Similarly, UAV consumes 15% lesser energy than the conventional scheme for the same sum rate provided by both the schemes in a UAV-centric applications.

5.7 Conclusion

In this chapter, we provide a generalized framework that can be applied to any predefined trajectory and optimizes the velocity-acceleration profile to optimize a given performance metric. In this chapter, we considered two performance measures namely, sum throughput and energy consumption. Through our proposed velocity-acceleration framework, we enable the UAV to traverse the same trajectory efficiently. This is achieved in the presence of an accurate energy consumption model that depends on the velocity and acceleration of the UAV, UAV mobility, and mission completion time constraints. The problems framed are non-convex, we utilize the alternating optimization to obtain the velocity-acceleration and time profile. Simulation results demonstrate the effectiveness of the proposed approach over the conventional schemes.

Chapter 6

UAV Replacement for Coverage Continuity

6.1 Introduction

In Chapters 3-5, we studied the optimal deployment location, communication-oriented trajectory design, and the optimal velocity-acceleration and time profile for the specified UAV trajectory while considering the UAV mobility constraints and onboard energy availability constraints. In other words, the previous chapters address several UAV challenges, such as deployment location, where a UAV must be deployed to deliver fruitful service, and the UAV trajectory to maximize the system's performance when the UAV is available with limited onboard energy. Though we have efficiently designed the trajectory of the UAV, the limited energy availability is still a concern that inhibits the UAV from delivering long-term service.

To fully utilize the benefits of the UAV as an ABS, we need to find a way to provide a long-term service rather than short-term. Notably, in missions that requires long battery endurance, the battery limitation problem cannot be solved by improving the energy efficiency or energy management. As a result, for the practical implementation of UAV applications, UAV battery recharge or replacement is essential [25]. Therefore, the UAV must be grounded frequently at the charging station to replenish its battery. That is, if one UAV gets low on battery, another fully charged UAV can take its place to provide continuous coverage to the ground users. As another UAV is launched for replacement, multiple key challenges like resource allocation and multi-UAV trajectory planning must be addressed by the communication system designer in the presence of UAV energy consumption constraints.

Motivated by the UAV replacement scenario and its challenges, this chapter presents a novel framework for maintaining coverage continuity in a UAV-assisted wireless communication system by launching a fully charged UAV to replace the existing UAV,

which is low on energy. This framework includes optimizing the 3D multi-UAV trajectory and bandwidth allocation to maximize the minimum achievable data rate by the ground users in the presence on onboard energy availability constraints.

6.1.1 Related Works

In general, in UAV-assisted wireless communication system, one line of research is to minimize the UAV's energy consumption for example, [90] and another line focuses on maximizing the user's data rate while considering energy availability as a constraint. In this work, our interest lies in the latter case. Towards this end, the authors in [91] maximized the minimum user throughput by jointly optimizing the multi-UAV trajectory and power allocation, while assuming the UAV to fly at a fixed altitude. In [92], the authors considered the wireless power system with downlink and uplink with sub-time slot. First, in the downlink sub-time slot, the power is transferred from the UAV to the ground user and then, in the uplink sub-time slot, the user uploads data to the UAV. They optimized the 2D multi-UAV trajectory, scheduling and power to maximize the minimum average rate among all ground users in the presence of harvested energy constraints. The same objective was also considered in [93]. The authors in [94] maximized the number of admitted users while satisfying the rate requirement constraint and jointly optimized the bandwidth, power allocation, and multi-UAV trajectory. In the above works, [91, 92, 93], the system was designed such that in a particular time, the UAV was deployed to serve one ground user. Moreover, they have optimized the 2D trajectory of the UAV.

In [95, 96, 97], the authors optimized the 3D multi-UAV trajectory while considering the LoS-dominant channel between the UAV and the user. For dense environments, the A2G channel is prone to blockage due to the presence of high-rise buildings. Thus, considering the assumption that UAV will always remain in LoS is not true and such analysis cannot be applied to dense scenarios, where the UAV can also experience NLoS link. Thus, a more practical channel model, such as probabilistic LoS channel model where the UAV can experience LoS and NLoS link with certain probabilities needs to be considered. On the same note, the authors in [98] optimized the 3D trajectory to maximize the total downlink coverage capacity by leveraging the UAV mobility under the presence of coverage constraints. However, all the existing works [91]−[98] have not taken into account the energy consumption of the UAV.

Noting the importance of UAV's limited onboard energy, the authors in [99] considered an uplink scenario. They optimized the 3D multi-UAV trajectory when the UAV and the

Table 6.1: Key differences between the related existing literature with our work. PLoS here stands for probabilistic LoS channel.

Ref.	Objective	Design	A2G model	Bandwidth allocation	Energy constraint	Application	Fair
[91]	Max-min throughput over all users	2D	LoS	Orthogonal channels	×	UAV associates with atmost one user	✓
[92]	Max-min average rate among all users	2D	LoS	Same bandwidth	Harvested energy constraint	User uploads data to UAV: One UAV associates to atmost one user	✓
[93]	Max-min throughput over all ground users	2D	LoS	Same bandwidth	×	Each UAV serves atmost one user and vice versa	✓
[94]	Number of admitted users while satisfying requirement constraints	2D	LoS	✓	×	-	-
[95]	Improve the minimum throughput	3D	LoS	Same bandwidth	×	One UAV can associate with only one user	✓
[96]	Aggregate sum rate of the UAV	3D	LoS	Same bandwidth	×	No. of UAVs should be equal to no. of users	×
[97]	Max-min throughput among UAV-served users	3D	LoS	Same bandwidth	×	Each UAV serves up one requester	✓
[98]	Maximize the total downlink capacity	3D	PLoS	Same bandwidth	×	Downlink setup: UAV provides coverage to multiple users	×
[99]	Max-min achievable rate among all users	3D	PLoS	Orthogonal channels	✓ harvested energy constraint	User uploads data to UAV: One UAV associates to atmost one user	✓
Ours	Max-min aggregate throughput among all users over all time	3D	PLoS	✓	✓	Downlink setup: UAV provides coverage to multiple users and users can connect to multiple UAVs	✓

user experiences a probabilistic LoS channel model to maximize the minimum throughput among all the users. However, there are some limitations of their system. First, they have considered the uplink communication system, where only one user could connect to the UAV to upload the data, and each UAV can only be connected to atmost one user. Second, such a system will only ensure that the user will receive a reasonable data rate in certain time slots (time slots for which the user is connected to the UAV) but not throughout the service time. Third, they assumed that an equal bandwidth is allocated to all the users.

Considering the above limitations, the analysis done in [99] cannot be applied to the downlink communication system, where the multiple users must be served by the UAV providing sufficient data rate in every time slot and allocates bandwidth depending upon the channel conditions to further improve the user's throughput. Also, none of the works have considered the importance and need for UAV replacement when the UAV goes low on energy. Although the prior works have considered UAV's onboard energy but have not provided how continuous long-term communication can be achieved using the multiple UAVs. Thus while designing the downlink communication system, it is critical to consider the above factors.

6.1.2 Contributions and Organization

In this chapter, we consider a novel UAV replacement framework where the existing UAV low on energy is replaced by an another fully charged UAV. This is done to maintain the service continuity and provide long-term coverage to the ground users. We maximize the minimum achievable rate of the ground user during the total flight time of the UAV by jointly optimizing the 3D multi-UAV trajectory and bandwidth allocation in the presence of UAV mobility, energy consumption constraint, and the minimum rate required by the ground user at each time instant. This work is carried out by considering a realistic A2G channel model comprising both LoS and NLoS links, *i.e.,* the probabilistic LoS channel model. As per the author's knowledge, there is no related work reported in the literature for the UAV replacement problem. Thus, this work fills the lacuna in providing continuous coverage to the users using UAVs.

This setup can be applied to many practical applications such as sports events, rescue and search operations, events taking place in urban environments, etc., where temporary coverage for upto several hours is required. The key contributions of this work are as follows:

- We consider a UAV replacement framework, where the existing UAV low on energy is replaced by an another fully charged UAV.

- We formulate a joint optimization problem that jointly optimizes the UAV trajectory and resource allocation to maximize the minimum rate achievable by the user.

- The formulated problem is non-convex. We propose an alternating optimization scheme based on successive convex approximation (SCA) methods to obtain the solution.

- Numerical results are plotted to show key insights and compares the performance of proposed scheme with the benchmark schemes.

The organization of this chapter is as follows. Section 6.2 describes the communication model with multiple UAVs and describes the performance metric. Section 6.3 describes the problem statement. The solution methodology is proposed in Section 6.4, followed by the overall algorithm and complexity in Section 6.5. Section 6.6 presents the numerical results. Finally, we conclude the chapter in Section 6.7.

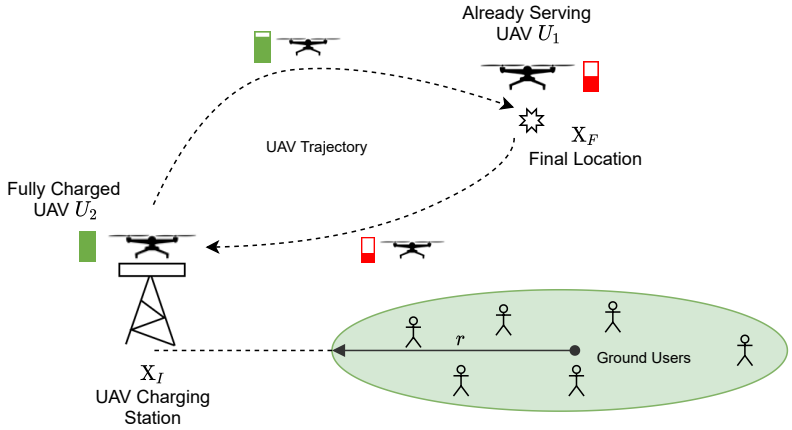

Figure 6.1: Model representing the UAV replacement framework.

6.2 System Model

6.2.1 Communication Model

We consider a UAV-assisted wireless communication system as shown in Figure 6.1 with $\mathcal{K} = \{1, \cdots, K\}$ ground users (or users) that are distributed over a circular field of radius r. Location of the k^{th}-user is given by $\mathbf{w}_k = [x_k, y_k]$, where $k \in \mathcal{K}$. The users are assumed to be stationary and their location is known. To consider the UAV replacement scenario, we consider $m \in \mathcal{M}$ UAVs, where $\mathcal{M} = \{1, 2\}$. One is the currently serving UAV, denoted by $U_1(m = 1)$ and the other one is a fully charged UAV, denoted by $U_2(m = 2)$. At the start of the replacement process, we assume that U_1 is located at the final location $\mathbf{X}_F = [\mathrm{x}^{\mathrm{F}}, \mathrm{y}^{\mathrm{F}}, \mathrm{z}^{\mathrm{F}}]$ and is serving users while U_2 is at the charging station $\mathbf{X}_I = [\mathrm{x}^{\mathrm{I}}, \mathrm{y}^{\mathrm{I}}, \mathrm{z}^{\mathrm{I}}]$ and proceeding towards $\mathbf{X}_F$ to replace U_1. Over time T, the replacement of the UAV takes place with U_2 taking position $\mathbf{X}_F$ while U_1 returning back to the launch station $\mathbf{X}_I$.

The UAV location at the n^{th}-time slot is given by $\mathbf{X}_m[n] = [\mathbf{q}_m[n], z_m[n]]$, where $m \in \{1, 2\}$, and $\mathbf{q}_m[n]$ and $z_m[n]$ are the horizontal and vertical coordinates of the m^{th}-UAV, respectively. Then, the constraint on the UAV locations with respect to time is given as

$$\mathbf{X}_1[0] = \mathbf{X}_F, \mathbf{X}_1[N_f] = \mathbf{X}_I, \mathbf{X}_2[0] = \mathbf{X}_I, \mathbf{X}_2[N] = \mathbf{X}_F. \tag{6.1}$$

The slot index $N_f \leq N$ is the number of time slots taken by the UAV U_1 to reach $\mathbf{X}_I$. Accordingly, if $N_f < N$, then after N_f time slots only UAV U_2 will provide communication to the ground users considering that the UAV U_1 has reached the charging station and has terminated its service. Note that, in our work, we consider two-UAVs for better insights but this work is also valid for more than two UAVs.

We assume the maximum flying velocity of the UAV is constrained by V_{max} such that $v_m[n] \leq V_{max}, \forall n, m \in \{1, 2\}$, where $v_m[n]$ is the velocity of m^{th}-UAV at time slot n. $v_m[n] = d_m[n]/\tau$, where $d_m[n] = \|\mathbf{X}_m[n] - \mathbf{X}_m[n-1]\|$ is the distance travelled by the m^{th}-UAV in the n^{th}-time slot. Also, we assume the minimum separation distance required to avoid collision between the two UAVs is D_{min}.

Note that after UAV U_1 has reached the charging station only UAV U_2 will serve the ground users from the final location. Therefore, the final location should be the optimal location where the performance is optimal. In this work, to better understand the replacement mechanism, we have considered the final location to be any location in 3D space and did not impose any constraint on the final location. However, this work is equally applicable when final location is an optimal location.

Since only UAV U_1 is low on energy, in this work, we consider the onboard energy constraint for UAV U_1 only, which is given by

$$\sum_{n=1}^{N_f} e_1[n] \leq E_{left}, \tag{6.2}$$

where $e_1[n]$ is defined in (2.2), Chapter 2, and E_{left} is the energy left with the UAV U_1.

6.2.2 Performance Metric

Since the A2G link is more prone to blockage due to the presence of obstacles and buildings, such as in the urban environment, we consider probabilistic LoS channel model (as described in Chapter 2). Then, the average path loss $h_{k,m}[n]$ between the m^{th}-UAV and the k^{th}-user at time slot n is expressed as

$$h_{k,m}[n] = \beta_0 \frac{(1-\kappa)P^L_{k,m}[n] + \kappa}{\|\mathbf{q}_m[n] - \mathbf{w}_k\|^2 + z_m[n]^2}. \tag{6.3}$$

Equation (6.3) is an extended form of (2.13) when multiple UAVs are present. Similarly, $P^L_{k,m}[n]$ can be written as

$$P^L_{k,m}[n] = \frac{1}{(1 + C\exp\left(-D[\phi_{k,m}[n] - C]\right))}, \tag{6.4}$$

which describes the LoS probability of the m^{th}-UAV with the k^{th}-user at time slot n, where C and D are parameters describing either the suburban, urban, or dense urban environment. $\phi_{k,m}[n] = \tan^{-1}\left(\frac{z_m[n]}{\|\mathbf{q}_m[n] - \mathbf{w}_k\|}\right)$ in (6.4) is the elevation angle between the m^{th}-UAV and the k^{th}-user at time slot n.

We consider a downlink communication setup where the UAV uses FDMA scheme for sharing resources among the ground users. Let $b_{k,m}[n]$ denote the bandwidth allocated by the m^{th}-UAV to the k^{th}-user in the n^{th}-time slot from the total bandwidth B (Hz) available. Then, the bandwidth allocation is given as

$$\sum_{k=1}^{K}\sum_{m=1}^{2} b_{k,m}[n] = B. \tag{6.5}$$

We assume the UAV transmits with equal power P_{tr} to all the users. Then, the achievable data rate by averaging over the small-scale fading effects at the k^{th}-user by the m^{th}-UAV at time slot n is given by

$$r_{k,m}[n] \approx b_{k,m}[n]\log_2\left(1+\frac{P_{tr}h_{k,m}[n]}{b_{k,m}[n]\sigma^2}\right), \tag{6.6}$$

where σ^2 is the receiver's noise power density. Consequently, the achievable data rate of the k^{th}-user during the flight time T is expressed as

$$R_k \triangleq \sum_{n=1}^{N_f} r_{k,1}[n] + \sum_{n=1}^{N} r_{k,2}[n]. \tag{6.7}$$

6.3 Problem Formulation

In this work, we intend to maximize the minimum rate among all the users in a UAV-assisted wireless communication system. We define $\mathbf{B} = \{b_{k,m}[n], \forall k \in \mathcal{K}, m \in \mathcal{M}, n \in \mathcal{N}\}$, and $\mathbf{T} = \{\mathbf{X}_m[n], \forall m \in \mathcal{M}, n \in \mathcal{N}\}$ as bandwidth, and multi-UAV trajectory, respectively. Then, the optimization problem is formulated as

$$\text{(P1)}: \max_{\mathbf{B},\mathbf{T}} \quad \min_{k} \quad R_k \triangleq \sum_{n=1}^{N_f} r_{k,1}[n] + \sum_{n=1}^{N} r_{k,2}[n],$$

$$s.t. \quad \mathbf{X}_1[0] = \mathbf{X}_F, \mathbf{X}_1[N_f] = \mathbf{X}_I, , \mathbf{X}_2[0] = \mathbf{X}_I, \mathbf{X}_2[N] = \mathbf{X}_F, \tag{6.8a}$$

$$v_m[n] \leq V_{max}, \forall m, n, \tag{6.8b}$$

$$\|\mathbf{X}_m[n] - \mathbf{X}_j[n]\|^2 \geq D_{min}^2, \forall n, m \neq j, \tag{6.8c}$$

$$\sum_{n=1}^{N_f} e_1[n] \leq E_{left}, N_f \leq N, \tag{6.8d}$$

$$r_{k,1}[n] + r_{k,2}[n] \geq R_{th}, \forall k, n, \tag{6.8e}$$

$$\sum_{k=1}^{K}\sum_{m=1}^{2} b_{k,m}[n] = B, \tag{6.8f}$$

where constraints (6.8a), (6.8b), and (6.8c) are the the initial and final location, maximum velocity, and collision avoidance constraints, respectively. Constraint (6.8d) is the energy consumption constraint, (6.8e) ensures a minimum rate R_{th} is ensured to each user at every time slot, and (6.8f) is the bandwidth constraint.

It can be observed that problem (P1) is highly complex and is difficult to be solved due to the following reasons. First, the objective function (*i.e.,* rate expression) is non-convex. Second, the constraints (6.8c) − (6.8e) are non-convex, which either contain the bandwidth and trajectory coupled together or contain individual variables. Therefore, the formulated problem is non-convex and NP-hard that cannot be solved using the existing methods. In the following section, we propose a method to obtain a sub-optimal solution.

6.4 Proposed Methodology

In this section, we first transform the max-min problem defined in (P1) to a maximization problem by introducing an auxiliary variable $\mathcal{R} = \min_{k} R_k$, as a function of $\mathbf{B}$ and $\mathbf{T}$. Then, the problem is defined as

$$\begin{aligned} (\text{P1.1}) : \max_{\mathcal{R},\mathbf{B},\mathbf{T}} \quad & \mathcal{R} \\ s.t. \;\; & R_k \geq \mathcal{R}, \forall k \in \mathcal{K}, \qquad (6.9a) \\ & (6.8a) - (6.8f). \end{aligned}$$

The problem (P1.1) is still non-convex with additional non-convex constraint in (6.9a). We solve this problem by decoupling it into two sub-problems, namely bandwidth optimization and UAV trajectory optimization. Thereafter, we apply alternating optimization to solve this problem. In alternating optimization, we solve the two subproblems alternatively. In particular, we first solve the bandwidth optimization under the initially given UAV trajectories using linear programming. Then, the UAV trajectory optimization problem is solved to obtain the optimal trajectory using the SCA approach. This repeats until the difference in the objective value between the two successive iterations is below an acceptable tolerance. Furthermore, we show the analytical complexity and convergence of the proposed iterative algorithm.

6.4.1 Bandwidth Optimization

For given UAV trajectories $\mathbf{T}$, the bandwidth optimization problem can be formulated as

$$(\text{P2}): \max_{\mathcal{R},\mathbf{B}} \quad \mathcal{R}$$
$$s.t.\ (6.9a), (6.8e), (6.8f).$$

It can be observed that $r_{k,m}[n]$ defined in (6.6) is convex in $b_{k,m}[n]$ and so is R_k defined in (6.9a). Furthermore, the constraints (6.9a) and (6.8e) are also convex along with the linear constraint in (6.8f). As a result, problem (P2) is a covex optimization problem and it can be efficiently solved using interior point method.

6.4.2 Trajectory Optimization

We optimize the UAV trajectories $\mathbf{T}$ for a given bandwidth allocation $\mathbf{B}$. The trajectory optimization problem is formulated as follow

$$(\text{P3}): \max_{\mathcal{R},\mathbf{T}} \quad \mathcal{R}$$
$$s.t.\ (6.9a), (6.8a) - (6.8e).$$

It can be observed that due to the presence of non-convex constraints in (6.9a), (6.8c) – (6.8e), the problem (P3) is non-convex. To tackle this difficulty efficiently, we solve for $\mathbf{q}_m[n]$ (horizontal) and $z_m[n]$ (vertical) trajectory coordinates separately in trajectory optimization. Thereafter, we propose an iterative algorithm that optimizes the horizontal and vertical coordinates iteratively.

Horizontal Coordinate Optimization

Given the vertical coordinates of the UAVs *i.e.,* $\{z_m[n], \forall m, n\}$, the horizontal coordinate problem is formulated as follows

$$(\text{P3.1}): \max_{\mathcal{R},\{\mathbf{q}_m[n],\forall m,n\}} \quad \mathcal{R}$$
$$s.t.\ (6.9a), (6.8a) - (6.8e).$$

Note that the problem (P3.1) is non-convex due to non-convex constraints in (6.9a), (6.8c) – (6.8e). To obtain a solution to this problem, we apply SCA method to convert the non-convex constraints to convex.

Since R_k in (6.9a) is a non-negative sum function of $r_{k,m}[n]$, to make this a concave function, we need to prove the concavity of $r_{k,m}[n], \forall m \in \{1, 2\}$ [100]. The $r_{k,m}[n]$ defined in (6.6) is a logarithmic function of average channel gain $h_{k,m}[n]$. As from [100], we know

that the logarithmic function preserves the concavity, therefore, we only need to deal with $h_{k,m}[n]$.

To transform $h_{k,m}[n]$, let us introduce an auxiliary variable $\alpha_{k,m}[n]$, such that

$$\alpha_{k,m}[n] \leq \frac{(1-\kappa)P^L_{k,m}[n] + \kappa}{\|\mathbf{q}_m[n] - \mathbf{w}_k\|^2 + z_m[n]^2}. \tag{6.13}$$

Then, the $r_{k,m}[n]$ defined in constraints (6.9a) and (6.8e) can be written in the form

$$\bar{r}_{k,m}[n] = b_{k,m}[n] \log_2(1 + \tilde{\gamma}_o \alpha_{k,m}[n]), \tag{6.14}$$

where $\tilde{\gamma}_o = \frac{P_{tr}\beta_0}{\sigma^2}$. As a consequence, the constraints (6.9a) and (6.8e) results in a convex constraints in $\alpha_{k,m}[n]$. The constraint introducing the auxiliary variable *i.e.,* (6.13) is however a non-convex constraint.

Lemma 6. *The non-convex constraint in* (6.13) *can be written in its equivalent forms represented by equations* (A.3.1)*,* (A.3.2)*,* (A.3.3)*,* (A.3.4)*,* (A.3.5)*, defined in Appendix A.3.1.*

Proof. See Appendix A.3.1. □

Accounting Lemma 6, the problem (P3.1) can now be represented as (P3.1.1)

$$\begin{aligned}
&(\text{P3.1.1}): \max_{\mathcal{R},\{\mathbf{q}_m[n],\forall m,n\},\mathcal{X}} \quad \mathcal{R} \\
&s.t.\ (6.8a) - (6.8d), (A.3.1) - (A.3.5) \\
&\bar{r}_{k,1}[n] + \bar{r}_{k,2}[n] \geq R_{th}, \forall k, n, && (6.15a) \\
&\sum_{n=1}^{N_f} \bar{r}_{k,1}[n] + \sum_{n=1}^{N} \bar{r}_{k,2}[n] \geq \mathcal{R}, \forall k, && (6.15b)
\end{aligned}$$

where $\mathcal{X} = \{\alpha_{k,m}[n], \Phi_{k,m}[n], y_{k,m}[n], \beta_{k,m}[n]\}, \forall k, m, n$. The constraints (6.15a) and (6.15b) are the modifications of constraints (6.8e) and (6.9a) in (P3.1), respectively, by introducing the auxiliary variable $\alpha_{k,m}[n]$ with $\bar{r}_{k,m}[n]$ defined in (6.14). In problem (P3.1.1), the constraints (6.8c), (6.8d), (A.3.1), (A.3.2), and (A.3.4) belong to a non-convex set. Accordingly, we utilize SCA method to obtain an approximate solution to (P3.1.1). We first introduce the following lemmas to convexify the non-convex constraints.

Lemma 7. *The constraint* (A.3.1) *can be represented in the convex form using the SCA method given as*

$$\frac{1}{2}\left(\Phi_{k,m}[n] + \|\mathbf{q}_m[n] - \boldsymbol{w}_k\|\right)^2 - \lambda_{k,m}[n] \leq z_m[n], \tag{6.16}$$

where $\lambda_{k,m}[n]$ *is defined in* (A.3.8).

Proof. See Appendix A.3.2. □

In a similar fashion as in Lemma 7, we can transform (A.3.2) to obtain

$$P_{\Phi_{k,m}[n]} - \left(\frac{1}{y^r_{k,m}[n]} + \frac{(y_{k,m}[n] - y^r_{k,m}[n])}{y^r_{k,m}[n]^2}\right) \leq 0, \tag{6.17}$$

where $P_{\Phi_{k,m}[n]} = 1 + C\exp\left(-D\left[\tan^{-1}\Phi_{k,m}[n] - C\right]\right)$. Similarly, (A.3.4) can be replaced by its convex form which is given by

$$\frac{1}{2}\left(\alpha_{k,m}[n] + \|\mathbf{q}_m[n] - \mathbf{w}_k\|^2\right)^2 + \alpha_{k,m}[n]z_m[n]^2 - \gamma_{k,m}[n] \leq \beta_{k,m}[n], \tag{6.18}$$

where $\gamma_{k,m}[n] = \frac{1}{2}(\alpha^r_{k,m}[n]^2 + \|\mathbf{q}^r_m[n] - \mathbf{w}_k\|^4) + \alpha^r_{k,m}[n](\alpha_{k,m}[n] - \alpha^r_{k,m}[n]) + \|\mathbf{q}^r_m[n] - \mathbf{w}_k\|^2(\|\mathbf{q}_m[n] - \mathbf{w}_k\|^2 - \|\mathbf{q}^r_m[n] - \mathbf{w}_k\|^2)$. To deal with the non-convex set (6.8c) and (6.8d), we introduce the following lemma

Lemma 8. *The collision constraint in* (6.8c) *can be transformed into its convex form given in* (A.3.10) *and the energy constraint in* (6.8d) *can be written as* $\sum_{n=1}^{N_f} \tilde{e}_1[n] \leq E_{left}$*, along with the additional convex constraint defined in* (A.3.12)*, where* $\tilde{e}_1[n]$ *is given as*

$$\tilde{e}_1[n] = \tau P_o\left(1 + \frac{3v_1^{xy}[n]^2}{U_{tip}^2}\right) + P_i g_1[n] + \frac{\tau}{2}d_0\rho S A v_1^{xy}[n]^3 + W v_1^z[n]. \tag{6.19}$$

Proof. See Appendix A.3.3. □

Accounting all the above discussion and lemmas to convexify the constraints, it can be observed that the problem (P3.1.1) can now be approximated to a convex optimization problem. Thus, interior point method can be employed to obtain the optimal solution. By adopting the first-order Taylor expansion to compute the bounds on the non-convex constraints, the solution to problem (P3.1.1) can be thought of as a subset of problem (P3.1). Therefore, the value of objective function obtained from (P3.1.1) is always lesser or equal to the solution obtained from (P3.1). This implies (P3.1.1) converges to atleast one locally optimal solution.

Vertical Coordinate Optimization

Given the horizontal coordinates $\{\mathbf{q}_m[n], \forall m, n\}$ obtained from the horizontal coordinate optimization subproblem, the vertical coordinate optimization subproblem is given as

$$(\text{P3.2}): \max_{\mathcal{R},\{z_m[n],\forall m,n\}} \quad \mathcal{R}$$
$$s.t.\ (6.9a), (6.8a) - (6.8e).$$

It can be observed that the problem is non-convex due to the non-convex constraints (6.9a), (6.8c), and (6.8e). Following the same procedure as done for the horizontal coordinate optimization problem, the problem (P3.2) can be written as

$$(\text{P3.2.1}): \max_{\{z_m[n],\forall m,n\},\mathcal{X}} \quad \mathcal{R}$$
$$s.t.\ (6.8a) - (6.8d), (6.15a), (6.15b), (A.3.1) - (A.3.5).$$

where $\mathcal{X} = \{\alpha_{k,m}[n], \Phi_{k,m}[n], y_{k,m}[n], \beta_{k,m}[n]\}, \forall k, m, n$. The constraints (6.15a), (6.15b), (A.3.1) − (A.3.5) are obtained using the same procedure as defined in horizontal coordinate optimization. It can be observed that the problem is non-convex due to the constraints (6.8c), (A.3.2), and (A.3.4).

Utilizing similar methods as used in the previous subsection, the constraint (6.8c) can be written as (A.3.10) with $\mathbf{X}_m^r[n] = (\mathbf{q}_m[n], z_m^r[n])$ and $\mathbf{X}_j^r[n] = (\mathbf{q}_j[n], z_j^r[n])$, and the constraint (A.3.2) can be transformed to a convex function as (6.17). Similarly, non-convex constraint (A.3.4) can be written in convex form as

$$\frac{1}{2}\left(\alpha_{k,m}[n] + z_m[n]^2\right)^2 + \alpha_{k,m}[n]\|\mathbf{q}_m[n] - \mathbf{w}_k\|^2 - \gamma_{k,m}^v[n] \leq \beta_{k,m}[n], \tag{6.22}$$

where $\gamma_{k,m}^v[n] = \frac{1}{2}(\alpha_{k,m}^r[n]^2 + z_m^r[n]^4) + \alpha_{k,m}^r[n](\alpha_{k,m}[n] - \alpha_{k,m}^r[n]) + z_m^r[n]^2(z_m[n]^2 - z_m^r[n]^2)$. Accounting the first-order Taylor expansions, the problem (P3.2.1) is now convex and can be solved using the interior point method. Similar to the horizontal coordinate subproblem, (P3.2.1) also converges to locally optimal solution of (P3.2).

Finally, using the subproblems (P3.1.1) and (P3.2.1), we obtain the sub-optimal trajectories $\mathbf{T}$ of the both UAVs U_1 and U_2 for a given bandwidth $\mathbf{B}$. Algorithm 10 presents the procedure to obtain $\mathbf{T}$ using alternating optimization. Here, in the first stage $\{\mathbf{q}_m[n], \forall m, n\}$ is solved for a fixed $\{z_m[n], \forall m, n\}$, and in the second stage $\{z_m[n], \forall m, n\}$ is solved for the obtained $\{\mathbf{q}_m[n], \forall m, n\}$. These two stages are iteratively executed until the objective function $\mathcal{R}$ converges.

6.5 Overall Algorithm

In this section, we present the overall algorithm to obtain the solution to problem (P1.1), its computational complexity, and convergence. Note that we have initialized the UAV

Algorithm 10 Trajectory optimization algorithm

Input: $\mathbf{X}_I$, $\mathbf{X}_F$, $\mathbf{w}_k, \forall k \in \mathcal{K}$, V_{max}.

1: Initialize $\mathbf{B}^0$, $\{\mathbf{q}_m[n]^0, \forall m, n\}$, $\{z_m[n]^0, \forall m, n\}$. Set acceptable tolerance $\epsilon = 10^{-4}$, and iteration count $r = 0$.
2: **Repeat**
3: Fix $\{z_m[n]^r, \forall m, n\}$ and solve for $\{\mathbf{q}_m[n]^{r+1}, \forall m, n\}$ in problem (P3.1.1).
4: Fix $\{\mathbf{q}_m[n]^{r+1}, \forall m, n\}$ and solve for $\{z_m[n]^{r+1}, \forall m, n\}$ in problem (P3.2.1).
5: Set $r = r + 1$, and calculate $\mathcal{R}^{r+1}$.
6: **Until** $\mathcal{R}^{r+1} - \mathcal{R}^r \leq \epsilon$.

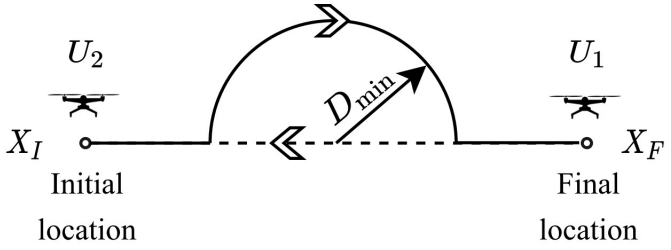

Figure 6.2: Trajectory initialization based on straight-line path.

trajectory in Algorithm 10. In general, the converged solution and the performance of the iterative algorithms depend on the initialization schemes. Therefore, we first present a low-complexity trajectory initialization strategy.

6.5.1 Trajectory Initialization Strategy

In this subsection, we present a low-complexity strategy to initialize the UAV trajectories that is based on straight flight trajectory. The strategy is as follows. First, we develop a straight-line between the initial and the final location. Second, to keep a safe distance between the UAVs, a semicircle of radius equal to D_{min} is formed from the centre of the straight line connecting the initial and the final location. The following two paths formed by considering the semicircle is shown in Figure 6.2. One path is the solid line while the other one is dashed line between the initial and the final location. Third, since the UAV launched from the initial location is full on energy, the UAV U_2 will take a semicircle path to reach the final location, and the other UAV U_1 takes a straight line path. Furthermore, in this initial trajectory design, the UAV moves with a fixed speed $0 \leq v_m[n] \leq V_{max}$ which is same for both the UAVs. This velocity $v_m[n]$ is obtained based on the energy available with the energy-constraint UAV, which is given by $v_m[n] = E_{left}/N$. The initial trajectory design is specifically chosen because of its low-complexity and systematic design.

6.5.2 Overall Algorithm

In this subsection, we present the overall algorithm design. Based on the analysis provided by decomposing the problem into subproblems, we present an alternating optimization

Algorithm 11 Overall algorithm to obtain solution of (P1.1)

Input: $\mathbf{X}_I$, $\mathbf{X}_F$, $\mathbf{w}_k, \forall k \in \mathcal{K}$, V_{max}.
1: Initialize $\mathbf{B}^0$, $\mathbf{T}^0$, set acceptable tolerance $\epsilon = 10^{-4}$, and iteration count $r = 0$.
2: **Repeat**
3: Fix $\mathbf{T}^r$ and solve for $\mathbf{B}^{r+1}$ in problem (P2).
4: Fix $\mathbf{B}^{r+1}$, call Algorithm 10 to obtain $\mathbf{T}^{r+1}$.
5: Update $\{\mathbf{T}^r, \mathbf{B}^r\}$ with $\{\mathbf{T}^{r+1}, \mathbf{B}^{r+1}\}$.
6: Set $r = r + 1$, and calculate $\mathcal{R}^{r+1}$.
7: **Until** $\mathcal{R}^{r+1} - \mathcal{R}^r \leq \epsilon$.

algorithm to obtain a sub-optimal solution. The overall algorithm is presented in Algorithm 11. The steps in the Algorithm 11 are as follows. In step 1, we initialize the bandwidth allocation $\mathbf{B}^0$, and multi-UAV trajectory $\mathbf{T}^0$. Step 2 to Step 7 involve the steps corresponding to alternating optimization, where bandwidth allocation and multi-UAV trajectory are optimized iteratively by fixing the other design variables. Particularly, in Step 3, for any given multi-UAV trajectory $\mathbf{T}^r$, we optimize the bandwidth allocated to each user by solving a linear programming problem. In Step 4, for an optimized bandwidth $\mathbf{B}^{r+1}$, the UAV trajectories $\mathbf{T}^{r+1}$ are optimized using Algorithm 10. The algorithm returns a solution when the difference in the objective function of the current iteration to the previous iteration is below the pre-defined tolerance ϵ.

6.5.3 Complexity and Convergence

The computational complexity of the overall algorithm depends on the complexity involved in solving the trajectory optimization subproblem. In particular, it depends on the iterative scheme (Algorithm 10) that solves the horizontal and vertical coordinate optimization subproblem iteratively, for (P3.1.1) and (P3.2.1), respectively. The complexity to solve problem (P3.1.1) is given by $C_{hor} \triangleq \mathcal{O}((4KMN + (M + 1)N)^{3.5} \log(1/\epsilon))$, where $4KMN+(M+1)N$ represents the number of variables that are to be optimized and ϵ represents the solution accuracy [88]. Similarly, the complexity to solve problem (P3.2.1) is given by $C_{ver} \triangleq \mathcal{O}((4KMN+MN)^{3.5} \log(1/\epsilon))$, where $4KMN+MN$ represents the number of variables to be optimized for vertical coordinate optimization. Let R_{iter} indicates the number of iteration to achieve convergence of Algorithm 10, then the overall complexity is given by $\mathcal{O}(R_{iter} \max(C_{hor}, C_{ver}))$.

Since we have solved the approximate problems to obtain the multi-UAV trajectory and allocated bandwidth to each user, we need to ensure the convergence of the alternating optimization method. This is proved by showing that the objective value increases in each iteration in a maximization problem. Here, we first present the convergence of Algorithm 10. Then, using that, we prove the convergence of the overall algorithm.

We define $\mathcal{R}(\mathbf{Q},\mathbf{Z})$, $\mathcal{R}^{lb}_{hor}(\mathbf{Q},\mathbf{Z})$, and $\mathcal{R}^{lb}_{ver}(\mathbf{Q},\mathbf{Z})$ as the objective value of (P3), horizontal coordinate optimization problem P3.1.3, and the vertical coordinate optimization problem (P3.2.1), respectively, with $\mathbf{Q} = \{\mathbf{q}_m[n], \forall m, n\}$ and $\mathbf{Z} = \{z_m[n], \forall m, n\}$. In Algorithm 10, for a fixed $\mathbf{Z}^r$, $\mathbf{Q}^{r+1}$ is optimized by solving P3.1.3. Then, we have

$$\begin{aligned}\mathcal{R}(\mathbf{Q}^r,\mathbf{Z}^r) &\overset{(a)}{=} \mathcal{R}^{lb}_{hor}(\mathbf{Q}^r,\mathbf{Z}^r)\\ &\overset{(b)}{\leq} \mathcal{R}^{lb}_{hor}(\mathbf{Q}^{r+1},\mathbf{Z}^r)\\ &\overset{(c)}{\leq} \mathcal{R}(\mathbf{Q}^{r+1},\mathbf{Z}^r),\end{aligned} \tag{6.23}$$

where (a) holds because of the tightness of the first-order Taylor expansion of the constraints at the local point, (b) holds since the optimal solution $\mathbf{Q}^{r+1}$ is obtained for the approximate problem with the given $\mathbf{Z}^r$, and (c) holds because the approximate problem is the lower bound of the original problem at $\mathbf{Q}^{r+1}$. Thus, (6.23) implies the objective function is non-decreasing after each iteration. Since the procedure to compute $\mathbf{Z}$ is similar to $\mathbf{Q}$, then we have

$$\mathcal{R}(\mathbf{Q}^{r+1},\mathbf{Z}^r) \leq \mathcal{R}(\mathbf{Q}^{r+1},\mathbf{Z}^{r+1}). \tag{6.24}$$

Through (6.23) and (6.24), we obtain $\mathcal{R}(\mathbf{Q}^r,\mathbf{Z}^r) \leq \mathcal{R}(\mathbf{Q}^{r+1},\mathbf{Z}^{r+1})$. This implies that the objective value of Algorithm 10 is non-decreasing after each iteration by solving for both the horizontal and vertical coordinate optimization problems. Therefore, the trajectory optimization algorithm *i.e.,* Algorithm 10 guarantees convergence.

Since we have followed the alternating optimization approach in Algorithm 11 to obtain $\mathbf{B}^{r+1}$ and $\mathbf{T}^{r+1}$, then we can directly write

$$\mathcal{R}(\mathbf{B}^r,\mathbf{T}^r) \leq \mathcal{R}(\mathbf{B}^{r+1},\mathbf{T}^{r+1}). \tag{6.25}$$

This shows that Algorithm 11 guarantees convergence. It is known that for alternating optimization algorithms, the performance of the converged solution in general depends on the initialization methods [93]. In our work, we have considered a low-complexity and simple trajectory initialization as discussed in Section 6.5.1.

6.6 Results and Discussions

In this section, to evaluate the performance of our proposed scheme, we consider three scenarios. In Scenario 1, we consider a single user because when a single user is present, the

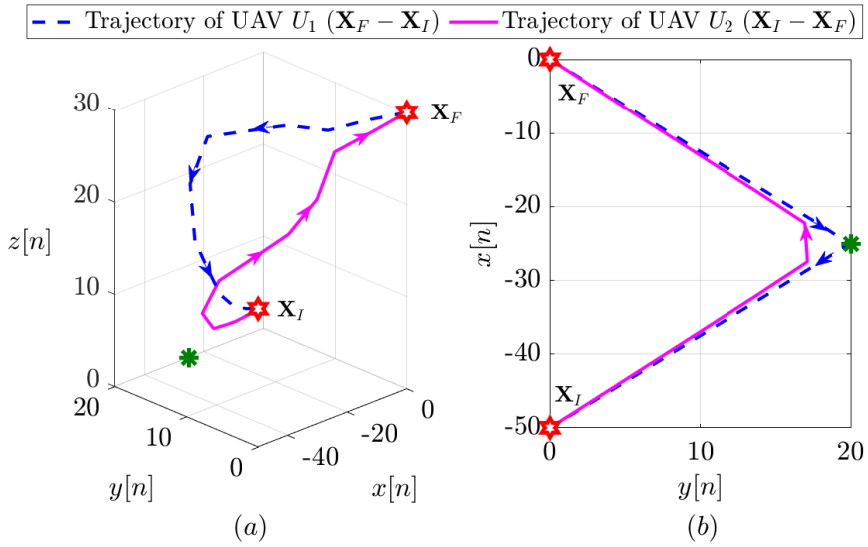

Figure 6.3: UAV trajectories for both UAV U_1 and UAV U_2 with $E_{left} = 5000$ J in (a) 3D-plane, and (b) XY-plane.

algorithm maximizes the user's throughput instead of max-min. Therefore, the max-min problem (P1.1) will be equivalent to a maximization problem. In Scenario 2, we consider a multi-user UAV replacement mechanism. In Scenario 3, we consider the case when $K = 12$ users forming three clusters.

In our system, we consider reference distance $\beta_0 = 1$ m and the environment parameters are set to $C = 10$, and $D = 0.6$. We consider the pathloss exponent and additional attenuation as $\bar{\alpha} = 2.3$, and $\kappa = 0.2$, respectively [9]. The time slot duration τ is set to 0.2 s with $N = 24$ time slots. Note that to keep the understanding of the UAV replacement mechanism simple we have considered a smaller value of N and smaller field with closer initial and final locations. In general, this approach can also be applied to a larger value of N. The UAV's starting location $\mathbf{X}_I = (-50, 0, 0)$ m, and $\mathbf{X}_F = (0, 0, 30)$ m. The total communication power available with each UAV is $P_{tr} = 0.1$ W [97], and the total communication bandwidth B of the system is set to 20 MHz unless specified. The UAV's maximum velocity is set to $V_{max} = 30$ m/s. The minimum safe distance between the UAVs to avoid collision is set to $D_{min} = 10$ m. The parameters in energy consumption model are taken as follows: $P_o = 79.86$ W, $P_i = 88.63$ W, $v_o = 4.03$ m/s, $d_0 = 0.6$, $U_{tip} = 120$, $\rho = 1.225$ kg/m^3, $S = 0.05$, $W = 20$ N and $A = 0.503$ [101].

6.6.1 Scenario 1: Single-user UAV Replacement Mechanism

In this sub-section, we study a single-user UAV replacement mechanism. Figure 6.3 and Figure 6.4 exhibit the UAV trajectories for two different onboard energies, *i.e.*, $E_{left} =$

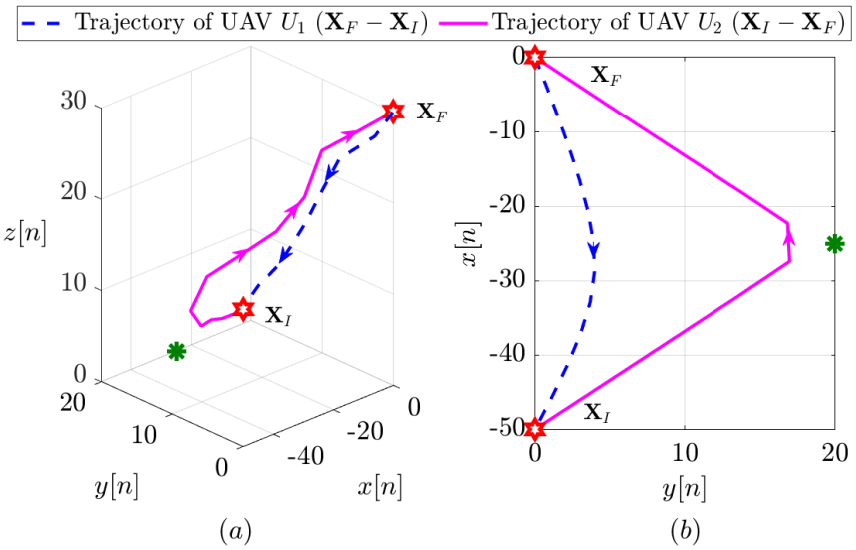

Figure 6.4: UAV trajectories for both UAV U_1 and UAV U_2 with E_{left} = 2000 J in (a) 3D-plane, and (b) XY-plane.

5000 J and E_{left} = 2000 J, respectively. In this single user case, it is intuitive that the UAVs would fly near to the users. The same can be observed from Figure 6.3 wherein both the UAVs tend to fly close to the user, and try to get as close as possible to minimize path loss. To avoid collision, the UAVs maintain a safe distance with each other as shown in Figure 6.3(a). As the UAV U_1 is low on energy due to which replacement is required, a lesser energy will restrict the UAV to approach close to the user. As a result, it forces the UAV to take a path closer to the straight line between the deployment and the charging station to reach the charging station without exhausting its full energy, as shown in Figure 6.4. To achieve a better performance, the ground user will connect only to a UAV with better channel conditions instead of associating with both the UAVs in a particular time slot. As a result, the whole system bandwidth is allocated to the user by the UAV with better channel condition.

6.6.2 Scenario 2: Multi-user UAV Replacement Mechanism

Here, we consider two users and observe how the proposed scheme achieves fairness among the two ground users by adjusting the UAV trajectory and bandwidth allocation. Figure 6.5 and Figure 6.6 depicts the optimized trajectories of the UAVs based on different onboard energy available with the UAV U_1. It is worth noting that when two users are present, the UAV must move close to each user to provide a higher rate. However, to maintain fairness among the ground users (corresponding to our max-min problem), the UAV must maintain equal coverage to both the users for the whole flight duration. The

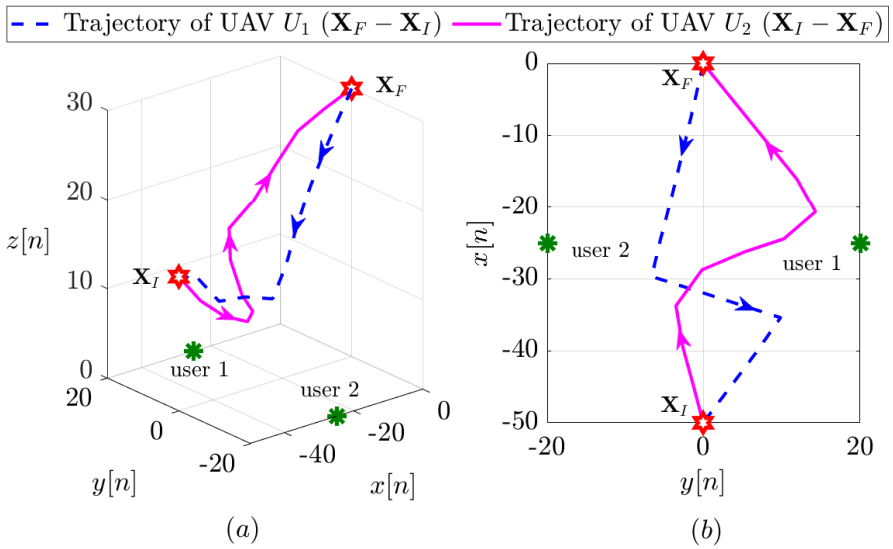

Figure 6.5: UAV trajectories for both UAV U_1 and UAV U_2 with $E_{left} = 5000$ J in (a) 3D-plane, and (b) XY-plane for Scenario 2.

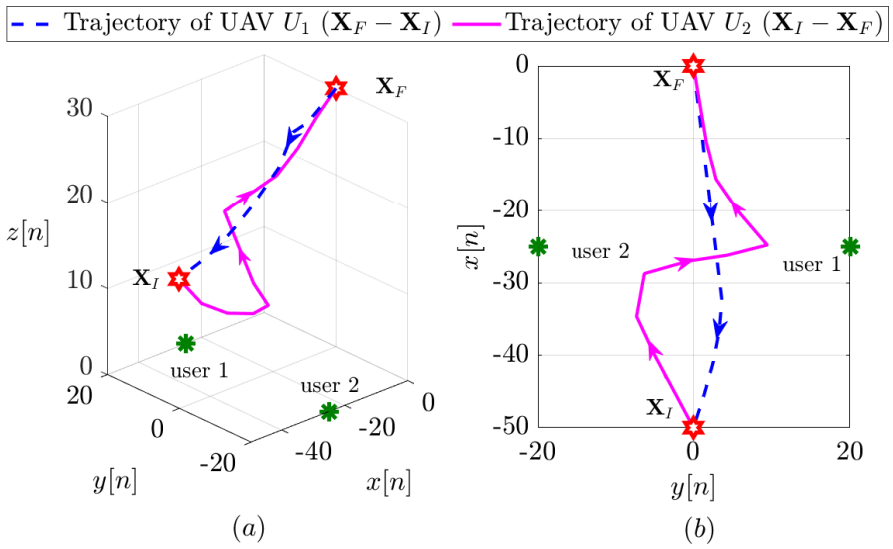

Figure 6.6: UAV trajectories for both UAV U_1 and UAV U_2 with $E_{left} = 2000$ J in (a) 3D-plane, and (b) XY-plane for Scenario 2.

term fairness here describes that a user must be provided with a sum rate equal to or comparable to other users during the service duration. The max-min problem achieves this fairness by maximizing the minimum rate provided to the users and finally, the solution returns the sum rate, which is equal or comparable to all the users. Similar to a single-user case, when the UAV U_1 has lesser energy available, the UAV U_1 takes a shorter path (straight line) to reach the charging station.

To illustrate how much bandwidth is allocated to each user, we plot Figure 6.7, and Figure 6.8, with both $E_{left} = 5000$ J, and $E_{left} = 2000$ J, respectively. Note that to ensure that the user is under coverage in a particular time slot, we have applied a minimum rate constraint. As a result, the user will experience a minimum rate R_{th} within a time slot.

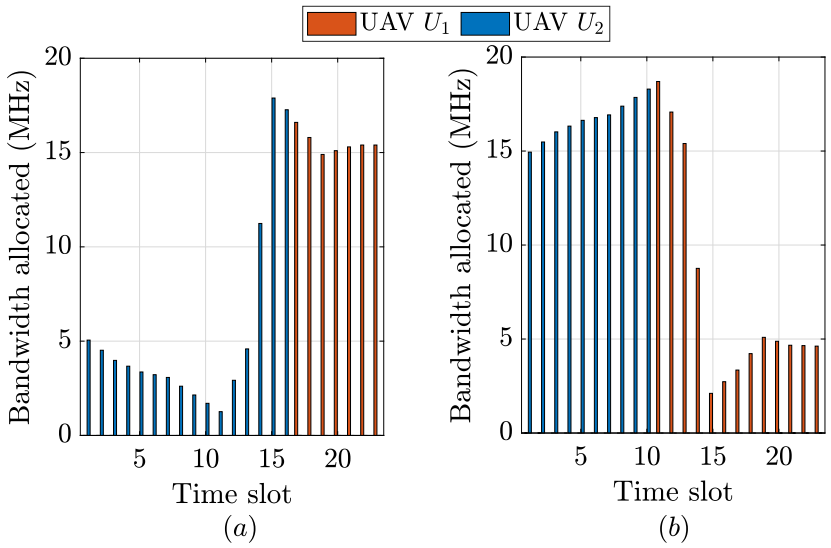

Figure 6.7: Optimal bandwidth allocated to (a) the user 1, and (b) user 2, when E_{left} = 5000 J.

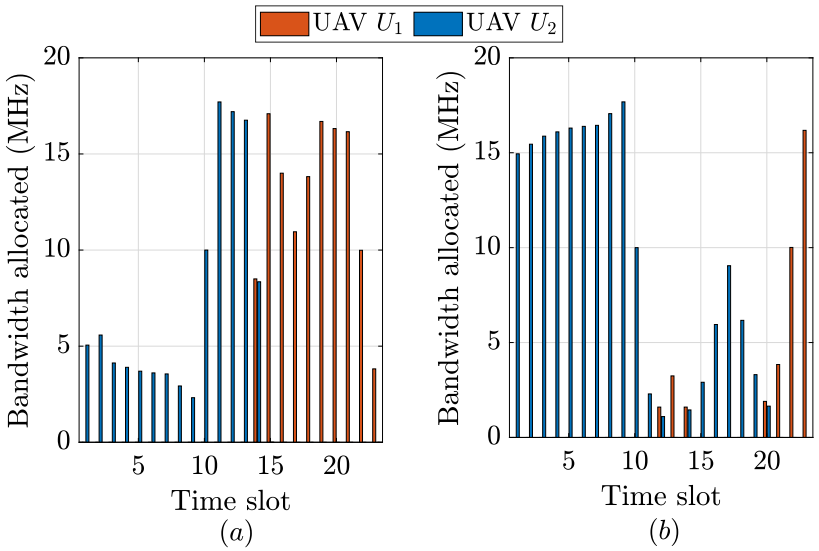

Figure 6.8: Optimal bandwidth allocated to (a) the user 1, and (b) user 2, when E_{left} = 2000 J.

It can be seen from Figure 6.7, as the UAV U_2 moves toward user 2, it allocates the majority of the system's bandwidth to user 2 as a better channel is experienced by user 2. However, to maintain fairness among users at the later stages, the UAV allocates a higher bandwidth to user 1. The same can also be observed when lesser energy is available with UAV U_1 in Figure 6.8.

To verify the performance of the proposed scheme, we consider four benchmark schemes as follows. (i) Straight flight trajectory [102]; (ii) Straight flight trajectory with bandwidth optimization (BWO); (iii) Ellipsoidal trajectory [103], [104]; (iv) Ellipsoidal trajectory with BWO. In a straight flight trajectory, the UAV travels in a straight line to reach the final location ensuring a minimum safe distance between the UAVs. In an ellipsoidal

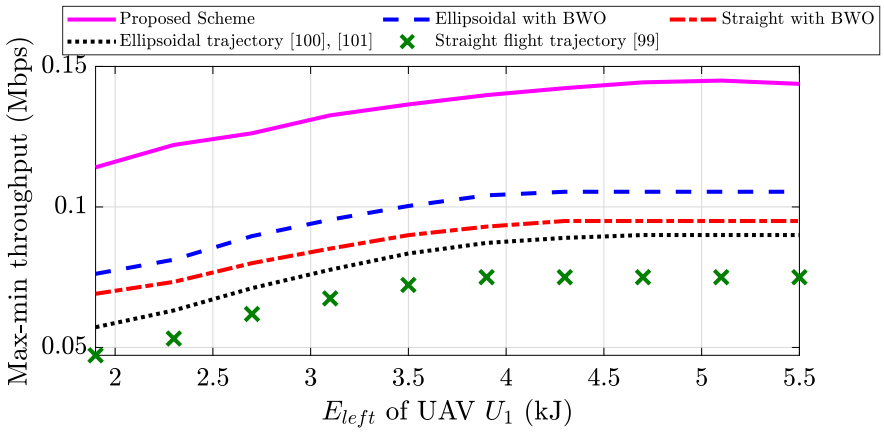

Figure 6.9: Comparison of proposed schemes with conventional schemes with different energy levels for Scenario 2.

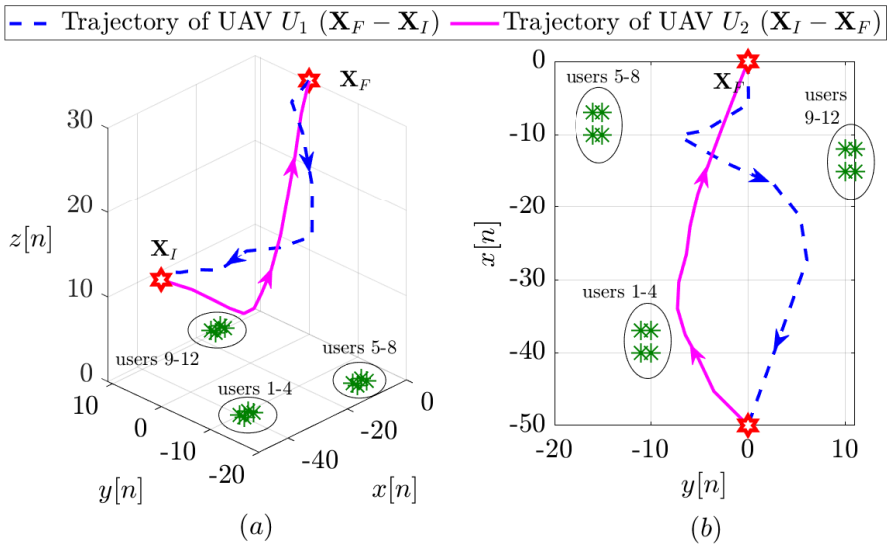

Figure 6.10: UAV trajectories for both UAV U_1 and UAV U_2 with $E_{left} = 5000$ J in (a) 3D-plane, and (b) XY-plane for Scenario 3.

trajectory, UAVs travel by forming an arc in the opposite direction to reach their respective location, resulting in a trajectory that resembles an ellipse. For both the straight flight and ellipsoidal trajectory, the equal amount of bandwidth is allocated to each user from each UAV irrespective of the channel conditions. Under BWO scheme, the problem (P2) (BWO) is solved for the pre-specified path of the UAVs, *i.e.,* straight flight and ellipsoidal trajectory, such that the bandwidth is optimized to provide a fair rate to each user.

It can be observed from Figure 6.9 that the proposed scheme provides better max-min rate compared to the other schemes as the energy availability increases. This is because as the energy level increases, the UAV has more freedom to get closer to the users and thereby providing higher rates. However, in the other schemes, such as straight flight and ellipsoidal trajectory with BWO, straight flight trajectory, and ellipsoidal trajectory, the throughput is significantly lower than the proposed scheme. This is because, in the other

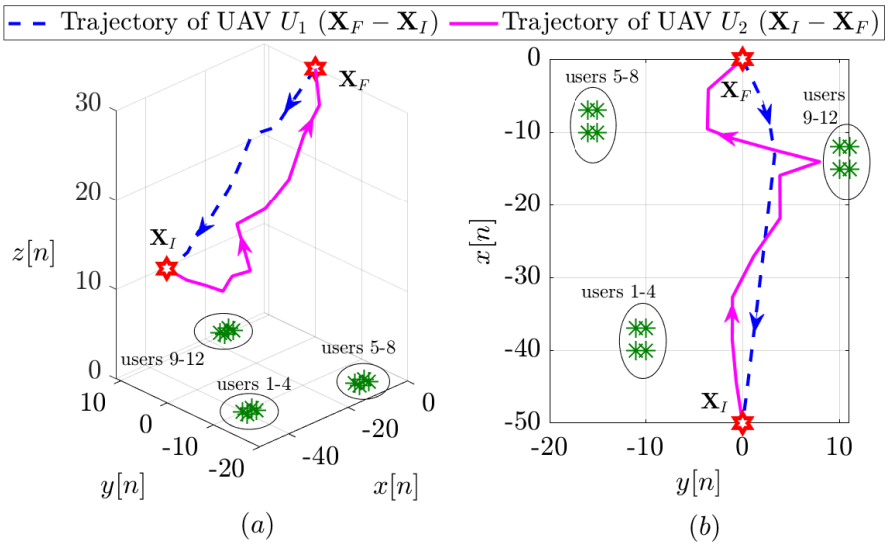

Figure 6.11: UAV trajectories for both UAV U_1 and UAV U_2 with E_{left} = 2000 J in (a) 3D-plane, and (b) XY-plane for Scenario 3.

schemes, the UAV follows a predefined path, and the user's throughput only increases if the users are present along the UAV's path. As a result, the user suffers from worse channel conditions and achieves a lower throughput. Therefore, optimizing the UAV trajectory and bandwidth allocation leads to a multi-fold performance enhancement in comparison to the benchmark schemes. Specifically, our proposed scheme provides on an average 42% improvement over the ellipsoidal with BWO (best performing benchmark schemes) and 110% improvement over the straight flight trajectory (poorer performing benchmark).

6.6.3 Scenario 3: Clustered-users UAV Replacement Mechanism

Similar to Scenario 1 and Scenario 2, Figure 6.10, and Figure 6.11 show the optimized trajectories for E_{left} = 5000 J and E_{left} = 2000 J energy levels, respectively. In this scenario, instead of following the user's individual locations, the UAV treats the group of users as a cluster and optimizes its trajectory.

The comparison of the proposed scheme for Scenario 3 with other schemes is shown in Figure 6.12. Apart from this, we also present the sum throughput obtained by each user during the total flight time in comparison to the benchmark schemes in Figure 6.13. It can be observed that the benchmark schemes, such as straight flight trajectory and ellipsoidal trajectory provide a better rate to only some of the ground users that are closer to the trajectory of the UAVs. As a result, the other ground users get a significantly lesser rate. Furthermore, it is also challenging to maintain fairness between the ground users under such schemes. However, schemes such as straight flight with BWO and ellipsoidal with BWO can achieve fairness but at a lesser rate. In comparison to the benchmark schemes,

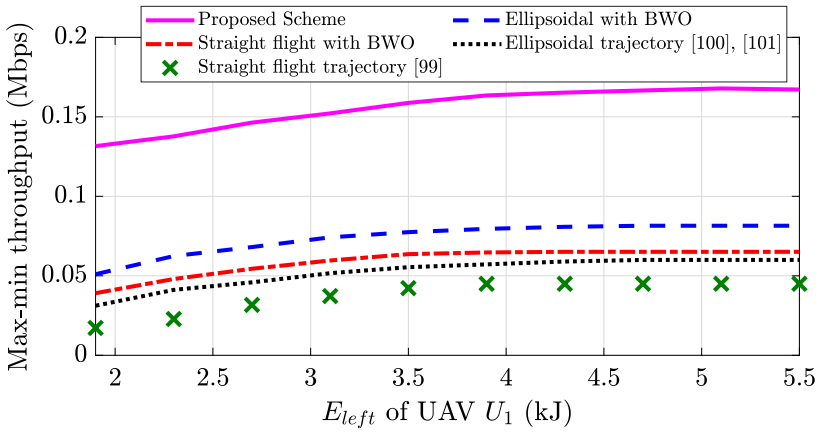

Figure 6.12: Comparison of max-min throughput with different energy levels for a clustered-user UAV replacement scenario.

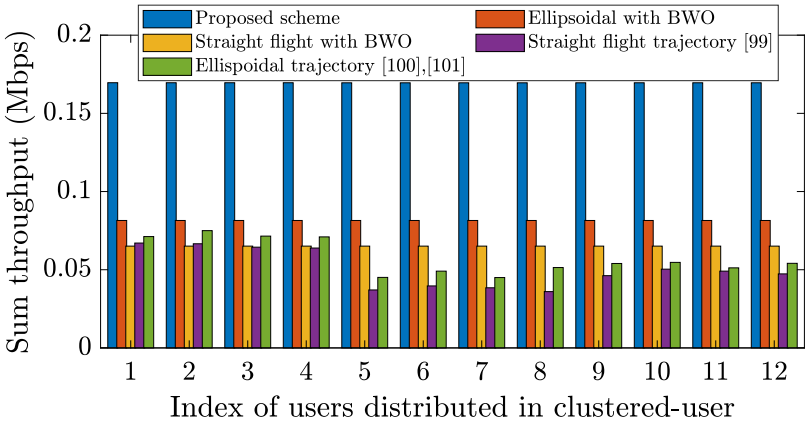

Figure 6.13: Comparison of achievable sum throughput of $K = 12$ users using different schemes for Scenario 3.

multi-fold enhancement is achieved due to the joint optimization of multi-UAV trajectory and bandwidth allocation. In particular, we observe that our proposed scheme provides 110% and 250% improvement in the minimum rate provided to the users in comparison to the ellipsoidal with BWO and straight flight trajectory, respectively. Thus, we conclude that the rate provided by the proposed scheme is fair and is significantly higher than the benchmark schemes for all the considered scenarios.

6.7 Conclusion

Given the UAV's limited onboard energy availability, in this work, we design a UAV replacement scheme to maintain coverage continuity in a UAV-assisted wireless communication system. A fully charged UAV is launched from the charging station to replace an energy depleted UAV. Service fairness to all ground users is ensured by formulating a max-min throughput optimization problem to jointly optimize the 3D

multi-UAV trajectory and resource allocation. The formulated problem is non-convex and an efficient iterative alternating optimization approach is proposed based on the SCA method to solve the optimization problem. Numerical results present insights on the UAV trajectories. Furthermore, our proposed scheme provides multi-fold performance enhancement in achievable sum rate due to the joint optimization of multi-UAV trajectory and bandwidth allocation in comparison to the benchmark schemes. In the future, UAVs can use various energy sources to prolong battery endurance. In such instances, managing the scheduling of communication and energy resources between the UAVs while considering their cooperation is essential.

In a multi-UAV network, to achieve a higher communication rate, the ground user associates with one of the UAVs based on the received signal strength. In this chapter, we assume that the user associates with both the UAVs, but to achieve better communication service to the ground user, the user primarily connects to the UAV with better received signal strength. The same can also be observed from Figure 6.8, where a user connects to one UAV by allocating sufficient bandwidth to the ground user at a particular time.

Therefore, in the next chapter, we study the association probability model for UAV-assisted wireless communication systems, which defines the probability that the ground user is connected to a particular UAV. Furthermore, we also study the impact of fading on the association probability.

Chapter 7

Impact of Fading on Association Probability

7.1 Introduction

7.1.1 Motivation

The advancements in wireless communication networks, ranging from emergency assistance to remote communication enable the use of UAVs as an ABSs. They are an essential means to provide seamless connectivity, improved scalability, and higher data-rate support in various scenarios, such as improved data transmission scalability to the IoT devices, non-terrestrial networks, etc. [101]. Consider a scenario where multiple UAVs are deployed to provide communication to the ground users spread over a given area. The A2G channel can be characterized by path loss, probability of presence of LoS link, etc. To achieve a higher communication rate, the user associates with one of the UAV based on the received signal strength, and the ground user association probability is defined as the probability that the ground user is connected to a particular UAV.

In general, the user is associated with the UAV that is closest. In a UAV-assisted wireless communication networks, the A2G channel is classified into LoS and NLoS based on the channel fading conditions. In such a system, it may happen that a closer UAV may be in NLoS or may experience deep fade than a farther UAV with a LoS channel. Thus, instead of associating with the closest UAV, the ground user may want to associate with another UAV with better channel for better communication.

Nevertheless, the small-scale effect is most often neglected while obtaining the association probability models for UAV-assisted wireless communication networks. Owing to the emergence of UAV-assisted wireless communication networks and the impact of small-scale fading, we study an association probability model for data transmission in a UAV-assisted wireless communication networks where the A2G links are characterized by LoS or NLoS UAV by taking fading into account. Since the channel between the UAV

and the user is estimated through obtaining the instantaneous SNR which includes fading, therefore, it is necessary to study the impact of fading on the association probability.

We assume that the user is associated with either the closest LoS or NLoS UAV by considering a realistic channel model with Nakagami-m fading. To this extent, we derive an exact and closed-form approximate analytical expressions using stochastic geometry for LoS association probability *i.e.,* the user is connected to the closest LoS UAV while considering fading. We also discuss the impact of various parameters, such as the altitude and spatial density of UAV, pathloss exponent, and the scale parameter of Nakagami-m fading on the LoS association probability. At last, we provide a comparison of our analytical model with the average fading model.

7.1.2 Related Works

Stochastic geometry has been extensively used to model the terrestrial networks. However, few works have used such an approach for UAV-assisted communication networks. The authors in [105] analyzed the performance of UAV-assisted communication networks where the location distribution of UAV forms a Poisson point process (PPP). They considered the heterogeneous system consisting of UAV and derived the association probability of the typical receiver by considering the strongest average received power (*i.e.,* the typical receiver is connected to closest UAV). The authors in [106] and [107] analyzed the performance of the UAV-assisted communication network by considering LoS and NLoS components while assuming the typical user is connected to the closest UAV and UAV are distributed according to PPP, however, they have not considered the impact of fading in their model. The work in [108] studied a finite network of UAVs with a LoS channel model distributed over a disc located at a fixed altitude following a 2D binomial point process. However, UAVs in LoS conditions with the users may not be justified if the UAVs hover below buildings or in dense environments. On a similar note, the recent work in [109] evaluated the network performance by considering the association of UAV based on the strongest average received power. Considering the blockage effect, the authors in [110] derived the coverage probability when the user is associated to the closest visible UAV.

In the above works [105]-[110], the authors have considered the user to be associated with the UAV which is closer. In a practical scenario, considering closest UAV may not result in better performance due to the obstruction in signal strength that may even cause deep fade. Also, the characterization of the A2G channel is determined by its instantaneous SNR. Therefore, this work bridges the gap in understanding how fading

affects the network's performance. In particular, from analysis, we conclude that if the user associates with the UAV while accounting fading, we get an average improvement of 10% in the ergodic capacity. Furthermore, the results show that considering fading in addition to pathloss is beneficial for low-altitude scenarios, as it provides a significant increase in the user association probability compared to the average fading scenario.

This work is different from the analysis done on terrestrial networks because the channel model for UAV-assisted communication network includes both the LoS and the NLoS links between the UAV and the user. Also, the pathloss of the A2G channel depends on the distance and elevation angle, whereas in the terrestrial networks, it increases monotonically with distance.

7.2 System Model

7.2.1 Aerial Network Deployment

We consider a UAV-assisted communication network comprising of multiple UAVs to serve the set of users. We assume the UAVs are deployed to hover at a constant height H and are distributed according to PPP, $\mathbf{\Phi} \triangleq \{x_i\}$ with density λ, where x_i denotes the 3D location of the i^{th}-UAV. Note that the practical deployment of base station is not random, however, the PPP assumption allows useful analytical tools from stochastic geometry and provides much tractability to track the real deployment of base stations [111]. Indeed, the authors in [112] showed that even with the PPP used for base station locations, the resulting model is about as accurate as the grid model. Furthermore, we assume that all UAVs transmit at power P_B and are equipped with adequate backhaul links (sufficient bandwidth). To simplify our analysis, we consider a typical user to be present at the origin.

7.2.2 A2G channel model

The A2G channel model is characterized by a combination of large-scale attenuation and small-scale fading. According to [113], the A2G links comprise of both the LoS and the NLoS that considers the occurrence probabilities of both the links separately. The large-scale attenuation due to pathloss is modelled as $\mathcal{L}(X) = X^{-\alpha_s}$, where $s \in \{L, N\}$ represents the type of sight *i.e.,* L for LoS and N for NLoS. $X = \sqrt{r^2 + H^2}$ is the distance between UAV and a typical user, where r denotes the 2D distance from the projection of UAV onto the ground and the typical user. α_s denotes the pathloss exponent, where

$\alpha_s = \alpha_L$ with probability $P_L(X)$ and $\alpha_s = \alpha_N$ with probability $P_N(X)$.

The probability $P_L(X)$ is the probability of LoS transmissions which depends upon the height and density of the buildings, and elevation angle between the typical user and UAV. The probability $P_L(X)$ is given by

$$P_L(X) = \frac{1}{1 + C\exp(-D(\omega - C))}, \tag{7.1}$$

where C and D are environment-dependent constants, and $\omega = \frac{180}{\pi}\sin^{-1}(H/X)$ is the elevation angle between the typical user and the UAV. Then, $P_N(X)$ is the probability of NLoS transmission given by $P_N(X) = 1 - P_L(X)$.

The typical user experiences either a LoS or NLoS channel with each UAV independently depending on the probability of pathloss $P_L(X)$ in (7.1). Therefore, from the user's view point, we decomposed the set of UAVs $\mathbf{\Phi}$ into two independent PPP, *i.e.,* $\mathbf{\Phi} = \mathbf{\Phi}_N \bigcup \mathbf{\Phi}_L$. $\mathbf{\Phi}_N$ and $\mathbf{\Phi}_L$ denote the set of UAV that are in NLoS and LoS with the typical user, respectively. The above two sets are disjoint *i.e.,* $\mathbf{\Phi}_N \bigcap \mathbf{\Phi}_L = \varnothing$.

In this work, we assume the LoS and NLoS links undergo independent small-scale Nakagami-m fading. The Nakagami-m parameters for LoS and NLoS links are given by (m_L, θ_L) and (m_N, θ_N), respectively, where m_L and m_N are shape parameters, and θ_L and θ_N are the scale parameters. Accordingly, the channel power gain H_{s,x_i}, $s \in \{L, N\}$ between the UAV located at x_i and the typical user, follow Gamma distribution with probability density function (PDF) given by

$$f_{H_{s,x_i}}(h_s) = \frac{1}{\alpha^m \Gamma(m)} h^{m-1} e^{-h_s/\theta}, h_s > 0, \forall\, x_i \in \mathbf{\Phi}, \tag{7.2}$$

where $s \in \{L, N\}$, $m \in \{m_L, m_N\}$ and $\Gamma(.)$ is the Gamma function. The received power at the typical user from LoS UAV and NLoS UAV located at point x_i is given by

$$P_{s,x_i} = P_B H_{s,x_i} X_{s,x_i}^{-\alpha_s}, \forall\, x_i \in \mathbf{\Phi}_s, \tag{7.3}$$

where $s \in \{L, N\}$, respectively. X_{s,x_i}, represents the distances between the typical user and the i^{th}-UAV located at x_i for s^{th}-transmissions, respectively. Next, we introduce a framework to derive the user association probability.

7.3 Association Probability Analysis

In this section, we first describe the key statistical results required to provide the analysis of association probability. Further, the exact analytical expression of association probability along with its special case is derived. Note that to avoid ping-pong effect due to rapid channel fluctuations, the notion of hysteresis discussed in [114] can be employed.

7.3.1 Key Statistical Results

Let U and V be the two independent random variables, and $R_1 = \frac{V}{U}$. Then, the PDF of R_1 according to the ratio property [115] is given as

$$f_{R_1}(r) = \int_u^\infty u f_V(ru) f_U(u)\, \mathrm{d}u. \tag{7.4}$$

Let $R_2 = U \cdot V$, then the PDF of R_2 according to the product property [115] is given as

$$f_{R_2}(r) = \int_v^\infty \frac{1}{v} f_U\left(\frac{r}{v}\right) f_V(v)\, \mathrm{d}u. \tag{7.5}$$

Let $V = U^{\frac{1}{a}}$, then $\left|\frac{\mathrm{d}u}{\mathrm{d}v}\right| = \left|av^{(a-1)}\right|$. Using transformation of random variable [115], the PDF of V is given by

$$f_V(v) = f_U(v^a) \left|\frac{\mathrm{d}u}{\mathrm{d}v}\right|. \tag{7.6}$$

Using the above key results, we next derive the exact analysis of association probability.

7.3.2 Exact Association Probability

We assume that the user is connected to the closest LoS UAV or the closest NLoS UAV. The probability that it will be connected with the second closest UAV is very less given that the minimum distance between any two UAVs is greater than some threshold distance to avoid collision. Here, we make note that the fading introduces small channel variations in the signal than the pathloss. Then, the serving UAV y_i when the typical user is connected to the closest UAV of sight $s \in \{L, N\}$ is given by

$$y_i = arg\max_{y_i} P_B H_{s,x_i} X_{s,x_i}^{-\alpha_s}, \tag{7.7}$$

where X_{s,x_i} denotes the distance from the typical user to the closest UAV from $\mathbf{\Phi}_s$ with density $P_s(X_{s,x_i})\lambda$. The PDF of distance X_{s,x_i} is taken as in [109], given by

$$f_{X_{s,x_i}}(x) = 2\pi x P_s(x)\lambda \exp\left(\mathcal{X}(x)\right), x \geq H, x_i \in \mathbf{\Phi}_s, \tag{7.8}$$

$$\text{with} \quad \mathcal{X}(x) = -\int_0^{\sqrt{x^2-H^2}} 2\pi u P_s\left(\sqrt{u^2+H^2}\right)\lambda \, \mathrm{d}u, \tag{7.9}$$

and $s \in \{L, N\}$. Due to LoS and NLoS, there exists two possible cases in the association of typical user: typical user associated with LoS UAV and NLoS UAV. According to the law of probability, if the typical user is associated with the LoS UAV with probability $\mathcal{P}_{LoS}$, then $\mathcal{P}_{NLoS} = 1 - \mathcal{P}_{LoS}$, represents the association probability with the NLoS UAV. Therefore, in this work, we focus on $\mathcal{P}_{LoS}$, *i.e.,* $\mathcal{P}_{LoS} \triangleq \mathbb{P}[s = L]$. Next, we introduce a lemma to obtain $\mathcal{P}_{LoS}$.

Lemma 9. *The probability of the typical user to be associated with the LoS UAV is given by*

$$\mathcal{P}_{LoS} = \mathcal{A}_1 \int_{q=\frac{H}{z}}^{\infty} \exp\left(\mathcal{X}\left(qz\right)\right) \Bigg\{ \int_{H^{\frac{\alpha_L}{\alpha_N}}}^{\infty} P_L\left(b^{\frac{\alpha_N}{\alpha_L}}\right) \left(\left(\frac{q}{b}\right)^{\alpha_N}\right)^{m_N} \times b^{\frac{2\alpha_N}{\alpha_L}-1} \left(\left(\frac{q}{b}\right)^{\alpha_N} + 1\right)^{-m_L-m_N} \exp\left(\mathcal{X}\left(b^{\frac{\alpha_N}{\alpha_L}}\right)\right) \mathrm{d}b \Bigg\} \mathrm{d}q, \tag{7.10}$$

where $\mathcal{A}_1 = \frac{2\pi\alpha_N\lambda}{\alpha_L \beta(m_L, m_N)}$.

Proof. See Appendix A.4.1. □

With the above exact expression of $\mathcal{P}_{LoS}$, we next describe the special case of $\mathcal{P}_{LoS}$.

7.3.3 Special Case: Rayleigh Fading

Taking $m_L = m_N = 1$, this scenario reduces to the Rayleigh fading model. Then, the probability of association of typical user to the LoS UAV for Rayleigh fading channel denoted by $\mathcal{P}^R_{LoS}$ is given by

$$\mathcal{P}^R_{LoS} = \frac{2\pi\alpha_N\lambda}{\alpha_L \beta(m_L, m_N)} \int_{q=\frac{H}{z}}^{\infty} q^{\alpha_N} \exp\left(\mathcal{X}\left(qz\right)\right) \Bigg\{ \int_{H^{\frac{\alpha_L}{\alpha_N}}}^{\infty} p_L\left(b^{\frac{\alpha_N}{\alpha_L}}\right) \frac{b^{\frac{2\alpha_N}{\alpha_L}+\alpha_N-1}}{(b^{\alpha_N} + q^{\alpha_N})^2} \exp\left(\mathcal{X}\left(b^{\frac{\alpha_N}{\alpha_L}}\right)\right) \mathrm{d}b \Bigg\} \mathrm{d}q. \tag{7.11}$$

To gain more analytical insights and obtain the closed-form expression for the user

association probability with the closest LoS UAV, we approximate (7.11). The validity of the approximated closed-form association probability is discussed later in Section 7.5.1.

7.4 Approximate Association Probability

Since the $\mathcal{P}_{LoS}$ in (7.11) takes into account the regularized LoS probability of form $P_L(X)$ as defined in (7.1) which is a function of distance between the typical user and UAV. This makes (7.11) difficult to handle. To address this issue, one way is to use a homogeneous approximation of the LoS probability, where the LoS probability is set to the value corresponding to the most likely elevation angle. This reduces $P_L(X)$ to a scalar value, lets say P_L. Then, (7.8) reduces to

$$f_{X_{s,x_i}}(x) = 2\pi x\, P_s\lambda \exp\left(-\pi P_s\lambda(x^2 - H^2)\right), x \geq H, \tag{7.12}$$

where $s \in \{L, N\}$. Thereafter, we present a lemma to obtain the approximate expression of association probability.

Lemma 10. *The approximate LoS association probability of a typical user to be associated with LoS UAV is given by* $\widetilde{\mathcal{P}}_{LoS} = \exp(-s_N H^2)\mathcal{T}$*, where* $\mathcal{T}$ *is given by*

$$\begin{aligned}\mathcal{T} = \mathcal{A}_2 \int_H^\infty q \exp(-s_N z^2 q^2) G_{1,2}^{2,1}\left(s_L\, q^2 \,\middle|\, \begin{matrix} -1 \\ 0 \quad 0 \end{matrix}\right) \mathrm{d}q \\ - \mathcal{A}_2 \int_H^\infty \frac{1}{q^3} \exp(-s_N z^2 q^2) \sum_{k=0}^{\infty} \frac{(-s_L)^k}{k!} \frac{(H^2)^{k+2}}{k+2} \\ \times\ {}_2F_1(2, k+2; k+3; \frac{-H^2}{q^2})\, \mathrm{d}q,\end{aligned} \tag{7.13}$$

with $\mathcal{A}_2 = 2\pi\, P_L\lambda \exp(\pi P_L\lambda H^2)$*,* $G_{1,2}^{2,1}(.)$ *is the Meijer-G function and* ${}_2F_1(\cdot;\cdot;\cdot)$ *is the Gauss hypergeometric function [116].*

Proof. See Appendix A.4.2. □

Since the closed-form expression of approximate LoS association probability $\widetilde{\mathcal{P}}_{LoS}$ is difficult to obtain, we present a special case of $\widetilde{\mathcal{P}}_{LoS}$ in the next sub-section to obtain a closed-form expression.

7.4.1 Special Case: Low Altitude UAVs

While obtaining the approximate LoS association probability in (A.4.17), it can be observed that for low heights UAVs, $f_Q(q) \approx f_{Q_1}(q)$. Then, $F_Z(z)$ in (A.4.24) can be

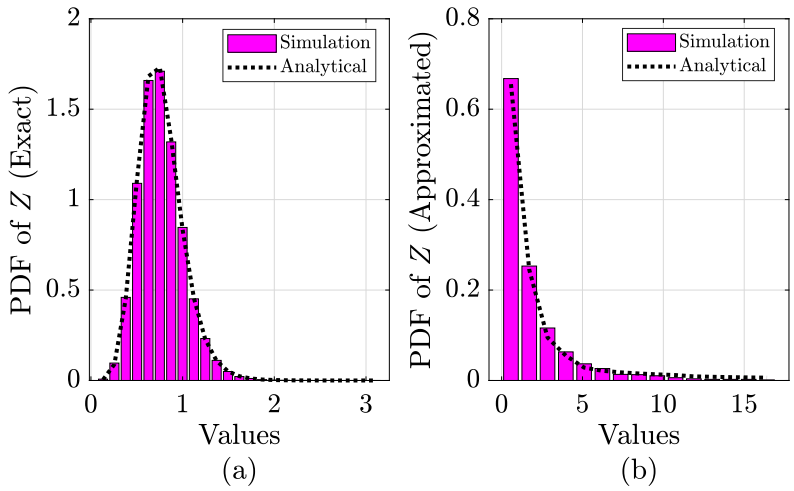

Figure 7.1: Validation of exact and closed-form expression with the simulation runs.

written as $F_Z(z) \triangleq 1-\exp(-s_N H^2)\widehat{\mathcal{T}}$, and association probability $\widehat{\mathcal{P}}_{LoS} = \exp(-s_N H^2)\widehat{\mathcal{T}}$, where

$$\widehat{\mathcal{T}} = \mathcal{A}_2 \int_0^\infty q \exp(-s_N z^2 q^2) G_{1,2}^{2,1}\left(s_L\, q^2 \,\middle|\, \begin{matrix} -1 \\ 0 \quad 0 \end{matrix} \right) \mathrm{d}q, \tag{7.14}$$

with $\mathcal{A}_2 = 2\pi\, P_L \lambda \exp(\pi P_L \lambda H^2)$. Substituting $q^2 = t$ to transform integral and then using property [116, Eq. 07.34.21.0088.01], we get

$$\widehat{\mathcal{T}} = \frac{\mathcal{A}_2}{2 s_N z^2} G_{2,2}^{2,2}\left(\frac{s_L}{s_N z^2} \,\middle|\, \begin{matrix} 0 & -1 \\ 0 & 0 \end{matrix} \right) \mathrm{d}q. \tag{7.15}$$

Then, using (7.15) and $\widehat{\mathcal{P}}_{LoS}$, we can obtain the closed-form expression of association probability of a typical user with closest LoS UAV for low heights UAVs, for example, rural areas.

7.5 Result and Discussions

In this section, we first validate the exact and approximate expressions derived for association probability under fading. Later, we discuss the impacts of various parameters on the association probability. We use Matlab for performing Monte Carlo simulation. The association probability is obtained by averaging over 10^5 simulation runs.

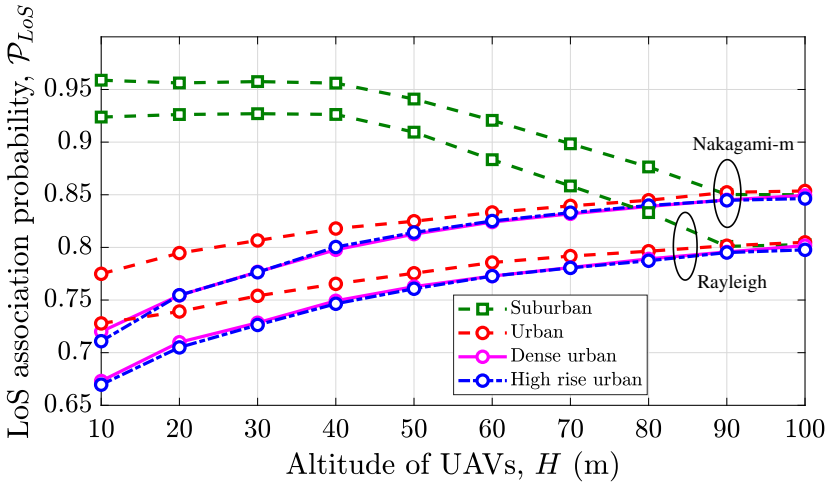

Figure 7.2: Impact of UAV's altitude on the LoS association probability for different environment scenarios.

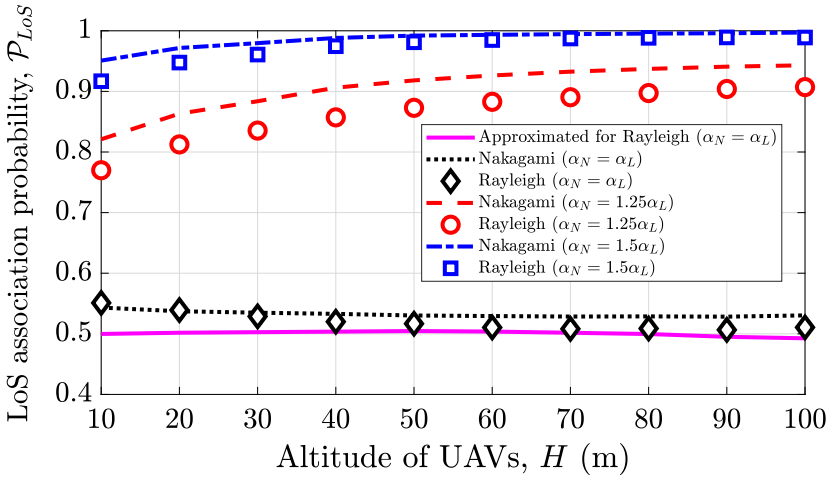

Figure 7.3: Comparison of different fading scenario and validation of approximation LoS association probability.

7.5.1 Validation of Association Probability

To validate the analytical expression and closed-form approximate expression obtained for association probability, we plot Figure 7.1. Figure 7.1(a) shows the validation of PDF of Z (with Nakagami fading) obtained from the CDF defined in (7.10) with the simulation runs. Similarly, Figure 7.1(b) validates the approximated Z defined in (7.15) with simulation runs. From Figure 7.1, we conclude that the analytical expressions match the simulations with negligible errors.

7.5.2 Performance Analysis

In Figure 7.2 and Figure 7.3, we show the impact of height on the association probability for different environments and pathloss variations. Figure 7.2 is plotted by taking $\alpha_N = 2.3$,

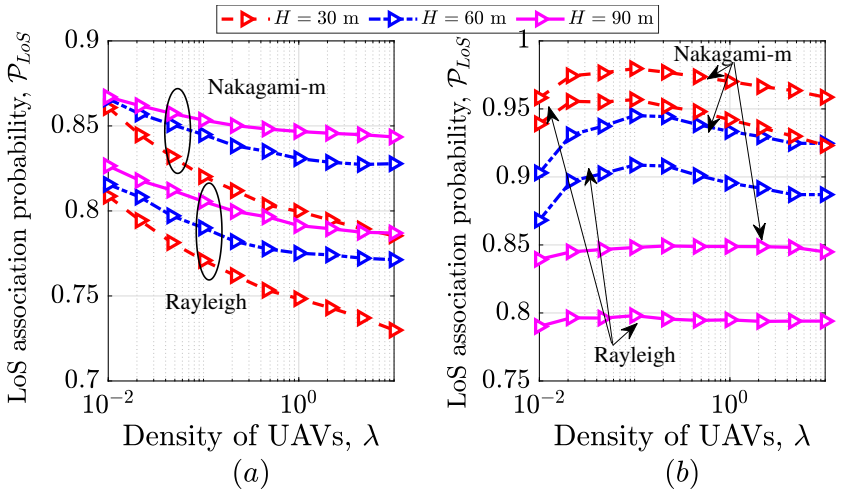

Figure 7.4: Impact of UAV density, λ on the LoS association probability for (a) dense urban scenario, (b) sub-urban scenario.

$\alpha_L = 2$, $\lambda = 5$, and $m_L = 1.3$, $m_N = 1.2$ for Nakagami-m fading model and $m_L = m_N = 1$, for Rayleigh fading model. It can be observed that as the environment becomes dense for a particular fading scenario, the association probability with LoS UAV decreases for a particular height, and with the increase in the height of the UAV, the chances to experience LoS links increases and certainly the typical user will associate towards the LoS UAV in comparison to the NLoS UAV. However, for suburban, it first increases and then decreases after a particular height. This is because that in suburban environment, increasing altitude results in poor channel conditions between the UAV and the user despite the fact that the A2G links are usually LoS. Also, the association probability for Nakagami-m fading is higher than the Rayleigh fading, because for LoS UAV, Nakagami-m is assumed to be better than the Rayleigh fading as there exists the chances to maintain LoS links and thus the received power increases.

Figure 7.3 is plotted by varying the value of pathloss exponent for urban environment scenario. It can be observed that association probability of LoS UAV increases as the α_N increases due to the better connectivity with the LoS UAV because the pathloss difference between α_N and α_L increases. Also, for the approximated case, the association probability is approximately close or lesser than the association probability of Rayleigh when $\alpha_N \approx \alpha_L$. This is because of considering the most likely value of probability of LoS instead of exact LoS probability defined in (7.1).

To get further insights on the association probability, we show the impact of BS density λ on association probability in Figure 7.4(a), and Figure 7.4(b) for dense urban and suburban scenario, respectively. Here, $H = \{30, 60, 90\}$ m, $\alpha_N = 2.3$, $\alpha_L = 2$, $m_L = 1.3$, $m_N = 1.2$ for Nakagami-m fading and $m_L = m_N = 1$, for Rayleigh fading model. In

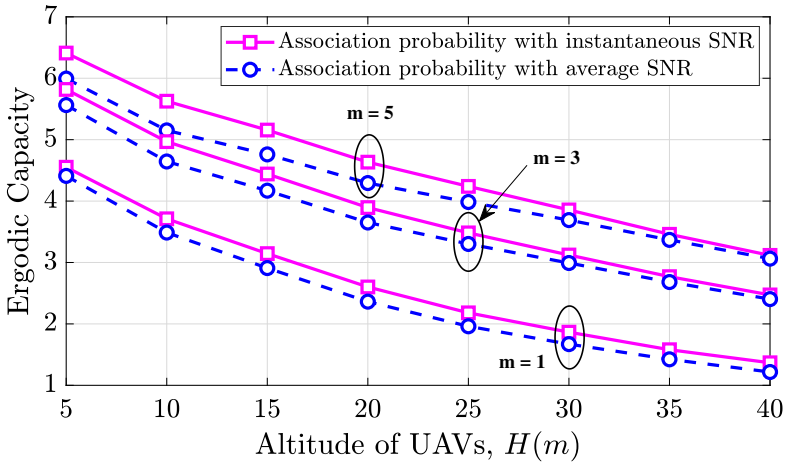

Figure 7.5: Comparison of ergodic capacity of our proposed UAV scheme with the closest UAV scheme.

Figure 7.4(a), the decreasing trend of association probability with the increase in the base station density is desired because for a dense-urban environment, due to large number of obstacles, the increase in the density of UAV results in increasing the UAV which are in NLoS with the typical user. Thus, the probability to associate with LoS decreases as λ increases. However, for a particular λ, increasing altitude result in increasing the association probability as shown in Figure 7.2. In Figure 7.4(b) for a suburban scenario, increasing density at high altitudes does not have much impact on the LoS association probability. This is because most of the UAV are already in LoS with the typical user. However, at low-altitudes, the increase in density will increase the probability of serving with LoS UAV. Thus, the desired received signal strength increases significantly.

7.5.3 Performance Comparison

To show the effectiveness of user associating with the UAV on the basis of instantaneous received signal strength, we compare it to the user associating with the average fading scenario in Figure 7.5 and Figure 7.6. It is plotted by varying the altitude of the UAV for different shape parameter $m_L = \{1, 3, 5\}$ and keeping $m_N = 1$. Figure 7.5 shows the ergodic capacity of typical user to be associated with LoS UAV versus altitude of UAV which is given by $\mathcal{P}_{LoS}\mathbb{E}[\log_2(1 + \text{SNR})]$ (bps/Hz) [105], where SNR is signal-to-noise ratio defined as received power in (7.3). The values of transmit power P_B and noise power for simulation is taken as 32 dBm and -174 dbm/Hz, respectively. It is clear from Figure 7.5 that the average improvement in the ergodic capacity of the considered system is around 10% in comparison to the average fading scenario. This can also be inferred from Figure 7.6 that shows the variation in association probability with the height of UAV

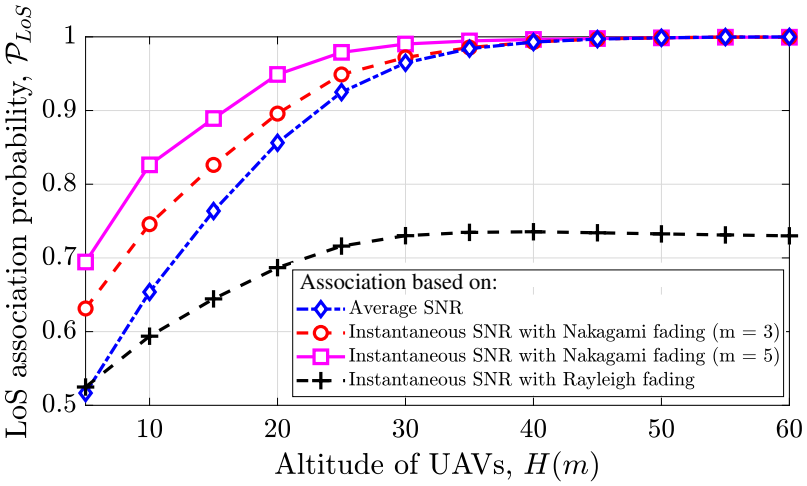

Figure 7.6: Comparison of LoS association probability of our proposed scheme with the closest UAV.

for association based on instantaneous SNR and average SNR. Furthermore, it is observed that for low altitude scenario, inclusion of fading is more beneficial in comparison to the average fading, where as for high altitude scenarios, the association probability is nearly the same as that of average fading. Due to low gain for LoS link in case of $m_L = 1$, the association probability for that case is comparative lesser than the average fading.

7.6 Conclusion

In this work, we presented a stochastic geometry framework to derive the association probability of the user in a UAV-assisted communication network. In general, the channel between the UAV and the user is estimated through obtaining the instantaneous SNR which includes fading, therefore, it is necessary to study the impact of fading on the association probability. As a result, this framework considers instantaneous channel that comprises of both the LoS and NLoS transmission with Nakagami-m fading for A2G links. Utilizing this model, we obtain the exact and approximated closed-form expressions for the LoS association probability. Furthermore, we validated the analytical expressions and studied the impact of various system parameters, such as altitude and density of UAV, pathloss exponent, scale parameter of Nakagami-m fading on the LoS association probability. In particular, with an increase in altitude and pathloss exponent, the LoS association probability increases, whereas it decreases with an increase in UAV density. Also, compared to the average fading scenario, as we increase the shape parameter of Nakagami-m fading, the association probability is higher until some altitude. Later, at higher altitudes, it converges to the average fading scenario. The average improvement in

the ergodic capacity of the considered system is around 10% in comparison to the average fading scenario. Thus, the inclusion of fading at low-altitude UAV applications is more beneficial to the association probability compared to the average fading scenario.

Chapter 8

Conclusion and Future Scope

UAVs as ABS can extend the capability of existing terrestrial cellular infrastructure. However, as we have seen, there exists a certain lacuna in this technology, which we have tried to address in this dissertation. Namely, we addressed the problems of UAV trajectory design, optimal deployment location, UAV replacement for uninterrupted services, resource allocation, and user association. From the results, we have diligently shown the improvement in performance our algorithm brings compared to the existing ones.

The technology and algorithms suggested in this dissertation are analyzed on various input parameters to show how the algorithm responds to variance. Thus, these algorithms can be easily realized in practice by incorporating them as application-level software in 5G communication networks along with the current needs and requirements. In this context, the application of this dissertation lies in providing coverage continuity for practical UAV deployments and related applications. This includes the UAV radio node to support terrestrial RANs, which can be used to extend the coverage or provide communication in isolated regions. As discussed in the previous chapters, it enables rapid deployment in emergency scenarios, such as supporting evacuation in disaster-affected areas or they can be used to provide on-demand communication at hotspot events. Moreover, in contrast to several assumptions such as the static ground users and sufficient backhauling capacity, user mobility and backhauling constraint can be taken into the account to get a more insightful results.

However, there is still more way to go to completely realize this UAV-assisted wireless communication system for on-demand coverage. Some of the challenges are

- The explosive growth and heterogeneous appearance of terrestrial users necessitate dynamic utilization of resources, and adaptation according to the service requirements.

- There is still a need to develop a cross-layer design of MAC and PHY to optimally support a variety of traffic.

- The multi-UAV network encounter several network level issues, such as periodic rearrangement, optimum routing and handovers.

Thus, the UAV-assisted communication system for on-demand coverage still requires robust algorithms to keep the network organized even when the UAV goes out of energy to replenish its battery. That is, the network must have self-arrangement capabilities.

In the next few years, UAV-assisted wireless communication is heading towards the non-terrestrial networks (integration of satellites, UAVs, and terrestrial infrastructure), reconfigurable smart surfaces deployment on UAVs to create an intermediate path between the ground base station and the isolated user, artificial intelligence for UAV-assisted wireless communication networks, etc.

Chapter A

Appendix Title

A.1 Detailed Proofs of Chapter 3

A.1.1 Proof of Lemma 1: Individual Concave regions for step approximation

We know $\widetilde{R}_k^S = \frac{B}{K}\log_2(1+S_k^S)$, where $S_k^S = \frac{\tilde{\gamma}_o}{((x-x_k)^2+(y-y_k)^2+z^2)^{\alpha}}$. Since logarithm $\log_2(.)$ preserves the concavity [100], the concave region of $\widetilde{R}_k^S$ is equivalent to S_k^S. The double derivative of S_k^S is given by

$$\frac{\partial^2 S_k^S}{\partial x^2} = 2\alpha\tilde{\gamma}_o\left((2\alpha+1)(x-x_k)^2-(y-y_k)^2-z^2\right) \times\left((x-x_k)^2+(y-y_k)^2+z^2\right)^{-\alpha-2}, \tag{A.1.1}$$

$$\frac{\partial^2 S_k^S}{\partial y^2} = 2\alpha\tilde{\gamma}_o\left((2\alpha+1)(y-y_k)^2-(x-x_k)^2-z^2\right) \times\left((x-x_k)^2+(y-y_k)^2+z^2\right)^{-\alpha-2}, \tag{A.1.2}$$

$$\frac{\partial^2 S_k^S}{\partial z^2} =2\alpha\tilde{\gamma}_o\left(2\alpha z^2-x^2+2xx_k-x_k^2-y^2+2yy_k-y_k^2+z^2\right) \times\left((x-x_k)^2+(y-y_k)^2+z^2\right)^{-\alpha-2}. \tag{A.1.3}$$

On solving for $\{\frac{\partial^2 S_k^S}{\partial x^2}, \frac{\partial^2 S_k^S}{\partial y^2}, \frac{\partial^2 S_k^S}{\partial z^2}\} \leq 0$, we obtain the regions as $\mathcal{R}_{xs}^k$, $\mathcal{R}_{ys}^k$, and $\mathcal{R}_{zs}^k$ defined by $x \in (x_k^{lb}, x_k^{ub})$ given (y,z), $y \in (y_k^{lb}, y_k^{ub})$ given (x,z), and $z \in (z_k^{lb}, z_k^{ub})$ given (x,y), respectively, where the function is individually concave. ψ_k^{lb} and ψ_k^{ub} denote the lower and upper bounds of ψ for k^{th}-user, respectively, where $\psi \in \{x,y,z\}$ and are given by

$$\{x_k^{lb}, x_k^{ub}\} =\frac{1}{2\alpha+1}\Bigg(\alpha x_k \pm \left(2\alpha y^2-4\alpha y y_k+2\alpha y_k^2+2\alpha z^2 +y^2-2yy_k+y_k^2+z^2\right)^{-\frac{1}{2}}+x_k\Bigg), \tag{A.1.4}$$

$$\{y_k^{lb}, y_k^{ub}\} = \frac{1}{2\alpha+1}\Big(\alpha y_k \pm \big(2\alpha x^2 - 4\alpha x x_k + 2\alpha x_k^2 + 2\alpha z^2 + x^2 - 2x x_k + x_k^2 + z^2\big)^{-\frac{1}{2}} + y_k\Big), \tag{A.1.5}$$

$$\{z_k^{lb}, z_k^{ub}\} = \pm\frac{\sqrt{x^2 - 2x x_k + x_k^2 + y^2 - 2y y_k + y_k^2}}{\sqrt{2\alpha+1}}. \tag{A.1.6}$$

Then, for K users, we obtain K regions corresponding to each user where the function is concave in either x, y or z. The overall region over which $\widetilde{Q}^S \triangleq \sum_{k=1}^{K} \widetilde{R}_k^S$ is individually concave is given by

$$\mathcal{R}_x^S = \bigcap_{k=1}^{K} \mathcal{R}_{xs}^k, \mathcal{R}_y^S = \bigcap_{k=1}^{K} \mathcal{R}_{ys}^k, \text{ and } \mathcal{R}_z^S = \bigcap_{k=1}^{K} \mathcal{R}_{zs}^k. \tag{A.1.7}$$

Hence, $\widetilde{Q}^S$ is concave with respect to x, y, and z, individually, in the region $\mathcal{R}_x^S$, $\mathcal{R}_y^S$, and $\mathcal{R}_z^S$, respectively.

A.1.2 Proof of Lemma 2: Individual Concave regions for linear approximation

We know $\widetilde{R}_k^L = \frac{B}{K}\log_2(1+\tilde{\gamma}_o S_k^L)$, where $S_k^L = \frac{\frac{(1-\kappa)z}{\sqrt{(x-x_k)^2+(y-y_k)^2+z^2}}+\kappa}{((x-x_k)^2+(y-y_k)^2+z^2)^{\alpha}}$. Since logarithm $\log_2(.)$ preserves concavity [100], to find the concave region of $\widetilde{R}_k^L$ we consider S_k^L. Next, we provide the regions in which S_k^L is individually concave in x, y, and z. Later, we find out the overall region for individual concavity of $\widetilde{Q}^L \triangleq \sum_{k=1}^{K} \widetilde{R}_k^L$ in x, y, and z.

Individual Concavity with Respect to x and y

To check the concavity of S_k^L with respect to x, the double derivative of S_k^L with respect to x is given by

$$\frac{\partial^2 S_k^L}{\partial x^2} = \mathcal{A}_1^{-\alpha-\frac{5}{2}}\big(\big((y-y_k)^2+z^2\big)\big((2\alpha+1)(\kappa-1)z - 2\alpha\kappa\sqrt{\mathcal{A}_1}\big) - 2(2\alpha+1)(x-x_k)^2\big((\alpha+1)(\kappa-1)z - \alpha\kappa\sqrt{\mathcal{A}_1}\big)\big), \tag{A.1.8}$$

where $\mathcal{A}_1 = \big((x-x_k)^2 + (y-y_k)^2 + z^2\big)$. On solving $\frac{\partial^2 S_k^L}{\partial x^2} = 0$, (A.1.8) reduces to

$$u_1^2 u_5^2 - 4u_3^2 u_5^3 = (x-x_k)^2\big(2u_1 u_2 u_4 u_5 - 4u_3^2 u_4 u_5^2 + 4u_3^2 u_5^2\big) + (x-x_k)^4\big(-u_2^2 u_4^2 + u_3^2 u_4^2 u_5 - 4u_3^2 u_4 u_5\big) + u_3^2 u_4^2 (x-x_k)^6, \tag{A.1.9}$$

$$\{\gamma_3,\gamma_z\} \triangleq -\frac{\left(1+i\sqrt{3}\right)}{6\sqrt[3]{2}q_1}\sqrt[3]{\sqrt{\left(\pm 27q_1^2q_4+9q_1q_2q_3-2q_2^3\right)^2+4\left(3q_1q_3-q_2^2\right)^3}\pm 27q_1^2q_4+9q_1q_2q_3-2q_2^3}$$
$$-\frac{q_2}{3q_1}+\frac{\left(1-i\sqrt{3}\right)\left(3q_1q_3-q_2^2\right)}{3\ 2^{2/3}q_1\sqrt[3]{\sqrt{\left(\pm 27q_1^2q_4+9q_1q_2q_3-2q_2^3\right)^2+4\left(3q_1q_3-q_2^2\right)^3}\pm 27q_1^2q_4+9q_1q_2q_3-2q_2^3}}. \tag{A.1.11}$$

where $u_1 = (2\alpha+1)(\kappa-1)z$, $u_2 = (\alpha+1)(\kappa-1)z$, $u_3 = \alpha\kappa$, $u_4 = 2(1+2\alpha)$, and $u_5 = ((y-y_k)^2+z^2)$. Substituting $w = (x-x_k)^2$ in (A.1.9), (A.1.9) reduces to a cubic linear equation with variable w and is given by

$$w^3u_3^2u_4^2+w^2\left(-u_2^2u_4^2+u_3^2u_4^2u_5-4u_3^2u_4u_5\right)+w\left(2u_1u_2u_4u_5 - 4u_3^2u_4u_5^2+4u_3^2u_5^2\right)=u_1^2u_5^2-4u_3^2u_5^3. \tag{A.1.10}$$

Next, we find the roots of the cubic equation. Since $w = (x-x_k)^2$, we will obtain six roots which divides the search range into seven intervals. Out of seven, we will find the intervals where $\frac{\partial^2 S_k^L}{\partial x^2} < 0$. On solving, we get the overall range where $\frac{\partial^2 S_k^L}{\partial x^2} < 0$. That is S_k^L is concave over the domain x is given by $\mathcal{R}_{xl}^k$ defined by $x \in (-\sqrt{\gamma_3}+x_k, \sqrt{\gamma_3}+x_k)$ given (y,z). The closed form expression for γ_3 is defined in (A.1.11), where $q_1 = u_4^2u_3^2$, $q_2 = u_4^2u_5u_3^2-u_2^2u_4^2-4u_4u_5u_3^2$, $q_3 = 4u_5^2u_3^2-4u_4u_5^2u_3^2+2u_1u_5u_2u_4$, and $q_4 = u_1^2u_5^2-4u_5^3u_3^2$.

Since in S_k^L, the behaviour of y is similar to x, then the region for x is also applicable for y. To find the region of y, except $u_5 = ((x-x_k)^2+z^2)$, rest all the variable will remain the same and we will form the cubic equation in $w = (y-y_k)^2$. The individual concave region where the function is concave in y is given by $\mathcal{R}_{yl}^k$ defined by $y \in (-\sqrt{\gamma_3}+y_k, \sqrt{\gamma_3}+y_k)$ for a given (x,z). Note that $\mathcal{R}_{xl}^k$, and $\mathcal{R}_{yl}^k$ denote the individual concave regions for $\widetilde{R}_k^L$.

Concavity With Respect to z

The double derivative of S_k^L with respect to z is given by

$$\frac{\partial^2 S_k^L}{\partial z^2} = \mathcal{A}_1^{-\alpha-\frac{5}{2}}\Big(-2\alpha(2\alpha+1)z^2\big((\kappa-1)z-\kappa\sqrt{\mathcal{A}_1}+ ((x-x_k)^2+(y-y_k)^2)\big(3(2\alpha+1)(\kappa-1)z-2\alpha\kappa\sqrt{\mathcal{A}_1}\big)\big)\Big), \tag{A.1.12}$$

where $\mathcal{A}_1 = \big((x-x_k)^2+(y-y_k)^2+z^2\big)$. Simplifying $\frac{\partial^2 S_k^L}{\partial z^2} = 0$, (A.1.12) reduces to

$$\begin{aligned} &z^6\big(4\alpha^2u_1^2(\kappa-1)^2 - 4\alpha^2u_1^2\kappa^2\big) + z^4\big(8\alpha^2f_2\kappa^2 - 4\alpha^2u_1f_2\kappa^2 \\ &- 12\alpha u_3f_2(\kappa-1)\big) - 4\alpha^2u_2^3\kappa^2 + z^2\big(-4\alpha^2u_2^2\kappa^2 \\ &+ 8\alpha^2u_2f_2\kappa^2 + 9f_1^2\big) = 0, \end{aligned} \tag{A.1.13}$$

where $u_1 = 1+2\alpha$, $u_2 = (x-x_k)^2+(y-y_k)^2$, $u_3 = (1+2\alpha)(-1+\kappa)$, $f_1 = u_2u_3$, and $f_2 = u_1u_2$. Substituting $w = z^2$ in (A.1.13) turns it into a cubic linear equation. Since $z > 0$, we will get three roots which will divide the whole range into four intervals. We obtain the concave region by taking a value within each interval and computing $\frac{\partial^2 S_k^L}{\partial z^2}$. The interval where the $\frac{\partial^2 S_k^L}{\partial z^2} < 0$, is taken as the region where the function is concave. On solving, we obtain the region $\mathcal{R}_{zl}^k$ where S_k^L is individually concave in z is defined as $z \in (0, \sqrt{\gamma_z})$ for a given (x, y). The closed form expression for γ_z is shown in (A.1.11), where $q_1 = 4\alpha^2u_1^2(-1+\kappa)^2 - 4\alpha^2u_1^2\kappa^2$, $q_2 = 8\alpha^2f_2\kappa^2 - 4\alpha^2u_1f_2\kappa^2 - 12\alpha f_2u_3(-1+\kappa)$, $q_3 = 9f_1^2 - 4\alpha^2u_2^2\kappa^2 + 8\alpha^2f_2u_2\kappa^2$, and $q_4 = 9f_1^2 - 4\alpha^2u_2^2\kappa^2 + 8\alpha^2f_2u_2\kappa^2$.

Thus, the regions obtained for individual concavity of $\widetilde{R}_k^L$ in x, y, and z are defined as $\mathcal{R}_{xl}^k$, $\mathcal{R}_{yl}^k$, and $\mathcal{R}_{zl}^k$, respectively. When K users are present, we will obtain K regions each for x, y, and z. Then, the overall region for individual concavity of $\widetilde{Q}^L \triangleq \sum_{k=1}^K \widetilde{R}_k^L$ in x, y, and z is given as

$$\mathcal{R}_x^L = \bigcap_{k=1}^K \mathcal{R}_{xl}^k,\ \mathcal{R}_y^L = \bigcap_{k=1}^K \mathcal{R}_{yl}^k, \text{ and } \mathcal{R}_z^L = \bigcap_{k=1}^K \mathcal{R}_{zl}^k. \tag{A.1.14}$$

A.2 Detailed Proofs of Chapter 4

A.2.1 Proof of Lemma 3: Pseudoconvexity of $e[n]$ with respect to $v[n]$

In this section, we prove the pseudoconvexity of $e[n]$ with respect to $v[n]$. Since $e[n]$ expression defined in (2.2) is difficult to investigate due to the second term being a square root. We consider first-order Taylor approximation of the second term when $v[n] \gg v_o$, where v_o is the mean rotor induced velocity. The approximation is given as [9, Eq. 13]

$$\mathcal{E}(v[n]) \approx \tau P_o\left(1+\frac{3v[n]^2}{U_{tip}^2}\right) + \tau P_i\frac{v_o}{v[n]} + \frac{1}{2}\tau D_{en}\rho\psi A_{en}v[n]^3, \tag{A.2.1}$$

where $U_{tip} = \Omega R_{en}$. Differentiating $e[n]$ with respect to $v[n]$, we get

$$\frac{\partial e[n]}{\partial v[n]} = \frac{6\tau P_o v[n]}{U_{tip}^2} - \frac{\tau P_i v_o}{2v[n]^2} + \frac{3}{2}\tau D_{en}\rho\psi A_{en}\tau v[n]^2. \tag{A.2.2}$$

Equating $\frac{\partial e[n]}{\partial v[n]} = 0$, we obtain two roots (one negative and other positive). Since velocity is positive, we discard the negative root. The positive root is given by

$$\begin{aligned} V_0 \triangleq v[n] = &-\sqrt{\frac{P_o^2}{h_e^2} + \frac{\sqrt[3]{2}\sqrt[3]{w_e}}{6h_e} - \frac{2^{2/3}P_i U_{tip}^2 v_o}{6\sqrt[3]{w_e}}} - \frac{P_o}{h_e} \\ &+ \Bigg(- \frac{\sqrt[3]{2}\sqrt[3]{w_e}}{6h_e} + \frac{2^{2/3}P_i U_{tip}^2 v_o}{6\sqrt[3]{w_e}} + \frac{2P_o^2}{h_e^2} \\ &+ \frac{2\sqrt{6}P_o^3}{h_e^2\sqrt{-\frac{2^{2/3}h_e^2 P_i U_{tip}^2 v_o}{\sqrt[3]{w_e}} + \sqrt[3]{2}h_e\sqrt[3]{w_e} + 6P_o^2}} \Bigg)^{1/2}, \end{aligned} \tag{A.2.3}$$

where $g_e = 2A_{en}^3 D_{en}^3 P_i^3 \rho^3 \psi^3 U_{tip}^{12} v_o^3 + 81 P_o^4 P_i^2 U_{tip}^4 v_o^2$, $h_e = A_{en} D_{en} \rho \psi U_{tip}^2$ and $w_e = \sqrt{g_e} - 9P_o^2 P_i U_{tip}^2 v_o$.

It can be seen by solving (A.2.2), $\frac{\partial e[n]}{\partial v[n]} < 0$ for $v[n] \in [0, V_0)$ and $\frac{\partial e[n]}{\partial v[n]} > 0$ for $v[n] \in (V_0, \infty]$. This proves the pseudoconvexity of (A.2.1) with respect to $v[n]$.

As the approximation error is small, we assume $e[n]$ defined in (2.2) to be a pseudoconvex function of $v[n]$.

A.2.2 Proof of Lemma 4: Individual Pseudoconvexity of $\bar{P}_{out}$ in (x, y) for Fixed z and in z for fixed (x, y)

We will omit [n] throughout this proof. $\bar{P}_{out} = \frac{1}{N}\sum_{k=1}^{K} \widehat{P}_{out}^k$. Firstly, we prove $\widehat{P}_{out}^k$ to be jointly convex in x and y for a given z. Thereafter $\bar{P}_{out}$ is proved to be jointly convex using the non-negative sum property of convex functions [100]. Considering

$$L_k = \sqrt{(x - x_k)^2 + (y - y_k)^2}, \forall i \in \mathcal{N} \tag{A.2.4}$$

where L_k represents the horizontal distance between the projection of UAV on the ground and the k^{th}-user. It can also be written in form of $L_k = \sqrt{f(x, y)}$, where $f(x, y) = (x - x_k)^2 + (y - y_k)^2$. The function $f(x, y)$ has $\frac{\partial^2 f(x,y)}{\partial x^2} = 2$, $\frac{\partial^2 f(x,y)}{\partial y^2} = 2$, and $\frac{\partial^2 f(x,y)}{\partial y \partial x} = \frac{\partial^2 f(x,y)}{\partial x \partial y} = 0$, then, $det[\mathcal{H}(f(x, y))] > 0$, where Hessian $\mathcal{H}(f(x, y)) = \begin{bmatrix} \frac{\partial^2 f(x,y)}{\partial x^2} & \frac{\partial^2 f(x,y)}{\partial x \partial y} \\ \frac{\partial^2 f(x,y)}{\partial y \partial x} & \frac{\partial^2 f(x,y)}{\partial y^2} \end{bmatrix}$. This implies that $f(x, y)$ is jointly convex in x and y. Since square root is a monotonic increasing function, therefore it preserves the convexity [100]. Substituting L_k in $\widehat{P}_{out}^i$

defined in (4.5), we get,

$$\widehat{P}_{out}^{k} \triangleq \frac{\frac{\gamma_{th}}{\tilde{\gamma}_o}(L_k^2+z^2)^{\alpha}}{\frac{(1-\kappa)}{1+C\exp\left(-D\left[\frac{180}{\pi}\sin^{-1}\left(\frac{z}{\sqrt{(L_k^2+z^2)}}\right)-C\right]\right)}+\kappa}. \tag{A.2.5}$$

Since L_k is jointly convex in x and y, then proving convexity of $\widehat{P}_{out}^{k}$ defined in (A.2.5) with respect to L_k will result in joint convexity of $\widehat{P}_{out}^{k}$ in x and y.

The double derivative of $\widehat{P}_{out}^{k}$ with respect to L_k is given as

$$\frac{\partial^2 \widehat{P}_{out}^{k}}{\partial L_k^2} = \mathcal{A}\left[\frac{w_k D z}{\alpha\pi}\left(\frac{(2\alpha-1)L_k}{(w_k\kappa+1)^2}+\frac{90Dz(1-w_k\kappa)}{\pi(w_k\kappa+1)^3}\right)+\frac{(w_k+1)\Big((2\alpha-1)L_k^2+z^2\Big)}{180(1-\kappa)(w_k\kappa+1)}\right], \tag{A.2.6}$$

where $\mathcal{A}=360\alpha\frac{\gamma_{th}}{\tilde{\gamma}_o}(1-\kappa)\big(L_k^2+z^2\big)^{\alpha-2}$ and $w_k = C\exp\Big(-D\Big(\frac{180}{\pi}\sin^{-1}\Big(\frac{z}{\sqrt{L_k^2+z^2}}\Big)-C\Big)\Big)$. It is observed that, $\frac{\partial^2 \widehat{P}_{out}^{k}}{\partial L_k^2}$ is positive for all values of L_k when z is fixed. This implies the convexity of $\widehat{P}_{out}^{k}$ in L_k. Then, due to non-negative sum property, $\bar{P}_{out}$ is also convex in L_k. As a result, $\bar{P}_{out}$ is jointly convex (also psuedoconvex) in x and y for fixed z [117].

To show the pseudoconvexity of $\widehat{P}_{out}^{k}$ with z for fixed x and y, let $z_0 \triangleq \left\{z\middle|\left(\frac{\partial \bar{P}_{out}}{\partial z}=\mathcal{G}_1-\mathcal{G}_2=0\right)\right\}$, where

$$\mathcal{G}_1 \triangleq 2\alpha\frac{\gamma_{th}}{\tilde{\gamma}_o}z\sum_{k=1}^{K}\frac{(1+w_k)\mathcal{A}_k}{1+w_k\kappa}, \tag{A.2.7}$$

$$\mathcal{G}_2 \triangleq 180\frac{\gamma_{th}}{\tilde{\gamma}_o}D\sum_{k=1}^{K}\frac{w_k(1-\kappa)\mathcal{A}_k\sqrt{(x-x_k)^2+(y-y_k)^2}}{\pi(w_k+1)^2}, \tag{A.2.8}$$

$\mathcal{A}_i=\big[(x-x_k)^2+(y-y_k)^2+z^2\big]^{\alpha-1}$ and $w_i = C\exp\Big(-D\Big(\frac{180}{\pi}\sin^{-1}\Big(\frac{z}{\sqrt{(x-x_k)^2+(y-y_k)^2+z^2}}\Big)-C\Big)\Big)$. Using (A.2.7) and (A.2.8), we observe that $\mathcal{G}_1 > \mathcal{G}_2$ for $z > z_0$ and $\mathcal{G}_1 < \mathcal{G}_2$, otherwise. This implies $\frac{\partial \bar{P}_{out}}{\partial z} > 0$ *i.e.,* increasing function for $z > z_0$ and $\frac{\partial \bar{P}_{out}}{\partial z} < 0$ *i.e.,* decreasing function for $z < z_0$. This proves the pseudoconvexity of $\bar{P}_{out}$ with respect to z for given x and y.

A.2.3 Proof of Lemma 5: Conditional Joint Convexity of $\bar{P}_{out}$ in x, y, and z

Although $\bar{P}_{out}$ is non-convex with respect to x, y, and z, we can still find the region where $\bar{P}_{out}$ is jointly convex. As stated in Appendix A.1.2, (A.2.4) is jointly convex in L_k for a fixed z. Thus, if we prove that $\widehat{P}^k_{out}$ is conditionally jointly convex in L_k, and z, the same can be applied to x, y, and z. The Hessian of $\widehat{P}^k_{out}$ is given as $\mathcal{H}(\widehat{P}^k_{out})=\begin{bmatrix} \frac{\partial^2 \widehat{P}^k_{out}}{\partial L_k^2} & \frac{\partial^2 \widehat{P}^k_{out}}{\partial L_k \partial z} \\ \frac{\partial^2 \widehat{P}^k_{out}}{\partial z \partial L_k} & \frac{\partial^2 \widehat{P}^k_{out}}{\partial z^2} \end{bmatrix}$, where $\frac{\partial^2 \widehat{P}^k_{out}}{\partial L_k^2}$ is given by (A.2.6) and $\frac{\partial^2 \widehat{P}^k_{out}}{\partial z \partial L_k}=\frac{\partial^2 \widehat{P}^k_{out}}{\partial L_k \partial z}$ is given as

$$\frac{\partial^2 \widehat{P}^k_{out}}{\partial z \partial L_k} =\frac{\mathcal{A}_1}{2}\Bigg[\frac{(\alpha-1)(w_k+1)L_k z}{45D(1-\kappa)}+\Bigg(\frac{180DL_k z(w_k\kappa-1)}{\pi^2(w_k\kappa+1)^2} - \frac{(2\alpha-1)(L_k^2-z^2)}{\pi(w_k\kappa+1)}\Bigg)\times\frac{w_k}{\alpha}\Bigg], \tag{A.2.9}$$

$$\frac{\partial^2 \widehat{P}^k_{out}}{\partial z^2} =\mathcal{A}_1\Bigg[\frac{w_k L_k}{\alpha\pi}\Bigg(\frac{(2\alpha+1)z}{(w_k\kappa+1)}+\frac{90DL_k(1-w_k\kappa)}{\pi(w_k\kappa+1)^2}\Bigg) + \frac{(w_k+1)\Big((2\alpha-1)z^2+L_k^2\Big)}{180D(1-\kappa)}\Bigg], \tag{A.2.10}$$

where $\mathcal{A}_1 = 360D\alpha\frac{\gamma_{th}}{\tilde{\gamma}_o}\frac{(1-\kappa)}{(w_k\kappa+1)}\left(L_k^2+z^2\right)^{\alpha-2}$ and $w_k = C\exp\Big(-D\Big(\frac{180}{\pi}\sin^{-1}\Big(\frac{z}{\sqrt{L_k^2+z^2}}\Big)-C\Big)\Big)$. From (A.2.6), $\frac{\partial^2 \widehat{P}^k_{out}}{\partial L_k^2} > 0, \quad \forall\, L_k, z$ and from (A.2.10), $\frac{\partial^2 \widehat{P}^k_{out}}{\partial z^2} > 0, \quad \forall\, L_k$, and $z > L_k/4.5$. To show $det[\mathcal{H}(\widehat{P}^k_{out})] > 0$, we need to show that $\mathcal{K}_1 \triangleq \frac{\partial^2 \widehat{P}^k_{out}}{\partial L_k^2} - \frac{\partial^2 \widehat{P}^k_{out}}{\partial z \partial L_k} > 0$, and $\mathcal{K}_2 \triangleq \frac{\partial^2 \widehat{P}^k_{out}}{\partial z^2} - \frac{\partial^2 \widehat{P}^k_{out}}{\partial z \partial L_k} > 0$. By substituting any value for $z > L_k/4.5$, say $z = L_k/4$ in $\mathcal{K}_1$ and $\mathcal{K}_2$, we get,

$$\mathcal{K}_1 =\mathcal{A}_2\Bigg(\frac{2070(2\alpha-1)w_k D}{\pi(w_k\kappa+1)^2}+\frac{\alpha(24\alpha-7)(w_k+1)}{(w_k\kappa+1)(1-\kappa)}+ \frac{81000w_k D^2(1-w_k\kappa)}{\pi^2(w_k\kappa+1)^3}\Bigg), \tag{A.2.11}$$

$$\mathcal{K}_2 =\mathcal{A}_2\Bigg(\frac{90\pi(46\alpha-7)w_k D}{\pi(w_k\kappa+1)^2}+\frac{\alpha(23-6\alpha)(w_k+1)}{(w_k\kappa+1)(1-\kappa)} + \frac{324000w_k D^2(1-w_k\kappa)}{\pi^2(w_k\kappa+1)^3}\Bigg), \tag{A.2.12}$$

where $\mathcal{A}_2 = 2^{5-4\alpha}17^{\alpha-2}\frac{\gamma_{th}}{\tilde{\gamma}_o}(1-\kappa)\left(L_k^2\right)^{\alpha-1}$. It can be easily observed that $\mathcal{K}_1 > 0$ and $\mathcal{K}_2 > 0$ from (A.2.11) and (A.2.12), respectively. This alongwith (A.2.6) and (A.2.10)

proves that $\widehat{P}_{out}^{k}$ is jointly convex in L_k and z with condition $z > L_k/4.5$. From L_k, the above condition can be written as $\mathcal{R}_C^k \triangleq z^k > \frac{\sqrt{(x-x_k)^2+(y-y_k)^2}}{4.5}$. The region $\mathcal{R}_C^k$ represents an inverted cone with center at (x_k, y_k). For each user we obtain similar cones. So, the overall the region ($\mathcal{R}_C$) over which $\bar{P}_{out}$ is jointly convex is given as the intersection region of all these cones as

$$\mathcal{R}_C = \bigcap_{k=1}^{K} \mathcal{R}_C^k. \tag{A.2.13}$$

A.3 Detailed Proofs of Chapter 6

A.3.1 Proof of Lemma 6

For ease of representation of $P_{k,m}^{L}[n]$ defined in (6.4), we take

$$\Phi_{k,m}[n] = \frac{z_m[n]}{\|\mathbf{q}_m[n] - \mathbf{w}_k\|}, \tag{A.3.1}$$

such that $P_{k,m}^{L}[n]$ can be expressed as

$$P_{k,m}^{L}[n] = \big(1 + C\exp\big(-D[\tan^{-1}\Phi_{k,m}[n] - C]\big)\big)^{-1}.$$

Then by introducing a variable $y_{k,m}[n]$, such that $0 \leq y_{k,m}[n] \leq P_{k,m}^{L}[n]$ we have

$$\big(1 + C\exp\big(-D[\tan^{-1}\Phi_{k,m}[n] - C]\big)\big) \leq \frac{1}{y_{k,m}[n]}, \tag{A.3.2}$$

$$y_{k,m}[n] \geq 0. \tag{A.3.3}$$

Substituting $y_{k,m}[n]$ in (6.13), we get $\alpha_{k,m}[n]\left(\|\mathbf{q}_m[n] - \mathbf{w}_k\|^2 + z_m[n]^2\right) \leq (1-\kappa)y_{k,m}[n] + \kappa$. To simplify further, we introduce $\beta_{k,m}[n]$, where

$$\alpha_{k,m}[n](\|\mathbf{q}_m[n] - \mathbf{w}_k\|^2 + z_m[n]^2) \leq \beta_{k,m}[n], \tag{A.3.4}$$

$$(1-\kappa)y_{k,m}[n] + \kappa \geq \beta_{k,m}. \tag{A.3.5}$$

With the above substitutions and introduction of auxiliary variables, it can be observed that the inequality constraint (6.13) is now equivalent to (A.3.2), (A.3.3), (A.3.4), (A.3.5).

A.3.2 Proof of Lemma 7

Here, to tackle the difficulty of (A.3.1), we change the equality to inequality, represented as

$$\Phi_{k,m}[n] \leq \frac{z_m[n]}{\|\mathbf{q}_m[n] - \mathbf{w}_k\|}, \forall k, m, n. \tag{A.3.6}$$

In the problem (P3.1.1) with (A.3.6) instead of (A.3.1) (we name this problem as (P3.1.2)), the optimal solution can only be achieved when (A.3.6) is active, that is, $\Phi_{k,m}[n] = \frac{z_m[n]}{\|\mathbf{q}_m[n]-\mathbf{w}_k\|}, \forall k, m, n,$. This can be proved by the contradiction. We assume that the optimal solution to (P3.1.2) is $\mathcal{R}^*, \mathbf{q}_{k,m}[n]^*, \mathcal{X}^*$, which satisfies $R_i\left(\alpha_{i,m}[n]^*\right) > \mathcal{R}^*, \exists i \in k$, and $R_k\left(\alpha_{k,m}[n]^*\right) = \mathcal{R}^*, k \neq i$. Then the value of $R_i\left(\alpha_{i,m}[n]^*\right)$ to make $R_i\left(\alpha_{i,m}[n]^*\right) = \mathcal{R}^*$ hold, whereas the objective function $\mathcal{R}^*$ does not change. Then to make this happen, we need to decrease the $b_{i,m}[n]$, which will not return a feasible solution as the value of $b_{i,m}[n]$ is fixed from the bandwidth optimization problem. This is in contraction to the optimal solution. Therefore, the constraint (A.3.6) need to be active while obtaining the optimal solution to (P3.1.2). Then, it can be observed that the problem (P3.1.2) has the same condition on constraints as of (P3.1.1). Moreover, due to the presence of same objective function, the solution to (P3.1.1) can be obtained while solving (P3.1.2). Thus, problem (P3.1.2) is equivalent to (P3.1.1).

Since (A.3.6) is of the form "convex $\times$ convex $\leq$ constant", we use square of sum formula to make (A.3.6) a difference of convex function. Then, we get

$$\frac{1}{2}\left(\Phi_{k,m}[n] + \|\mathbf{q}_m[n] - \mathbf{w}_k\|\right)^2 - \frac{1}{2}\left(\Phi_{k,m}[n]^2 + \|\mathbf{q}_m[n] - \mathbf{w}_k\|^2\right) \leq z_m[n]. \tag{A.3.7}$$

It can be observed that the (A.3.7) is of the form $f - g$, where f and g are both convex. To make (A.3.7) a convex constraint, g must be affine. Thus, we use first-order Taylor series expansion at any feasible point [99]. Then, g can be approximated as

$$\begin{aligned}\lambda_{k,m}[n] = &\frac{1}{2}\left(\Phi^r_{k,m}[n]^2 + \|\mathbf{q}^r_m[n] - \mathbf{w}_k\|^2\right) + \left(\Phi_{k,m}[n] - \Phi^r_{k,m}[n]\right) \\ &\Phi^r_{k,m}[n] + \|\mathbf{q}^r_m[n] - \mathbf{w}_k\|\left(\|\mathbf{q}_m[n] - \mathbf{w}_k\| - \|\mathbf{q}^r_m[n] - \mathbf{w}_k\|\right),\end{aligned} \tag{A.3.8}$$

where $\Phi^r_{k,m}[n], \mathbf{q}^r_m[n]$ is the value of $\Phi_{k,m}[n], \mathbf{q}_m[n]$ in the $r^{th}-$iteration, respectively. Using (A.3.8) in (A.3.7), the constraint in (A.3.6) is approximated to a convex constraint given in (6.16).

A.3.3 Proof of Lemma 8

To deal with the non-convex constraint in (6.8c), we introduce an auxiliary variable $D_{m,j}[n] = \{\mathbf{X}_m[n] - \mathbf{X}_j[n], \forall n, j \neq m\}$. Then, (6.8c) can be written as $\|D_{m,j}[n]\|^2 \geq D_{min}^2, \forall n, j \neq m$, so that the left side $\|D_{m,j}[n]\|^2$ is convex in $D_{m,j}[n]$. Using first order Taylor expansion to obtain the global lower bound of convex function, we get

$$\|D_{m,j}[n]\|^2 \geq 2\left(D_{m,j}^r[n]\right)^T\left(D_{m,j}[n] - D_{m,j}^r[n]\right) + \|D_{m,j}^r[n]\|^2, \tag{A.3.9}$$

for a given $D_{m,j}^r[n]$. Using (6.8c), (A.3.9) is converted into

$$\begin{aligned} &2\left(\mathbf{X}_m^r[n] - \mathbf{X}_j^r[n]\right)^T\left(\mathbf{X}_m[n] - \mathbf{X}_j[n] - \mathbf{X}_m^r[n] - \mathbf{X}_j^r[n]\right) + \\ &\|\mathbf{X}_m^r[n] - \mathbf{X}_j^r[n]\|^2 \geq D_{min}^2, \end{aligned} \tag{A.3.10}$$

where $\mathbf{X}_m^r[n] = (\mathbf{q}_m^r[n], z_m[n])$ and $\mathbf{X}_j^r[n] = (\mathbf{q}_j^r[n], z_j[n])$.

From (6.8d), it can be observed that the energy constraint is the non-negative sum of $e_1[n]$, where $e_1[n]$ is defined in (2.2). It can be observed that the first and third term is convex, where as the second term is non-convex. To deal with the second term, we follow the same procedure as described in [9] and add an additional non-convex constraint to make $e_1[n]$ convex. The additional non-convex constraint is given by

$$\frac{\tau^4}{g_1[n]^2} = g_1[n]^2 + \frac{\Delta_1[n]^2}{v_o^2},\ g_1[n] \geq 0,\ \forall n, \tag{A.3.11}$$

where $\Delta_1[n] = \|\mathbf{q}_1[n+1] - \mathbf{q}_1[n]\|$. Then the first order taylor expansion can be utilized to obtain its global lower bound, which is given by

$$\begin{aligned} g_1[n]^2 + \frac{\Delta_1[n]}{v_o^2} \geq\ & g_1^r[n]^2 + 2g_1^r[n]\left(g_1[n] - g_1^r[n]\right) - \frac{\Delta_1^r[n]}{v_o^2} \\ &+ \frac{2}{v_o^2}\left(\mathbf{q}_1^r[n+1] - \mathbf{q}_1^r[n]\right)^T\left(\mathbf{q}_1^r[n+1] - \mathbf{q}_1[n]\right), \end{aligned} \tag{A.3.12}$$

where $\Delta_1^r[n] = \|\mathbf{q}_1^r[n+1] - \mathbf{q}_1^r[n]\|$, and $g_1^r[n], \mathbf{q}_1^r[n]$, and $\mathbf{q}_1^r[n+1]$ are the values of $g_1[n], \mathbf{q}_1[n]$, and $\mathbf{q}_1[n+1]$ at r^{th}-iteration, respectively.

A.4 Detailed Proofs of Chapter 7

A.4.1 Proof of Lemma 9: Association probability of typical user with the LoS UAV

The probability of the typical user to be associated with the LoS UAV is given by

$$\mathcal{P}_{LoS} = \mathbb{P}[P_{L,x_k} > P_{N,x_k}] \tag{A.4.1}$$

$$\overset{(a)}{=} \mathbb{P}[P_B X_{L,x_k}^{-\alpha_L} H_{L,x_k} > P_B X_{N,x_k}^{-\alpha_N} H_{N,x_k}] \tag{A.4.2}$$

$$= \mathbb{P}\left[X_{N,x_k} > (X_{L,x_k})^{\frac{\alpha_L}{\alpha_N}} \left(\frac{H_{N,x_k}}{H_{L,x_k}}\right)^{\frac{1}{\alpha_N}}\right] \tag{A.4.3}$$

$$= \mathbb{P}\left[Z > 1\right] \tag{A.4.4}$$

$$\overset{(b)}{=} \bar{F}_Z(z), \tag{A.4.5}$$

where, $Z = \frac{X_{N,x_k}}{(X_{L,x_k})^{\frac{\alpha_L}{\alpha_N}} (H_{N,x_k}/H_{L,x_k})^{\frac{1}{\alpha_N}}}$. $\bar{F}_Z(z)$ denotes the complementary cumulative density function (CCDF) of Z. In the above equation, (a) is based on the definition of the association policy, and (b) is derived according to the definition of CCDF. Thus, to find the association probability, we compute the CCDF of Z defined in (A.4.5).

To this extent, let $Y = \frac{H_{N,x_k}}{H_{L,x_k}}$, where the PDF of H_{N,x_k} and H_{L,x_k} are given in (7.2). Then, according to the definition given in (7.4), we get

$$f_Y(y) = \frac{y^{m_N-1}}{\alpha^{m_L+m_N}\Gamma(m_L)\Gamma(m_N)} \int_0^\infty h_L^{m_L+m_N-1} e^{\frac{-h_L(1+y)}{\alpha}} \mathrm{d}h_L$$

$$= \frac{1}{\beta(m_L, m_N)} y^{m_N-1}(1+y)^{-m_L-m_N}, y \geq 0, \tag{A.4.6}$$

where $\beta(.)$ denote the beta distribution. Further, let $W = \left(\frac{H_{N,x_k}}{H_{L,x_k}}\right)^{\frac{1}{\alpha_N}}$, then the PDF of W is computed using the transformation of random variable as described in (7.6). Then, $f_W(w)$ is given by

$$f_W(w) = f_Y(w^{\alpha_N})\alpha_N w^{(\alpha_N-1)}, w \geq 0. \tag{A.4.7}$$

Using (A.4.6), the PDF of W with $w \geq 0$ is given by

$$f_W(w) = \frac{\alpha_N}{w\beta(m_L, m_N)} (w^{\alpha_N})^{m_N} (1+w^{\alpha_N})^{-m_L-m_N}. \tag{A.4.8}$$

Similarly, let $B = (X_{L,x_k})^{\frac{\alpha_L}{\alpha_N}} = (X_{L,x_k})^{1/A}$, where $A = \frac{\alpha_N}{\alpha_L}$ and PDF of X_{L,x_k} is defined

in (7.8). Then, the PDF of B $f_B(b)$ obtained using transformation in (7.6) is given by

$$\begin{aligned} f_B(b) &= f_{X_L}(b^A).Ab^{A-1} \\ &= \frac{2\pi\alpha_N}{\alpha_L} b^{\frac{2\alpha_N}{\alpha_L}-1} P_L\left(b^{\frac{\alpha_N}{\alpha_L}}\right) \lambda \exp\left(\mathcal{X}\left(b^{\frac{\alpha_N}{\alpha_L}}\right)\right), b \geq H^{\frac{\alpha_L}{\alpha_N}}, \end{aligned} \tag{A.4.9}$$

where $\mathcal{X}(.)$ is defined in (7.9). Since random variable X_{L,x_k} takes value greater than or equal to H, accordingly $b \geq H^{\frac{\alpha_L}{\alpha_N}}$. Next, we need to compute the PDF for $Q = (X_{L,x_k})^{\frac{\alpha_L}{\alpha_N}} \left(\frac{H_{N,x_k}}{H_{L,x_k}}\right)^{\frac{1}{\alpha_N}}$ *i.e.,* $Q = W.B$. Using product property of positive random variable defined in (7.5) and substituting the PDF of W and B from (A.4.8), and (A.4.9), respectively in (7.5), we get

$$\begin{aligned} f_Q(q) = \frac{2\pi\alpha_N^2\lambda}{\alpha_L\beta(m_L,m_N)} \int_{b=H^{\frac{\alpha_L}{\alpha_N}}}^{\infty} \Bigg\{ \frac{1}{q} P_L\left(b^{\frac{\alpha_N}{\alpha_L}}\right) b^{\frac{2\alpha_N}{\alpha_L}-1} \\ \times \left(\left(\frac{q}{b}\right)^{\alpha_N}\right)^{m_N} \left(\left(\frac{q}{b}\right)^{\alpha_N}+1\right)^{-m_L-m_N} \exp\left(\mathcal{X}\left(b^{\frac{\alpha_N}{\alpha_L}}\right)\right) \Bigg\} \mathrm{d}b. \end{aligned} \tag{A.4.10}$$

The cumulative density function (CDF) of $Z = \frac{X_{N,x_k}}{Q}$ defined in (A.4.4) can be obtained as

$$F_Z(z) = \int_{H/z}^{\infty} F_{X_{N,x_k}}(qz) f_Q(q) \mathrm{d}q, \tag{A.4.11}$$

where $F_{X_{N,x_k}}(qz)$ is the CDF of X_{N,x_k} obtained by using the PDF $f_{X_{N,x_k}}(x)$ defined in (7.8), which is given by $F_{X_{N,x_k}}(qz) = 1 - \exp\left(\mathcal{X}(qz)\right)$ with $\mathcal{X}(.)$ defined in (7.9). Since $X_{N,x_k} \geq H$, then $q \geq H/z$. Therefore, the lower limit of the CDF in (A.4.11) is set to $q = H/z$.

Then, $\bar{F}_Z(z)$ defined in (A.4.5) *i.e.,* the user association probability with closest LoS UAV, $\mathcal{P}_{LoS}$ is given by

$$\mathcal{P}_{LoS} \triangleq \bar{F}_Z(z) \triangleq 1 - F_Z(z). \tag{A.4.12}$$

Using (A.4.10) and $F_{X_{N,x_k}}(qz)$ in (A.4.12), we obtain $\mathcal{P}_{LoS}$ defined in (7.10).

A.4.2 Proof of Lemma 10: Approximate association probability of typical user with LoS UAV

Here we again need to compute the CDF of $Z = \frac{X_{N,x_k}}{Q}$, where $Q = W.B$. To ensure the analytical tractability, the α_N is chosen such that $\alpha_N \approx \alpha_L$, then PDF of B as described

in (A.4.9) is equal to the PDF of X_{L,x_k}, which is given by

$$f_B(b) = \mathcal{A}_2\, b\, \exp\left(-\pi P_L \lambda\, b^2\right), \quad b \geq H, \tag{A.4.13}$$

where $\mathcal{A}_2 = 2\pi\, P_L \lambda\, \exp(\pi P_L \lambda H^2)$. Following the same procedure as described in (A.4.7) to compute the PDF of W, with $m_L = m_N = 1$, we get

$$f_W(w) = \frac{\alpha_N w^{\alpha_N - 1}}{(1 + w^{\alpha_N})^2}, \quad w \geq 0. \tag{A.4.14}$$

Similarly using the product property, PDF of Q (by taking $\alpha_N \approx \alpha_L = 2$) is given by

$$f_Q(q) = 2\,\mathcal{A}_2\, q \int_{b=H}^{\infty} \frac{b^3}{\left(b^2 + q^2\right)^2} \exp\left(-s_L b^2\right) \mathrm{d}b, \tag{A.4.15}$$

where $s_L = \pi P_L \lambda$. Substituting $b^2 = \tilde{x}$ to transform the integral, we get

$$f_Q(q) = \mathcal{A}_2\, q \int_{\tilde{x}=H^2}^{\infty} \frac{\tilde{x}}{\left(\tilde{x} + q^2\right)^2} \exp\left(-s_L\, \tilde{x}\right)\, \mathrm{d}\tilde{x}. \tag{A.4.16}$$

Since (A.4.16) is difficult to solve, we break the integral into two parts, which is given by

$$\begin{aligned} f_Q(q) = &\underbrace{\mathcal{A}_2\, q \int_{\tilde{x}=0}^{\infty} \frac{\tilde{x}}{\left(\tilde{x} + q^2\right)^2} \exp\left(-s_L\, \tilde{x}\right)\, \mathrm{d}\tilde{x}}_{f_{Q_1}(q)} \\ &- \underbrace{\mathcal{A}_2\, q \int_{\tilde{x}=0}^{H^2} \frac{\tilde{x}}{\left(\tilde{x} + q^2\right)^2} \exp\left(-s_L\, \tilde{x}\right)\, \mathrm{d}\tilde{x}}_{f_{Q_2}(q)}. \end{aligned} \tag{A.4.17}$$

Representing exponential term in $f_{Q_1}(q)$ into Meijer-G form, we get

$$f_{Q_1}(q) = \mathcal{A}_2\, q \int_{\tilde{x}=0}^{\infty} \frac{\tilde{x}}{\left(\tilde{x} + q^2\right)^2} G_{0,1}^{1,0}\left(s_L \tilde{x} \,\middle|\, \begin{matrix} - \\ 0 \end{matrix} \right) \mathrm{d}\tilde{x}, \tag{A.4.18}$$

Then using [116, Eq. 07.34.21.0086.01], we get

$$f_{Q_1}(q) = \frac{\mathcal{A}_2 q}{\Gamma(2)} G_{1,2}^{2,1}\left(s_L\, q^2 \,\middle|\, \begin{matrix} -1 \\ 0 \quad 0 \end{matrix} \right). \tag{A.4.19}$$

On the other hand, representing exponential in series form, $f_{Q_2}(q)$ can be simplified into

$$f_{Q_2}(q) = \mathcal{A}_2\, q \sum_{k=0}^{\infty} \frac{(-s_L)^k}{k!} \int_{\tilde{x}=0}^{H^2} \frac{\tilde{x}^{k+1}}{(\tilde{x}+q^2)^2}\, \mathrm{d}\tilde{x}. \tag{A.4.20}$$

Using the integral property [118, Eq. 3.194], we get

$$f_{Q_2}(q) = \frac{\mathcal{A}_2}{q^3} \sum_{k=0}^{\infty} \frac{(-s_L)^k}{k!} \frac{(h^2)^{k+2}}{k+2}\, {}_2F_1(2, k+2; k+3; \frac{-h^2}{q^2}), \tag{A.4.21}$$

where ${}_2F_1(\cdot;\cdot;\cdot)$ is the Gauss hypergeometric function. Then, $F_Z(z)$ as obtained in (A.4.11) is given as

$$F_Z(z) = \int_H^{\infty} F_{X_{N,x_k}}(qz) f_Q(q) \mathrm{d}q, \tag{A.4.22}$$

where $F_{X_{N,x_k}} = 1 - \exp(-s_N(x^2 - H^2))$, is obtained by using the PDF of X_{N,x_k}, defined in (7.12), where $s_N = \pi P_N \lambda$. Then, $F_Z(z)$ in (A.4.22) is written as

$$F_Z(z) = \int_H^{\infty} f_Q(q) \mathrm{d}q - \mathcal{A}_3 \int_H^{\infty} \exp(-s_N z^2 q^2) f_Q(q) \mathrm{d}q, \tag{A.4.23}$$

where $\mathcal{A}_3 = \exp(-s_N H^2)$. Since $Q = W.B$ then according to (A.4.13), and (A.4.14), $q \geq H$, then $\int_H^{\infty} f_Q(q)\mathrm{d}q = 1$. Thus, we get

$$F_Z(z) = 1 - \mathcal{A}_3 \int_H^{\infty} \exp(-s_N z^2 q^2) f_Q(q) \mathrm{d}q. \tag{A.4.24}$$

According to the definition of association probability, $\bar{F}_Z(z) = 1 - F_Z(z)$. Then, the approximated association probability, denoted by $\widetilde{\mathcal{P}}_{LoS}$ is given by $\widetilde{\mathcal{P}}_{LoS} \triangleq \bar{F}_Z(z) = \exp(-s_N H^2)\mathcal{T}$, where $\mathcal{T}$ is defined in (7.13).

References

[1] K. P. Valavanis and G. J. Vachtsevanos. *Handbook of unmanned aerial vehicles*, volume 1. Amsterdam, The Netherlands: Springer, 2014.

[2] R. Austin. *Unmanned aircraft systems: UAVs design, development and deployment.* Hoboken, NJ, USA: Wiley, 2011.

[3] M. A. Lahmeri, M. A. Kishk, and M. S. Alouini. Charging techniques for UAV-assisted data collection: Is laser power beaming the answer? *IEEE Commun. Mag.*, 60(5):50–56, May 2022.

[4] Y. Zeng, R. Zhang, and T. J. Lim. Wireless communications with unmanned aerial vehicles: Opportunities and challenges. *IEEE Commun. Mag.*, 54(5):36–42, May 2016.

[5] B. Li, Z. Fei, and Y. Zhang. UAV communications for 5G and beyond: Recent advances and future trends. *IEEE Internet Things J.*, 6(2):2241–2263, Dec. 2019.

[6] Y. Zeng, X. Xu, and R. Zhang. Trajectory design for completion time minimization in UAV-enabled multicasting. *IEEE Trans. Wireless Commun.*, 17(4):2233–2246, Apr. 2018.

[7] G. Ding, Q. Wu, L. Zhang, Y. Lin, T. A. Tsiftsis, and Y. D. Yao. An amateur drone surveillance system based on the cognitive internet of things. *IEEE Commun. Mag.*, 56(1): 29–35, Jan. 2018.

[8] L. Nagpal and K. Samdani. Project loon: Innovating the connectivity worldwide. In *Proc. IEEE Int. Conf. Recent Trends in Electronics, Information & Commun. Technol. (RTEICT), Bangalore, India*, pages 1778–1784, May 2017.

[9] Y. Zeng, J. Xu, and R. Zhang. Energy minimization for wireless communication with rotary-wing UAV. *IEEE Trans. Wireless Commun.*, 18(4):2329–2345, Apr. 2019.

[10] Y. Zeng and R. Zhang. Energy-efficient UAV communication with trajectory optimization. *IEEE Trans. Wireless Commun.*, 16(6):3747–3760, June 2017.

[11] Q. Wu, J. Xu, Y. Zeng, D. W. K. Ng, N. Al-Dhahir, R. Schober, and A. L. Swindlehurst. A comprehensive overview on 5G-and-beyond networks with UAVs: From communications to sensing and intelligence. *IEEE J. Selected Areas Commun.*, 39(10):2912–2945, Jun. 2021.

[12] Z. Ullah, F. Al-Turjman, and L. Mostarda. Cognition in UAV-aided 5G and beyond communications: A survey. *IEEE Trans. Cognitive Commun. Netw.*, 6(3):872–891, Jan. 2020.

[13] G. Gui, M. Liu, F. Tang, N. Kato, and F. Adachi. 6G: Opening new horizons for integration of comfort, security, and intelligence. *IEEE Wireless Commun.*, 27(5):126–132, Oct. 2020.

[14] E. Chaalal, S. M. Senouci, and L. Reynaud. A new framework for multi-hop ABS-assisted 5G-networks with users' mobility prediction. *IEEE Trans. Veh. Technol.*, 71(4):4412–4427, Apr. 2022.

[15] M. Coupechoux, J. Darbon, J. M. Kelif, and M. Sigelle. Optimal trajectories of a UAV base station using hamilton-jacobi equations. *IEEE Trans. Mobile Computing*, pages 1–1, Mar. 2022. doi: 10.1109/TMC.2022.3156822.

[16] Rheinmettal Defence Australia Pty. Ltd. URL www.mobilecorp.com.au/blog/mobilecorp-is-the-lead-technology-partner-for-5G-innovation-initiative-grant/.

[17] IEEE draft standard for aerial communications and networking standards. *IEEE P1920.1/D4*, pages 1–85, Aug. 2020.

[18] Y. Zeng, J. Lyu, and R. Zhang. Cellular-connected UAV: Potential, challenges, and promising technologies. *IEEE Wireless Commun.*, 26(1):120–127, Feb 2019.

[19] A. S. Abdalla and V. Marojevic. Machine learning-assisted UAV operations with the UTM: Requirements, challenges, and solutions. In *Proc. IEEE 92nd Veh. Technol. Conf. (VTC2020-Fall), Victoria, BC, Canada*, pages 1–5, Dec. 2020.

[20] Y. Zeng, R. Zhang, and T. J. Lim. Wireless communications with unmanned aerial vehicles: Opportunities and challenges. *IEEE Commun. Mag.*, 54(5):36–42, May 2016.

[21] P. Yang, X. Cao, C. Yin, Z. Xiao, X. Xi, and D. Wu. Proactive drone-cell deployment: Overload relief for a cellular network under flash crowd traffic. *IEEE Trans. Intell. Transp. Syst.*, 18(10):2877–2892, Oct. 2017.

[22] M. Mozaffari, W. Saad, M. Bennis, Y. Nam, and M. Debbah. A tutorial on UAVs for wireless networks: Applications, challenges, and open problems. *IEEE Commun. Surveys Tuts.*, 21 (3):2334–2360, Mar. 2019.

[23] M. Mozaffari, W. Saad, M. Bennis, and M. Debbah. Drone small cells in the clouds: Design, deployment and performance analysis. In *Proc. IEEE Global Commun. Conf. (GLOBECOM), San Diego, CA, USA*, pages 1–6, Dec. 2015.

[24] A. R. S. Bramwell, G. Done, and D. Balmford. *Bramwell's helicopter dynamics (Butterworth-Heinemann)*. 2nd ed. Washington, DC, USA:AIAA, 2001.

[25] Yuntao W., Z. Su, N. Zhang, and R. Li. Mobile wireless rechargeable UAV networks: Challenges and solutions. *IEEE Commun. Mag.*, 60(3):33–39, Mar. 2022.

[26] H. Sallouha, M. M. Azari, A. Chiumento, and S. Pollin. Aerial anchors positioning for reliable RSS-based outdoor localization in urban environments. *IEEE Wireless Commun. Lett.*, 7 (3):376–379, June 2018.

[27] G. Han, J. Jiang, C. Zhang, T. Q. Duong, M. Guizani, and G. K. Karagiannidis. A survey on mobile anchor node assisted localization in wireless sensor networks. *IEEE Commun. Surveys Tuts.*, 18(3):2220–2243, Mar. 2016.

[28] Q. Hu, Y. Cai, G. Yu, Z. Qin, M. Zhao, and G. Y. Li. Joint offloading and trajectory design for UAV-enabled mobile edge computing systems. *IEEE Internet Things J.*, 6(2):1879–1892, Apr. 2019.

[29] Z. Yang, W. Xu, and M. Shikh-Bahaei. Energy efficient UAV communication with energy harvesting. *IEEE Trans. Veh. Technol.*, 69(2):1913–1927, Feb. 2020.

[30] T. Zhang, G. Liu, H. Zhang, W. Kang, G. K. Karagiannidis, and A. Nallanathan. Energy-efficient resource allocation and trajectory design for UAV relaying systems. *IEEE Trans. Commun.*, 68(10):6483–6498, Oct. 2020.

[31] Z. Liu, R. Sengupta, and A. Kurzhanskiy. A power consumption model for multi-rotor small unmanned aircraft systems. In *Proc. Int. Conf. Unmanned Aircraft Sys. (ICUAS), Miami, FL, USA*, pages 310–315, June 2017.

[32] A. Al-Hourani, S. Kandeepan, and S. Lardner. Optimal LAP altitude for maximum coverage. *IEEE Wireless Commun. Lett.*, 3(6):569–572, Dec. 2014.

[33] M. Mozaffari, W. Saad, M. Bennis, and M. Debbah. Unmanned aerial vehicle with underlaid device-to-device communications: Performance and tradeoffs. *IEEE Trans. Wireless Commun.*, 15(6):3949–3963, Feb. 2016.

[34] M. Mozaffari, W. Saad, M. Bennis, and M. Debbah. Efficient deployment of multiple unmanned aerial vehicles for optimal wireless coverage. *IEEE Commun. Lett.*, 20(8): 1647–1650, June 2016.

[35] J. Lyu, Y. Zeng, R. Zhang, and T. J. Lim. Placement optimization of UAV-mounted mobile base stations. *IEEE Commun. Lett.*, 21(3):604–607, Mar. 2017.

[36] R. I. Bor-Yaliniz, A. El-Keyi, and H. Yanikomeroglu. Efficient 3D placement of an aerial base station in next generation cellular networks. In *Proc. IEEE Int. Conf. Commun. (ICC), Kuala Lumpur, Malaysia*, pages 1–5, May 2016.

[37] M. Alzenad, A. El-Keyi, and H. Yanikomeroglu. 3D placement of an unmanned aerial vehicle base station for maximum coverage of users with different QoS requirements. *IEEE Wireless Commun. Lett.*, 7(1):38–41, Feb. 2018.

[38] X. Zhong, Y. Huo, X. Dong, and Z. Liang. QoS-compliant 3D deployment optimization strategy for UAV base stations. *IEEE Sys. J.*, pages 1–9, Aug. 2020. doi: 10.1109/JSYST.2020.3015428.

[39] H. He, S. Zhang, Y. Zeng, and R. Zhang. Joint altitude and beamwidth optimization for UAV-enabled multiuser communications. *IEEE Commun. Lett.*, 22(2):344–347, Nov. 2018.

[40] M. Alzenad, A. El-Keyi, F. Lagum, and H. Yanikomeroglu. 3D placement of an unmanned aerial vehicle base station (UAV-BS) for energy-efficient maximal coverage. *IEEE Wireless Commun. Lett.*, 6(4):434–437, Aug. 2017.

[41] I. Valiulahi and C. Masouros. Multi-UAV deployment for throughput maximization in the presence of co-channel interference. *IEEE Internet Things J.*, 8(5):3605–3618, Mar. 2021.

[42] Q. Wu, Y. Zeng, and R. Zhang. Joint trajectory and communication design for UAV-enabled multiple access. In *Proc. IEEE Global Commun. Conf. (GLOBECOM), Singapore*, pages 1–6, Dec. 2017.

[43] Y. Zeng, R. Zhang, and T. J. Lim. Throughput maximization for UAV-enabled mobile relaying systems. *IEEE Trans. Commun.*, 64(12):4983–4996, Dec. 2016.

[44] Q. Wu, Y. Zeng, and R. Zhang. Joint trajectory and communication design for multi-UAV enabled wireless networks. *IEEE Trans. Wireless Commun.*, 17(3):2109–2121, Mar. 2018.

[45] M. Hua, L. Yang, C. Pan, and A. Nallanathan. Throughput maximization for full-duplex UAV aided small cell wireless systems. *IEEE Wireless Commun. Lett.*, 9(4):475–479, Apr. 2020.

[46] F. Cheng, S. Zhang, Z. Li, Y. Chen, N. Zhao, F. R. Yu, and V. C. M. Leung. UAV trajectory optimization for data offloading at the edge of multiple cells. *IEEE Trans. Veh. Techol.*, 67 (7):6732–6736, Mar. 2018.

[47] N. Gupta, D. Mishra, and S. Agarwal. 3D-trajectory design for outage minimization in UAV-assisted 5G communication system. In *Proc. IEEE IEEE Consumer Commun. Net. Conf. (CCNC), Las Vegas, USA*, pages 1–6, Jan. 2021.

[48] N. Gupta, D. Mishra, and S. Agarwal. 3D-trajectory design for outage minimization in UAV-assisted 5G communication system. In *Proc. IEEE Consumer Commun. Net. Conf. (CCNC), Las Vegas, USA*, pages 1–6, Jan. 2021.

[49] F. Zeng, Z. Hu, Z. Xiao, H. Jiang, S. Zhou, W. Liu, and D. Liu. Resource allocation and trajectory optimization for QoE provisioning in energy-efficient UAV-enabled wireless networks. *IEEE Trans. Veh. Technol.*, 69(7):7634–7647, July 2020.

[50] M. Hua, Y. Wang, C. Li, Y. Huang, and L. Yang. Energy-efficient optimization for UAV-aided cellular offloading. *IEEE Wireless Commun. Lett.*, 8(3):769–772, June 2019.

[51] F. Wu, D. Yang, L. Xiao, and L. Cuthbert. Energy consumption and completion time tradeoff in rotary-wing UAV enabled WPCN. *IEEE Access*, 7:79617–79635, June 2019.

[52] J. Gu, H. Wang, G. Ding, Y. Xu, Z. Xue, and H. Zhou. Energy-constrained completion time minimization in UAV-enabled internet of things. *IEEE Internet Things J.*, 7(6):5491–5503, June 2020.

[53] S. Eom, H. Lee, J. Park, and I. Lee. UAV-aided wireless communication designs with propulsion energy limitations. *IEEE Trans. Veh. Technol.*, 69(1):651–662, Jan. 2020.

[54] H. Dai, H. Bian, C. Li, and B. Wang. UAV-aided wireless communication design with energy constraint in space-air-ground integrated green IoT networks. *IEEE Access*, 8:86251–86261, May 2020.

[55] X. Jing and C. Masouros. UAV trajectory design and bandwidth allocation for coverage maximization with energy and time constraints. In *Proc. IEEE Int. Sym. Personal, Indoor and Mobile Radio Commun., London, UK*, pages 1–6, Sep. 2020.

[56] Y. Cai, Z. Wei, R. Li, D. W. Kwan Ng, and J. Yuan. Energy-efficient resource allocation for secure UAV communication systems. In *Proc. IEEE Wireless Commun. Net. Conf. (WCNC), Marrakech, Morocco*, pages 1–8, Apr. 2019.

[57] S. Ahmed, M. Z. Chowdhury, and Y. Jang. Energy-efficient UAV-to-user scheduling to maximize throughput in wireless networks. *IEEE Access*, 8:21215–21225, Jan 2020.

[58] Y. Chang. N-dimension golden section search: Its variants and limitations. In *Proc. BMEI, Tianjin, China*, pages 1–6, Oct. 2009.

[59] C. Cartis, N. IM Gould, and P. L. Toint. *On the complexity of the steepest-descent with exact linesearches*. Science & Technol. Facilities Council, Sep. 2012.

[60] A. Alsharoa, H. Ghazzai, M. Yuksel, A. Kadri, and A. E. Kamal. Trajectory optimization for multiple UAVs acting as wireless relays. In *Proc. IEEE Int. Conf. Commun. Workshops (ICC Workshops), Kansas City, USA*, pages 1–6, May 2018.

[61] H. Lee, Y. Kim, Y. Han, and C. Y. Park. Centroid-based movement assisted sensor deployment schemes in wireless sensor networks. In *Proc. IEEE Veh. Technol. Conf. Fall, Anchorage, AK, USA*, pages 1–5, Sep. 2009.

[62] X. Yuan, T. Yang, Y. Hu, J. Xu, and A. Schmeink. Trajectory design for UAV-enabled multiuser wireless power transfer with nonlinear energy harvesting. *IEEE Trans. Wireless Commun.*, 20(2):1105–1121, Feb. 2021.

[63] S. Zhang, H. Zhang, Q. He, K. Bian, and L. Song. Joint trajectory and power optimization for UAV relay networks. *IEEE Commun. Lett.*, 22(1):161–164, Jan. 2018.

[64] S. Zeng, H. Zhang, K. Bian, and L. Song. UAV relaying: Power allocation and trajectory optimization using decode-and-forward protocol. In *Proc. IEEE Int. Conf. Commun. Workshops (ICC Workshops), Kansas City, United States*, pages 1–6, May 2018.

[65] C. You, X. Peng, and R. Zhang. 3D trajectory design for UAV-enabled data harvesting in probabilistic LoS channel. In *Proc. IEEE Global Commun. Conf. (GLOBECOM), Puako, Hawaii, United States*, pages 1–6, Dec. 2019.

[66] C. D. Franco and G. Buttazzo. Energy-aware coverage path planning of UAVs. In *Proc. IEEE Int. Conf. Auton. Robot Syst. and Competitions, Vila Real, Portugal*, pages 111–117, Apr. 2015.

[67] S. Ahmed, M. Z. Chowdhury, and Y. M. Jang. Energy-efficient UAV relaying communications to serve ground nodes. *IEEE Commun. Lett.*, 24(4):849–852, Apr. 2020.

[68] G. Yang, R. Dai, and Y. C. Liang. Energy-efficient UAV backscatter communication with joint trajectory design and resource optimization. *IEEE Trans. Wireless Commun.*, 20(2): 926–941, Feb. 2021.

[69] M. T. Nguyen and L. B. Le. Flight scheduling and trajectory control in UAV-based wireless networks. In *Proc. IEEE Wireless Commun. and Netw. Conf. (WCNC), Seoul, Korea (South)*, pages 1–6, May 2020.

[70] X. Jing, J. Sun, and C. Masouros. Energy aware trajectory optimization for aerial base stations. *IEEE Trans. Commun.*, 69(5):3352–3366, May 2021.

[71] T. Zhang, J. Lei, Y. Liu, C. Feng, and A. Nallanathan. Trajectory optimization for UAV emergency communication with limited user equipment energy: A safe-DQN approach. *IEEE Trans. Green Commun. & Netw.*, 5(3):1236–1247, Sep. 2021.

[72] Y. Gao, L. Xiao, F. Wu, D. Yang, and Z. Sun. Cellular-connected UAV trajectory design with connectivity constraint: A deep reinforcement learning approach. *IEEE Trans. Green Commun. & Netw.*, 5(3):1369–1380, Sep. 2021.

[73] N. Gupta, S. Agarwal, and D. Mishra. Trajectory design for throughput maximization in UAV-assisted communication system. *IEEE Trans. Green Commun. & Netw.*, 5(3): 1319–1332, Sep. 2021.

[74] A. Meng, X. Gao, Y. Zhao, and Z. Yang. Three-dimensional trajectory optimization for energy-constrained UAV-enabled IoT system in probabilistic LoS channel. *IEEE Internet Things J.*, 9(2):1109–1121, Jan. 2022.

[75] A. M. Hayajneh, S. A. R. Zaidi, D. C. McLernon, and M. Ghogho. Optimal dimensioning and performance analysis of drone-based wireless communications. In *Proc. IEEE Globecom Workshops, Washington, D.C., United States*, pages 1–6, Dec. 2016.

[76] A. Girdher, A. Bansal, and A. Dubey. On the performance of SLIPT-enabled df relay-aided hybrid OW/RF network. *IEEE Sys. J.*, pages 1–12, Jan. 2022. doi: 10.1109/JSYST.2021.3135957.

[77] D. Mishra, S. De, and C. Chiasserini. Joint optimization schemes for cooperative wireless information and power transfer over rician channels. *IEEE Trans. Commun.*, 64(2):554–571, Feb. 2016.

[78] U. Niesen, D. Shah, and G. Wornell. Adaptive alternating minimization agorithms. In *Proc. IEEE Int. Symp. Inf. Theory, Nice, France*, pages 1641–1645, June 2007.

[79] J. C. Meza. Steepest descent. *Wiley Interdisciplinary Reviews: Computational Statistics*, 2 (6):719–722, Dec. 2010.

[80] C. Cartis, N. I. M. Gould, and P. Toint. *On the complexity of the steepest-descent with exact linesearches*. NAXYS Technical Report. FUNDP. Namur center for complex systems, 2012.

[81] G. Prasad, D. Mishra, K. Tourki, A. Hossain, and M. Debbah. QoS- and energy-aware optimal resource allocations in DF relay-assisted FSO networks. *IEEE Trans. Green Commun. & Netw.*, 4(3):914–926, Sep. 2020.

[82] A. Brown and D. Anderson. Trajectory optimization for high-altitude long-endurance UAV maritime radar surveillance. *IEEE Trans. Aerospace & Electronic Sys.*, 56(3):2406–2421, Jun. 2020.

[83] H. Teng, I. Ahmad, A. Msm, and K. Chang. 3D optimal surveillance trajectory planning for multiple UAVs by using particle swarm optimization with surveillance area priority. *IEEE Access*, 8:86316–86327, May 2020.

[84] C. Zhan, Y. Zeng, and R. Zhang. Energy-efficient data collection in UAV enabled wireless sensor network. *Wireless Commun. Lett.*, 7(3):328–331, June 2018.

[85] Q. Hu, Y. Cai, A. Liu, G. Yu, and G. Y. Li. Low-complexity joint resource allocation and trajectory design for UAV-aided relay networks with the segmented ray-tracing channel model. *IEEE Trans. Wireless Commun.*, 19(9):6179–6195, Sep. 2020.

[86] Y. Li, W. Liang, W. Xu, Z. Xu, X. Jia, Y. Xu, and H. Kan. Data collection maximization in IoT-sensor networks via an energy-constrained UAV. *IEEE Trans. Mobile Computing*, 22 (1):159–174, Jan. 2023.

[87] A. Kamal, A. Y. Javaid, V. K. Devabhaktuni, D. Kaur, J. Zaientz, and Robert M. A novel approach to air corridor estimation and visualization for autonomous multi-UAV flights. In *Proc. IEEE Int. Conf. Electro Inf. Technol. (EIT), Naperville, USA*, pages 370–377, Sep. 2020.

[88] C. You and R. Zhang. 3D trajectory optimization in rician fading for UAV-enabled data harvesting. *IEEE Trans. Wireless Commun.*, 18(6):3192–3207, June 2019.

[89] H. Yan, Y. Chen, and S. H. Yang. New energy consumption model for rotary-wing UAV propulsion. *IEEE Wireless Commun. Lett.*, 10(9):2009–2012, Sep. 2021.

[90] X. Qin, Z. Song, Y. Hao, and X. Sun. Joint resource allocation and trajectory optimization for multi-UAV-assisted multi-access mobile edge computing. *IEEE Wireless Commun. Lett.*, 10(7):1400–1404, July 2021.

[91] Y. Xu, L. Xiao, D. Yang, Q. Wu, and L. Cuthbert. Throughput maximization in multi-UAV enabled communication systems with difference consideration. *IEEE Access*, 6:55291–55301, Sep. 2018.

[92] J. Wang, Z. Na, and X. Liu. Collaborative design of multi-UAV trajectory and resource scheduling for 6G-enabled internet of things. *IEEE Internet Things J.*, 8(20):15096–15106, Oct. 2021.

[93] Q. Wu, Y. Zeng, and R. Zhang. Joint trajectory and communication design for multi-UAV enabled wireless networks. *IEEE Trans. Wireless Commun.*, 17(3):2109–2121, March 2018.

[94] M. T. Nguyen and L. B. Le. Resource allocation, trajectory optimization, and admission control in UAV-based wireless networks. *IEEE Networking lett.*, 3(3):129–132, Sep. 2021.

[95] Y. Wu, W. Fan, W. Yang, X. Sun, and X. Guan. Robust trajectory and communication design for multi-UAV enabled wireless networks in the presence of jammers. *IEEE Access*, 8:2893–2905, Dec. 2020.

[96] C. Shen, T. H. Chang, J. Gong, Y. Zeng, and R. Zhang. Multi-UAV interference coordination via joint trajectory and power control. *IEEE Trans. Signal Processing*, 68:843–858, Jan. 2020.

[97] J. Ji, K. Zhu, D. Niyato, and R. Wang. Joint cache placement, flight trajectory, and transmission power optimization for multi-UAV assisted wireless networks. *IEEE Trans. Wireless Commun.*, 19(8):5389–5403, Aug. 2020.

[98] W. Zhang, Q. Wang, X. Liu, Y. Liu, and Y. Chen. Three-dimension trajectory design for multi-UAV wireless network with deep reinforcement learning. *IEEE Trans. Veh. Technol.*, 70(1):600–612, Jan. 2021.

[99] W. Luo, Y. Shen, B. Yang, S. Wang, and X. Guan. Joint 3-d trajectory and resource optimization in multi-UAV-enabled IoT networks with wireless power transfer. *IEEE Internet Things J.*, 8(10):7833–7848, May 2021.

[100] S. Boyd and L. Vandenberghe. *Convex optimization*. Cambridge university press, 2004.

[101] N. Gupta, S. Agarwal, and D. Mishra. Trajectory design for throughput maximization in UAV-assisted communication system. *IEEE Trans. Green Commun. Netw.*, 5(3):1319–1332, June 2021.

[102] C. Zhan, Y. Zeng, and R. Zhang. Energy-efficient data collection in UAV enabled wireless sensor network. *IEEE Wireless Commun. Lett.*, 7(3):328–331, June 2018.

[103] D. C. Gandolfo, L. R. Salinas, A. Brandão, and J. M. Toibero. Stable path-following control for a quadrotor helicopter considering energy consumption. *IEEE Trans. Control Syst. Technol.*, 25(4):1423–1430, July 2017.

[104] C. Villaseñor, A. A. Gallegos, G. Lopez-Gonzalez, J. Gomez-Avila, J. Hernandez-Barragan, and N. Arana-Daniel. Ellipsoidal path planning for unmanned aerial vehicles. *Applied Sciences*, 11(17), Aug. 2021.

[105] M. Alzenad and H. Yanikomeroglu. Coverage and rate analysis for vertical heterogeneous networks (VHetNets). *IEEE Trans. Wireless Commun.*, 18(12):5643–5657, Dec. 2019.

[106] M. Alzenad and H. Yanikomeroglu. Coverage and rate analysis for unmanned aerial vehicle base stations with LoS/NLoS propagation. In *Proc. IEEE Globecom Workshops (GC Wkshps)*, pages 1–7, Dec. 2018.

[107] E. Turgut and M. C. Gursoy. Downlink analysis in unmanned aerial vehicle (UAV) assisted cellular networks with clustered users. *IEEE Access*, 6:36313–36324, May 2018.

[108] V. V. Chetlur and H. S. Dhillon. Downlink coverage analysis for a finite 3D wireless network of unmanned aerial vehicles. *IEEE Trans. Commun.*, 65(10):4543–4558, Oct. 2017.

[109] H. Sun, X. Wang, Y. Zhang, and T. Q. S. Quek. Performance analysis and cell association design for drone-assisted heterogeneous networks. *IEEE Trans. Veh. Technol.*, 69(11): 13741–13755, Nov. 2020.

[110] W. Tang, H. Zhang, and Y. He. Tractable modelling and performance analysis of UAV networks with 3D blockage effects. *IEEE Wireless Commun. Lett.*, 9(12):2064–2067, Dec. 2020.

[111] H. S. Dhillon, R. K. Ganti, F. Baccelli, and J. G. Andrews. Modeling and analysis of k-tier downlink heterogeneous cellular networks. *IEEE J. Selected Areas Commun.*, 30(3):550–560, Apr. 2012.

[112] J. G. Andrews, F. Baccelli, and R. K. Ganti. A tractable approach to coverage and rate in cellular networks. *IEEE Trans. Commun.*, 59(11):3122–3134, Nov. 2011.

[113] A. Al-Hourani, S. Kandeepan, and A. Jamalipour. Modeling air-to-ground path loss for low altitude platforms in urban environments. In *Proc. IEEE Global Commun. Conf. (GLOBECOM), Austin, TX USA*, pages 2898–2904, Dec. 2014.

[114] S. K. Singh, R. Singh, and B. Kumbhani. mm-Wave micro-wave integrated Sub-RAN for CRAN performance enhancement. *IET Commun.*, (15):1045–1052, Nov. 2021.

[115] A. Papoulis and H. Saunders. Probability, random variables and stochastic processes. 1989.

[116] Wolfram. The wolfram functions site. URL "https://functions.wolfram.com/".

[117] M. S. Bazaraa, H. D. Sherali, and C. M. Shetty. *Nonlinear programming: Theory and algorithms*. John Wiley & Sons, 2013.

[118] I. S. Gradshteyn and I. M. Ryzhik. *Table of integrals, series, and products*. Academic press, 2014.